

**AN INVESTIGATION OF GENOTOXICITY AND ANTIOXIDANT  
TREATMENT ON DNA REPAIR IN HUMAN CELLS**

**by**

**Pratibha Mistry BSc (Hons) MSc**

**A thesis submitted for the degree of  
Doctor of Philosophy  
at the University of Leicester  
2002**

**Department of Pathology  
Centre for Mechanisms of Human Toxicity  
University of Leicester  
Leicester**

UMI Number: U161436

All rights reserved

INFORMATION TO ALL USERS

The quality of this reproduction is dependent upon the quality of the copy submitted.

In the unlikely event that the author did not send a complete manuscript and there are missing pages, these will be noted. Also, if material had to be removed, a note will indicate the deletion.



UMI U161436

Published by ProQuest LLC 2013. Copyright in the Dissertation held by the Author.  
Microform Edition © ProQuest LLC.

All rights reserved. This work is protected against  
unauthorized copying under Title 17, United States Code.



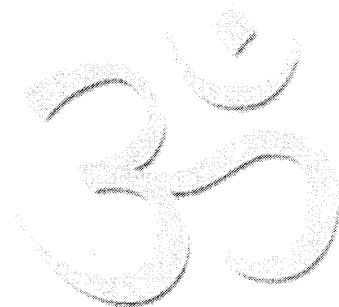
ProQuest LLC  
789 East Eisenhower Parkway  
P.O. Box 1346  
Ann Arbor, MI 48106-1346

## **ABSTRACT**

Understanding the mechanisms defying endogenous and exogenous processes that threaten DNA integrity remains critical to the elucidation of cancer, disease processes and ageing. The research presented in this thesis examines the formation and the removal of two distinctly different DNA lesions in human cell culture systems. Significant differences in the formation of cyclobutane pyrimidine dimers following monochromatic ultraviolet irradiations at 305nm and 315nm in cultured keratinocytes and DNA were demonstrated immunochemically, offering a non-invasive model to gauge wavelength-specific damage and their potencies. The formation of the oxidative lesion, 7, 8-dihydro-8-oxo-2'-deoxyguanosine (8-oxodG), was also demonstrated immunochemically and by HPLC with electrochemical detection. In addition the measurement of intracellular reactive oxygen species generation was monitored by a fluorimetric assay. All three approaches clearly illustrated that sub-lethal doses of hydrogen peroxide caused a dose-dependent increase in the genotoxic potential in cultured human cells. Further to the confirmation of this prooxidant condition, the generation of a potentially antioxidant environment was achieved through the uptake and/or regeneration of ascorbic acid, confirmed by capillary electrophoresis measurements of intracellular extracts. The modulation of two base excision repair enzymes, human 8-oxoguanine glycosylase (hOGG1) and human apurinic/apyrimidinic endonuclease (hAPE), important in the removal of 8-oxodG, was investigated in response to prooxidant and antioxidant treatments. No significant change in mRNA and protein expression of hOGG1 and hAPE was observed under either experimental condition. In conclusion however, there may be modulation of these repair enzymes at the post-translational level possibly in response to the changes in cellular redox status and the formation of 8-oxodG. Therefore measuring repair activities alongside genotoxicity may provide useful indications of perturbations that can lead to potential mutational events and cellular dysfunction. Appreciating the interplay of multiple DNA repair pathways presents an interesting challenge for future studies.

**To my family and friends**

**Thank you**



## **ACKNOWLEDGMENTS**

I wish to thank Drs Karl Herbert and Jacqui Shaw for their assistance and encouragement in the completion of this thesis. A special thank you Dr Karl Herbert for his valued scientific input and motivation throughout my work.

I would like to acknowledge the financial contributors to this PhD: Prof I Lauder and Dr K Herbert, Department of Pathology; Prof J Lunec, Division of Chemical Pathology; Dr P Hutchinson, Department of Dermatology, Leicester Royal Infirmary and the Scottish Office.

I would also like to thank my colleagues of the CMHT for their valued assistance and guidance. It was a pleasure to be part of such a unit.

And finally, my heart felt thanks to those closest to me who have given me enormous strength and support during troubled times.

## CONTENTS

	<b>Page</b>
Abstract	II
Dedication	III
Acknowledgments	IV
Contents	V
Index of Figures	VII
Index of Tables	IX
Abbreviations	X

### CHAPTER ONE: Introduction

	<b>Page</b>	
1.1	Genotoxicity	2
1.2	Cellular defences against genotoxicity	4
1.2.1	Base excision repair	6
1.2.2	Nucleotide excision repair: global genome and transcription-coupled	11
1.2.3	Repair of double-strand breaks: homologous recombination and end-joining	15
1.2.4	Mismatch repair	15
1.3	Diseases associated with genotoxicity and DNA repair systems	18
1.3.1	Base excision repair and cancer	18
1.3.2	Nucleotide excision repair and cancer	18
1.3.3	Double-strand break repair and cancer	22
1.3.4	Mismatch repair and cancer	22
1.4	Aims	23

### CHAPTER TWO: Materials & Methods

	<b>Page</b>	
2.1	Materials	25
2.2	Equipment	32
2.3	Methods	35

### CHAPTER THREE: Detection of direct UV-induced DNA damage & repair in human skin cells & tissues

	<b>Page</b>	
3.1	Introduction	58
3.2	Aims	62
3.3	Methods	63
3.4	Results	66
3.5	Discussion	88

**CHAPTER FOUR:** Cellular oxidative stress induced by hydrogen peroxide & the uptake of ascorbic acid

	<b>Page</b>
<b>4.1</b> Introduction	99
<b>4.2</b> Aims	102
<b>4.3</b> Methods	103
<b>4.4</b> Results	106
<b>4.5</b> Discussion	126

**CHAPTER FIVE:** The expression of base excision repair enzymes specific for the removal of 8-oxoguanine lesions

	<b>Page</b>
<b>5.1</b> Introduction	135
<b>5.2</b> Aims	138
<b>5.3</b> Methods	139
<b>5.4</b> Results	142
<b>5.5</b> Discussion	167

**CHAPTER SIX:** General Discussion & Future Work

	<b>Page</b>
<b>6.1</b> General Discussion	180
<b>6.2</b> Future Work	186

**APPENDICES**

	<b>Page</b>
Appendix I: Composition of cell culture media	189
Appendix II: Spectrophotometric assessment of hydrogen peroxide molarity	191
Appendix III: Excitation and emission spectra of fluorochromes	192
Appendix IV: Emission spectra of UV sources	194
Appendix V: Calculation of UV dose and coefficient of variation of irradiation	195
Appendix VI: hOGG1 peptide synthesis data	196
Appendix VII: $\beta$ -actin, hOGG1 and hAPE primer positions	198
Appendix VIII: Endonuclease nicking assay experimental approaches	199
Appendix IX: $\beta$ -actin, hOGG1 and hAPE PCR product sequencing data	200
Appendix X Potential ARE and AP-1 transcription binding sites of <i>hOGG1</i> and <i>hAPE</i>	206
Appendix XI Publications arising from this thesis	207

<b>REFERENCES</b>	<b>208</b>
-------------------	------------

**INDEX OF FIGURES**

	<b>Page</b>
<b>1.1</b> Genotoxicity typical of endogenous and exogenous agents	3
<b>1.2</b> Genotoxicity and interplay between the cellular defence and DNA repair mechanisms	5
<b>1.3</b> Human base excision repair pathways	9
<b>1.4</b> Human nucleotide excision repair pathway	14
<b>1.5</b> Human double strand break repair pathways	16
<b>1.6</b> Human mismatch repair pathway	17
<b>3.1</b> UV-induced DNA lesions.	59
<b>3.2</b> Immunocytochemical staining of cytokeratins in cultured keratinocytes	67
<b>3.3</b> Optimisation of pyrimidine dimer ELISA with native and UVC irradiated calf thymus DNA	68
<b>3.4</b> Immunochemical detection of CPD in THEK cells and formalin-fixed paraffin embedded human skin sections	70
<b>3.5</b> The effect of photoreversal on the immunochemical detection of pyrimidine dimers	72
<b>3.6</b> The effect of enzymic photoreversal on the detection of CPD	73
<b>3.7</b> Ultrastructural localisation of the pyrimidine dimer antibody in NHEK and THEK cells irradiated with UVB	74
<b>3.8</b> Comparison of CTD detection by ELISA with gas chromatography-mass spectrometry values	75
<b>3.9</b> Quantitation of CTD by ELISA	77
<b>3.10</b> Immunofluorescence comparison of CTD formation with 305nm and 315nm UVB irradiation	78
<b>3.11</b> Immunofluorescence investigation of CTD repair in THEK cells	81
<b>3.12</b> Changes in ultrastructure of THEK cells following UVB irradiation	82
<b>3.13</b> Optimisation of CTD competition ELISA	83
<b>3.14</b> A direct-binding ELISA assessment of cell culture medium salt concentration on the binding of the CTD antibody to UVC treated DNA	84
<b>3.15</b> A competition ELISA comparison of desalting and purification procedures for repair oligonucleotides	86
<b>3.16</b> Repair of CTD by THEK cells	87
<b>4.1</b> Representative HPLC chromatograms of deoxyguanosine and 8-oxodG	106
<b>4.2</b> High performance liquid chromatography with electrochemical detection of 8-oxodG	107
<b>4.3</b> Immunocytochemical staining of 8-oxodG in THEK cells	108
<b>4.4</b> Immunohistochemical detection of 8-oxodG and cytosine glyoxal in formalin-fixed paraffin embedded human normal skin and basal cell carcinoma sections	109
<b>4.5</b> Optimisation of CM-H <sub>2</sub> DCFDA for the measurement of endogenous ROS in THEK cells	114
<b>4.6</b> Background fluorescence measurements of cell culture medium and treatment reagents at excitation and emission of 485 and 535nm	114
<b>4.7</b> The effects of hydrogen peroxide on intracellular ROS activity in NHEK and THEK cells	117
<b>4.8</b> The effects of ascorbic acid and dehydroascorbic acid on intracellular ROS activity in THEK cells	118

4.9	Extracellular ascorbic acid concentrations in cultures of THEK cells	120
4.10	Typical calibration curve of ascorbic acid and representative capillary electropherograms of ascorbic acid with isoascorbic acid internal standard	122
4.11	Capillary electrophoresis measurements of ascorbic acid in cell culture medium following supplementation of cell cultures with 0-400 $\mu$ M ascorbic acid of THEK and CCRF cells	123
4.12	Capillary electrophoresis measurements of intracellular ascorbic acid following supplementation of cell cultures with 0-400 $\mu$ M ascorbic acid or dehydroascorbic acid in CCRF and THEK cells	124
5.1	The interaction of hOGG1 and hAPE: their enzymatic potentials in the repair of the oxidative lesion 8-oxoguanine	136
5.2	Effects of hydrogen peroxide, ascorbic acid and dehydroascorbic acid on cytotoxicity	142
5.3	Cell cycle profiles of CCRF cells following 48hr serum starvation, comparison with non-serum starved cells	143
5.4	Electrophoretic mobility shift assay measuring AP-1 DNA binding activity in THEK nuclear extracts	144
5.5	Optimisation of MgCl <sub>2</sub> concentration for <i>hOGG1</i> and <i>hAPE</i> PCR	146
5.6	Optimal PCR annealing temperature for <i>hOGG1</i> and <i>hAPE</i> primers	147
5.7	Optimal PCR cycle number for <i><math>\beta</math>-actin</i> , <i>hOGG1</i> and <i>hAPE</i> to study gene expression changes	148
5.8	A comparison of RT-PCR products with genomic DNA PCR products amplified by <i><math>\beta</math>-actin</i> , <i>hOGG1</i> and <i>hAPE</i> primers	149
5.9	Effect of hydrogen peroxide on <i>hOGG1</i> and <i>hAPE</i> mRNA expression in THEK and CCRF cells	152
5.10	Effect of ascorbic acid on <i>hOGG1</i> and <i>hAPE</i> mRNA expression in THEK and CCRF cells	153
5.11	Direct-binding ELISA data of anti-hOGG1 peptide antibodies	156
5.12	Immunoglobulin sub-class identification for anti-hOGG1 peptide immune sera from rabbits 807 and 808 by direct-binding ELISA	157
5.13	Isolation of IgG anti-hOGG1 peptide antibody from whole serum of rabbits 807 and 808	157
5.14	Coomassie blue stained IgG isolated from pre-immune serum and hOGG1 peptide immune serum from rabbit 808	158
5.15	Validation of anti-hOGG1 peptide antibody specificity	158
5.16	A comparison of protein levels determined by Ponceau S staining followed by Western blot analysis of $\beta$ -actin protein	159
5.17	Western blot detection of hOGG1 and $\beta$ -actin proteins in cell lysates	160
5.18	Western blot analysis of hOGG1 protein expression following hydrogen peroxide, ascorbic acid and dehydroascorbic acid, in THEK and CCRF cells	161
5.19	Immunochemical localisation of hOGG1 protein in THEK cells	162
5.20	Metaphor <sup>®</sup> agarose electrophoresis verification of double-stranded repair oligonucleotide	163
5.21	Detection of 11 and 21mer oligonucleotides by denaturing-polyacrylamide gel electrophoresis	164
5.22	Measurement of 8-oxodG repair activity by capillary electrophoresis	165
5.23	Effect of hydrogen peroxide on hOGG1 and hAPE repair activity in CCRF cells	166

## INDEX OF TABLES

		<b>Page</b>
<b>1.1</b>	Human DNA glycosylases, nomenclature and species equivalents	7
<b>1.2</b>	Molecular and biochemical profiles of some human DNA glycosylases	8
<b>1.3</b>	Protein components of nucleotide excision repair	13
<b>1.4</b>	Xeroderma pigmentosum complementation groups	20
<b>1.5</b>	Human syndromes defective in DSB repair	22
<b>2.1</b>	Primary & secondary antibodies for immunochemical experiments	27
<b>2.2</b>	<i>hOGG1</i> , <i>hAPE</i> and $\beta$ - <i>Actin</i> , primer sequences, gene positions and predicted PCR product size	49
<b>2.3</b>	Oligonucleotide sequences of DNA repair oligonucleotides used for the Endonuclease Nicking Assay	50
<b>3.1</b>	Coefficients of variation (CV) in ELISA quantitation of cyclobutane thymine dimer compared to gas chromatography-mass spectrometry measurements	76
<b>4.1</b>	The assessment of homogeneity of transformed and primary human keratinocyte growth in 96-well plates	112
<b>5.1</b>	Automated sequencing data $\beta$ - <i>actin</i> , <i>hOGG1</i> and <i>hAPE</i> PCR products	150

## ABBREVIATIONS

ADP	Adenosine diphosphate
ALS	Amyotrophic lateral sclerosis
AP-1	Activator protein-1
AP endonuclease/ APE	Apurinic/aprimidinic endonuclease
AP lyase	Apurinic/aprimidinic lyase
APS	Ammonium persulphate
ATM	Ataxia telangiectasia mutated
ATP	Adenosine triphosphate
ATR	Ataxia telangiectasia related
BER	Base excision repair
BRCA	Breast cancer
BSA	Bovine serum albumin
CAK	Cdk-activating kinase
CCRF-HSB-2	Human caucasian acute human T-lymphoblastic leukaemia cells
Cdk	Cyclin-dependant protein kinase
cDNA	Complementary deoxyribonucleic acid
CE	Capillary electrophoresis
CM-H <sub>2</sub> DCFDA	5-(and-6)-chloromethyl-2',7'-dichlorodihydrofluorescein diacetate
CNS	Central nervous system
CS	Cockayne's syndrome
CSA	Cockayne's syndrome complementation group A
CSB	Cockayne's syndrome complementation group B
CSC	Cockayne's syndrome complementation group C
Cys	Cysteine
dA	Deoxyadenosine
DCFDA	Dichlorodihydrofluorescein
dC	Deoxycytidine
dCTP	Deoxycytidine triphosphate
DFO	Desferrioxamine
dG	Deoxyguanosine
dGTP	Deoxyguanosine triphosphate
DMEM	Dulbecco's modified Eagles medium
DMSO	Dimethyl sulphoxide
DNA	Deoxyribonucleic acid
DNA-PK	DNA protein kinase
DNA Pol	DNA polymerase
dNTP	Deoxynucleotide triphosphate
dpm	Disintegrations per minute
dRPase	Deoxyribophosphodiesterase
DSB	Double-strand breaks
dT	Thymidine
DTPA	Diethylenetriaminepentaacetic acid
DTT	Dithiothreitol
ECL	Enhanced chemiluminescence
E. coli	Escherichia coli
EDTA	Ethylenediaminetetraacetic acid
EJ	End-joining
ELISA	Enzyme linked immunosorbent assay
EM	Electron microscopy
EMSA	Electrophoretic mobility shift assay

ERCC	Excision repair cross complementation
Fapy-A	2,6-diamino-4-hydroxy-5-formamidoadenine
Fapy-G	2,6-diamino-4-hydroxy-5-formamidoguanine
FEN1	Flap structure-specific endonuclease 1
FITC	Fluorescein Isothiocyanate
GG-NER	Global Genome-Nucleotide Excision Repair
Hams F12	Ham's Nutrient Mixture F-12
hAPE	Human Apurinic/aprimidinic Endonuclease
HEPES	N-(2-hydroxyethyl) piperazine-N'-(2-ethanesulfonic acid)
hHR23B	Human homologue Rad23
HiFCS	Heat-inactivated foetal calf serum
hMBD4	Human mismatch thymine glycosylase
hMLH	Human MutL homologue
hMMH	Human MutM homologue
hMPG	Human methylpurine glycosylase
hMSH	Human MutS homologue
hMTH	Human MutT homologue
hMYH	Human MutY homologue
hNEIL	Human nei endonuclease VIII-like
HNPCC	Human non-polyposis colorectal cancer
hNTH	Human endonuclease III homologue
hOGG1	Human 8-oxoguanine glycosylase 1
HPLC	High performance liquid chromatography
HPMS1	Human postmeiotic segregation increased 1
HR	Homologous recombination
HRP	Horseradish peroxidase
hSMUG1	Human 5-hydroxymethyluracil glycosylase
hTDG	Human thymine DNA glycosylase
hUDG	Human uracil DNA glycosylase
hUNG	Human uracil DNA glycosylase
IAA	Isoascorbic acid
IgG	Immunoglobulin G
IgM	Immunoglobulin M
Ig's	Immunoglobulins
KBM	Keratinocyte basal medium
KGM	Keratinocyte growth medium
KLH	Keyhole limpet haemocyanin
LPS	Lipopolysaccharide
MAT1	Ménage-a-trois protein 1
MED	Minimal erythematous dose
Mfd	Mutation frequency decline
MMR	Mismatch repair
MnSOD	Manganese superoxide dismutase
MPA	Metaphosphoric acid
MRE11	Meiotic recombination protein
MutL $\alpha$	hMLH1/hPMS2
MutL $\beta$	hMLH1/hPMS1
MutS $\alpha$	hMSH2/6
MutS $\beta$	hMSH2/3
NBS	Nijmegen breakage syndrome
nCaRE	Negative calcium-responsive element

NER	Nucleotide excision repair
NGS	Normal goat serum
NHEK-Ad	Normal human epidermal keratinocytes-adult
8-oxoG	8-oxoguanine
8-oxodG	7, 8-dihydro-8-oxo-2'-deoxyguanosine
PAGE	Polyacrylamide gel electrophoresis
PARP	Poly (ADP)-ribose polymerase
PBS	Phosphate buffered saline
PCR	Polymerase chain reaction
PMSF	Phenylmethylsulfonyl fluoride
PCNA	Proliferating cell nuclear antigen
Poly (dI)-(dC)	Polydeoxyinosinic-deoxycytidylic acid
PUVA	Psoralen-UVA
PVDF	Polyvinylidene difluoride
RAD	Radiation-sensitive mutations
RFC	Replication factor C
RNA	Ribonucleic acid
RNA Pol	RNA polymerase
ROS	Reactive oxygen species
RPA	Replication protein A
RPMI-1640	Roswell Park Memorial Institute medium 1640
RT	Room temperature
RT-PCR	Reverse transcriptase-polymerase chain reaction
<i>S. cerevisiae</i>	<i>Saccharomyces cerevisiae</i>
SDS	Sodium dodecyl sulphate
Ser	Serine
SLE	Systemic lupus erythematosus
SOD	Superoxide dismutase
<i>S. pombe</i>	<i>Saccharomyces pombe</i>
SSB	Single-strand breaks
SSL1	Suppressor of stem-loop protein 1
THEK	Simian virus 40 transformed human epidermal keratinocytes
TBE	Tris-borate EDTA
TBS	Tris buffered saline
TC-NER	Transcription coupled-nucleotide excision repair
TE	Tris-EDTA
TEMED	N, N, N', N'- tetramethylethyldiamine
TFIIF	RNA Pol II transcription factor IIF
TFB1	RNA Pol II transcription factor B protein 1
TRCF	Transcription-repair coupling factor
TTD	Trichothiodystrophy
UP	Ultrapure
USF	Upstream factor
UV	Ultraviolet
UVA	Ultraviolet A (320-400nm)
UVB	Ultraviolet B (280-320nm)
UVC	Ultraviolet C (100-280nm)
VHL	Von Hippel-Lindau disease
XP	Xeroderma pigmentosum
XPA	Xeroderma pigmentosum complementation group A
XPB	Xeroderma pigmentosum complementation group B
XPC	Xeroderma pigmentosum complementation group C

XPD	Xeroderma pigmentosum complementation group D
XPE	Xeroderma pigmentosum complementation group E
XPF	Xeroderma pigmentosum complementation group F
XPG	Xeroderma pigmentosum complementation group G
XRCC1	X-ray repair cross-complementing protein 1

# **CHAPTER ONE**

## **INTRODUCTION**

## **1.0 INTRODUCTION**

Genes encoded in DNA control development and the maintenance of life. Defying endogenous and exogenous processes that threaten DNA integrity is essential for our existence. Understanding these mechanisms remains critical for elucidation of cancer development, other disease processes and ageing. In particular, the continued research into the effective treatment of diseases and the preservation of life highlights the need to add to our knowledge of the role of damage to DNA and the interplay of protective mechanisms in cellular systems.

### **1.1 Genotoxicity**

DNA consists of two long unbranched polymers, composed of four types of deoxyribonucleotides, held together by complementary hydrogen bonding of bases. Each deoxyribonucleotide consists of a nitrogen-containing base, either a purine (adenine or guanine) or a pyrimidine (cytosine or thymine), a 5-carbon sugar (deoxyribose) and a phosphate. Genes encoded in selected regions of DNA produce a functional RNA molecule during transcription. Each triplicate nucleotide sequence (codon) in the RNA molecule in turn specifies a particular amino acid of a protein during the translation process. DNA is compartmentalised in the nucleus where it is tightly coiled around histone octamers to form nucleosomes, and these are further packed into chromatin. During metaphase of the cell cycle the chromatin structure of DNA is further condensed to assist efficient separation of replicated chromosomes.

Despite the complexities of the structure of DNA and protective proteins, the integrity of DNA is subject to continual stresses; DNA lesions can arise from a variety of mechanisms involving external insults and/or endogenous physiological metabolism, such as chemical toxins, infection, inflammation, xenobiotic metabolism and the mitochondrial electron transport chain (Ames 1989; Halliwell and Gutteridge 1999, Lindahl 1993). The resulting damage can be characteristic of the nature of insult, such as pyrimidine dimers following ultraviolet (UV) light exposure, or can be more non-specific such as those resulting from oxidative modifications; some of these DNA lesions are detailed in Figure 1.1. Single base lesions do not tend to distort the DNA helix, whilst covalent alterations in DNA such as those seen with bulky adducts can significantly distort the DNA.

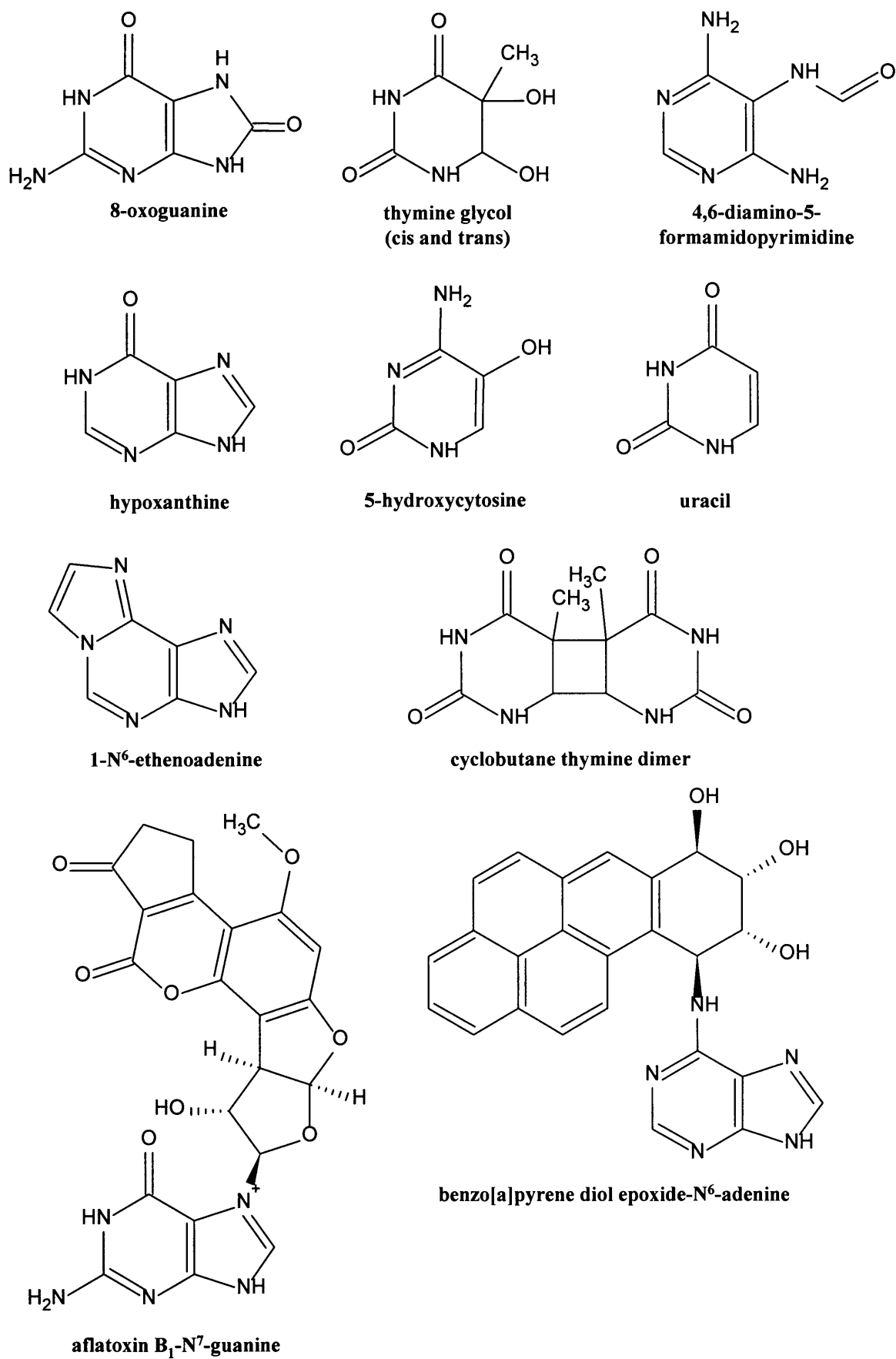


**Figure 1.1:** Genotoxicity typical of endogenous and exogenous agents

DNA replication is a highly accurate process involving several proofreading mechanisms, however rarely these processes can skip or add a few nucleotides, or cause mispairing of bases (Schär, 2001). Such mutational events can have deleterious consequences for a cell, where the inactivation of a crucial protein can lead to cell dysfunction or even death. Not all mutations however affect cellular homeostasis, some mutations can be 'silent' and pose little change to cells, and some mutations may even be beneficial and improve protein function. A lifetime of 'spontaneous' mutations does not alone account for the genetic instability driving tumourigenesis (Loeb, 1991; Loeb, 2001); indeed many links between acquired and inherited defects in DNA protection systems have been associated with cancer development.

## **1.2 Cellular defences against genotoxicity**

The effects of DNA damage can be divided into acute effects such as cell cycle arrest or cell death, and more long-term effects such as mutations or chromosomal aberrations. The integrity of DNA relies on a network of integrated processes involving DNA damage recognition and repair, replication, transcription, cell cycle regulation as well as cell death mechanisms (Rich *et al.*, 2000). In addition to these processes, cellular detoxification and antioxidant mechanisms are equally important. A major group of detoxification enzymes include the glutathione-*S*-transferase (GST) multi-gene family found in the endoplasmic reticulum. Particular isoforms of GST determine the toxicity of a given insult to cells. In humans there are distinct differences in isoenzyme expression, and certain polymorphisms influence cancer risk/progression, chemoprotection and drug resistance (Hayes and Pulford, 1995; Smith *et al.*, 1996).

The importance of antioxidant mechanisms in maintaining the integrity of DNA has been highlighted. Intracellular enzymes such as catalase, superoxide dismutase, glutathione peroxidase catalyse the removal of specific ROS (Röhrdanz and Kahl, 1998; Taniguchi, 1992), whilst glutathione, a low molecular weight polypeptide and a cofactor of glutathione peroxidase, has also non-specific scavenging capacities (Anderson, 1998; Bray *et al.*, 1998; Meister, 1981). Protection against endogenous free radicals can also be provided by dietary antioxidants, such as vitamins C and E, flavonoids and selenium (Collins, 1999; Halliwell, 2002; Loft and Poulsen, 2000). Despite these cellular protection mechanisms, the integrity of DNA is continually challenged. Some DNA aberrations are removed by direct reversal, such as single-strand breaks at undamaged sites which can be directly rejoined by the action of DNA ligase. Similarly, O<sup>6</sup>-guanine and O<sup>4</sup>- thymine alkylations are repaired by reversal, where O<sup>6</sup>-methylguanine DNA methyltransferase (MGMT) transfers the methyl group from

O<sup>6</sup>- and O<sup>4</sup>- DNA alkylations to its cysteine residue (Grombacher and Kaina, 1995; Sekiguchi *et al.*, 1996). However, the majority of DNA lesions are repaired by DNA excision pathways (described in sections 1.2.1 to 1.2.4), and these orchestrated repair responses are often specific to the nature of the insult (Bohr, 1995; Bohr and Anson, 1995; Wilson and Thompson, 1997).

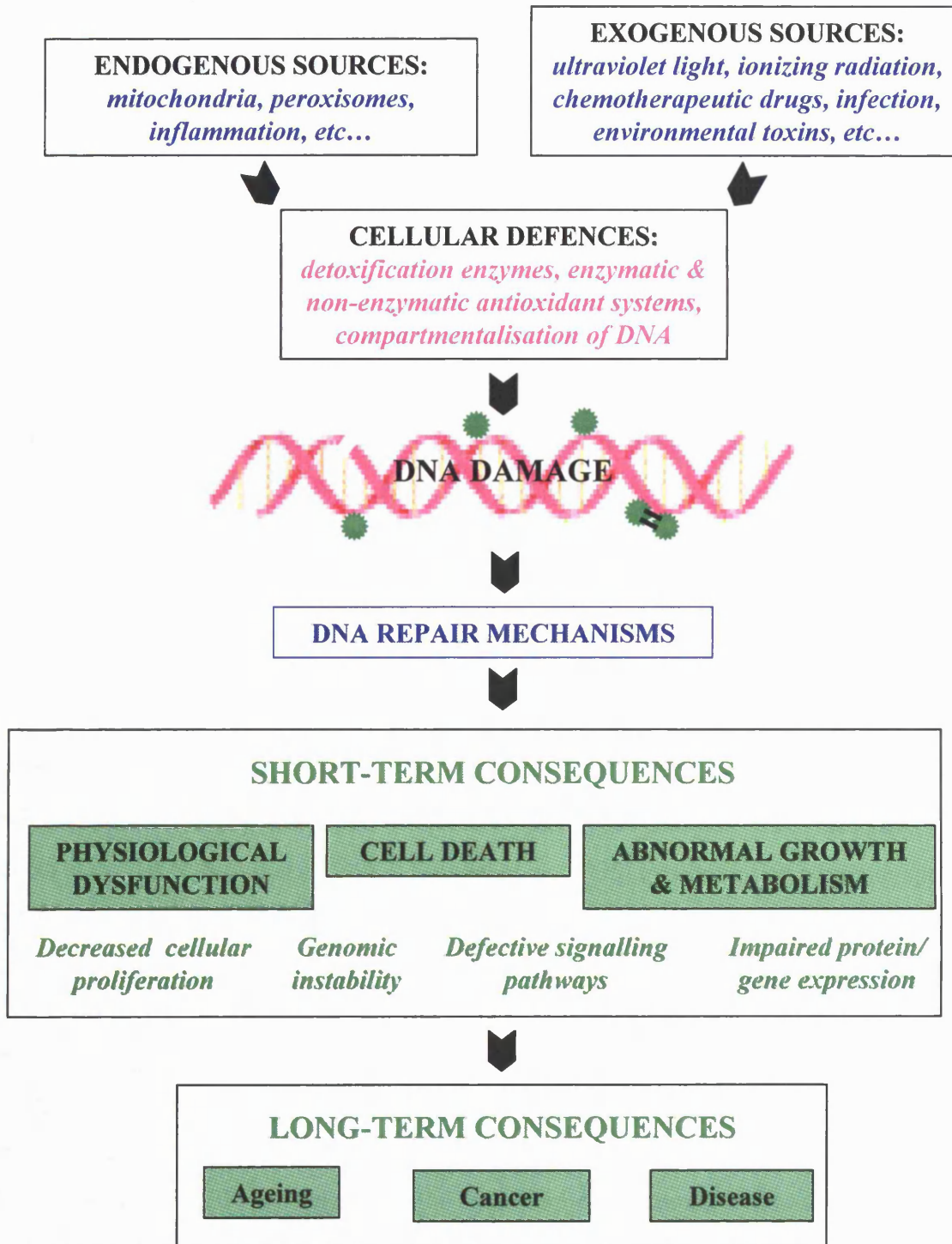


**Figure 1.2:** Genotoxicity and the interplay between the cellular defence and DNA repair mechanisms: long and short-term consequences to cellular function.

### 1.2.1 Base excision repair (BER)

Spontaneous and induced non-bulky base lesions, typically derived from reactive oxygen species, methylation, deamination and hydroxylation events, are substrates for base excision enzymes (Cunningham, 1997; Demple and Harrison, 1994; Krokan *et al.*, 1997; Seeberg *et al.*, 1995). The multistep process of base excision repair (BER) is initiated by the damage-specific glycosylases which tend to be small monomeric proteins that cleave the N-C1' glycosylic bond between the damaged base and the deoxyribose-phosphate backbone (Table 1.1). The base is released and resulting abasic site is further processed (Figure 1.3). There are however two types of glycosylases either monofunctional or bifunctional, the latter possessing the typical glycosylase property as well as a  $\beta$ -lyase activity that cleaves the phosphodiester bond 3' to the abasic site (Table 1.2). Interestingly, mammalian glycosylases, unlike their bacterial counterparts, have N-terminal extensions that determine whether the enzyme targets repair of mitochondrial or nuclear DNA (Otterlei, 1999).

The abasic site is removed by the action of apurinic/apyrimidinic (AP) endonuclease and this may proceed into either 'short patch repair' or 'long patch repair' pathways (Matsumoto *et al.*, 1999; Pascucci *et al.*, 1999). As the names suggest, short patch repair involves a single nucleotide whilst long patch repair involves 2-8 nucleotides to repair the gap generated by excision (Figure 1.3a and b respectively). The type of glycosylase initiating repair and possibly the cell cycle status governs which pathway of BER is followed (Krokan *et al.*, 2000). The gap filling involves either proliferating cell nuclear antigen (PCNA)-independent DNA polymerase (DNA Pol)  $\beta$  action in short patch repair or PCNA-dependent DNA Pols  $\beta$ ,  $\delta$  and  $\epsilon$  action in long patch repair (Frosina *et al.*, 1996; Jónsson and Hübscher, 1997; Pascucci *et al.*, 1999; Shivji *et al.*, 1992; Singhal *et al.*, 1995) involving flap structure-specific endonuclease 1 (FEN1;). The final stage of base excision repair requires the recruitment of a DNA ligase (I or III), involving the scaffold protein x-ray repair cross-complementing gene/protein 1 (XRCC1), for the ligation of a nucleotide to its neighbour and thus sealing the DNA strand (Frosina *et al.*, 1996; Pascucci *et al.*, 1999; Prasad *et al.*, 1996; Hoeijmakers, 2001). Poly-(ADP-ribose) polymerase (PARP) activity, which has been shown to increase as a result of strand breaks (deMurcia *et al.*, 1994), and the recently described polynucleotide kinase (Whitehouse *et al.*, 2001) are believed to be important during repair synthesis when BER is activated through single-strand breaks (SSB).

Name	Human abbreviation	Species equivalents	References
Methylpurine DNA glycosylase	hMPG	<i>E.coli</i> (tag) <i>E.coli</i> (alkA) <i>S.cerevisiae</i> (MAG) <i>S.pombe</i> (mag1) <i>A. thaliana</i> (MPG) <i>Mus Musculus</i> (MPG)	Engelward <i>et al.</i> , 1997 Elder <i>et al.</i> , 1998
Mut Y homologue	hMYH	<i>E.coli</i> (mutY)	Krokan <i>et al.</i> , 1997
nei endonuclease VIII-like 1	hNEIL1	<i>E.coli</i> (mutM/Nei)	Harza <i>et al.</i> , 2002 <sup>1</sup>
nei endonuclease VIII-like 2	hNEIL2	<i>E.coli</i> (mutM/Nei)	Harza <i>et al.</i> , 2002 <sup>2</sup>
Endonuclease III homologue	hNTH1	<i>E.coli</i> (endonuclease III & VII) <i>S.cerevisiae</i> (NTG1) <i>S.pombe</i> (nth) <i>Mus Musculus</i> (mNTH1)	Dizdaroglu <i>et al.</i> , 1999 "
8-oxoguanine glycosylase	hOGG1	<i>E.coli</i> Fpg <i>S.cerevisiae</i> yOGG1 <i>S.cerevisiae</i> yOGG2 <i>D.melanogaster</i> S3 <i>Mus Musculus</i> (mogg1)	Arai <i>et al.</i> , 1997 Radicella <i>et al.</i> , 1997 Roldán-Arjona <i>et al.</i> , 1997 Rosenquist <i>et al.</i> , 1997
Thymine/uracil mismatch DNA glycosylase	hMBD4		Hendrich <i>et al.</i> , 1999
	hSMUG1		Haushalter <i>et al.</i> , 1999
	hTDG	<i>E.coli</i> MUG	Neddermann and Jiricny, 1994
Uracil DNA glycosylase	hUNG1	<i>S.cerevisiae</i> UNG1	Haug <i>et al.</i> , 1998
	hUNG2		Nilsen <i>et al.</i> , 1997
	hUDG2		Krokan <i>et al.</i> , 2000

**Table 1.1:** Human DNA glycosylases, nomenclature and species equivalents, adapted from Griffiths *et al.* (1998), Krokan *et al.* (1997) and Krokan *et al.* (2000).

Glycosylase	Lyase Activity	Cellular Compartment	Size (aa)	Substrate specificity	Chromosome localisation
<b>Alkylbases</b>					
hMPG	×	-	293	3-meA, 7-meA, 3-meG, 7-meG, 8-oxoG, hypoxanthine, εA, εG	16p(telomere)
<b>Adenine-specific mismatch bases</b>					
hMYH	✓? ✓?	Nuclei Mitochondria	521 535	misincorporated A:8-oxoG, A:G, A:C	1p32.1-p34.3
<b>Oxidised purines and pyrimidines</b>					
hNEIL1	✓	Nuclei	390	possible association with stalled replication, see transcription coupled repair (section 1.2.2).	15q22.33
hNEIL2	✓	Nuclei	332	Oxidised cytosine & 5-hydroxyuracil	8p
<b>Oxidized &amp; ring-fragmented pyrimidines</b>					
hNTH1	✓	Nuclei Mitochondria?	312 304?	T/C-glycol, fapy, dihydrouracil,	16p13.2-13.13
<b>Oxidised &amp; ring-fragmented purines</b>					
hOGG1	✓ ✓	Nuclei (α) Mitochondria (β)	345 424	mefapyG:C>>fapyG:C> >8-oxoG:C>>8-oxoG:T	3p25
<b>Uracil and thymine mismatches</b>					
hMBD4	?	-	580	U or T in U/TpG:5-meCpG	3q21
hSMUG1	×		270	ssU>U:A, U:G	12q13.1-q14
hTDG	×	Nuclei	410	U:G>εC:G>T:G	12q24.1
<b>Uracil in DNA</b>					
hUNG1	×	Mitochondria	304	ssU>U:G>U:A, 5-FU, poor repair of 5-hydroxy U, isodialuric acid, alloxan	12q24.1
hUNG2	×	Nuclei	313		
hUDG2	×	-	327	U:A	5

**Table 1.2:** Molecular and biochemical profiles of some human DNA glycosylases, adapted from Krokan *et al.* (1997) and Krokan *et al.* (2000). Known substrate specificities are described for adenine (A), cytosine (C), guanine (G), thymine (T), uracil (U), single-stranded (ss), methyl (me) and etheno (ε) adducts.

a Short-patch repair

Damage to DNA can be in the form of adducts or abasic sites

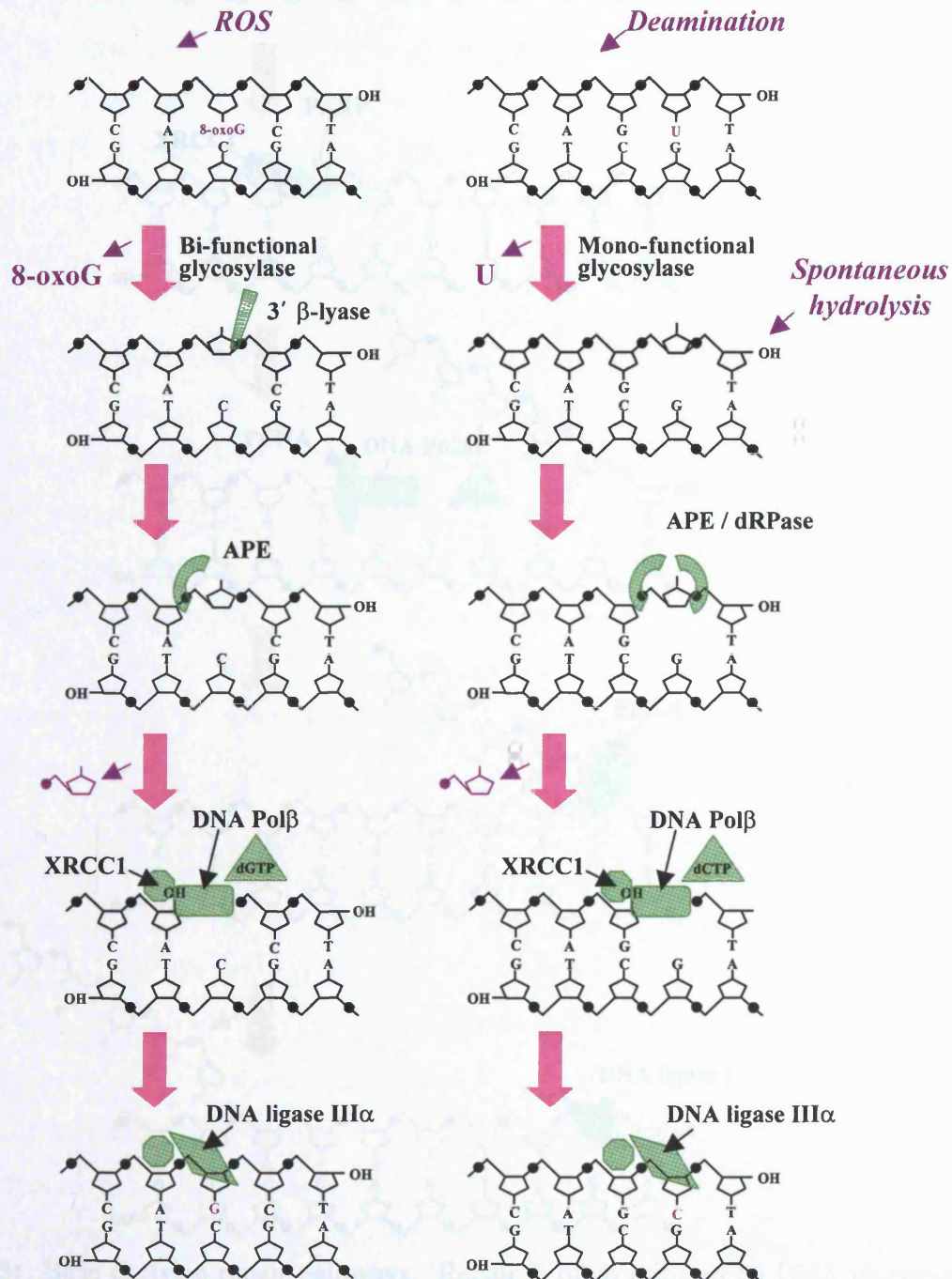
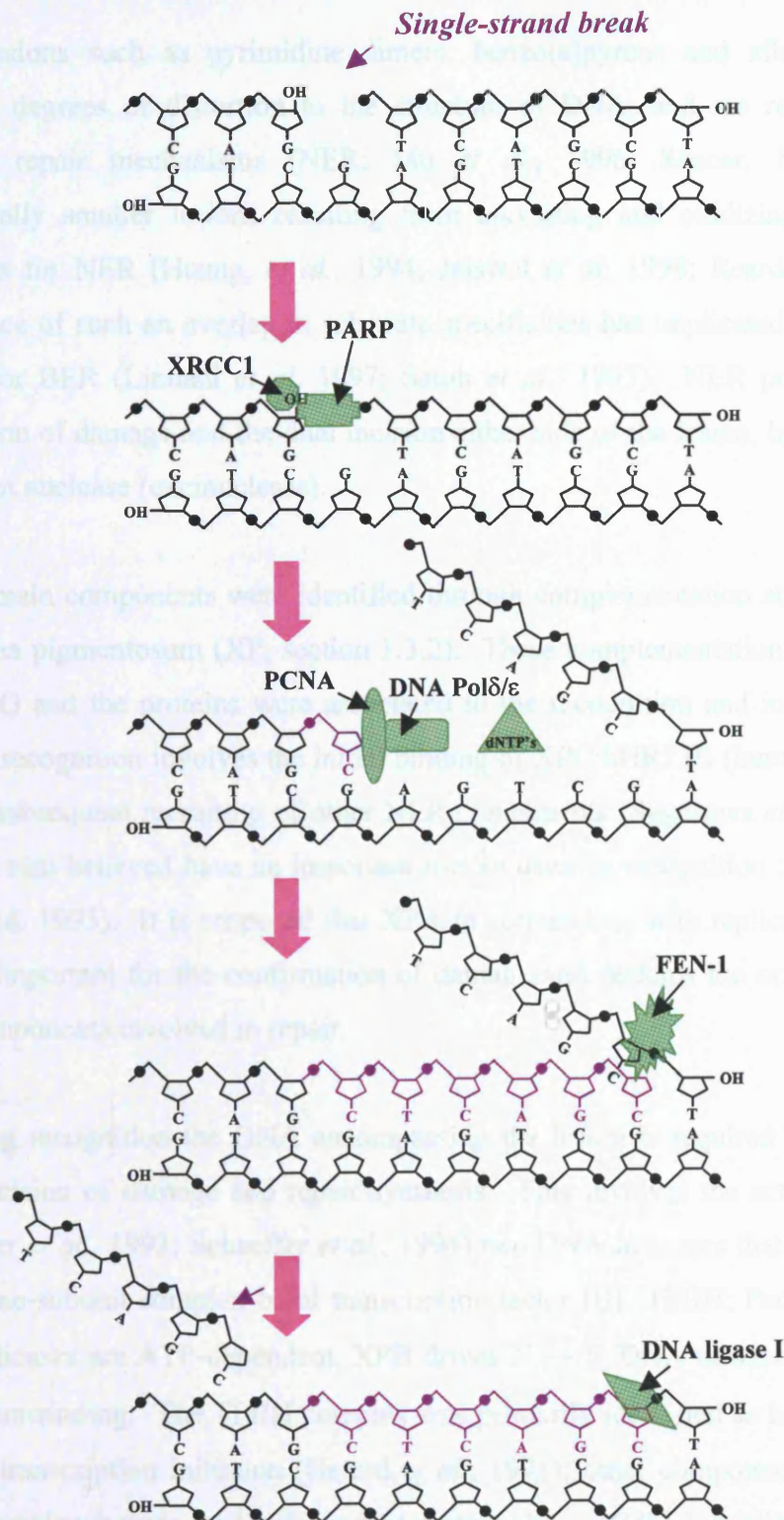


Figure 1.3: Short-patch repair of DNA damage. DNA damage can be repaired through the use of monofunctional or bifunctional enzyme activities, and the resulting abasic site can be further processed through either a short-patch (a) or a long-patch (b) pathway adapted from Nilver & Kasian (2001) and Florynski et al. (2001). Abbreviations: apurinic/apyrimidinic endonuclease (APE), deoxycytosine triphosphate (dCTP), deoxyguanosine triphosphate (dGTP), deoxynucleoside triphosphate (dNTP), DNA polymerase (DNA Pol), deoxyribose phosphodiesterase (dRPase), flap structure-specific endonuclease 1 (FSE-1), poly(ADP-ribose) polymerase (PARP), proliferating cell nuclear antigen (PCNA), and cross-complementing gene-1 protein-1 (XRCC1).

Figure 1.3 continued...

## b Long-patch repair



**Figure 1.3:** Base excision repair pathways. Repair is often initiated by DNA glycosylases through their monofunctional or bifunctional enzyme activities; and the resulting abasic site is further processed through either a short-patch (a) or a long-patch (b) pathway; adapted from Nilsen & Krokan (2001) and Hoeijmakers (2001). Abbreviations: apurinic/apyrimidinic endonuclease (APE), deoxycytosine triphosphate (dCTP), deoxyguanine triphosphate (dGTP), deoxynucleotide triphosphate (dNTP), DNA polymerase (DNA Pol), deoxyribophosphodiesterase (dRPase), flap structure-specific endonuclease 1 (FEN1), poly-(ADP)-ribose polymerase (PARP), proliferating cell nuclear antigen (PCNA), and x-ray repair cross-complementing gene/protein 1 (XRCC1).

### 1.2.2 Nucleotide excision repair: global genome and transcription-coupled

Bulky lesions such as pyrimidine dimers, benzo(a)pyrene and aflatoxin adducts, cause differing degrees of distortion to the structure of DNA, and are removed by nucleotide excision repair mechanisms (NER: Mu *et al.*, 1996; Sancar, 1995<sup>1</sup>; Sancar 1996). Additionally smaller lesions resulting from alkylating and oxidizing agents can also be substrates for NER (Huang, *et al.*, 1994; Jaiswal *et al.* 1998; Reardon *et al.* 1997). The importance of such an overlap in substrate specificities has implicated NER to be a back-up system for BER (Lindahl *et al.*, 1997; Satoh *et al.*, 1993). NER principally involves the recognition of damage and the dual incision either side of the lesion, by a multisubunit ATP-dependent nuclease (excinuclease).

Several main components were identified through complementation studies of the syndrome xeroderma pigmentosum (XP, section 1.3.2). These complementation groups were assigned XPA to G and the proteins were associated to the recognition and incision stages of NER. Damage recognition involves the initial binding of XPC:hHR23B (human homologue Rad23) and the subsequent recruiting of other NER components (Sugasawa *et al.*, 1998). XPA and XPE are also believed have an important role in damage recognition (He *et al.*, 1995; Jones and Wood, 1993). It is proposed that XPA in conjunction with replication protein A (RPA) may be important for the confirmation of damage and perhaps the ordered assembly of the other components involved in repair.

Following recognition the DNA encompassing the lesion is required to unwind in order to allow excision of damage and repair synthesis. This involves the action of XPB and XPD (Schaeffer *et al.*, 1993; Schaeffer *et al.*, 1994) two DNA helicases that comprise components of the nine-subunit complex basal transcription factor IIIH (TFIIH; Park *et al.*, 1995<sup>1</sup>). Both DNA helicases are ATP-dependent, XPB drives 3' → 5' DNA unwinding while XPD drives 5' → 3' unwinding. The TFIIH complex was primarily identified as having an essential role in basal transcription initiation (Gerard *et al.*, 1991); other components associated with the TFIIH complex include cyclin-dependent protein kinase (Cdk) 7, cyclin H and ménage-a-trois (MAT) 1 that constitute the Cdk-activating kinase (CAK) complex (Nigg, 1996). This CAK complex is involved in the phosphorylation of Cdks important in cell cycle regulation and the phosphorylation of the C-terminal domain of RNA polymerase II (RNA Pol II; Nigg, 1996).

The incision stage of NER in *E.coli* requires three subunits whilst in humans many more proteins are required (Table 1.3; Araújo and Wood, 1999; Mu *et al.*, 1996; Sancar, 1995<sup>2</sup>;

Sancar 1996). In both *E.coli* and humans, the excinuclease cuts the 5<sup>th</sup> phosphodiester bond 3' to the lesion of the unwound DNA; however at the 5' end the position of the cut varies such that the excised oligomer generated is a 12-13mer in *E.coli* and a 24-29mer in humans (Figure 1.4). These dual incisions are performed by XPG and XPF at the 3' and 5' sites to the lesion respectively (Bessho, *et al.*, 1997; Brookman *et al.*, 1996; Matsunaga, *et al.*, 1995; Park, *et al.*, 1995<sup>2</sup>). Once the oligonucleotide containing the lesion dissociates from DNA, repair synthesis resumes involving the action of RPA, replication factor C (RFC), proliferating cell nuclear antigen (PCNA) and DNA polymerases (DNA Pol), namely Pol $\delta$  and Pol $\epsilon$  (Balajee *et al.*, 1998; Shivji *et al.*, 1992; Wood and Shivji, 1997). After the excision gap is filled the sequence is sealed into place by the action of one of four DNA ligases (Lindahl *et al.*, 1998).

DNA repair rates are heterogeneous throughout the genome; active genes are repaired far more efficiently compared to inactive ones (Bohr *et al.*, 1985; Madhani *et al.*, 1986; Hanawalt, 1995). Ruven *et al.*, 1993 described the selective removal of cyclobutane pyrimidine dimers (CPD) from transcriptionally active genes in the epidermis of hairless mice. Similarly, lesions in the template strand within a transcribed sequence are repaired more rapidly than lesions in the non-transcribed (coding) strand (Friedberg, 1996). There are many factors that govern repair rates (Hanawalt, 1994) such as: the configuration of chromatin structure, accessibility to damage, level of CpG methylation and the interaction with the nuclear matrix. The relationship between DNA excision repair and repair of transcribed strands has been investigated in both prokaryotic and eukaryotic systems and two mechanisms of NER have been proposed: global genome NER (GG-NER) and transcriptional coupled NER (TC-NER) differing essentially in the recognition of damage.

GG-NER is initiated by XPC:hHR23B (Reardon, *et al.*, 1996) as described above whilst TC-NER is instigated by the stalled RNA Pol II complex (de Boer and Hoeijmakers, 2000). Studies in *E. coli* revealed a 130kDa protein referred to as transcription-repair coupling factor [TRCF or mutation frequency decline (Mfd)] to be involved in the displacement of the stalled RNA Pol II, and the promotion of repair via binding to the damage recognition subunit (UvrA) of the excision nuclease (Selby & Sancar, 1993). In humans, two gene products: Cockayne's syndrome (CS)A/ERCC8 and CSB/ERCC6 appear to be involved in the recognition and promotion of repair of transcription blocking lesions (Sancar, 1996). CSA, CSB and RNA Pol II have been demonstrated to interact *in vivo* (Henning *et al.*, 1995; van Gool, 1997), and therefore CSA and CSB may have potential roles in processing stalled RNA Pol II (de Boer and Hoeijmakers, 2000).

Complex	Protein components (M <sub>r</sub> )/rodent and yeast homologues	Proposed Activity In Repair
<b>Damage recognition</b>		
XPC- hHR23B	XPC (p125)/RAD4 hHR23B (p58)/RAD 23	Recognition of damage in non-transcribed DNA, initiator of GG-NER
RNA Pol II		Stalled polymerase triggers TC-NER
CSA/CSB		Recognition and promotion of TC-NER
XPA-RPA	XPA (p31)/RAD14 RPA (HSSB) p70	XPA recruits trimeric RPA and the XPA-RPA complex recruits TFIIH and XPF-ERCC1 complex
<b>DNA unwinding &amp; excision</b>		
TFIIH	XPB(p89)/ERCC3/RAD25 XPD(p80)/ERCC2/RAD3 [other components include: yeast TFB1 (p73) and SSL1 (p53), Cdk7 (p41), Cyclin H (p38), MAT1 (p36)]	XPB and XPD are ATP-dependent helicases that aid unwinding of DNA, XPB has (3'→5' polarity) and XPD has (5'→3' polarity) allowing dual incision. The basal transcription initiation factor TFIIH forms part of the preincision complex
XPF-ERCC1	XPF(p103)/ERCC4/RAD1 ERCC1 (p33)/RAD 10	5' -incision endonuclease activity: hydrolase
XPG	XPG(p133)/ERCC5/RAD2	3'-incision endonuclease activity: β-lyase
<b>Repair synthesis &amp; ligation</b>		
RFC		Assists recruitment of PCNA
PCNA		Assists positioning of RFC
DNA Pol		Repair synthesis
DNA ligase		Seals DNA nicks

**Table 1.3:** Protein components of human nucleotide excision repair. XP refers to the complementation groups of the human disease xeroderma pigmentosum, ERCC indicates the rodent excision repair cross complementing genes and RAD refers to their yeast radiation-sensitive counterparts. Abbreviations: Cockayne's syndrome (CS), cyclin-dependent protein kinase 7 (Cdk7), DNA polymerase (DNA Pol), human homolog of Rad 23 (hHR23B), human single stranded DNA binding protein (HSSB), ménage-a-trois protein 1 (MAT), proliferating cell nuclear antigen (PCNA), replication factor C (RFC), RNA polymerase II (RNA Pol II), replication protein A (RPA), suppressor of stem-loop protein 1 (SSL1), RNA Pol II basal transcription factor IIIH (TFIIH), RNA Pol II transcription factor B protein 1 (TFB), x-ray repair cross-complementing protein 1 (XRCC1), xeroderma pigmentosum complementation groups (XPA, XPC, XPF and XPG).

## 1.2.3 Repair of double-strand breaks: homologous recombination and end joining

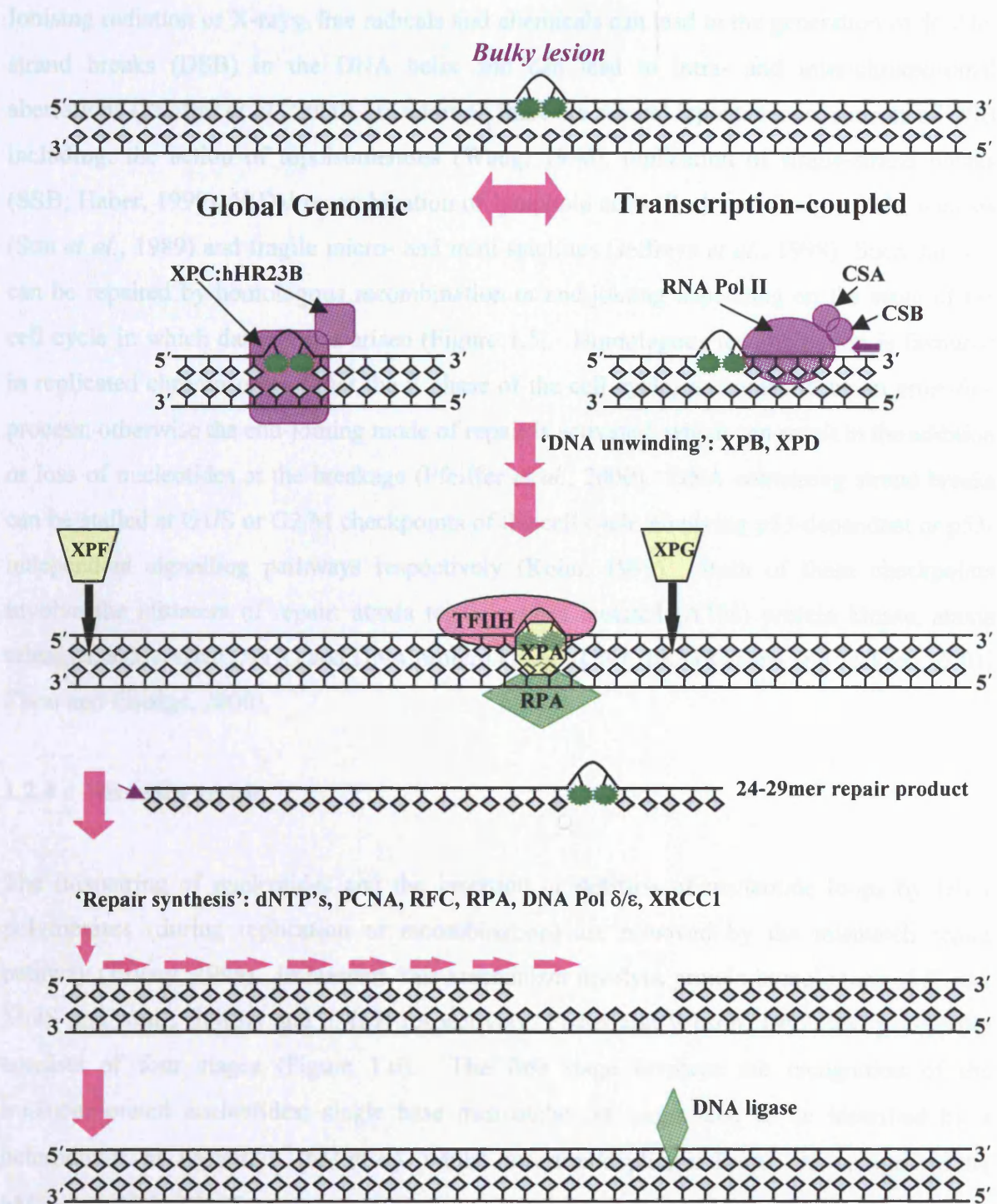


**Figure 1.4:** Proposed model for nucleotide excision repair (NER) pathways in humans: global genome (GG) and transcription-coupled (TC); adapted from Griffiths *et al.* (1998) and Hoeijmakers (2001). Abbreviations: Cockayne’s syndrome proteins (CSA and CSB), deoxynucleotide triphosphate (dNTP), DNA polymerase (DNA Pol), human homolog of Rad23 (hHR23B), proliferating cell nuclear antigen (PCNA), replication factor C (RFC), RNA polymerase II (RNA Pol II), replication protein A (RPA), RNA polymerase basal transcription factor IIIH (TFIIH), x-ray repair cross-complementing gene/protein 1 (XRCC1), Xeroderma pigmentosum proteins (XPA, XPB, XPC, XPD, XPF and XPG).

### 1.2.3 Repair of double-strand breaks: homologous recombination and end-joining

Ionising radiation or X-rays, free radicals and chemicals can lead to the generation of double-strand breaks (DSB) in the DNA helix and can lead to intra- and inter-chromosomal aberrations (Pfeiffer *et al.*, 2000). In addition there are several 'spontaneous' sources of DSB including: the action of topoisomerases (Wang, 1996), replication of single-strand breaks (SSB; Haber, 1999), V(D)J recombination of lymphoid cells (Roth and Craig, 1998), meiosis (Sun *et al.*, 1989) and fragile micro- and mini-satellites (Jeffreys *et al.*, 1998). Such damage can be repaired by homologous recombination or end-joining depending on the stage of the cell cycle in which damage has arisen (Figure 1.5). Homologous recombination is favoured in replicated chromosomes (after the S phase of the cell cycle) and tends to be an error-free process; otherwise the end-joining mode of repair is activated, which can result in the addition or loss of nucleotides at the breakage (Pfeiffer *et al.*, 2000). DNA containing strand breaks can be stalled at G1/S or G2/M checkpoints of the cell cycle involving p53-dependent or p53-independent signalling pathways respectively (Kohn, 1999). Both of these checkpoints involve the initiators of repair: ataxia telangiectasia mutated (ATM) protein kinase, ataxia telangiectasia related (ATR) and DNA protein kinase (DNA-PK) (Khanna and Jackson, 2001; Zhou and Elledge, 2000).

### 1.2.4 Mismatch repair

The mispairing of nucleotides and the insertion or deletion of nucleotide loops by DNA polymerases (during replication or recombination) are removed by the mismatch repair pathway (Jiricny, 1998). In humans, this mechanism involves protein homologues of *E. coli* MutS and MutL (hMSH and hMLH respectively; Fishel and Wilson, 1997) and principally consists of four stages (Figure 1.6). The first stage involves the recognition of the misincorporated nucleotides; single base mismatches or loops tend to be identified by a heterodimer of hMSH2/6 (hMutS $\alpha$ ), whilst insertion/deletion loops are recognised by hMSH2/3 (hMutS $\beta$ ) (Drummond *et al.*, 1995; Palombo *et al.*, 1996). Following recognition further factors are recruited including heterodimers of hMLH-like 1 and human postmeiotic segregation increased 1 (hPMS) proteins [hMLH1/hPMS2 (hMutL $\alpha$ ) and hMLH1/hPMS1 (hMutL $\beta$ )] and replication factors (Li and Modrich, 1995; Prolla *et al.*, 1994). The incorrectly synthesised strand is degraded by exonucleases and then resynthesized involving factors such as DNA polymerases  $\delta$  and  $\epsilon$ , RPA, PCNA, RFC and FEN 1 (Hoeijmakers, 2001; Jiricny, 1998).

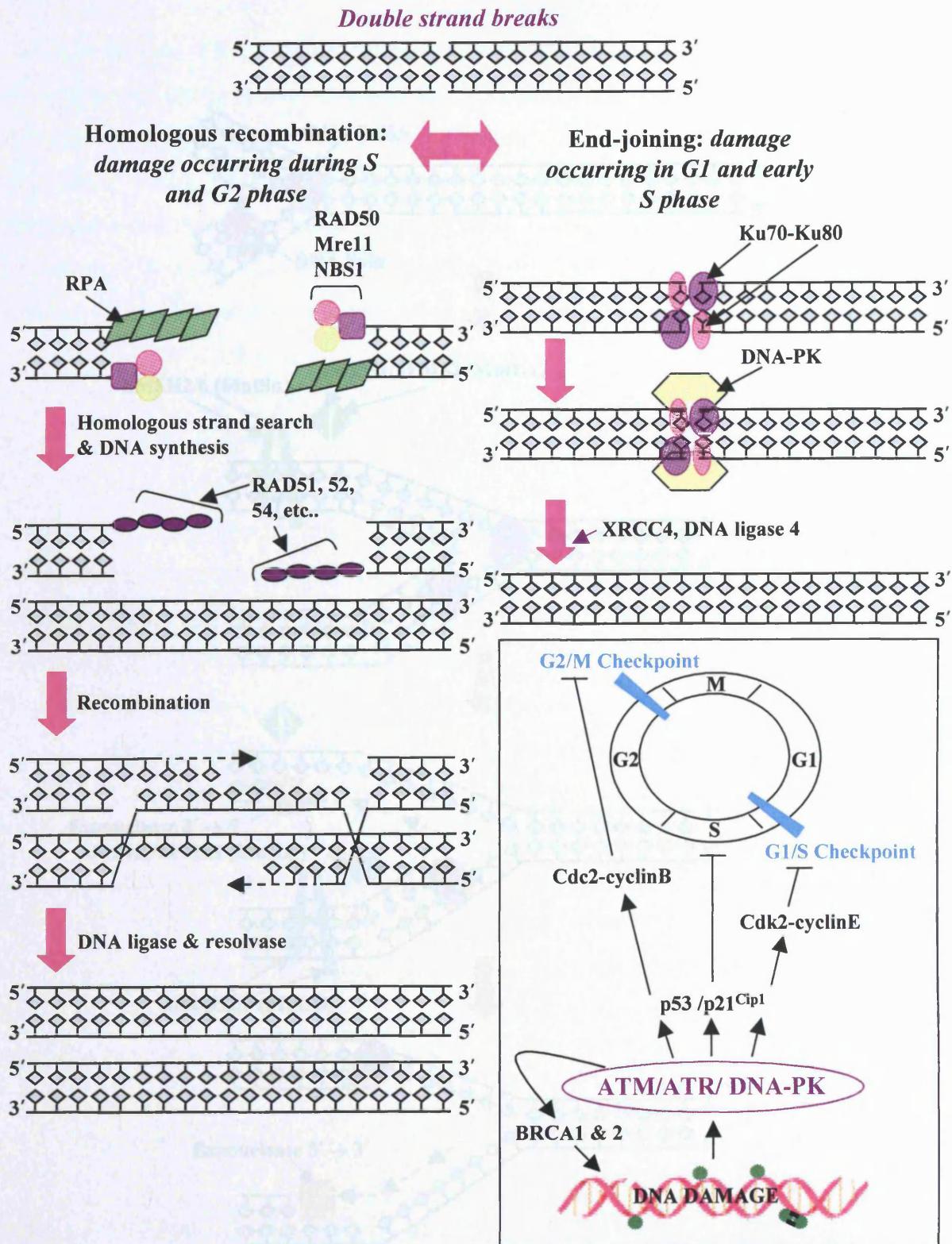


**Figure 1.5:** An overview of the repair of double-strand breaks (DSB) in humans: homologous recombination and end-joining; adapted from Hoeijmakers (2001). A simplistic overview of cell signalling mechanisms controlling the interplay of DNA damage and cell cycle progression (Box); see Kohn (1999) for a detailed interaction map. Abbreviations: ataxia telangiectasia mutated (ATM) protein kinase, ataxia telangiectasia related (ATR), breast cancer (BRCA), cell division cycle protein (cdc), cyclin-dependent kinase (Cdk) DNA protein kinase (DNA-PK), meiotic recombination (Mre), Nijmegen breakage syndrome (NBS), radiation-sensitive yeast protein (RAD), replication protein A (RPA), x-ray repair cross-complementing gene/ protein 4 (XRCC4)

### 1.3.1.1. Mismatch repair associated with genotoxicity and DNA repair systems

Copyright © 2009, Elsevier B.V.

The accumulation of lesions and mutations has long been considered to be an important factor of ageing and the progression of cancer (Hollman, 2000; Friedel and Holbrook, 2000). Although there are a number of mechanisms specific to DNA repair defects in DNA repair mechanisms, for example, the mismatch repair (MMR) system, it is also required to repair the TUNER site and more of the DNA repair mechanisms. For example, the MMR system is also required by BER mechanisms, can also be repaired via the TUNER site and more of the DNA repair mechanisms within the repair pathway, a component of BER, NER, and MMR.

### 1.3.1.1.1. MMR and Cancer

Copyright © 2009, Elsevier B.V.

To date, no human disease has been reported. Mice lacking models of glycosylase (Eick et al., 1998; Engstrand and Mead, 1999) and deficiency in MMR (Eick et al., 1998; Engstrand and Mead, 1999) are reported to be similar to human MMR.

Copyright © 2009, Elsevier B.V.

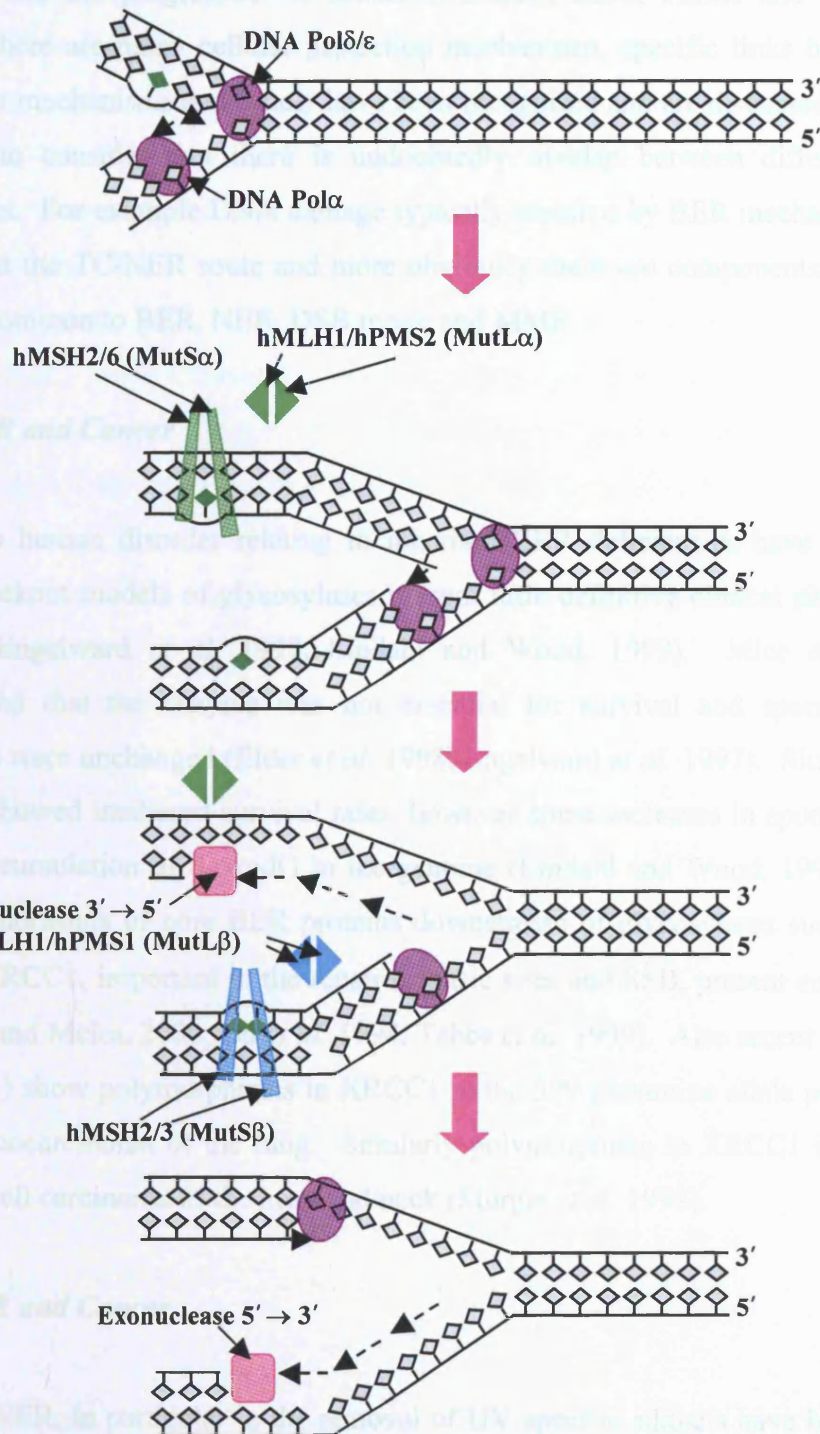


**Figure 1.6:** A model of mismatch repair in humans, adapted from Hoeijmakers (2001). Abbreviations: human MutL (hMLH), human MutS homologue (hMSH), human PMS homologue (hPMS).

### 1.3 Diseases associated with genotoxicity and DNA repair systems

The accumulation of lesions and mutations has long been considered to be an important factor of ageing and the progression of cancer (DePinho, 2000; Finkel and Holbrook, 2000). Although there are many cellular protection mechanisms, specific links between defects in DNA repair mechanisms and cancer have been recognised and are discussed below. It is also important to consider that there is undoubtedly overlap between different DNA repair mechanisms. For example DNA damage typically repaired by BER mechanisms can also be repaired via the TC-NER route and more obviously there are components within the repair pathways common to BER, NER, DSB repair and MMR.

#### 1.3.1 *BER and Cancer*

To date no human disorder relating to inherited BER deficiencies have been recognized. Mouse knockout models of glycosylases present little definitive clinical phenotype (Elder *et al.* 1998, Engelward *et al.* 1997, Lindahl and Wood, 1999). Mice deficient in MPG demonstrated that the enzyme was not essential for survival and spontaneous mutation frequencies were unchanged (Elder *et al.* 1998, Engelward *et al.* 1997). Similarly, knockouts of OGG1 showed unaltered survival rates, however some increases in spontaneous mutation rate and accumulation of 8-oxodG in the genome (Lindahl and Wood, 1999). Interestingly however, knockouts of core BER proteins downstream of glycosylases such as APE, DNA Pol $\beta$  and XRCC1, important in the repair of basic sites and SSB, present embryonic lethality (Friedberg and Meira, 2000; Gu *et al.* 1994, Tebbs *et al.* 1999). Also recent studies by Divine *et al.* (2001) show polymorphisms in XRCC1 at the 399 glutamine allele poses an increased risk of adenocarcinoma of the lung. Similarly polymorphism in XRCC1 is associated with squamous cell carcinoma of the head and neck (Sturgis *et al.* 1999).

#### 1.3.2 *NER and Cancer*

Defects in NER, in particular in the removal of UV-specific adducts have been implicated in the pathogenesis of skin cancer (Camplejohn, 1996; Wei *et al.*, 1994), as well as rare recessive photosensitive disorders: xeroderma pigmentosum (XP; Kraemer *et al.*, 1994), Cockayne's syndrome (CS; Lehmann, 1982; Schmickel *et al.*, 1977) and trichothiodystrophy (TTD; Itin and Pittelkow, 1990).

***Xeroderma Pigmentosum***

Cleaver (1968) first proposed through experiments with cultured fibroblasts that XP was linked to defects in the repair of DNA lesions generated by UV light. The clinical characteristics of homozygous individuals include extreme sensitivity of sunlight-exposed areas of skin showing pigmentation abnormalities and premalignant lesions. The incidence of skin cancers, basal cell carcinoma, squamous cell carcinoma and malignant melanomas are increased in these individuals by up to 4000-fold (Ford and Hanawalt, 1996). The development of ocular neoplasms is also accelerated by 30-50 years when compared with the normal population (Ford and Hanawalt, 1996). XP individuals have also been shown to have a 10-20 fold increase in the incidence of 'internal' cancers, *i.e.* those of non-UV exposed sites (Kraemer *et al.*, 1994; Cleaver & Kraemer, 1989); and about a fifth of sufferers display progressive neurological degeneration involving peripheral neuropathy, sensorineural deafness, progressive mental retardation and cerebellar/pyramidal tract involvement (Robbins 1988). Overall the life expectancy of XP sufferers is reduced by approximately 30 years. Epidemiological data show the incidence of XP is 1 in 250,000 in USA and Europe, whilst the incidence in Japan and Egypt is 1 in 40,000.

The genetic heterogeneity and the biochemical complexities of this disease have been highlighted. Studies have shown that the defect in cells from most XP individuals is in their nucleotide excision repair (NER) processes (Figure 1.4). However there are a small number of cases, referred to as XP variant, which appear to have normal NER but display a defect in post-replication repair (Codonier and Fuchs 1999; Lehmann, 1975; Masutani *et al.*, 1999; Wang *et al.*, 1993; Wood, 1999), whereby there is error-prone replication on a template containing photoproducts. Complementation analysis provided evidence for genetic heterogeneity within XP. Such studies revealed the main complementation groups, XPA to G, with the respective protein/enzymes being important in the recognition, unwinding, and incision stages of NER, and subsequent clinical phenotype (Table 1.4).

Cultured cells from different XP complementation groups show varying degrees of UV sensitivity, the most sensitive being XP groups A, B, D and G. However, Runger *et al.*, 1995 transfected lymphoblast cell lines from patients with XP complementation groups A, C, D, E and variant with either UVB treated or methylene blue and visible light (which generates singlet oxygen) treated plasmid pRSVcat. The results showed that all cell lines had varied but reduced repair of UVB-induced damage, and XP-A, D, E and the variant cells were efficient in the repair of singlet oxygen induced damage. However, three of four XPC cell lines

showed marked reduction in the latter capacity to repair indirect UV damage. Such difference in the capacity to process direct and indirect UV-induced damage proposes difficulties in assessing UV exposure risk in XP patients and clinical phenotype. Reardon *et al.*, 1997 proposed that the 20-30 % of XP individuals suffering neurological abnormalities may be explained by their inability to repair reactive oxygen species generated lesions (such as 8-oxoguanine and thymine glycol) since TC-NER pathway can also actively excise these adducts. This was further supported by the lack of neurological abnormalities presented in XPC patients (Kraemer *et al.*, 1994), suggesting that alternative pathways such as BER were efficiently repairing oxidative lesions in non-transcribed DNA.

In an attempt to correlate the defect in repair processes and the initiation of skin tumours in XP patients, Dumaz *et al.*, 1993 used reverse transcription-PCR and single-stranded conformation polymorphism analysis to determine the mutation spectra of the p53 gene in more than 40 XP tumours. They found 40% contained at least one point mutation of the gene. All mutations were located at dipyrimidine sites, 61% of which were tandem CC→TT mutations, those unique to UV-induced damage. Such levels were significantly higher than those previously observed in non-XP tumours (Sarasin, 1999). Similarly, Daya-Grosjean *et al.* (1993) showed a higher level of mutations as well as amplification and rearrangement in the *ras* oncogene of repair-deficient XP skin tumours compared to tumours from normal individuals. Such studies have highlighted the importance of unrepaired UV-induced DNA damage in genes essential for growth regulation.

XP Group	Involvement in XP Pathogenesis	References
XPA XPB XPD XPG	Cells demonstrate severe loss of GG-NER and TC-NER. Patients often suffer severe/moderate neurological abnormalities. XPB, XPD and XPG patients displaying some CS-like symptoms; and XPD patients have associated TTD phenotypes.	Evans <i>et al.</i> , 1993 Winkler and Hoeijmakers, 1998
XPC XPE XPF	All three groups are not associated with neurological abnormalities. XPC are deficient in the overall GG-NER and not TC-NER. The exact role of XPE in NER has yet to be defined, however cell-free extracts have reduced excision and repair synthesis.	Kantor <i>et al.</i> , 1990; Kraemer <i>et al.</i> , 1994 Venema <i>et al.</i> , 1990, 1991;
XP-variant	Cells demonstrate defects in post-replication repair.	Codonnier and Fuchs 1999; Masutani <i>et al.</i> , 1999 Wood, 1999

**Table 1.4:** Xeroderma Pigmentosum (XP) complementation groups: their role in pathogenesis and clinical phenotype.

**Cockayne's syndrome**

Cockayne's syndrome (CS) is a premature aging disorder. Similar to XP, this too is an autosomal recessive disease with defective repair of UV induced DNA lesions, namely cyclobutane pyrimidine dimers (Schmickel *et al.*, 1977; Kraemer *et al.*, 1994). CS and XP share some clinical and biochemical similarities such as cutaneous photosensitivity, mental retardation and neurological abnormalities. The neurological defects affecting only some XP individuals are predominantly due to primary neuronal degeneration (Stary & Sarasin, 1996), whilst in CS individuals disease is caused by primary demyelination (Leech *et al.*, 1985). Some CS specific clinical features include cachectic dwarfism, skeletal abnormalities, pigmentary retinal degeneration, cataracts, progressive intracranial calcification and deafness (Timme & Moses, 1988). Unlike XP, CS sufferers are not at increased risk for developing skin cancers, however the life expectancy is only 12 years (Nance & Berry, 1992).

Studies into the genetic heterogeneity of CS have revealed at least three complementation groups, termed CS-A to C (Lehmann, 1982). The XP and CS complementation groups have been classified based on their genetic defect. Studies by Robbins *et al.* 1974 showed that XP-B, D and G individuals also shared clinical features of CS; such similarities between these XP and CS complementation groups are often referred to as XPB/CSC, XPD/CS and XP-D/CS, respectively. Vermeulen *et al.*, 1994 identified two XPB siblings with neurological and cutaneous features similar to XP and CSC, but both not developing skin cancer beyond 40yrs. Further molecular analysis revealed a single-base missense mutation in a conserved region of both XPB/CSC patients. These results indicated defects in certain repair genes do not necessarily predispose an individual to developing cancers typical of UV exposure.

**Trichothiodystrophy**

The hallmark clinical phenotype of Trichothiodystrophy (TTD) includes sulphur-deficient brittle hair (Itin and Pittelkow, 1990). This phenotype can be combined with ichthyosis (scaly skin) and/or mental and physical retardation. The heterogeneity in clinical phenotype leads to the description of many other syndromes, now all believed to be associated with TTD; these include: Amish brittle hair syndrome, Marinesco-Sjögren syndrome, Pollitt syndrome, Sabinas syndrome and Tay's syndrome (de Boer and Hoeijmakers, 2000). The majority of TTD cases have associated photosensitivity arising from defective XPD (de Boer *et al.*, 1999; Stefanini *et al.*, 1986). Interestingly mutations in XPD present great clinical diversity, however no clear correlation of specific defects in conserved protein domains explains the contribution of XPD to XP, CS and TTD phenotypes (Broughton *et al.*, 1995; Taylor *et al.*, 1997).

### 1.3.3 DSB Repair and Cancer

Many human syndromes have been identified relating to defects in homologous recombination and end-joining DSB repair reactions, these are summarised in Table 1.5. Numerous mouse knockout models of components of HR, including ATR, BRCA1, BRCA 2 and the combined knockout of ATM and DNA-PK, have indeed shown embryonic lethality (Gurley and Kemp, 2001).

Syndrome	Disease phenotype	Specific defect	References
Ataxia telangiectasia (AT)	Lymphomas	DSB response & repair	Lavin <i>et al.</i> , 1999 Rotman & Shiloh, 1998
AT-like disorder	Lymphomas	DSB response & repair	Lavin <i>et al.</i> , 1999
Bloom syndrome	Leukaemia, lymphomas & other cancers	HR? (RecQ helicase)	Hickson <i>et al.</i> , 2001 Wu <i>et al.</i> , 1999
BRCA1/BRCA2	Breast (ovarian) cancer	HR	Futaki & Liu, 2001 Scully & Livingstone, 2000 Moynahan <i>et al.</i> , 2001
Fanconi anaemia	Leukaemia and various disease	HR	Ahmad <i>et al.</i> , 2002 Grompe and D'Andrea, 2001
Ligase IV deficiency (isolated case)	Leukaemia?	EJ	Riballo <i>et al.</i> , 1999
Nijmegen breakage syndrome	Lymphomas	DSB response & repair	Digweed <i>et al.</i> , 1999
Rothmund-Thomson syndrome	Osteosarcoma	HR? (RecQ helicase)	Kitao <i>et al.</i> , 1999 <sup>1</sup> Kitao <i>et al.</i> , 1999 <sup>2</sup>
Werner syndrome	Various cancers, premature ageing	translesion lesion synthesis? & HR? (RecQ helicase)	Shen and Loeb, 2000 Wu <i>et al.</i> , 1999

**Table 1.5:** Human syndromes defective in double strand breaks (DSB) repair. Most defects in homologous recombination (HR) events lead to chromosomal aberrations or recombination fidelity in end-joining (EJ) defects; adapted from Hoeijmakers (2001)

### 1.3.4 MMR and Cancer

The links between defects in MMR and colorectal, endometrial, ovarian and other cancers have yet to be fully clarified (Duval and Hamelin, 2002; Fishel and Kolodner, 1995; Hoeijmakers, 2001; Jiricny 1994). However the majority of hereditary non-polyposis colorectal cancers (HNPCC) are linked to germline mutations in *hMLH1* and *hMLH2* (Gonda *et al.*, 2002; Heinen *et al.*, 2002), whilst some cases of late-onset atypical HNPCC have been associated with *hMSH6* mutations (Leach *et al.*, 1993).

## 1.4 Aims and Objectives.

Understanding the mechanisms of DNA damage and repair and how these processes can be modulated may provide possibilities for the treatment of common diseases including cancer. The aim of this thesis was to establish human cell culture model systems in order to examine the formation and repair of two distinctly different forms of DNA damage: UV-specific pyrimidine dimers and 8-oxodG. Such models would provide the basis of future investigations applicable to clinical situations.

For UV studies, the main objective was to assess the relative potency of specific wavelengths of solar UVB and to gauge UV exposure with particular focus for the calibration of phototherapy and the potential application to predict minimal erythema dose. The achievement of this objective involved the following experimental steps:

- Establish and characterise primary and transformed keratinocyte cell culture models
- Complete characterisation of immune serum raised to UVC-irradiated DNA
- Establish immunochemical methodologies to detect and quantitate direct UV-induced DNA damage *in situ* and in extracted DNA
- Compare the relative potencies of discrete biologically relevant narrow-band irradiations of UVB by the measurement of direct UV-induced damage
- Assess the repair kinetics of UV-specific DNA damage in cultured keratinocytes
- Establish an assay in order to measure the excision and removal of UV-specific DNA adducts in extracellular medium

For the potentially mutagenic lesion 8-oxodG, typically generated through ROS, the main objective was to investigate the modulation of key enzymes important in the BER-mediated removal of this lesion following prooxidant and antioxidant treatment. The achievement of this objective involved the following experimental steps:

- Establish and validate *in vitro* model systems to demonstrate the intracellular generation of the ROS and the formation of 8-oxodG
- Measure the internalisation and intracellular regeneration of the antioxidant, ascorbic acid
- Develop methods to measure the gene, protein and enzyme activity levels of hOGG1 and hAPE
- Assess the potential modulation of these enzymes following pro-oxidant and anti-oxidant treatments

## **CHAPTER TWO**

### **MATERIALS & METHODS**

## **2.0 MATERIALS AND METHODS**

### **2.1 Materials**

#### **2.1.1 *Animals, Cell Culture & Treatment Reagents***

##### **2.1.1.1 *Animals***

Two NZW male rabbits weighing 1-1.5kg were purchased by Biomedical Services, University of Leicester, Leicester, UK and used for polyclonal anti-hOGG1 antibody production.

##### **2.1.1.2 *Cell Lines***

Simian virus 40 transformed human epidermal keratinocytes (THEK) were a kind gift from Prof Irene Leigh, Department of Dermatology, London Hospital Medical College, London. Normal human epidermal keratinocytes from adult skin (NHEK-Ad) were purchased from Clonetics, BioWhittaker, Wokingham, UK and human Caucasian acute T-lymphoblastic leukaemia cell line (CCRF-HSB-2) was purchased from the European Collection of Cell Cultures, Salisbury, UK. Both THEK and CCRF-HSB-2 cell lines were screened for mycoplasma contamination by Mycoplasma Experience, Surrey, UK, and NHEK-Ad were certified mycoplasma free on purchase.

##### **2.1.1.3 *Cell Culture Media***

Dulbecco's Modified Eagles Medium with GlutaMAX™-1, 1000mg/L glucose and sodium pyruvate (DMEM), Ham's Nutrient Mixture F-12 with GlutaMAX™-1 (Ham's F12) and Roswell Park Memorial Institute medium (RPMI-1640) without glutamine were purchased from Gibco Life Technologies, Paisley, UK (for compositions see Appendix I). Serum-free Keratinocyte Growth Medium BulletKit® (KGM®-2 BulletKit) containing Keratinocyte Basal Medium (KBM®-2) and SingleQuot® growth supplements were obtained from Clonetics, UK (Appendix I). Other reagents included: heat inactivated foetal calf serum (HiFCS) (Batch No. 67H3355) from Sigma, Poole, UK; GlutaMAX™-1 and trypsin (EC 3.4.21.4), ethylenediaminetetraacetic acid (EDTA) 10x solution from Gibco Life Technologies and phosphate buffered saline (PBS, pH 7.3) from Oxoid, Basingstoke, UK.

#### **2.1.1.4 Treatment of Cells**

Reagents used to treat cell lines included: ascorbic acid (AA) from Fisher, Loughborough, UK, dehydroascorbic acid (DHAA) and 30% (w/w) hydrogen peroxide solution (Appendix II) from Sigma.

#### **2.1.2 Markers of Viability & Cellular Stress**

0.4% (w/v) Trypan Blue solution was purchased from Sigma and Hoechst 33342 and propidium iodide were purchased from Molecular Probes, Cambridge Bioscience, Cambridge, UK (Appendix III). Other reagents: absolute ethanol from Merck Ltd., Lutterworth, UK; PBS from Oxoid and ribonuclease type III-A, from bovine pancreas (EC 3.1.27.5) was from Sigma. 5-(and-6)-chloromethyl-2',7'-dichlorodihydrofluorescein diacetate [CM-H<sub>2</sub>DCFDA, Appendix III (50µg aliquots)] and methyl sulphoxide (DMSO) over a molecular sieve (H<sub>2</sub>O < 0.005%) were purchased from Molecular Probes and Fluka (Gillingham, Dorset, UK) respectively.

#### **2.1.3 Immunochemical Materials**

##### **2.1.3.1 Antibodies**

All the primary and secondary antibodies used for immunostaining, ELISA and Western blotting are listed in Table 2.1.

##### **2.1.3.2 Antibody Production**

Antigens: Calf thymus DNA was purchased from Calbiochem, Nottingham, UK and hOGG1 peptide (N-DKSQASRPTPDELEAVRKC-C) was synthesized by the Protein and Nucleic Acid Chemistry Laboratory (PNACL), University of Leicester, UK. Carrier proteins: methylated bovine serum albumin (BSA) from Sigma and Imject<sup>®</sup> Maleimide-activated Keyhole Limpet Haemocyanin (KLH) from Pierce, Rockford, Illinois, USA. Adjuvants: Freund's complete adjuvant from Sigma and Titer Max<sup>®</sup>Gold from Stratech Scientific Ltd., Luton, UK.

##### **2.1.3.3 Antibody Purification & Characterisation**

IgG fractions from rabbit serum were isolated using HiTrap<sup>®</sup> Protein G1 Affinity Columns from Pharmacia Biotech, St. Albans, UK and the following reagents from Sigma: glycine, sodium phosphate and Trizma<sup>®</sup>-HCl. Pyrimidine dimer antibody characterization experiments required an *E.coli* photolyase (EC 4.1.99.3) kit, PharMingen International, Becton Dickinson, Wheatley, UK.

ANTIBODIES	SOURCE
<b>Primary</b>	
Polyclonal anti-pyrimidine dimer (Ab529)	Dr K.E. Herbert, University of Leicester
Polyclonal anti-hOGG1 (Ab807 and Ab808)	This thesis
Polyclonal anti-hAPE	Alexis Biochemicals, Nottingham, UK
Monoclonal anti-8-oxoguanine (N45.1)	Genox Corporation, Baltimore, USA
Monoclonal anti-cytosine glyoxal (F3/9)	Dr P Butler, University of Leicester
Monoclonal anti- $\beta$ -actin (clone AC-15)	Sigma
Monoclonal anti-cytokeratin 8/18 (clone 5D3)	Novocastra Labs. Ltd, Peterborough, UK
Monoclonal anti-cytokeratin 14 (clone LL002)	Novocastra
<b>Secondary</b>	
Goat anti-rabbit IgG- Alexa fluor <sup>TM</sup> 488	Molecular Probes (Appendix III)
Goat anti-rabbit IgG-biotin	Dako
Goat anti-rabbit IgG-Fluorescein Isothiocyanate (FITC)	Sigma (Appendix III)
Goat anti-rabbit IgG-fluoronanogold	Nanoprobes, Yaphank, USA
Goat anti-rabbit IgG- Horseradish Peroxidase (HRP)	Sigma
Goat anti-rabbit Igs-HRP	Dako Ltd., Cambridge, UK
Goat anti-mouse Igs-biotin	Dako
Goat anti-mouse IgG-FITC	Sigma
Goat anti-mouse IgM-FITC	Sigma
Sheep anti-mouse IgG-HRP	Sigma

**Table 2.1:** Primary and secondary antibodies used for immunochemical experimentation.

#### 2.1.3.4 Enzyme Linked Immunosorbent Assay (ELISA)

All reagents except calf thymus DNA (Calbiochem), dried skimmed milk powder and sulphuric acid (Fisher) were purchased from Sigma: *o*-phenylenediamine 10mg tablets, PBS, phosphate-citrate buffer with sodium perborate capsules, poly-L-lysine hydrobromide, oleyoxyethylenesorbitan monolaurate (Tween-20). 96-well plates (Nunc Immuno plate-Maxisorb surface) were purchased from Nunc Plasticware, Gibco Life Technologies.

#### 2.1.3.5 Western Blotting

With the exception of methanol and hydrochloric acid from Fisher and dried skimmed milk powder; all reagents were purchased from Sigma: Immobilon-P polyvinylidene difluoride (PVDF) membrane, Ponceau S, glycine, sodium chloride, sodium hydroxide, Trizma<sup>®</sup>- base and Tween-20. ECL<sup>TM</sup> reagents and Hyperfilm ECL<sup>TM</sup> were from Amersham, Little Chalfont, UK. Other materials included: sample bags for use with 1450 Microbeta<sup>TM</sup> counter (Perkin Elmer, Beaconsfield, UK) and Whatman<sup>®</sup> 3MM filter paper (Whatman International Ltd., Maidstone, UK).

### **2.1.3.6 Immunocytochemistry**

The following reagents were purchased from Sigma: 37% (v/v) formaldehyde, glycine, paraformaldehyde, PBS, t-octylphenoxypolyethoxyethanol (Triton-X-100) and Tween-20; from Fisher, acetone and methanol. Vectashield mounting medium containing propidium iodide from Vector Laboratories, Peterborough, UK; and MitoTracker<sup>®</sup> CMXRos and Hoechst 33258 from Molecular Probes (Appendix III). 8-well chambered slides were purchased from Nunc Plasticware and plastic coverslips from Oncor, Gaithersburg, Maryland, USA.

Electron microscopy (EM) reagents included: 30%(w/v) BSA solution, glycine, sodium chloride and Tween 20 from Sigma; ethanol and potassium ferrocyanide from Merck; glutaraldehyde and osmium tetroxide from Agar Scientific, Stanstead, UK; PBS from Oxoid; lead nitrate from Fisher; sodium cacodylate, uranyl acetate and TAAB Epoxy resin (TAAB Laboratories Equipment Ltd., Aldermaston, UK); and “Gold Enhance” (Nanoprobes, USA).

### **2.1.3.7 Immunohistochemistry**

The following general reagents, except ethanol (Merck) and hydrochloric acid and xylene (Fisher), were purchased from Sigma: FAST Fast Red TR-Naphthol AS-MX, gelatin, magnesium chloride, Mayer's Haematoxylin, sodium chloride, Triton-X-100, Trizma<sup>®</sup>-base, Trizma<sup>®</sup>-HCl and 1mg trypsin tablets, type II-S from Porcine pancreas (EC 3.4.21.4). Normal goat serum and Strept ABC complex labelled with alkaline phosphatase were purchased from Dako. Apathy's aqueous mountant was from R.A. Lamb, London, UK.

## **2.1.4 Extraction Materials**

### **2.1.4.1 DNA Extraction**

All reagents except absolute ethanol (Merck) and sodium iodide (Fisher) were purchased from Sigma: desferrioxamine (DFO), diethylenetriaminepentaacetic acid (DTPA), EDTA, isopropanol, *N*-lauroyl-sarcosine, magnesium chloride, sodium acetate, sodium chloride, sodium citrate, sucrose, Triton-X-100, Trizma<sup>®</sup>-base and Trizma<sup>®</sup>-HCl. Enzyme preparations for this procedure were also purchased from Sigma: ribonuclease type III-A, from Bovine pancreas (EC 3.1.27.5), Proteinase K from *Tritirachium album* (EC 3.4.23.6) and Protease type XIV from *Streptomyces griseus* (EC 3.4.24.31).

#### **2.1.4.2 RNA Extraction**

RNAzol™B was purchased from Biogenesis, Poole, UK and absolute ethanol from Merck. All other reagents used for RNA extraction were purchased from Sigma: isopropanol, chloroform, DNase and RNase free water.

#### **2.1.4.3 Oligonucleotide, Primer & PCR Product Extraction & Quantitation**

A NucleoTrap®Nucleic Acid purification kit was purchased from Clontech Laboratories, Basingstoke, UK. Dynabeads® M-280 Streptavidin supermagnetic polystyrene beads and Dynal® MPC magnet were purchased from Dynal®, Bromborough, UK. Other reagents included: absolute ethanol from Merck, phage λ DNA quantitation standards from Gibco, and EDTA, sodium acetate, sodium chloride, transfer RNA and Trizma®-HCl from Sigma.

#### **2.1.4.4 Cellular Lysate Extraction**

All reagents were purchased from Sigma: antipain, chymostatin, EDTA, leupeptin, magnesium acetate, β-mercaptoethanol, pepstatin A, potassium chloride and Trizma®-HCl.

#### **2.1.4.5 Nuclear Protein Extraction**

The following reagents were purchased from Sigma: dithiothreitol (DTT), EDTA, N-(2-hydroxyethyl) piperazine-N'-(2-ethanesulfonic acid) (HEPES), glycerol, leupeptin, magnesium chloride, potassium chloride, phenylmethylsulfonyl fluoride (PMSF), sodium fluoride, sodium orthovanadate and Triton X-100.

For cell lysate and nuclear protein quantitation, Bradford-based BioRad protein assay solution was purchased from BioRad, Hemel Hempstead, UK.

### **2.1.5 Molecular Biology Reagents**

#### **2.1.5.1 Reverse Transcription-Polymerase Chain Reaction (RT-PCR)**

All molecular biology reagents and enzyme preparations for this method were purchased from Gibco Life Technologies: random primers, Superscript™ II RNase H<sup>-</sup> Reverse Transcriptase (EC 2.7.7.49) supplied with 5X first strand buffer [250mM Tris-HCl (pH 8.3), 375mM potassium chloride and 15mM magnesium chloride] and 0.1M dithiothreitol (DTT), deoxynucleotide triphosphate (dNTP) mix, *Taq* DNA Polymerase, recombinant (EC 2.7.7.7) supplied with 10X PCR buffer [200mM Tris-HCl and 500mM potassium chloride] and 50mM magnesium chloride.

*β-actin*, *hOGG1* and *hAPE* primers (Appendix VII) were synthesised by PNACL, University of Leicester. Primers were cleaned up with ethanol (Fisher) and sodium acetate from Sigma. DNA quantitation standards were purchased from Gibco.

#### **2.1.5.2 Electrophoretic Mobility Shift Assay (EMSA)**

AP-1 and NFκB transcription factor consensus oligonucleotides and T4 polynucleotide kinase (EC 2.7.1.78) were purchased from Promega, Southampton, UK. [ $\gamma$ -<sup>32</sup>P] dATP was purchased from Amersham, UK, Nap5 columns from Pharmacia Biotech and 30% acrylamide/bis (29:1) from BioRad. All other reagents: ammonium persulfate (AMPS, DTT, Ficoll, polydeoxyinosinic-deoxycytidylic acid [poly (dI)-(dC)], N, N, N', N'-tetramethylethylenediamine (TEMED), as well as Kodak X-Omat film were purchased from Sigma.

#### **2.1.5.3 Endonuclease Nicking Assay**

All reagents were from Sigma: EDTA, potassium chloride, sodium acetate, tRNA, Trizma<sup>®</sup>-HCl. Fluorescein isothiocyanate conjugated and non-conjugated oligonucleotides for the endonuclease nicking assay detailed in Table 2.3 (section 2.3.5.3) were synthesized by Pharmacia Biotech.

### **2.1.6 Electrophoresis**

#### **2.1.6.1 Agarose Gel Electrophoresis & Photography**

All materials for agarose gel electrophoresis and photography were purchased from Sigma: agarose, boric acid, EDTA, ethidium bromide, gel loading solution type I [6x concentrate containing 0.25%(w/v) bromophenol blue, 0.25%(w/v) xylene cyanol FF and 40%(w/v) sucrose in water], 7-hydroxy-8-phenylazo-1,3-naphthalenedisulphonic acid (Orange G), sodium sulphite, sucrose, Trizma<sup>®</sup>-base, and Type 55 Polaroid positive-negative 4x5 Instant Sheet Film. 100bp DNA ladder and 10bp DNA ladder were purchased from Gibco and Metaphor<sup>®</sup> agarose from FMC BioProducts, Vallensbaek Strand, Denmark.

#### **2.1.6.2 Polyacrylamide Gel Electrophoresis (PAGE)**

The following electrophoresis grade reagents were from Sigma: ammonium persulfate (AMPS), boric acid, bromophenol blue, EDTA, formamide, glycine, sodium dodecyl sulphate (SDS), TEMED, Trizma<sup>®</sup>-base, urea. Acrylamide:bisacrylamide 29:1 and SeeBlue™ Pre-stained Standards were purchased from BioRad.

### **2.1.6.3 Capillary Electrophoresis (CE)**

CE detection of fluorescence tagged oligonucleotides used for the endonuclease nicking assay involved the use of BioCAP™ Oligonucleotide Analysis Capillary (75µm i.d. x 375µm o.d. x 30cm) and Run Buffer both purchased from BioRad. All reagents for the CE measurement of ascorbic acid were purchased from Sigma: ascorbic acid, isoascorbic acid, metaphosphoric acid, sodium hydroxide and Tricine, except ascorbate oxidase (EC 1.10.3.3) spatulas from Roche Diagnostics, Lewes, East Sussex, UK. Isoascorbic acid and ascorbic acid were separated on a fused silica capillary of 50µm internal diameter and 47cm capillary length (Composite Metal Services Ltd., Hallow, UK).

### **2.1.7 High Performance Liquid Chromatography (HPLC)**

The following reagents for ascorbic acid measurements were purchased from Sigma: metaphosphoric acid, EDTA, citric acid and sodium citrate. Glacial acetic acid and LiChrospher 100 NH<sub>2</sub> HPLC column, particle size 5µm, column size 250-4 and LiChrospher 100 NH<sub>2</sub> guard cartridges were purchased from Merck. Acetonitrile 190 (far UV) SPS was purchased from Romil Ltd., Cambridge, UK.

For DNA digestion and the HPLC measurement of 2'-deoxyguanosine (dG) and 8-oxodeoxyguanosine (8-oxodG) the following reagents were purchased from Sigma except 8-oxodG (Wako Pure Chemical Industries Ltd., Japan): 2'-deoxyguanosine, sodium acetate, Trizma®-HCl and zinc chloride. Enzymes, alkaline phosphatase from Bovine intestinal mucosa (EC 3.1.3.1) and Nuclease P1 from *Penicillium citrinum* (EC 3.1.30.1) were from Boehringer Mannheim and Calbiochem respectively. For the HPLC mobile phase, electrochemical grade methanol, sodium acetate and water were purchased from Fisher. 3µm Hypersil® ODS columns [octadecyl silane (C18) bonded to silica, 15cm x 4.6mm internal diameter] and guard column kit and cartridges from Hypersil, Runcorn, UK and Phenomenex, Macclesfield, Cheshire, UK respectively.

## **2.2 Equipment**

### **2.2.1 UV Source, Radiometry & Spectrometry**

Broad-band irradiations were performed using the following lamps: UVB (Model UVM-57 Chromato-vue® Lamp 302nm, UVP Inc, Knight Optical Technologies, Leatherhead, UK) and UVC (254nm UVC Lamp, Anderman, UK). Narrowband irradiation with a bandwidth of  $\pm 4.5\text{nm}$  were performed using a Thermal Jarrell Ash Model 18 Monochromator and a 1kW xenon-mercury arc lamp with post optics consisting of an 8mm liquid light guide (Knight Optical Technologies).

The emission spectra of the broad-band UVC lamp and of each monochromatic wavelength specified were taken every 6 months with a S2000 Fiber Optic Spectrometer with computerised Spectrawin 2000 software, Knight Optical Technologies (Appendix IV). The energy output from all UV sources was assessed using an Optical Radiometer with UVB and UVC sensors (Micropulse Technology, Knight Optical Technologies). The calculations of UV dose and the coefficient of variation of UV irradiation are described in Appendix V.

### **2.2.2 Spectrophotometry / Spectrofluorimetry**

Spectrophotometric measurements of 96-well plates using 492nm and 620nm filters were performed on an Anthos Reader 2001, Salzburg, Austria. Fluorescence detection of CM-H<sub>2</sub>DCFDA, Hoechst 33342 and propidium iodide in 96-well plates was performed on a Wallac 1420 Multilabel Counter, Perkin Elmer with WorkOut™ Applications Data Management System Computerized Software, version 1.5. The excitation / emission filters were 485 / 535nm for CM-H<sub>2</sub>DCFDA, 355 / 460nm for Hoechst 33342 and 530 / 615nm for propidium iodide.

DNA, RNA and oligonucleotide samples were quantified and the purities verified on a Lambda 2 UV/VIS Spectrophotometer, Perkin Elmer with Perkin Elmer Computerised Spectroscopy Software, version 4.3.

### **2.2.3 Electrophoresis**

All PAGE and Western blotting apparatus as well as Powerpac (model 300) were purchased from BioRad, UK. PCR products were assessed on a stackable agarose gel cask tank allowing simultaneous electrophoresis of 136 samples (produced and designed by Leicester University Workshop, UK).

A P/ACE™ 2050 Capillary Electrophoresis System with Laser Module 488 was used for the analysis of fluorescence-tagged oligonucleotides, and a P/ACE™ 2200 Capillary Electrophoresis System with UV detection for the measurement of ascorbic acid. Both CE systems were controlled by Beckman System Gold Software and purchased from Beckman, High Wycombe, UK.

#### **2.2.4 Chromatography**

Measurement of ascorbic acid in cell culture supernatants was performed using a Rheodyne 7125 injector fitted with a 20µL loop (Fisher, Loughborough, UK), Beckman 126 Solvent module with a Beckman 168 Diode Array Detector module and Graphic 1000 Chart Recorder from Lloyd Instruments Ltd., Fareham, UK.

Analysis of 8-oxoguanine involved a Shimadzu LC-10AD HPLC pump (Shimadzu, Milton Keynes, UK), Beckman 508 Autosampler and Beckman 168 Diode Array Detector module with ESA Coulochem II electrochemical detector with 5020 Guard cell, 5011 Analytic cell and pulse dampener (ESA, Aylesbury, UK). Sample processing and final data analysis were controlled by Beckman 32 Karat Windows Software.

#### **2.2.5 Microscopy**

Immunohistochemical data was photographed using an Olympus BH-2, Vanox SZH microscopy with Olympus Automatic Photomicrographic System (PM-10ADS) from Olympus Optical Co. Ltd., Middlesex, UK and Fuji Provia 1600ASA film. Immunocytochemical slides were analysed using a True Confocal Scanning microscope (Model: Leitz DM IRB/E TCS4D, Leica, Milton Keynes, UK). For ultrastructural analysis and gold labelling in cells, ultrathin sections were cut using an Ultracut UCT ultramicrotome (Leica Microsystems Ltd., Milton Keynes, UK) and sections examined on a Zeiss 902A electron microscope (LEO Electron Microscopy Ltd., Cambridge, UK).

#### **2.2.6 Imaging**

Agarose gels were photographed under UV light using a Polaroid MP4<sup>+</sup> Instant Camera System (model 44-16, Wheathampstead, UK) using Type 55 Polaroids. Western blotting Hyperfilm ECL was developed on a Compact X4 Automatic X-ray Film Processor, X-ograph Imaging Systems, Malmesbury, UK. Type 55 Polaroid negatives, Hyperfilm ECL and EMSA Kodak X-Omat negatives were analysed and quantified using a β-Imaging Computing Densitometer (Molecular Dynamics, Little Chalfont, UK) with MD Image Quant Software

version 3.3. PAGE gels were analysed on a BioRad Fluor-S™ MultiAnalyst with MultiAnalyst Software, version 1.1, BioRad.

### ***2.2.7 Miscellaneous Equipment***

RT-PCR was performed in a Techne Unit Progene Thermal Cycler, Techne Ltd., Cambridge, UK and PCR products were sequenced on an ABI 377 Automated Sequencer, Applied Biosystems, Warrington, UK. For radioactivity monitoring a Mini-monitor g.m Meter type 5.10, Mini Instruments Ltd., Essex, UK was used and EMSA gels were dried using a Slab Dryer Model 483 from BioRad. For freeze-drying of cell supernatants a Lyoprep-3000 Freeze Drier with Edwards RV5 pump from International Equipment Company, Dunstable, UK was required. For cell cycle analysis, a Becton Dickinson fluorescence-activated cell-sorting (FACS) Vantage Flow Cytometer (Wheatley, UK) was used.

## **2.3 Methods**

### **2.3.1 Cell Culture & Treatment**

All cells were cultured and experiments performed in a Sanyo incubator in a 5% CO<sub>2</sub> atmosphere at 37°C and routinely passaged. Adherent cell lines were detached in trypsin-EDTA solution (0.05%(w/v) trypsin, 0.02%(w/v) EDTA and 145mM sodium chloride) at 37°C for 3min. THEK cells of passage 35 were cultured in 3:1 (v/v) mixture of DMEM and Ham's F12 containing 10% HiFCS. Cells were subcultured every 2-3 days at a seeding density of 10,000/cm<sup>2</sup> up to passage 55. For serum starvation, cells at 60-70% confluence were maintained in 3:1 (v/v) DMEM: Ham's F12 without HiFCS for 48hr.

NHEK-Ad cells were cultured according to the supplier's recommendation in serum-free Keratinocyte Basal Medium (KBM<sup>®</sup>-2) containing SingleQuot<sup>®</sup> growth supplements. Cells were subcultured at a seeding density of 3500 cells/cm<sup>2</sup> and not grown beyond 15 population doublings. Population doubling time was estimated as approximately 24 hr.

CCRF-HSB-2 cells were grown in RPMI-1640 with 2mM GlutaMAX<sup>™</sup>-1 and 10% HiFCS. Cultures were maintained up to passage 15 between 2-3x10<sup>5</sup> cells/mL and not allowed to exceed a cell density of 2-3 x10<sup>6</sup> cells/mL. Cells were serum starved for 48hr prior to treatments at a density of 1x10<sup>6</sup> cells/mL in RPMI-1640 with 2mM GlutaMAX<sup>™</sup>-1 and 0.5% HiFCS.

Cells were treated with filter sterilized hydrogen peroxide (Appendix II), ascorbic acid or dehydroascorbic acid at doses of 0, 50, 100, 200 and 400μM diluted in serum-reduced medium as stated above. Cells were incubated at 37°C for periods ranging between 0 and 24hr. For treatments with UV, THEK cells were washed twice with PBS and irradiated in PBS, and either fixed or further incubated in serum deficient medium for periods up to 48hr.

### **2.3.2 Measurement of Viability & Oxidative Cellular Stress**

#### **2.3.2.1 Trypan Blue Exclusion**

Following the treatment of both THEK and CCRF with hydrogen peroxide, ascorbic acid and dehydroascorbic acid, viability was assessed by Trypan Blue exclusion. At each treatment timepoint an aliquot of CCRF cell suspension was added to an equal volume of 0.4%(w/v) Trypan Blue solution. Similarly, trypsinised cells and supernatants from THEK cell

incubations were pooled and assessed in the same manner. Triplicate haemocytometer counts of swollen, dark blue non-viable cells and small, round and refractile viable cells were performed; a minimum of 100 cells counted per measurement. The proportion of viable cells was represented as a percentage of total cells counted.

### **2.3.2.2 *Hoechst & Propidium Iodide***

Live cells were washed twice with sterile PBS and DNA stained with 50µg/mL Hoechst 33342 for 10min at 37°C. Cells were washed twice with PBS and fluorescence read (excitation of 355nm and emission of 460nm) on a fluorescence plate reader.

For dead cells, cells were initially washed twice with PBS and fixed with ice-cold 70%(v/v) ethanol in PBS for 30min on ice. Cells were washed twice with PBS and then stained for 30min at 37°C with 40µg/mL propidium iodide in PBS containing 100µg/mL heat de-activated RNase A. Cells were washed twice with PBS and fluorescence read (excitation of 530nm and emission of 615nm) on a fluorescence plate reader.

For flow cytometry studies, CCRF cells at  $2.5 \times 10^6$ /mL were washed and fixed as described above and stained with propidium iodide overnight at 4°C. To aid a single cell suspension, cells gently passed through a 25gauge syringe post fixation. Cells were analysed by flow cytometry (section 2.2.7).

### **2.3.2.3 *CM-H<sub>2</sub>DCFDA***

Each 50µg aliquot of CM-H<sub>2</sub>DCFDA was initially dissolved in 50µL DMSO and then immediately diluted to a 10µM working solution in PBS. The final amount of DMSO was <0.1% of the working solution to minimize cytotoxicity.

THEK cells were seeded at  $2 \times 10^4$  cells / well in 96-well plates, and allowed to adhere overnight at 37°C. Cells were washed twice with PBS and loaded with 10µM (CM-H<sub>2</sub>DCFDA) for 15 min at 37°C. After loading, cells were washed twice with PBS and treated for up to 1 hr with various concentrations of hydrogen peroxide, ascorbic acid or dehydroascorbic acid in PBS.

Intracellular fluorescence generation as a marker of reactive oxygen species (ROS) was assessed by reading the plates on the Wallac Multilabel Counter using an excitation of 485nm with an emission of 535nm.

### 2.3.3 Immunochemical Methods

#### 2.3.3.1 Antibody Preparations

##### *Pyrimidine Dimer Antibody (Ab529)*

Production of this polyclonal antiserum was previously described by Herbert *et al.* (1994)<sup>2</sup>. Briefly, rabbits were immunised with UVC (21Jcm<sup>-2</sup>) and UVA (34Jcm<sup>-2</sup>) irradiated calf thymus DNA conjugated to BSA and homogenized with Freund's complete adjuvant. Each rabbit received a total 0.8mL of immunogen subcutaneously at multiple sites and sera collected at week five after one booster injection at week four.

##### *hOGG1 Antibody*

hOGG1 peptide (N-DKSQASRPTPDELEAVRKC-C), as described by Hazra *et al.* 1998, was synthesized, analysed by HPLC and MALDI and kindly conjugated to Imject<sup>®</sup> Maleimide activated KLH at a molar ratio of 1:1, by the PNACL, University of Leicester (Appendix VI). The conjugated peptide was desalted by gel filtration and the protein concentration of two fractions (807 & 808) determined by the Bradford assay (section 2.3.4.4). Two rabbits were immunized with 100µg of either fraction 807 or 808 on each occasion. The immunisation mixture consisted of 100µg conjugated protein in sterile PBS and 50%(v/v) Titer Max<sup>®</sup>Gold in a final volume of 800µL.

Prior to immunization, rabbits were allowed to acclimatize for 2 weeks and pre-immune test bleeds taken. Each rabbit received four 200µL subcutaneous injections on three occasions, days 0, 7 and 28. Test bleeds were taken every week after booster injections and screened immediately alongside pre-immune sera by ELISA (section 2.3.3.3). Serum from pre-immune and immune test bleeds, as well as the final bleed (day 35), was collected by incubating the blood for 1hr at 37°C, dislodging the clots and then centrifuging at 9000g for 10 min. Serum was transferred and stored in aliquots at -80°C.

#### 2.3.3.2 IgG Purification from antiserum

IgG fractions from rabbit serum were isolated using HiTrap<sup>®</sup> Protein G1 Affinity Columns and the manufacturer's protocol. Briefly, the 20% ethanol gel column preservative was washed off with three column volumes of start buffer (20mM sodium phosphate, pH 7.0). The column was allowed to equilibrate for 30min with two column volumes of start buffer. 1mL of serum was placed onto the column with a syringe and then unbound material washed off with five column volumes of start buffer. Bound IgG was eluted off the protein G column

with five column volumes of 0.1M glycine-HCl (pH 2.7) collecting fractions of 1mL. To preserve activity of acid-labile IgG, 100 $\mu$ L 1M Trizma<sup>®</sup>-base (pH 9.0) was pre-added to each fraction collection tube.

### **2.3.3.3 Enzyme Linked Immunosorbent Assay (ELISA)**

#### *Pyrimidine dimer ELISA*

The ELISA was modified from that previously described by Herbert *et al.* (1994)<sup>2</sup>. Briefly, both single-stranded native and UV-damaged DNA at 50 $\mu$ g/mL in PBS were allowed to bind to 96-well plates (50 $\mu$ L/well). All incubations were at 37°C for 1hr in a humidified chamber. Plates were washed three times in PBS and free sites blocked with 4%(w/v) dried skimmed milk powder in PBS. Plates were washed with PBS and then incubated with sera from rabbits [diluted in 4%(w/v) milk in PBS]. Unbound antibody was washed off in three washes of 0.05%(v/v) Tween 20 in PBS (PBS-Tween). Plates were incubated with goat anti-rabbit IgG-HRP conjugated antibody diluted 1 in 5000 in 4%(w/v) milk in PBS. Plates were finally washed with PBS-Tween prior to detection of peroxidase with 0.5mg/mL *o*-phenylenediamine in 0.05M phosphate citrate (pH 5.0) containing 0.03%(w/v) sodium perborate (50 $\mu$ L/well). Plates were incubated in the dark for 15min and the reaction quenched with 2M H<sub>2</sub>SO<sub>4</sub> (25 $\mu$ L/well). Plates were read spectrophotometrically at 492nm in an ELISA plate reader.

Competitive ELISA for pyrimidine dimers was as described above except, solid phase antigen consisted of 7.5s UVC irradiated calf thymus DNA and competitors consisted of 7.5-120sec UVC irradiated calf thymus or THEK DNA, or 5min UVC irradiated oligonucleotide standard (5'-AAC AGT AAT ACA TTT GGA GAT AGC GTG-3'). Competitors were serially diluted and co-incubated with the primary antibody.

#### *hOGG1 Peptide ELISA*

Screening of pre-immune and immune rabbit sera involved coating 96-well plates with 20 $\mu$ g/mL of purified hOGG1 peptide (Appendix IV) in PBS. All incubations were at 37°C for 1hr in a humidified chamber. Plates were washed three times with PBS and non-specific sites blocked as described in 2.3.3.3. After three further washes in PBS, plates were incubated with rabbit serum serially diluted in blocking solution. Plates were washed with PBS-Tween and then incubated with goat anti-rabbit-HRP conjugated secondary antibody diluted 1 in 5000. Plates were finally washed in PBS-Tween and peroxidase activity detected as described for pyrimidine dimer ELISA (section 2.3.3.3).

#### **2.3.3.4 Western Blotting**

Immobilon-P membrane and four pieces of Whatman® 3MM paper were cut to the size of each SDS PAGE gel. The membranes were pre-soaked in methanol for 15sec, rinsed in de-ionized (milliΩ) water for 2min and then in freshly prepared transfer buffer [25mM Trizma®-base, 192mM glycine and 10% methanol in de-ionized water (pH8.3)] for 5min; whilst the papers were pre-soaked in transfer buffer only, for 2min. Each SDS PAGE gel (section 2.3.6.2) and membrane were sandwiched between sheets of Whatman® 3MM paper and inserted into a blotting cassette after ensuring all air bubbles were dispersed. Each cassette was placed into the mini-gel tank together with transfer buffer and the transfer conducted overnight at 30V. Membranes were either air dried and stored at 4°C or immediately rinsed in de-ionized water for 5min. Dried membranes were rehydrated in methanol for 15sec and then de-ionized water for 5min.

To confirm efficient transfer of protein, immobilon membranes were stained with 0.1 %(w/v) Ponceau S solution for 5min. Membranes were rinsed with ultrapure (UP) water and the blots photographed under white light. Prior to immunodetection the stain was removed by 30sec incubation in 0.1M sodium hydroxide and several rinses in de-ionized water. Membranes were washed twice in TBS [50mM Trizma®-HCl and 150mM NaCl, (pH 7.6)] for 2min and then blocked for 1hr in 10%(w/v) milk in 0.1%(v/v) Tween 20 in TBS. All incubations and washes were performed on a shaking platform at room temperature (RT). Membrane washes consisted of two brief rinses in 0.1%(v/v) Tween 20 in TBS, followed by one 15min and two 5min washes. Membranes were incubated with the appropriate primary antibody diluted in 0.1%(v/v) Tween 20 in TBS for 1hr and washes performed as described. Membranes were finally incubated for 1hr with HRP-conjugated goat anti-rabbit IgG antibody, diluted typically 1 in 10,000 in 0.1%(v/v) Tween 20 in TBS and then washed with an extra two 5min washes. Peroxidase activity was detected with ECL™ reagents according to the manufacturer's recommendation. Briefly, equal volumes of reagents 1 and 2 were mixed and the membranes incubated for 1min. Excess developing solution was blotted and the membranes heat-sealed in sample bags ready for exposure to Hyperfilm ECL™. The films were exposed for various periods of time and developed by a Compact X4 automatic x-ray film processor.

### 2.3.3.5 Immunocytochemistry

#### Confocal Microscopy

Immediately post treatment, cells were fixed in ice-cold 50:50 (v/v) acetone:methanol for 2min at RT, ice-cold 100% methanol for 10min at RT, or in aldehyde-based fixatives, either 4%(w/v) paraformaldehyde in PBS (pH 10.5) for 30-60min and the fixation was quenched in 50mM glycine in PBS for 5 min at RT, or 4%(w/v) formaldehyde in PBS (pH 7.4) for 30min at RT. Cells fixed in 50:50 (v/v) acetone:methanol were air dried for approximately 15min and stored at -80°C pending staining and brought to RT in a minimal volume of ice-cold 50:50% (v/v) acetone:methanol for 5min then rinsed three times in PBS (pH 7.4). Cells were permeabilized in 0.5 % (v/v) Tween 20 in PBS for 15min at RT or for aldehyde-based fixatives in 0.1% (v/v) Triton-X-100 in PBS for 10min at RT, rinsed three times in PBS and non-specific sites blocked with 4%(w/v) BSA in PBS or 5%(w/v) dried skimmed milk powder in PBS for 1hr at 37°C. The block was removed and primary antibody diluted in blocking solution (refer to results chapters for final antibody dilutions) was placed onto the cells for 1hr at 37°C. Slides were washed three times in 0.05%(v/v) Tween 20 in PBS then incubated overnight at 4°C or 1hr at 37°C with secondary antibody diluted in blocking solution (refer to results chapters for details of relevant antibodies and working dilutions). All blocking and antibody incubations were performed in a humidified chamber. After three washes with 0.05%(v/v) Tween 20 in PBS and a rinse in UP water, slides were mounted in Vectashield mounting medium containing propidium iodide. Control samples (sham treated cells) as well as negative controls, *i.e.* cells incubated without primary antibody were included in each staining run.

For co-localisation studies with anti-hOGG1 antibody, the mitochondria and nuclei were counterstained with MitoTracker<sup>®</sup> CMXRos and Hoechst 33258, respectively (Appendix III). MitoTracker<sup>®</sup> was loaded into the mitochondria of live cells prior to fixation with 4%(w/v) formaldehyde in PBS. This involved directly adding 500nM MitoTracker<sup>®</sup> to the cell culture medium and incubating the cells for 15min at 37°C. Cells were washed, fixed, permeabilised, blocked and incubated with antibodies prior to nuclear counterstaining with 300ng/mL Hoechst 33258 for 20min at RT.

All slides were kindly analysed by Mr Kulvinder Sikand (Centre for Mechanisms of Human Toxicity, University of Leicester, Leicester, UK) using a True Confocal Scanning microscope. Slides were scanned at 488nm for the Alex fluor<sup>™</sup> 488 fluorochrome which emits green fluorescence, at 568nm for propidium iodide and MitoTracker<sup>®</sup> which emits red and with UV

for Hoechst 33258 seen as blue (Appendix III). Cross talk between both scanning wavelengths was controlled for.

*Electron Microscopy (EM)*

Slides for routine EM were kindly processed by Mrs Judy McWilliam and Mr Tim Smith (MRC Toxicology Unit, Hodgkin Building, University of Leicester, Leicester, UK). After UV irradiation, slides were fixed overnight at 4°C in 2%(v/v) glutaraldehyde in 0.1M sodium cacodylate (pH 7.3) and then rinsed in cacodylate buffer (pH 7.3). Cells were post fixed for 2hr in 1%(w/v) osmium tetroxide in 0.1M sodium cacodylate and 0.04M potassium ferrocyanide, and stained overnight at 4°C in 2% (v/v) aqueous uranyl acetate. Cells were dehydrated through graded ethanols and embedded in TAAB Epoxy resin for 3 days. The resultant blocks (generated by the chambered wells) were detached from the glass slide by chilling in liquid nitrogen. Ultrathin sections (90-100nm) were stained with lead nitrate and examined by Dr David Dinsdale (MRC Toxicology Unit, Hodgkin Building, University of Leicester, Leicester, UK).

For immunostained EM work, cells were fixed with 4%(w/v) paraformaldehyde (pH 10.5) for 30-60min at RT after irradiation with UV. Fixation was quenched with 50mM glycine in PBS for 5 min at RT and the cells washed three times in PBS. Cells were permeabilised in 0.2% (v/v) Triton-X-100 in PBS for 10min at RT and then washed three times in PBS. Blocking of non-specific sites in 5%(w/v) dried skimmed milk powder in PBS, primary antibody incubation, and primary antibody post washes were as described in section 2.3.3.5. Cells were incubated in goat anti-rabbit IgG Fab-fluoronanogold, diluted 1 in 40 in blocking solution for 1hr at 37°C followed by three washes in 0.05%(v/v) Tween 20 in PBS. The above named EM personnel performed the remainder of the protocol. Briefly, cells were washed overnight in PBS, followed by three 30min washes in 50mM glycine in PBS, three 20min washes in PBS containing 0.5%(w/v) BSA, 0.05%(v/v) Tween 20 and 2%(w/v) sodium chloride and finally in three 10min washes in UP water. Gold labelling in cells was enhanced according to manufacturer's recommendation using "Gold Enhance" for 3min, and the cells subsequently fixed with 0.5% (w/v) osmium tetroxide in distilled water for 30min and stained in fresh 2%(w/v) aqueous uranyl acetate for 30min at 4°C. Embedding, sectioning and analyses of specimens was as described for routine EM above.

### **2.3.3.6 Immunohistochemistry**

Formalin-fixed paraffin-embedded tissue sections were dewaxed in xylene, rehydrated through graded ethanols and washed in UP water for 2min. Antigen retrieval pretreatments involved trypsin (1mg/mL) digestion for 25min at 37°C. The slides were washed in UP water and then TBS for 2min and immersed into blocking solution (1% (w/v) gelatin, 0.1% Triton X-100 in TBS). The sections were incubated in a humidified chamber with 5%(v/v) normal goat serum (NGS) diluted in blocking solution for 10min at RT. The blocking agent was drained off and the sections were incubated at RT for 1hr with primary antibody diluted in 5% NGS in blocking solution (refer to results chapters for final antibody dilutions). To ensure complete coverage and prevent drying, plastic coverslips were applied. After two washes in TBS, the sections were covered for 30min at RT with the biotinylated anti-mouse or rabbit secondary antibody diluted 1 in 400 in 5% NGS in blocking solution.

Following two washes in TBS, the bound secondary antibody was further amplified with preformed Strept ABC complex labelled with alkaline phosphatase, for 30min at RT. Final washes included two washes in TBS, one wash in UP water and then alkaline phosphatase buffer (100mM Trizma<sup>®</sup>-base, pH9.5, 50mM magnesium chloride hexahydrate, 100mM sodium chloride in UP water) for 5min. Alkaline phosphatase activity was detected using filtered Sigma FAST Fast Red TR-Naphthol AS-MX for 5-15min at RT. Excess stain was rinsed off in running tap water and the sections lightly counterstained (10sec) in Mayer's hematoxylin followed by a rinse in running tap water for 5 min. Slides were mounted in Apathy's aqueous mountant.

Controls were included with each staining run consisting of non-specific rabbit or mouse IgGs, non-secreting medium monoclonal cultures or secondary antibody only. Positive controls consisted of the *in vitro* treatment of tissue sections following dewaxing and rehydration steps. For Ab529, sections were irradiated in PBS with either UVC or UVB to generate thymine dimers, whilst for antibodies N45.1 and F3/9, sections were pretreated with 200µM hydrogen peroxide and 200µM ascorbic acid in UP water for 60min at 37°C.

Stained tissue sections were examined under a light microscope, photographed and the final magnifications calculated as: objective magnification times NFK photo eyepiece (2.5) times 3.

### 2.3.4 Extraction & Quantitation Methods

#### 2.3.4.1 DNA Extraction & Quantitation

##### *Pronase Method*

DNA used for UV irradiations or for  $\beta$ -actin, *hOGG1* and *hAPE* PCR was extracted from cells by the 'Pronase' method (Kendall *et al.*, 1991). Briefly, approximately  $6 \times 10^6$  cells were washed twice in PBS and centrifuged at 300g for 5min. The supernatant was removed and the pellets resuspended in 1.75mL of 5mM sodium citrate, 20mM NaCl (pH 6.5) and 2mL 20mM Trizma<sup>®</sup>-base, 20mM EDTA, 1.5% (w/v) *N*-lauroyl-sarcosine (pH 8.5) and vigorously mixed. RNase A (0.25mL of 20 Kunitz units ribonuclease type III-A from bovine pancreas) in RNase buffer (50mM Trizma<sup>®</sup>-HCl, 10mM EDTA, 10mM NaCl, pH 6.0), previously boiled to inactivate DNase activity, was added to the samples before incubation at 37°C for 60min. Pronase E (0.5mL equal to 11.2 units of protease, type XIV from *Streptomyces griseus* in 5mM sodium citrate, 20mM NaCl pH 6.5) was added to each sample before overnight incubation at 37°C.

After incubation, 2mL of 10mM Trizma<sup>®</sup>-HCl, 1mM EDTA (pH 7.5) and 0.5mL 7.5M sodium acetate was added and samples mixed by inversion. 18mL ice-cold ethanol was added to precipitate the DNA, which was then spooled and washed twice in ethanol before being air-dried. DNA was dissolved in water and purity and quantity assessed spectrophotometrically at 260nm and 280nm.

##### *Sodium Iodide Method*

DNA for 8-oxodG analyses was extracted using a method modified from that described for whole blood by Wang *et al.* (1994). After each treatment  $40 \times 10^6$  CCRFs or  $2-3 \times 10^6$  THEK cells were washed twice in PBS and transferred into a tube. The cell pellets were dispersed prior to the addition of 0.5mL lysis solution [10mM Trizma<sup>®</sup>-HCL, 5mM magnesium chloride, 320mM sucrose, pH7.5, 1%(w/v) Triton-X-100 with 0.1mM DFO added on the day of use]. The cells were vortexed for 30sec and pelleted at 8000g for 20sec. The supernatant was discarded and the process repeated with 1mL of lysis solution. To each pellet 0.2mL of enzyme reaction solution (20mM Trizma<sup>®</sup>-HCl, 5mM DTPA, 10mM NaCl, pH 6.0 with 0.1mM DFO added on the day of use) was added and mixed, followed by heat inactivated RNase A (0.1mL equal to 16 Kunitz units ribonuclease type III-A from bovine pancreas in enzyme reaction solution). The samples were incubated at 37°C for 15min, then 0.1mL equal

to 50 Kunitz units Proteinase K in enzyme reaction solution was added and the samples further incubated at 37°C for 60min.

Following incubation, 0.3mL sodium iodide solution (7.6M sodium iodide, 5mM DTPA and 40mM Trizma®-HCL, pH 8.0) and 0.5mL ice-cold isopropanol were added and the sample inverted. Once the DNA precipitate was visible the samples were centrifuged at 8000g for 20sec and the supernatants removed. The DNA was subsequently washed with 40%(v/v) ice-cold isopropanol and then 70%(v/v) ice-cold ethanol. The DNA pellets were allowed to dry before being reconstituted in 300-400µL 20mM sodium acetate (pH 4.8) and dissolved overnight at room temperature on a rotating mixer. DNA purity and quantity was assessed spectrophotometrically at 260 and 280nm.

#### **2.3.4.2 RNA Extraction & Quantitation**

Cells were washed twice in PBS before being lysed in RNAzol™B. The homogenates were transferred into sterile tubes and a tenth of the total volume of chloroform was added. The samples were vortexed for 15sec and then incubated on ice for 10min before centrifugation at 9000g for 10 min at 4°C. The upper aqueous layer containing RNA was collected, avoiding the interphase and organic phase. An equal volume of ice-cold isopropanol was added and the samples vortexed before storage at -20°C for 60min. Following centrifugation as before, the supernatants were discarded and the pellets washed in 75% (v/v) ethanol. After centrifugation, the ethanol was discarded and the pellets allowed to air dry for 30min before resuspension in 20µL sterile water.

Purity of RNA was assessed spectrophotometrically at 260nm and 280nm and the concentration of RNA was calculated based on the assumption that an optical density at 260nm of 1 corresponds to approximately 40µg/mL of RNA.

#### **2.3.4.3 Oligonucleotide Extraction & Quantitation**

##### *Oligonucleotide Extraction*

Oligonucleotides from cell supernatants were desalted and extracted either by sodium acetate /ethanol precipitation or by a NucleoTrap®Nucleic Acid purification kit. To cell culture supernatant samples, 6M sodium acetate and ice-cold absolute ethanol were added at 0.5 and 5 times the total volume of supernatant, respectively. Samples were incubated on dry ice for

30min and centrifuged at 9000g for 15min at 4°C. The pellets were washed in 80%(v/v) ice-cold ethanol, air-dried for 15min and reconstituted in UP water.

The NucleoTrap® Nucleic Acid purification kit was used according to the manufacturer's recommendation. To each supernatant sample (400µL), approximately 600µL NT2 buffer was added and vortexed. NucleoTrap® suspension (10µL) was added and the samples incubated with vortexing every 2-3min at RT for a total of 10min. The samples were centrifuged at 9000g for 30sec and 500µL NT3 buffer added to the pellets. The samples were centrifuged as above and pellets washed again in NT3 buffer before being air-dried for 15min. The oligonucleotides were eluted in UP water at RT for 10min (with periodic mixing) and the supernatants collected after centrifugation. The last step was repeated to ensure maximum yield.

#### *PCR Primer Extraction & Quantitation*

PCR primer sets were supplied in saturated ammonia at 40nmol and were purified by the addition of ice-cold absolute ethanol and 3M sodium acetate at 2.5 times and 0.1 times the starting volume respectively. Primers were kept at -20°C for 10min before centrifugation at 9000g for 5min. Subsequent washes included ice-cold 80% ethanol with 3M sodium acetate, followed by 80%(v/v) ethanol and then 70%(v/v) ethanol. The pellets were allowed to air dry before resuspension in 100µL sterile water. UV spectrophotometric readings were taken at 260nm and each primer concentration was calculated using the Nearest Neighbour Method (<http://www.williamstone.com/primers/calculator/>), which takes into account the molecular extinction coefficient of each base.

#### *PCR Product Extraction, Quantitation & Sequencing*

PCR products were purified in 3M sodium acetate and ice-cold absolute ethanol at a ratio of 1: 0.1: 3 respectively. Samples were incubated at -20°C for 1hr and then centrifuged at 9000g for 30min at 4°C. The pellets were washed in 75%(v/v) ice-cold ethanol and finally air-dried for 15min. Purified PCR products were reconstituted in UP water and resolved on 1.5%(w/v) agarose gels (section 2.3.6.1) alongside DNA quantitation standards. DNA quantitation standards consisted of six standardized solutions of phage λ DNA at concentrations ranging 15-500ng/6µL. Gels were photographed with Type 55 Polaroids and the negatives used for densitometry to quantify the PCR products (section 2.3.6.1). Purified PCR products (40ng) and primers (1pmol/µL) were supplied to the PNAFL, University of Leicester for sequence

analyses. Briefly, cycle sequencing reactions were performed using ABI BigDye terminator sequencing chemistry, unincorporated dye terminators removed by DyeEx columns and the resulting products analysed on an ABI 377 Sequencer. Chromatogram files were viewed on CHROMAS software ([www.technelysium.com.au/chromas.html](http://www.technelysium.com.au/chromas.html)).

#### *Endonuclease Nicking Assay Oligonucleotide Extraction*

Following the endonuclease nicking assay (section 2.3.5.3) repair oligonucleotides were extracted by two separate methods (Appendix VIII). Non-biotinylated double stranded repair oligonucleotides were extracted following incubation with cell lysates by the addition of an equal volume sodium acetate solution (300mM sodium acetate, 1mM EDTA and 0.4mg/mL yeast tRNA) and five volumes of ice-cold absolute ethanol. Samples were mixed by inversion and incubated on dry ice for 45min. Precipitated oligonucleotides were centrifuged at 9000g for 15min at 4°C and the pellets further washed in absolute ethanol, before being air-dried and reconstituted in water for denaturing-PAGE (section 2.3.6.2) analyses.

Biotinylated double stranded repair oligonucleotides were extracted by Streptavidin coated Dynabeads® for subsequent analysis by CE (section 2.3.6.3). The binding capacity of the Dynabeads® was assumed to be 10µg Dynabeads® per pmol of biotinylated oligonucleotide. The Dynabeads® were initially washed three times in bind / wash buffer [20mM Trizma®-HCl (pH 7.5), 2mM EDTA and 4M sodium chloride] and finally reconstituted in the same buffer before use.

Following the endonuclease nicking assay with biotinylated repair oligonucleotides, the samples were incubated with washed Dynabeads® for 15min at RT. The beads were pelleted in the magnet, washed in 0.5X bind / wash buffer and then competitor oligonucleotide in 100X excess was added (section 2.3.5.3). The samples were heated to 95°C for 5min and the beads finally precipitated on the magnet. The supernatant containing single stranded oligonucleotides was collected, and residual beads removed before CE analysis (section 2.3.6.3).

#### **2.3.4.4 Cellular Lysate Extraction & Quantitation**

CCRF cells ( $5 \times 10^6$ ) were washed twice in PBS by centrifugation at 200g for 3mins. Cells were lysed in lysis buffer [50mM Tris-HCl (pH 7.4), 50mM potassium chloride, 3mM EDTA, 5mM magnesium acetate and 3mM β-mercaptoethanol and 5µg/mL of each protease inhibitor: antipain, chymostatin, leupeptin and pepstatin] as previously described Yamaguchi

*et al.* (1996). Whole cell lysates were snap frozen on dry ice and stored at  $-80^{\circ}\text{C}$ . Lysates were thawed and homogenized on ice and for the endonuclease nicking assay (section 2.3.5.3) cellular debris was removed by centrifugation at 9,000g for 30min at  $4^{\circ}\text{C}$ .

The protein content of whole cell and supernatant lysates as well as nuclear extracts (section 2.3.4.5) was measured using the Bradford assay (Bradford, 1976). Briefly, extracts were serially diluted in lysis buffer and 25 $\mu\text{L}$  placed into a 96-well plate in triplicate. 200 $\mu\text{L}$  BioRad protein dye solution, pre-diluted 1 in 5, was added to each well. A BSA standard curve, diluted in lysis buffer or appropriate diluent, ranging from 0 $\mu\text{g}$  to 25 $\mu\text{g}$ , was included on each plate in triplicate. Plates were incubated at RT for 10min before being read spectrophotometrically at 620nm. The protein content in extracts was calculated using GraphPad Prizm software.

#### **2.3.4.5 Nuclear Protein Extraction and Quantitation**

Nuclear protein was extracted from THEK cells following the method described by Staal *et al.* (1990). At each timepoint post treatment, duplicate plates of THEKs were washed twice with ice-cold  $\text{Ca}^{2+}/\text{Mg}^{2+}$ -free PBS and the cells pooled, using a cell scraper, into a tube before being placed on ice. Cells were centrifuged at 50g for 10min and the pellets washed in 1mL  $\text{Ca}^{2+}/\text{Mg}^{2+}$ -free PBS. After centrifugation at 17,000g for 15sec at  $4^{\circ}\text{C}$ , cells were washed in 400 $\mu\text{L}$  of buffer containing 10mM HEPES/KOH (pH7.5), 10mM potassium chloride, 2mM magnesium chloride, 1mM DTT, 0.1mM EDTA, 0.4mM phenylmethylsulfonyl fluoride (PMSF), 0.2mM sodium fluoride, 0.2mM sodium orthovanadate and 0.3mg/mL leupeptin (wash buffer).

After 15min incubation on ice, cells were subsequently lysed in the wash buffer containing 1% (v/v) triton X-100. Cells were vigorously mixed and then centrifuged at 17,000g for 30sec at  $4^{\circ}\text{C}$ . The supernatant was discarded and the pelleted nuclei resuspended in 50 $\mu\text{L}$  of ice-cold, high salt buffer [50mM HEPES, (pH 7.8), 50mM potassium chloride, 300mM sodium chloride, 0.1mM EDTA, 1mM DTT, 0.4mM PMSF, 0.2mM sodium fluoride, 0.2mM sodium orthovanadate and 10% (v/v) glycerol]. Samples were mixed for 20 min on a rotating platform before being centrifuged at 14,000rpm for 5min at  $4^{\circ}\text{C}$ . The supernatant containing the nuclear protein extract was collected and stored at  $-80^{\circ}\text{C}$  pending analysis. The protein content of nuclear protein extracts was measured using the Bradford assay as described in section 2.3.4.4.

### 2.3.5 Molecular & Enzymatic Methods

#### 2.3.5.1 Reverse Transcription-Polymerase Chain Reaction (RT-PCR)

Reverse transcription-polymerase chain reaction (RT-PCR) was used to assess gene expression levels of hOGG1 and hAPE in RNA samples extracted from treated cells. All incubations for this procedure were performed on a Techne Unit Progene Thermal Cycler. Approximately 5µg total RNA was incubated at 25°C for 10min with 250ng random primers, consisting of mostly hexamers, in a final volume of 12µL RNase-DNase free water. To complete reverse transcription the following was added: 50mM Tris HCl (pH 8.3), 75mM KCl, 3mM MgCl<sub>2</sub>, 10mM dithiothreitol (DTT), 0.5mM dNTP mix (equal concentrations of dATP, dGTP, dCTP, dTTP in sterile water) and 100 units of Superscript™ II, in a final reaction volume of 20µL. Samples were pre-heated to 42°C for 2min prior to the addition of the reverse transcriptase. Samples were further incubated at 42°C for 50min and then at 72°C for 10min.

The synthesized complementary DNA (cDNA) was diluted 1 in 5 and then 30µL aliquots were used to amplify *β-actin*, *hOGG1* and *hAPE* sequences by PCR. Table 2.2 describes sequence specific primers for *β-actin*, *hOGG1* and *hAPE* together with gene positions and predicted PCR product size (Appendix VII). All PCR reactions were set up in a final volume of 50µL containing 20mM Tris HCl (pH 8.4), 50mM potassium chloride, 0.2mM dNTP mix, 2mM magnesium chloride for *hAPE* primers and 2.5mM magnesium chloride for *β-actin* and *hOGG1* primers, 500nM sense primer, 500nM anti-sense primer and 1.25 units *Taq* DNA polymerase. All three genes were simultaneously amplified using the same PCR cycling conditions: initial denaturation at 95°C for 5min, followed by 30 cycles of denaturation at 95°C for 1min, annealing at 55°C for 1min and extension at 72°C for 1min, followed by a final extension at 72°C for 10min. Controls consisted of water blanks to indicate experimental contamination, RNA from sham treated cells and batch to batch control specimens. PCR products were stored at 4°C and resolved in duplicate by agarose gel electrophoresis (section 2.3.6.1).

GENE / ACCESSION CODE	GENE POSITION OF PRIMER	PRIMER SEQUENCES	PCR PRODUCT
<i>hOGG1</i> / AJ13141	<i>Sense/Exon 2</i> <i>Anti-sense/Exon 3</i>	5' -TCA AGT ATG GAC ACT GAC TC -3' 5' -TGG AGG AAC AGA TAA AAG AG -3'	263bp
<i>hAPE</i> / M92444	<i>Sense/Exon 5</i> <i>Anti-sense/Exon 5</i>	5' -GGC ACA TGA AGA AAT TGA C-3' 5' -CAC ACA ATG CAG GTA ACA G-3'	251bp
<i>β-Actin</i> / M10277	<i>Sense/Exon 5</i> <i>Anti-sense/Exon 6</i>	5' -TTC AAC TTC ATC ATG AAG TGT GAC GTG -3' 5' -CTA AGT CAT AGT CCG CCT AGA AGC ATT -3'	310bp

**Table 2.2:** *hOGG1*, *hAPE* and *β-Actin*, primer sequences, gene positions and predicted PCR product size (Appendix VII).

### 2.3.5.2 Electrophoretic Mobility Shift Assay (EMSA)

Transcription factor activity was assessed by EMSA, nuclear extracts were incubated with a <sup>32</sup>P-labelled oligonucleotide (5' -CGCTTGAT**TGAGTCA**GCCCCGAA-3') containing a binding sites for AP-1. Non-labelled AP-1 consensus oligonucleotides and NFκB consensus oligonucleotides (5' -AGTTGAG**GGGACTTTCC**CAGG-3') were used as competitor and non-competitor controls respectively. (*N.B.* transcription factor binding sites have been highlighted in bold).

Double stranded oligonucleotides were kindly 5'-end labelled with [ $\gamma$ -<sup>32</sup>P] dATP using T4 polynucleotide kinase by Dr Steve Faux, MRC Toxicology, Hodgkin Building, University of Leicester, UK. Briefly, the 7pmol oligonucleotides were incubated for 30 min at 37°C with 8-10units T4 polynucleotide kinase in T4 polynucleotide kinase buffer [70mM Trizma<sup>®</sup>-HCl (pH 7.6), 10mM magnesium chloride and 5mM DTT] and 5μL [ $\gamma$ -<sup>32</sup>P] dATP (3000Ci/mmol at 10mCi/mL) in a 20μL final reaction volume. The reaction was stopped in Tris-EDTA buffer [TE: 10mM Trizma<sup>®</sup>-HCl and 1mM EDTA (pH 8.0)] and the oligonucleotides purified on a Nap5 column to remove unincorporated nucleotides. Eluted oligonucleotide fractions containing maximum radioactivity were pooled and the oligonucleotides precipitated overnight by the addition of 0.1 and 2.5 volumes of 5M sodium chloride and ethanol respectively. Oligonucleotides were centrifuged at 9000g for 30min and then re-dissolved in water.

EMSA was performed with the help of Dr Karen Holloway, Division of Chemical Pathology, University of Leicester, UK. 4 μg of nuclear protein extract were incubated at RT in DNA binding buffer containing 40mM HEPES buffer, 4% (v/v) Ficoll, 200ng of poly(dI).(dC)/L,

1mM magnesium chloride, 1mM DTT and 0.175pmol of <sup>32</sup>P-end-labelled double stranded oligonucleotide containing a consensus AP-1 site. Controls included: nuclear extracts from cells treated for 4hr with 16nM 12- O-tetradecanoylphorbol 13-acetate (TPA), a known inducer of AP-1, as a positive control. Other assay controls included incubation of nuclear extracts in the presence of <sup>32</sup>P labelled DNA as competitor, or with a <sup>32</sup>P labelled non-specific oligonucleotide as non-competitor. The binding of proteins to consensus sites was assessed by electrophoretic mobility on non-denaturing polyacrylamide gels (section 2.3.6.2).

### 2.3.5.3 Endonuclease Nicking Assay

Table 2.3 lists the sequences of both biotinylated and non-biotinylated repair oligonucleotides used in this assay. Double stranded repair substrate oligonucleotides were synthesized by combining an equal concentration of ss GF with ss C as control substrate and ss 8-GF with ss C as adduct containing substrate, to a final concentration of 1pmol/μL per oligonucleotide. Oligonucleotides were annealed on a Progene Thermal Cycler. They were initially denatured at 95°C for 5min and then annealed at a ramp time of -1°C/min to 20°C and then stored at 4°C. Annealing of oligonucleotides was confirmed by Metaphor<sup>®</sup> agarose electrophoresis (section 2.3.6.1).

Oligonucleotide sequence	Oligonucleotide length	Nomenclature
3'-CCA CCG GAC TGC GTA AGG GTT-5' *	21mer	ss C
F 5'-GGT GGC CTG ACG CAT TCC CAA-3'	21mer	ss 8-GF
F 5'-GGT GGC CTG ACG CAT TCC CAA-3'	21mer	ss GF
F 5'-GGT GGC CTG AC-3'	11mer	G11
5'-GGT GGC CTG ACG CAT TCC CAA-3'	21mer	Competitor

**Table 2.3:** Oligonucleotide sequences of DNA repair oligonucleotides used for the Endonuclease Nicking Assay. A, C, G, T represent adenine, cytosine, guanine and thymine respectively. G indicates 8-oxoguanine and F refers to 5' fluorescein isothiocyanate labeled oligonucleotide. \* Complementary strand (ss C) was biotinylated for double stranded oligonucleotides extracted by Dynal bead extraction system.

Double stranded control and adduct-containing oligonucleotides were incubated with 50-100μg cell lysate protein in triplicate. The samples were incubated for 2hr at 37°C, 0hr controls were also included in each run. After incubation the oligonucleotides were extracted from each sample (section 2.3.4.3) and resolved either on a denaturing polyacrylamide gel electrophoresis (denaturing PAGE, section 2.3.6.2) or by CE (section 2.3.6.3).

### 2.3.6 Electrophoretic Methods

#### 2.3.6.1 Agarose Gel Electrophoresis

##### *Agarose Gel Electrophoresis of PCR Products and Photography*

PCR products were resolved in 1.5%(w/v) agarose gels in a stackable gel cast tank allowing the simultaneous electrophoresis of up to 136 samples. The agarose was heated in a microwave oven in Tris borate-EDTA buffer [TBE: 89mM Tris-borate (pH 8.3) and 2mM EDTA]. Once dissolved, 25nM ethidium bromide was added, the gels poured and allowed to set for 1 hr at RT. PCR products were diluted in gel loading solution (either 0.25%(w/v) bromophenol blue, 0.25%(w/v) xylene cyanol FF and 40%(w/v) sucrose or 0.25%(w/v) Orange G and 40%(w/v) sucrose) at a ratio of 5:1 respectively. PCR samples (20 $\mu$ L) were loaded in duplicate wells and resolved by electrophoresis at 110V for 90 min in TBE buffer containing 50nM ethidium bromide together with a 100bp ladder prepared in the appropriate loading buffer.

Each gel was photographed under UV light using a Polaroid MP4<sup>+</sup> Instant Camera System. Polaroid Type 55 negatives were subsequently developed in 18% (w/v) sodium sulphite solution for 5min before overnight washing in UP water containing a few drops of washing-up liquid. Negatives were allowed to dry and stored pending densitometry analyses.

##### *Metaphor<sup>®</sup> Agarose Gel Electrophoresis*

Metaphor<sup>®</sup> agarose was used to resolve small DNA fragments (less than 80 base pairs). 5%(w/v) Metaphor<sup>®</sup> agarose gels were poured according to the manufacturer's recommendation. Briefly, the agarose powder was sprinkled into a continuously stirring pre-chilled TBE buffer and then allowed to rest for 15min to allow the agarose to soak. The vessel was weighed before and after microwaving and any losses were made up with hot UP water. The agarose was heated for 1min, allowed to stand for 15min, heated again for 1min and mixed, and then boiled for a further 1min. Ethidium bromide was added to a final concentration of 25nM, the gels poured and allowed to set for 1hr at RT. The gels were pre-chilled at 4°C before loading. Samples were diluted with non-denaturing gel loading solution [0.25%(w/v) bromophenol blue, 0.25%(w/v) xylene cyanol FF and 40%(w/v) sucrose] at ratio of 5:1 respectively. Oligonucleotides were resolved at 60V for 2hr alongside a 10bp ladder in a denaturing loading buffer [95%(v/v) formamide, 0.1%(w/v) bromophenol blue, 0.1%(w/v) xylene cyanol and 10mM EDTA in water].

### **2.3.6.2 Polyacrylamide Gel Electrophoresis (PAGE)**

#### *Sodium Dodecyl Sulphate-Polyacrylamide Gel Electrophoresis (SDS-PAGE)*

SDS-PAGE was used to study the expression of hOGG1 and hAPE proteins. 7mL of resolving gel consisting of 15%(v/v) acrylamide:bisacrylamide 29:1, 375mM Trizma<sup>®</sup>-HCl (pH 8.8), 0.1%(w/v) SDS, 4.4mM ammonium persulphate (APS) and 0.05%(v/v) N, N, N', N'- tetramethylethylenediamine (TEMED), was poured into a 9mL cast, and allowed to polymerize at RT for 40min. The gel was overlaid with water during polymerization and once set the water was removed. 1.5mL of stacking gel consisting of 4%(v/v) acrylamide:bisacrylamide 29:1, 125mM Trizma<sup>®</sup>-HCl (pH 8.8), 0.1%(w/v) SDS, 4.4mM APS and 0.1%(v/v) TEMED, was placed above the resolving gel with the appropriate comb and allowed to polymerize for 1hr. The comb was carefully removed and the wells thoroughly rinsed with water. The gel was placed into a mini-gel tank with SDS running buffer [0.1%(w/v) SDS, 192mM glycine and 25mM Trizma<sup>®</sup>-base (pH 8.3)].

20µg of cellular extract (section 2.3.4.4) were loaded into each well diluted in loading buffer [4%(w/v) SDS, 20%(w/v) glycerol, 500mM Trizma<sup>®</sup>-HCl (pH 6.8) and 0.02%(w/v) bromophenol blue] at a ratio of 2:1. SeeBlue<sup>™</sup> Pre-stained Standards were heated at 99°C for 5min and 5µL loaded into neighbouring wells. Proteins in cellular extracts were resolved by electrophoresis at 200V for 40min.

#### *Denaturing-Polyacrylamide Gel Electrophoresis (Denaturing-PAGE)*

Denaturing-PAGE was used to resolve repair substrate and product oligonucleotides between 11-22 bases in length that were used in the Endonuclease Nicking Assay (sections 2.3.4.3 and 2.3.5.3). Gels consisted of 20%(v/v) acrylamide:bisacrylamide 29:1, 7M urea, 2.2mM APS and 0.05%(v/v) TEMED in Tris-borate EDTA buffer [TBE: 89mM Trizma<sup>®</sup>-base, 89mM boric acid and 2mM EDTA (pH 8.3)], and were prepared in order to prevent 'smiling/frowning' of gels during running. Firstly, the acrylamide:bisacrylamide, urea and TBE was dissolved, filtered through a 0.2µM filter and then the mixture was degassed by bath sonication for 15min. The APS was added and the gel mixture carefully mixed by inversion to avoid excessive oxidation. Likewise the TEMED was added, the gels poured in 9mL casts and the appropriate comb positioned. Gels were allowed to set for 2hr at RT and then transferred to 4°C to pre-chill.

The gel casts were placed into a mini-tank and the tank filled with pre-chilled 500mL TBE. Oligonucleotide samples were heat denatured in an equal volume of loading buffer [90%(v/v) formamide, 10mM sodium hydroxide and 0.1% (w/v) bromophenol blue in TBE] for 5min at 95°C followed by a quick chill on ice, and then loaded. The entire gel tank was placed into an ice bucket containing ice to maintain chilled conditions during electrophoresis at 200V for 1hr.

#### *Non-denaturing-Polyacrylamide Gel Electrophoresis (Non-denaturing-PAGE)*

Non-denaturing polyacrylamide gels consisted of 4%(v/v) acrylamide:bisacrylamide, 3mM APS and 0.2%(v/v) TEMED in 0.25X TBE poured in 50mL casts. Prior to loading of samples the wells were thoroughly rinsed out and gels pre-run at 120V for 1hr. Samples were diluted with loading buffer [20%(v/v) glycerol, 2mM DTT and 0.1%(w/v) bromophenol blue in 0.25X TBE] at a ratio of 10:1 respectively. Samples (20µL) were loaded into each well and the gel shifts resolved by electrophoresis at 120V for 2hr in 0.25X TBE. Gels were dried onto Whatman® 3MM paper and visualised by autoradiography on Kodak X-Omat film.

#### **2.3.6.3** *Capillary Electrophoresis (CE)*

##### *Measurement of Endonuclease Nicking Assay Oligonucleotides*

Following the incubation of cell lysates with biotinylated double stranded repair oligonucleotides (section 2.3.5.3) repair products were extracted using Streptavidin coated Dynabeads® (section 2.3.4.3). The retrieved single-stranded FITC-conjugated repair oligonucleotides were assessed using a P/ACE™ 2050 Capillary Electrophoresis System with Laser Module 488 (with 488nm excitation and 535nm emission). Aliquots of supernatants (10-20µL) containing repair oligonucleotides of 11 and 21mer were placed into microvials, each sample was injected into a BioCAP™ Oligonucleotide Analysis Capillary (75µm i.d. x 375µm o.d. x 30cm) under 0.5psi pressure over 10sec. Oligonucleotides were separated in BioCAP™ run buffer under a constant voltage of 12kV (with a negative to positive polarity) over 15min (with 1min pre-rinse) at a constant temperature of 40°C. Each sample was analysed in duplicate and the peak areas generated by each oligonucleotide integrated using System Gold Software. The repair activity was expressed as the amount of 11mer oligonucleotide detected as a percentage of total oligonucleotide measured (*i.e.* the combined peak areas of the 21mer and 11mer oligonucleotides).

*Measurement of Ascorbic Acid*

THEK and CCRF cells were treated with ascorbic acid or dehydroascorbic acid. 500 $\mu$ L aliquots of cell culture medium were taken at 4, 8 and 12hr post incubation at 37°C and an equal volume of 6%(w/v) metaphosphoric acid containing 100 $\mu$ M isoascorbic acid (MPA-IAA) was added. 50x10<sup>6</sup> CCRFs or 10x10<sup>6</sup> trypsinised THEK cells per treatment dose and per time point were washed twice with PBS. Cell pellets were resuspended in 5mL PBS and a 50 $\mu$ L sample taken for protein quantitation by the Bradford assay (section 2.3.4.4). The cells were pelleted and lysed in 1mL MPA-IAA for CCRFs and 200 $\mu$ L MPA-IAA for THEK cells. The optimal percentage of MPA to efficiently precipitate proteins in cellular fractions was pre-determined by Mr A. Ladapo (BSc Undergraduate Student, DeMontfort University, Leicester). Cells were homogenized on ice and the supernatants collected following centrifugation at 8000g for 10min at 4°C. Samples were stored at -80°C for no more than two weeks pending analysis.

Ascorbic acid and isoascorbic acid were separated on a fused silica capillary of 50 $\mu$ m internal diameter and 47cm length. The capillary cartridge was kindly assembled by Ms J Nirwan (BSc Undergraduate Student, DeMonfort University, Leicester) and conditioned prior to use with 10min washes with 0.1M NaOH and then water followed by 0.1M tricine (pH 8.5). Aliquots of 10-20 $\mu$ L of either cell culture medium or cell extracts were placed into microvials, 25nL of each sample was injected into the capillary by applying positive pressure over 5sec. Ascorbic acid and isoascorbic acid were resolved under a constant voltage of 30kV (with a positive to negative polarity) over 8min at a constant temperature of 21°C and measured by absorbance at 254nm UV. Between each sample the capillary was rinsed for 20sec in 0.1M NaOH and 20sec water followed by 30sec 0.1M tricine (pH 8.5). Each sample was analysed in duplicate.

To confirm variations in migration times of ascorbic acid, a sample was treated with ascorbate oxidase, an enzyme that oxidizes ascorbic acid to dehydroascorbic acid. Oxidation of ascorbic acid would lead to the reduction or loss of the ascorbic acid peak. Peak areas of ascorbic acid measured in medium and cell lysate samples were integrated using System Gold Software, and the values were normalized to the internal standard, isoascorbic acid. Concentrations of ascorbic acid in cell extracts and cell culture medium were calculated from an ascorbic acid standard curve ranging 0-1000 $\mu$ M prepared in the MPA-IAA stock solutions

specific to each experiment. The final concentration of ascorbic acid in each cellular sample was expressed as  $\mu\text{mol}$  ascorbic acid per g of protein.

### **2.3.7 Chromatographic Methods**

#### **2.3.7.1 HPLC Measurement of Ascorbic Acid in Cell Culture Medium**

THEK cells were treated with 0, 100 and 400 $\mu\text{M}$  ascorbic acid in either PBS or standard cell culture medium for THEK cells (section 2.1.1.3). Aliquots of 750 $\mu\text{L}$  of medium or PBS, were taken at timepoints ranging from 0 to 4hr, and stabilized in an equal volume of ice-cold 10% (w/v) metaphosphoric acid (MPA). Samples were vortexed, followed by centrifugation at 2000g for 15min at 4°C. Two, 300 $\mu\text{L}$  aliquots of supernatant from each sample were collected and stored at -80°C for no more than two weeks pending analysis.

Samples for some experiments were kindly processed by Miss Helen Waller, Division of Chemical Pathology, University of Leicester, UK, using the method described by Lunec and Blake (1985). Briefly, MPA precipitated samples were thawed and EDTA solution (stock 10mM) was added to a final concentration of 1mM to prevent oxidation and an equal volume of 0.5M citric acid/ sodium citrate buffer, pH 3.6 was also added. Samples (20 $\mu\text{L}$ ) were injected in duplicate onto a LiChrospher 100  $\text{NH}_2$  HPLC column. Samples were eluted at 1mL/min with filtered acetonitrile, 40mM citric acid/sodium citrate buffer, pH3.2 and glacial acetic acid at ratios of 84.9:15:0.1 respectively. Ascorbic acid was detected by UV absorbance at 254nm and quantified using a standard curve of 0, 25, 50 and 100 $\mu\text{M}$  ascorbic acid. Samples of high ascorbic acid concentration were diluted with MPA prior to injection.

#### **2.3.7.2 HPLC Measurement of 8-oxodeoxyguanosine (8-oxodG)**

DNA extracted by the sodium iodide method (section 2.3.4.1) for 8-oxodG measurements was digested prior to analysis by HPLC-ECD. To each minimum 50 $\mu\text{g}$  aliquot of DNA in 190 $\mu\text{L}$  20mM sodium acetate, 10 $\mu\text{L}$  2mM DFO, 5 $\mu\text{L}$  1M sodium acetate containing 45mM zinc chloride (pH 4.8) and 0.1 Kunitz units/ $\mu\text{g}$  DNA Nuclease P1 in 20mM sodium acetate was added and the samples incubated at 37°C for 60min. Following incubation, 20 $\mu\text{L}$  1.5M Trizma<sup>®</sup>-HCl, pH 8.0 and 0.07 Kunitz units/ $\mu\text{g}$  DNA alkaline phosphatase in 100mM Trizma<sup>®</sup>-HCl, pH 8.0 were added and the samples further incubated at 37°C for 30min and stored on ice pending analysis.

In order to determine the concentration of 8-oxodG in DNA samples, 8-oxodG and dG standards were analysed using stocks solutions of 1mM dG and 100 $\mu$ M 8-oxodG prepared in water. To determine the exact concentration of these stocks, spectrophotometric absorbance measurements at 253nm for dG and 245nm for 8-oxodG were taken. The concentrations were then determined using their Extinction Coefficients, where  $E_{253} = 13.0\text{mM}^{-1}\text{cm}^{-1}$  and  $E_{245} = 12.3\text{mM}^{-1}\text{cm}^{-1}$  for dG and 8-oxodG respectively. The stock solutions of standards were further diluted to 200 $\mu$ M dG and 100nM 8-oxodG in 20mM sodium acetate containing 100 $\mu$ M DFO and then the following series of dilutions were prepared, for dG 2.5, 5, 10, 50 and 100 $\mu$ M and for 8-oxodG 0.25, 0.5, 1, 5 and 10nM. A 190 $\mu$ L aliquot of each standard was processed through the DNA digestion procedure to provide the nearest estimation of 8-oxodG in DNA samples.

Duplicate 50 $\mu$ L injections of deoxynucleoside standards or samples were separated by reversed-phase HPLC using a 3 $\mu$ m Hypersil<sup>®</sup> ODS column [octadecyl silane (C18) bonded to silica, 15cm x 4.6mm internal diameter] and mobile phase consisting of 75mM sodium acetate (pH 5.5) with 8%(v/v) methanol, pumped at a flow rate of 1mL/min. 2-deoxyguanosine was detected by its UV absorbance at 254nm and 8-oxodG by coulometric detection at 375mV (Guard cell output 700mV). Peaks were integrated using a Beckman 32 karat software package and the levels of 8-oxodG expressed per 10<sup>5</sup> dG. Results were processed and graphically presented using Microsoft Excel.

### **2.3.8 Data Analysis & Statistical Testing**

RT-PCR bands on polaroid negatives, AP-1 gel shift bands on Kodak X-Omat negatives and Hyperfilm ECL from Western experiments were quantified using a  $\beta$ -Imaging Computing Densitometer with MD Image Quant Software. hOGG1 and hAPE RT-PCR and hOGG1 protein levels were normalised to  $\beta$ -actin expression and results were expressed as fold increase of control. Similarly, AP-1 data was also expressed as fold increase of control. All calculations were performed in Microsoft Excel 2000.

Spectrophotometric data obtained from CM-H<sub>2</sub>DCFDA experiments were checked for normality (*i.e.* all data points were normally distributed) and the differences in ROS generation in response to treatment dose was compared by one-way Analysis of Variance (ANOVA) with Fisher's Least Squares Difference (LSD) post test. Statistical tests were performed using Minitab (version 10) and graphical presentation by using Microsoft Excel 2000.

## **CHAPTER THREE**

### **DETECTION OF DIRECT UV-INDUCED DNA DAMAGE & REPAIR IN HUMAN SKIN CELLS & TISSUES**

### **3.0 DETECTION OF DIRECT UV-INDUCED DNA DAMAGE AND REPAIR IN HUMAN SKIN CELLS AND TISSUES**

#### **3.1 INTRODUCTION**

Terrestrial ultraviolet radiation (UV) consists of 4.1% UVB (295-315nm) and 95.9% UVA (315-400nm), with the shorter wavelengths of UVB and UVC of the total UV spectrum being absorbed by oxygen in the upper atmosphere and therefore appearing to have no known biological significance (Gasparro and Brown, 2000). The deleterious effect of terrestrial UV is dependent not only on its intensity and the biological absorption spectrum, but also wavelength of UV (Arlett and Green, 1993; Griffiths *et al.*, 1998). Although UVB constitutes only a small fraction of the total solar UV, the potency and mutagenic potential of the shorter wavelengths on DNA has been well documented, since the energy carried by a photon is inversely proportional to wavelength (Frederick *et al.*, 1989). DNA weakly absorbs UVB whilst it is an even weaker absorber of UVA (Cadet *et al.*, 1992). DNA damage characteristics of solar UVB include cyclobutane pyrimidine dimers (CPD's) and 6-4 photoproduct and its corresponding Dewar isomer (Figure 3.1), which is formed by photoisomerisation at wavelengths longer than 290nm (Clingen *et al.*, 1995; Peak and Peak, 1989). Other less prominent DNA lesions induced by UVB include DNA strand breaks and ROS generated single base modifications such as 7, 8-dihydro-8-oxo-2'-deoxyguanosine (8-oxodG; Ahmed *et al.*, 1999).

Concerns in recent decades relating to stratospheric ozone depletion resulting from man-made hydrocarbons has heightened interest in establishing the specific biological effects of UV (Department of Environment, 1996; Diffey, 1991), particularly since links between sunlight exposure and skin cancers such as malignant melanoma (River, 1996), basal cell carcinoma and squamous cell carcinoma (de Laat and de Gruiji, 1996) have long been hypothesised, but the complexities surrounding the precise contribution to disease aetiology requires further elucidation. Similarly, defects in DNA repair mechanisms important in the removal of bulky UV adducts, namely nucleotide excision repair (NER; section 1.2.2) have been implicated in the pathogenesis of skin cancer (Camplejohn, 1996; Wei *et al.*, 1994), as well as photosensitive disorders (section 1.3.2) such as xeroderma pigmentosum (Kraemer *et al.*, 1984), Cockayne's syndrome (Lehmann, 1982; Schmickel *et al.*, 1977) and trichothiodystrophy (Itin and Pittelkow, 1990).

The mutagenic potential of sun exposure can be demonstrated by the presence of DNA mutations stemming from spontaneous deamination of cytosine to thymine. Mutations typical of UV exposure, such as characteristic C to T transitions, have been described in skin carcinomas and p53 and PCNA mutations from skin tumours (Bodak et al., 1999; Daya-Grosjean et al., 1993). The frequency of these mutations in skin tumours varies from 10% to 50% in normal DNA sequences (Daya-Grosjean et al., 1993; Saito et al., 1993). The frequency increases to 50-80% in tumours with partial loss of p53 or PCNA (Saito, 1999). The significance of skin cancer associated with UV exposure is clearly demonstrated by the fact that DNA repair proteins specific for UV-induced lesions are highly induced in skin (Daya-Grosjean et al., 1993; Saito et al., 1993). In addition, the high incidence of skin cancer related to UV exposure is associated with epidemiological studies that demonstrated a correlation between UV exposure and skin cancer (Chen et al., 1994; Hamada et al., 2000). A recent study by Xu et al. (2001) clearly demonstrated that DNA damage induced in vivo by UV phototherapy lamps and sunbeds is related to the formation of skin diseases and for recreational/esthetic tanning. Many skin products are treated by harmful UVB, UVA and UVA.

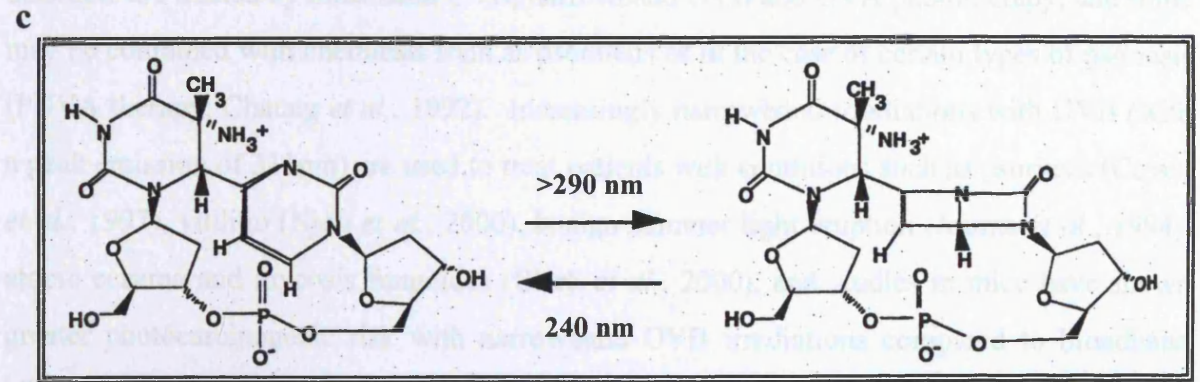
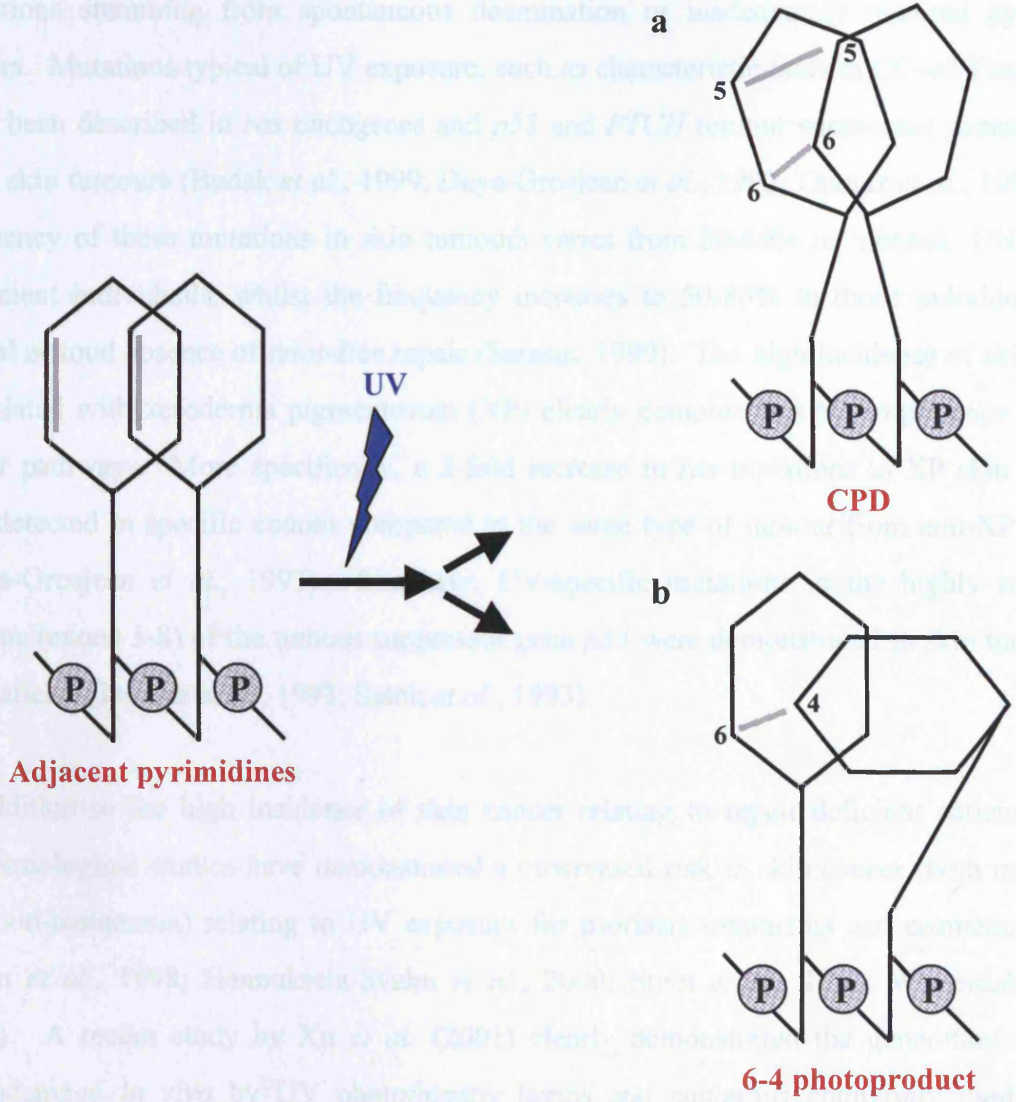


**Figure 3.1:** Ultraviolet (UV)-induced DNA lesions. Direct absorption of UV by adjacent pyrimidines leads to the formation of two major DNA lesions: cyclobutane pyrimidine dimers (CPD) (a) and 6-pyrimidine-4-pyrimidone product [6-4 photoproduct (b)]. The photoisomerisation of a thymine-cytosine 6-4 photoproduct into its corresponding Dewar valence isomer at wavelengths above 290nm (c). This figure has been adapted from van Steeg and Kraemer (1999) and Clingen *et al.* (1995).

The mutagenic potential of sun exposure can be demonstrated by the presence of DNA mutations stemming from spontaneous deamination or inadequately repaired pyrimidine dimers. Mutations typical of UV exposure, such as characteristic tandem CC→TT mutations, have been described in *ras* oncogenes and *p53* and *PTCH* tumour suppressor genes isolated from skin tumours (Bodak *et al.*, 1999; Daya-Grosjean *et al.*, 1993; Dumaz *et al.*, 1993). The frequency of these mutations in skin tumours varies from 30-60% in 'normal' DNA repair proficient individuals, whilst the frequency increases to 50-80% in those individuals with partial or total absence of error-free repair (Sarasin, 1999). The high incidence of skin cancer associated with xeroderma pigmentosum (XP) clearly demonstrates the importance of DNA repair pathways. More specifically, a 2-fold increase in *ras* mutations in XP skin tumours was detected in specific codons compared to the same type of tumour from non-XP patients (Daya-Grosjean *et al.*, 1993). Similarly, UV-specific mutations in the highly conserved regions (exons 5-8) of the tumour suppressor gene *p53* were demonstrated in skin tumours of XP patients (Dumaz *et al.*, 1993; Satoh *et al.*, 1993).

In addition to the high incidence of skin cancer relating to repair deficient patients, many epidemiological studies have demonstrated an increased risk in skin cancer (both melanoma and non-melanoma) relating to UV exposure for psoriasis treatments and cosmetic tanning (Chen *et al.*, 1998; Hannuksela-Svahn *et al.*, 2000; Stern *et al.*, 1997; Westerdahl *et al.*, 2000). A recent study by Xu *et al.* (2001) clearly demonstrated the generation of DNA photodamage *in vivo* by UV phototherapy lamps and sunlamps commonly used for the treatment of skin diseases and for recreational/cosmetic tanning purposes. Many skin disorders are treated by broadband UVB, narrowband UVB and UVA phototherapy; and some may be combined with chemicals such as psoralens as in the case of certain types of psoriasis (PUVA therapy; Chaung *et al.*, 1992). Increasingly narrowband irradiations with UVB (with a peak emission of 311nm) are used to treat patients with conditions such as psoriasis (Coven *et al.*, 1997), vitiligo (Njoo *et al.*, 2000), benign summer light eruption (Journe *et al.*, 1994), atopic eczema and mycosis fungoides (Clark *et al.*, 2000), and studies in mice have shown greater photocarcinogenic risk with narrowband UVB irradiations compared to broadband UVB irradiations (Flindt-Hansen *et al.*, 1991).

Research into the genotoxicity of UV can often be compromised by the source of UV used during *in vitro* experimentation. Often 'sunlamps' are used which provide irradiations containing both UVB and UVA, these experiments can generate false results as often filters required to eliminate biologically irrelevant contaminating sources of UVC and the shorter

wavelengths of UVB are not used (Woollons *et al.*, 1998<sup>1</sup>; Woollons *et al.*, 1998<sup>2</sup>). Also the proportions of UVB and UVA emitted by these lamps can be vastly different to those found in the natural environment which ultimately affect the amounts of different types DNA damage generated. In certain studies UVA has also been shown to also cause direct damage to DNA, typical of that generated by the UVB spectrum (Kuluncsics *et al.*, 1999). Mimicking solar UV is important for *in vitro* experimentation; however equally important is understanding the precise contribution of distinct portions of the UV spectrum, not only for the perspective of genotoxicity but also for the therapeutic potential of UV.

### 3.2 AIMS

The biological significance of UV-induced genotoxicity in relation to disease states has been well documented, however the precise contribution of each wavelength in the UV spectrum requires further definition in order to add to our understanding into the mechanisms of mutagenesis and pathogenesis, particularly for diseases associated with UV phototherapy and cosmetic tanning. This chapter aims to measure the direct genotoxic damage induced by discrete wavelengths of UVB and to monitor the repair processing of these DNA adducts in *in vitro* model systems. The initial focus will be complete characterisation of a rabbit antiserum raised against UVC treated DNA and establishment of immunochemical assays to detect pyrimidine dimers. The antibody will then be applied in immunochemical methods to detect and quantify pyrimidine dimers in cultured human keratinocytes and calf thymus DNA following biologically relevant narrow band irradiations at 305nm and 315nm using a monochromatic source of UV. The benefits and limitations of a monochromatic UV source for *in vitro* experimentation will also be discussed, as well as the potential use of such experiments for the calibration of phototherapy and establishing doses that relate to minimal erythemal dose (MED).

### **3.3 METHODS**

#### **3.3.1 Cells and DNA**

Normal human epidermal and transformed human epidermal keratinocytes (NHEK and THEK respectively) were cultured as described in sections 2.1.1.2, 2.1.1.3 and 2.3.1. Both cell types were plated onto 8-well chambered slides at a seeding density of  $5 \times 10^4$  cells/ well. Cells were allowed to adhere overnight then washed twice in PBS and irradiated in 300 $\mu$ L PBS.

Approximately  $6 \times 10^6$  transformed keratinocytes were washed twice in PBS by centrifugation at 200g for 5min. DNA was extracted from these cells by the Pronase method described in section 2.3.4.1, and calf thymus DNA used in these experiments was commercially obtained (section 2.1.3.4). Following spectrophotometric quantitation, DNA samples were UV irradiated at 1mg/mL in PBS in a 24-well tissue culture plate (1mL/ well).

#### **3.3.2 Characterisation of Keratinocyte Cell Lines**

Monoclonal antibodies to cytokeratins 14 (K14, clone LL002; Purkis *et al.*, 1990) and 8+18 (K8+18, clone 5D3; Angus *et al.*, 1987) were used to characterise both NHEK and THEK cell lines. Immunocytochemistry conditions for all three antibodies were optimised; the final method is described in section 2.3.3.5. The following parameters were investigated: fixation at room temperature in either 4%(v/v) formaldehyde in PBS for 15min, 50%(v/v) acetone: 50%(v/v) methanol for 2min or 100% methanol for 15min and the requirement for initial permeabilisation with 0.1%(v/v) Triton-X-100 for 15min and blocking with 4%(w/v) Bovine serum albumin (BSA) in PBS for 30min in formaldehyde fixed cells. Primary antibody dilutions were prepared in either blocking solution or PBS at concentrations recommended by the suppliers: 1 in 20 for K14 and 1 in 100 for K8+18. Primary antibody incubations consisted of 1hr at 37°C or overnight at 4°C. Bound primary antibody was detected with goat anti-mouse (Fab specific) conjugated to FITC secondary antibody at 1 in 250 for 1hr at 37°C and nuclei were counter stained with propidium iodide. Slides were examined at 488nm excitation for the FITC fluorochrome emitting green fluorescence and 568nm excitation for propidium iodide emitting red fluorescence with a Confocal Scanning microscope (section 2.2.5).

#### **3.3.3 UV source, dosimetry and irradiation**

Cells and DNA were irradiated with monochromatic UV at 305nm  $\pm$  4.5nm (doses ranging 12.5-50mJcm<sup>-2</sup>) and 315nm  $\pm$  4.5nm (doses ranging 125-500mJcm<sup>-2</sup>). For antibody

characterisation experiments, cells and DNA were also irradiated with  $313\text{nm} \pm 4.5\text{nm}$  (doses ranging  $500\text{-}4000\text{mJcm}^{-2}$  similar to those described by Mizuno *et al.*, 1991 and Mori *et al.*, 1988), and calf thymus DNA with approximately  $20\text{Jcm}^{-2}$  UVC. UV spectra of all lamps used are shown in appendix IV.

Irradiation doses at each wavelength for both cells in chambered slides and DNA in 24-well plates were calculated using Optical Radiometer readings ( $n=10$ ) prior to each experiment. All irradiations were performed from above the wells and the calculated doses accounted for the energy absorbed by the specified volume of PBS. The coefficients of variation of calculated irradiation doses achieved with an 8mm post-optic liquid light guide on chambered slides was  $\cong 5\%$  and on 24-well plates was  $\cong 10\%$  (Appendix V).

### **3.3.4 Characterisation of pyrimidine dimer antibody**

Immunisation and partial characterisation of the pyrimidine dimer antibody (antiserum 529) was previously described by Herbert *et al.*, 1994<sup>2</sup> (section 2.3.3.1). The sequence specificity for the antibody was determined however the distinction between cyclobutane pyrimidine dimer (CPD) and 6-4 photoproduct (and its corresponding Dewar isomer) was not made. Two approaches were taken; to assess detection of 6-4 photoproduct, cells and DNA were irradiated with 305nm followed by irradiation with 313nm, a wavelength known to induce photoisomerisation of 6-4 photoproduct (Patrick, 1970; Ikenaga *et al.*, 1970). The second approach involved repairing CPD's by treating UVC irradiated calf thymus DNA ( $50\mu\text{g/mL}$ ) with *E.coli* photolyase CSR603 ( $25\mu\text{g/mL}$ ; Sancar, 1994) in presence of the kit reaction buffer and 'black light', in this case 380nm UVA for 0-64 min (doses ranging  $0\text{-}4000\text{mJcm}^{-2}$ ).

### **3.3.5 Direct binding ELISA for pyrimidine dimer quantitation**

ELISA based detection of pyrimidine dimers in DNA was performed as previously described, Herbert *et al.*, 1994<sup>2</sup> with some modifications (sections 2.3.3.3). Dilutions of rabbit sera containing the primary antibody and secondary antibody were optimised. Comparisons were made between THEK DNA and calf thymus DNA as well as single and double stranded DNA as solid phase antigens. The pre-coating of ELISA plates with  $25\mu\text{g/mL}$  poly-L-lysine ( $50\mu\text{L/well}$ ) to assist antigen binding was also investigated. Pyrimidine dimers detected by ELISA were quantified by comparisons to GC-MS values obtained from a standard curve consisting of UVC irradiated calf thymus DNA (Podmore *et al.*, 1996).

### **3.3.6 Competition ELISA for pyrimidine dimer detection**

THEK cells grown in chambered slides were irradiated with UV and at 6, 12 and 24hr post irradiation cell culture medium was collected and pooled from 2 wells. 'Repair oligonucleotides' were extracted from THEK cell culture medium. The efficiency of optimal desalting and concentration of oligonucleotides was initially investigated by comparing a standard sodium acetate/ethanol extraction with a commercial kit form of extraction (both methods described in section 2.3.4.3) using a synthesised oligonucleotide diluted in cell culture medium or water. Dimer-containing oligonucleotides were detected by competition ELISA (section 2.2.5)

### **3.3.7 Immunocytochemical detection of pyrimidine dimers with confocal microscopy**

Immediately post UV irradiation, NHEK and THEK were fixed in 50:50% (v/v) acetone:methanol. Cells were stained for pyrimidine dimer formation, using 5%(w/v) milk in PBS as blocking agent (section 2.3.3.5). Both rabbit immune serum and Alexa fluor™ 488 conjugated goat anti-rabbit IgG secondary antibody dilutions were optimal at 1 in 500. Mounted slides were scanned at 488nm for the Alex fluor™ 488 fluorochrome which emits green fluorescence and 568nm for propidium iodide which emits red with a Confocal Scanning microscope (section 2.2.5).

### **3.3.8 Immunocytochemical detection of pyrimidine dimers with electron microscopy**

NHEK and THEK were fixed after UV irradiation either overnight at 4°C in 2%(v/v) glutaraldehyde in 0.1M sodium cacodylate (pH 7.3) for routine electron microscopy (EM) or 30-60min at RT in 4%(w/v) paraformaldehyde (pH 10.5) for immunocytochemical detection of pyrimidine dimer, as described in section 2.3.3.5. Immunochemical conditions for the pyrimidine dimer detection were as described in section 2.3.3.5 and the goat anti-rabbit IgG Fab-fluoronanogold secondary antibody concentration was optimised as 1 in 80. Ultrathin sections (90-100nm) were kindly analysed by Dr David Dinsdale (MRC Toxicology Unit, Hodgkin Building, University of Leicester, Leicester, UK).

### **3.3.9 Immunohistochemical detection of pyrimidine dimers by light microscopy**

The full methodology is described in section 2.3.3.6. Primary antibody was optimised as 1 in 500 and biotinylated goat anti-rabbit secondary antibody as 1 in 300. Suitable controls were included in each run consisting of a negative control (incubation of tissue with secondary antibody only) and an *in vitro* generated positive control. The latter involved irradiating dewaxed and rehydrated tissues with broadband UVB or UVC (section 2.3.3.6).

## **3.4 RESULTS**

### **3.4.1 Characterisation of keratinocytes**

Optimisation of immunochemical detection of cytokeratins was carried out in THEK cells. All fixation methods tested demonstrated similar staining patterns for the three cytokeratins (Figure 3.2a). Permeabilisation and blocking steps prior to primary antibody incubation slightly reduced background staining in negative controls (no primary antibody), whilst overnight incubation of cells with primary antibody generally increased background staining. Methanol fixation with no permeabilisation and blocking steps offered the optimal staining conditions and cellular morphology for all three cytokeratin antibodies; combined with the added advantage of a short staining protocol.

NHEK and THEK were stained with cytokeratin 14 and 8+18 (K14 and K8+18 respectively) to characterise the differences in cell types (Figure 3.2b). All NHEK cells were positive for K14 showing filamentous cytoplasmic staining, but lacked K8+18 staining (Figure 3.2 v), whilst THEK cells showed positive staining for both K14 and K8+18 (Figure 3.2 iv). However unlike NHEK, not all THEK cells were positive for K14, only those that appeared morphologically to have recently divided (Figure 3.2 iv). The slightly larger more 'mature' transformed keratinocytes appeared to lack K14 expression.

### **3.4.2 Optimisation of immunochemical methods**

In order to apply the pyrimidine dimer antibody, various immunochemical approaches were firstly optimised. Further to the basic ELISA method described by Herbert *et al.*, 1994<sup>2</sup>, a comparison of double stranded and single stranded DNA as solid phase antigen was investigated; the latter proved slightly more sensitive (Figure 3.3a). Furthermore pre-coating the plates with poly-L-lysine to facilitate electrostatic binding of DNA to plates was examined. No extra improvement to the binding of the antibody to the antigen was observed and so the use of poly-L-lysine was not adopted (Figure 3.3a and b). In order to validate the use of calf thymus DNA for studies relating to transformed keratinocytes, the rate of pyrimidine dimer formation with various doses of UVC irradiation was assessed in both types of DNA (Figure 3.3c). The amount of pyrimidine dimer detected was comparable at each dose of UVC irradiation for both calf thymus and transformed keratinocyte DNA.

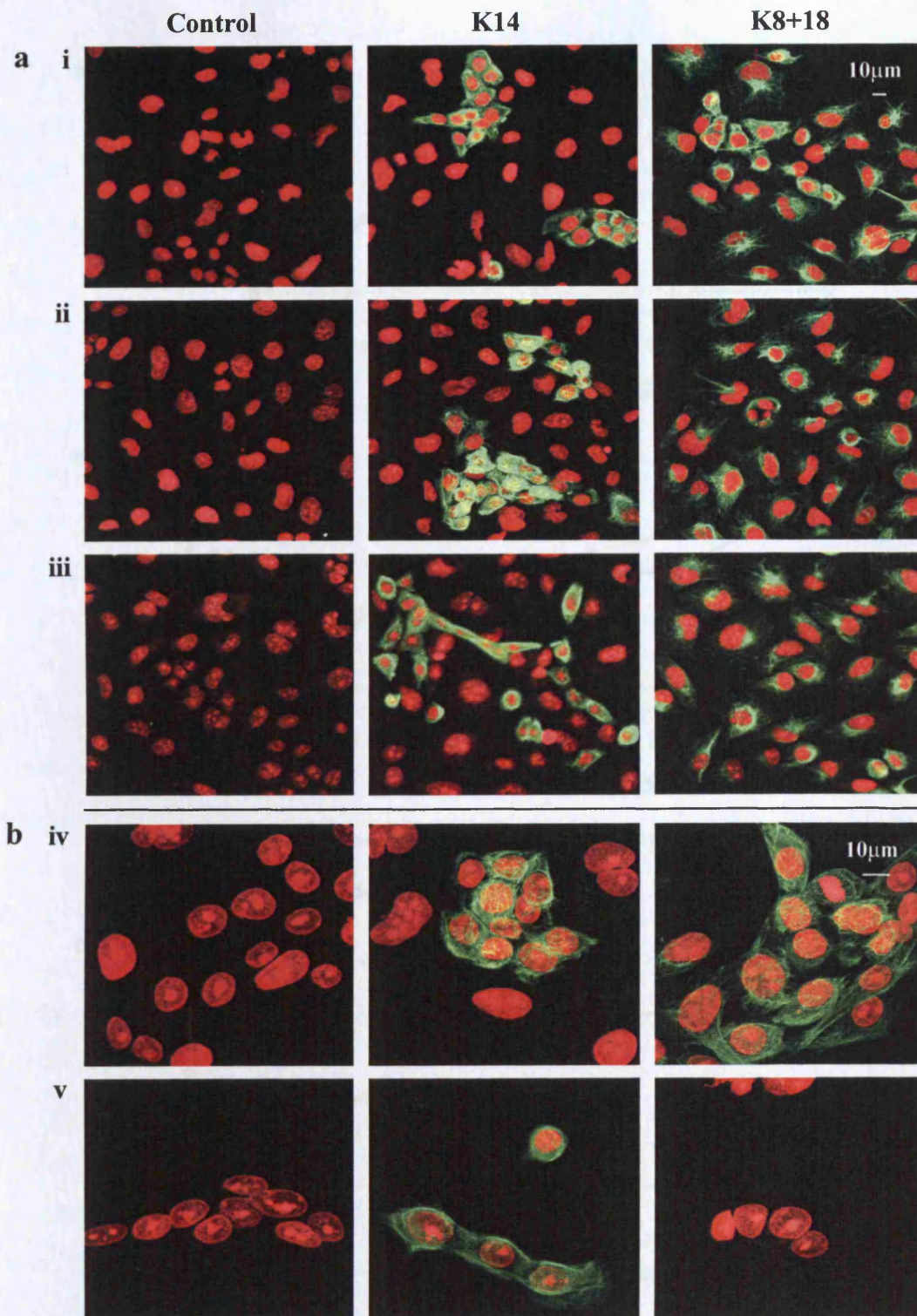


**Figure 3.2:** Immunocytochemical staining of cytokeratins in cultured keratinocytes: **(a)** optimisation of cellular fixation, where **(i)** 50:50% (v/v) acetone: methanol, **(ii)** 100% methanol and **(iii)** 4%(v/v) formaldehyde in PBS pH7.6, and **(b)** comparison of cytokerin staining in **(iv)** THEK and **(v)** NHEK cells. Confocal images show immunochemical localisation of no primary antibody (control), cytokerin 14 (K14) and cytokerin 8+18 (K8+18), as demonstrated by indirect fluorescence using goat anti-mouse (Fab specific) conjugated to FITC secondary antibody. The images represent the combined scans at 488nm for the FITC fluorochrome, seen as green fluorescence and 568nm for propidium iodide DNA counterstain, seen as red fluorescence.

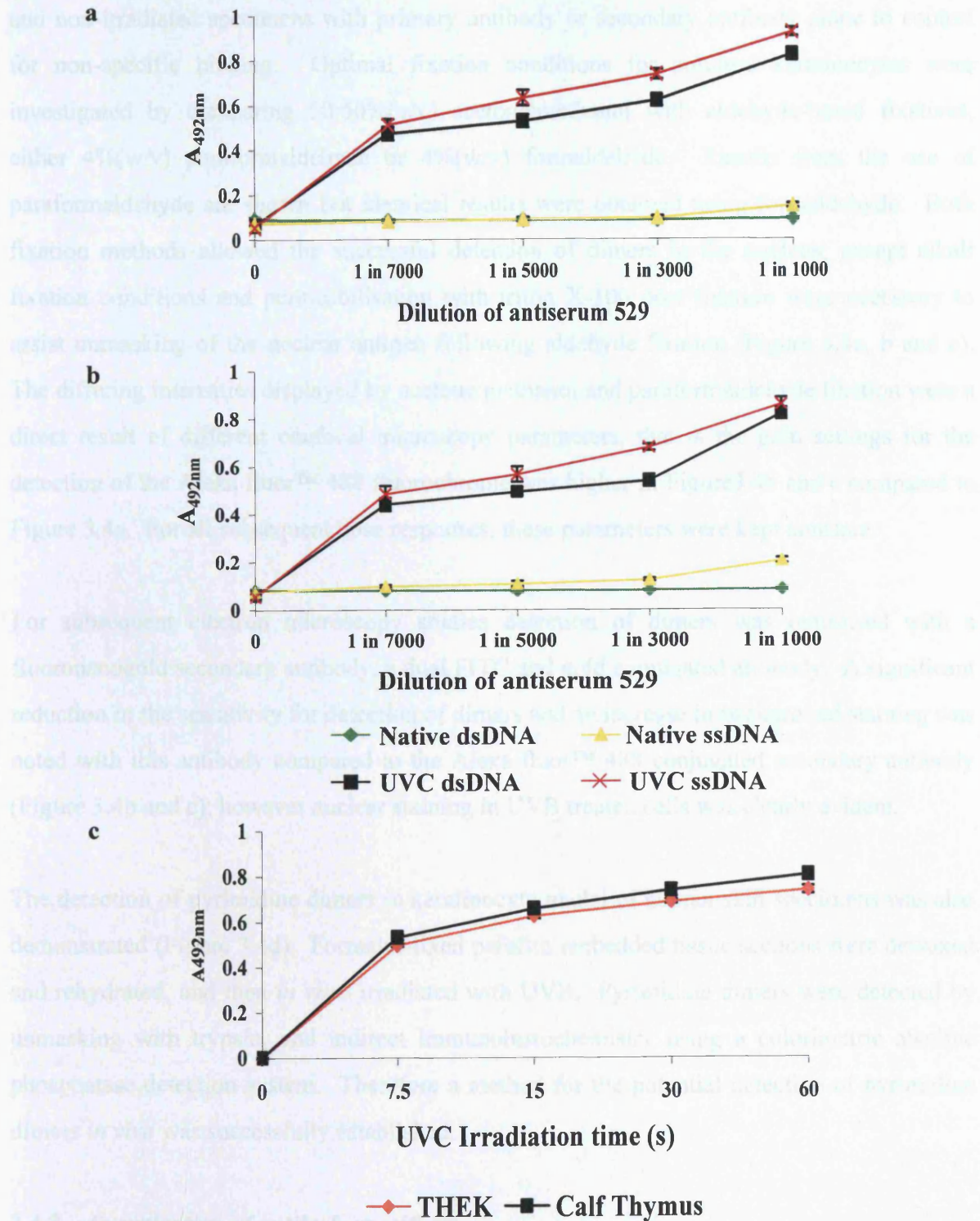


**Figure 3.3:** Optimisation of pyrimidine dimer ELISA with native and UVC irradiated calf thymus double-stranded DNA (dsDNA) and single-stranded DNA (ssDNA) as solid phase antigens, an assessment of non-coated (a) and poly-L-lysine pre-coated (b) ELISA plates. Pyrimidine dimer formation in THEK DNA and calf thymus DNA, a comparison of antigenicity detected with antiserum 529 diluted 1 in 5000 (c). The values represent the mean ( $\pm$  standard deviation) spectrophotometric absorbance at 492nm of three measurements.

Immunochemical detection of pyrimidine dimers in cells and tissues was optimised (Figure 3.4). For all immunochemical approaches controls included incubating both UVB irradiated and non-irradiated specimens with primary antibody or secondary antibody alone to control for non-specific binding. Optimal fixation conditions for cultured keratinocytes were investigated by comparing 50:50%(v/v) acetone:methanol with aldehyde-based fixatives, either 4%(w/v) paraformaldehyde or 4%(w/v) formaldehyde. Results from the use of paraformaldehyde are shown but identical results were obtained using formaldehyde. Both fixation methods allowed the successful detection of dimers in the nucleus, except alkali fixation conditions and permeabilisation with triton X-100 post fixation were necessary to assist unmasking of the nuclear antigen following aldehyde fixation (Figure 3.4a, b and c). The differing intensities displayed by acetone:methanol and paraformaldehyde fixation were a direct result of different confocal microscopy parameters, that is the gain settings for the detection of the Alexa fluor™ 488 fluorochrome was higher in Figure 3.4b and c compared to Figure 3.4a. For all subsequent dose responses, these parameters were kept constant.

For subsequent electron microscopy studies detection of dimers was optimised with a fluoronanogold secondary antibody, a dual FITC and gold conjugated antibody. A significant reduction in the sensitivity for detection of dimers and an increase in background staining was noted with this antibody compared to the Alexa fluor™ 488 conjugated secondary antibody (Figure 3.4b and c); however nuclear staining in UVB treated cells was clearly evident.

The detection of pyrimidine dimers in keratinocyte nuclei of human skin specimens was also demonstrated (Figure 3.4d). Formalin-fixed paraffin embedded tissue sections were dewaxed and rehydrated, and then *in vitro* irradiated with UVB. Pyrimidine dimers were detected by unmasking with trypsin, and indirect immunohistochemistry using a colorimetric alkaline phosphatase detection system. Therefore a method for the potential detection of pyrimidine dimers *in vivo* was successfully established.

### **3.4.3 Investigation of antibody specificity**

A rabbit antiserum raised against UVC irradiated calf thymus DNA was previously described to detect pyrimidine dimers, more specifically thymine dimers with an adjacent thymine (Herbert *et al.*, 1994<sup>2</sup>). In order to investigate the specificity further, transformed keratinocytes and calf thymus DNA irradiated with 305nm ( $\pm$  4.5nm) UVB were treated with increasing doses of 313nm ( $\pm$  4.5nm) UVB to induce photoisomerisation of 6-4 photoproduct to the Dewar isomer (Figure 3.5).

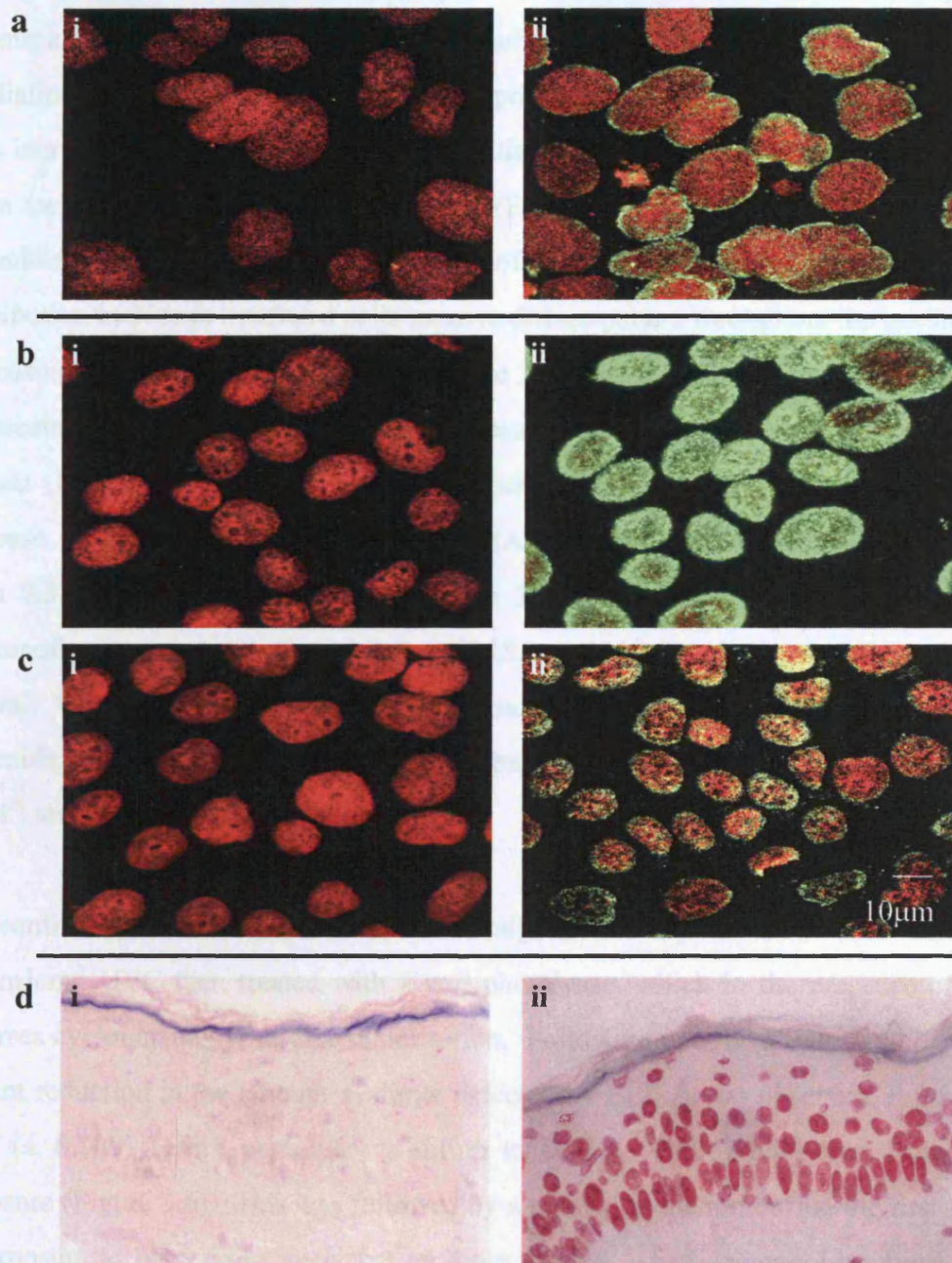


**Figure 3.4:** Immunochemical detection of cyclobutane pyrimidine dimers in transformed human keratinocytes (**a, b and c**) and formalin-fixed paraffin embedded human skin sections (**d**). Keratinocytes were sham treated (**i**) or irradiated with 305nm UVB (**ii**) and fixed in either 50%(v/v) acetone:methanol (**a**) or 4%(w/v) paraformaldehyde (**b and c**). The presence of pyrimidine dimers demonstrated by indirect immunofluorescence staining using an Alexa fluor™ 488 conjugated goat anti-rabbit IgG secondary antibody (**a and b**) or goat anti-rabbit IgG Fab-fluoronangold secondary antibody (**c**) in the presence of propidium iodide DNA counterstain. Formalin-fixed paraffin embedded skin sections were dewaxed and rehydrated through graded alcohols and irradiated with UVB in PBS. Control (**i**) and UVB treated (**ii**) sections were unmasked with trypsin and cyclobutane pyrimidine dimers were detected for light microscopy by goat anti-biotin secondary antibody and a Streptavidin biotin amplification system conjugated to horseradish peroxidase. Peroxidase activity was detected with Fast Red TR-Naphthol AS-MX and nuclei counterstained with haematoxylin blue (**d**, x300 magnification).

Reactivity of the antiserum to 6-4 photoproduct would have been demonstrated by a reduction of immunostaining observed in 305nm irradiated cells following increasing 313nm UVB irradiations, indicating the loss of 6-4 photoproduct. Instead an increase in antibody binding with increasing dose of 313nm UVB irradiation was observed in both 305nm pretreated and sham treated cells (Figure 3.5a) and DNA (Figure 3.5b), since 313nm continued to induce pyrimidine dimers. The nuclear appearance of immunofluorescence changed from a speckled distribution in 305nm irradiated cells to more diffuse pattern throughout the nucleus following increasing doses of 313nm irradiation (Figure 3.5a, panel 1). In control cells (without 305nm pre-treatment) a similar dose dependent increase in diffuse nuclear staining was observed with 313nm (Figure 3.5a, panel 2). In DNA increasing doses in 313nm irradiation caused an increase in spectrophotometric absorbance ( $A_{492nm}$ ) from 0.12 to 0.63 in control DNA and from 0.51 to 0.65 in DNA pretreated with 305nm (Figure 3.5b). The results from both immunofluorescence and direct binding ELISA experiments demonstrated good correlation. Overall the results suggested the main reactivity of the antiserum was to cyclobutane pyrimidine dimer, more specifically cyclobutane thymine dimers (CTDs, Herbert *et al.*, 1994<sup>2</sup>) and not to 6-4 photoproduct.

To confirm that CTD was indeed the antigen, calf thymus DNA was irradiated with  $20.1mJcm^{-2}$  UVC then treated with *E.coli* photolyase, which in the presence of black light reverses cyclobutane pyrimidine dimerisation. Following treatment with *E.coli* photolyase an instant reduction in the amount of dimer detected by ELISA was observed, from an  $A_{492nm}$  of  $0.83 (\pm 0.009)$  before photolyase addition to  $0.27 (\pm 0.006)$  following 1min black light exposure (Figure 3.6). This was followed by a gradual reduction during the first few minutes of exposure to black light, such that by 4min the  $A_{492nm}$  had decreased by more than 5 fold. Further addition of photolyase at 4 min had little effect. Similar results were obtained with native DNA, background CTDs were instantaneously reversed following the first addition of *E.coli* photolyase at 0 min (Figure 3.6). The spectrophotometric absorbance of UVC irradiated DNA did not quite reach native DNA levels post addition of *E.coli* photolyase and prolonged exposure to black light. This difference, albeit small ( $\approx 0.05$  absorbance units at 492nm), may be due to some immunoreactivity of the antiserum to other UVC lesions, such as oxidative DNA adducts and DNA strand breaks. Alternatively, this difference may be explained by the inability of the *E.coli* photolyase enzyme to efficiently reverse dimerization of all pyrimidine dimers for example in certain sequence context.

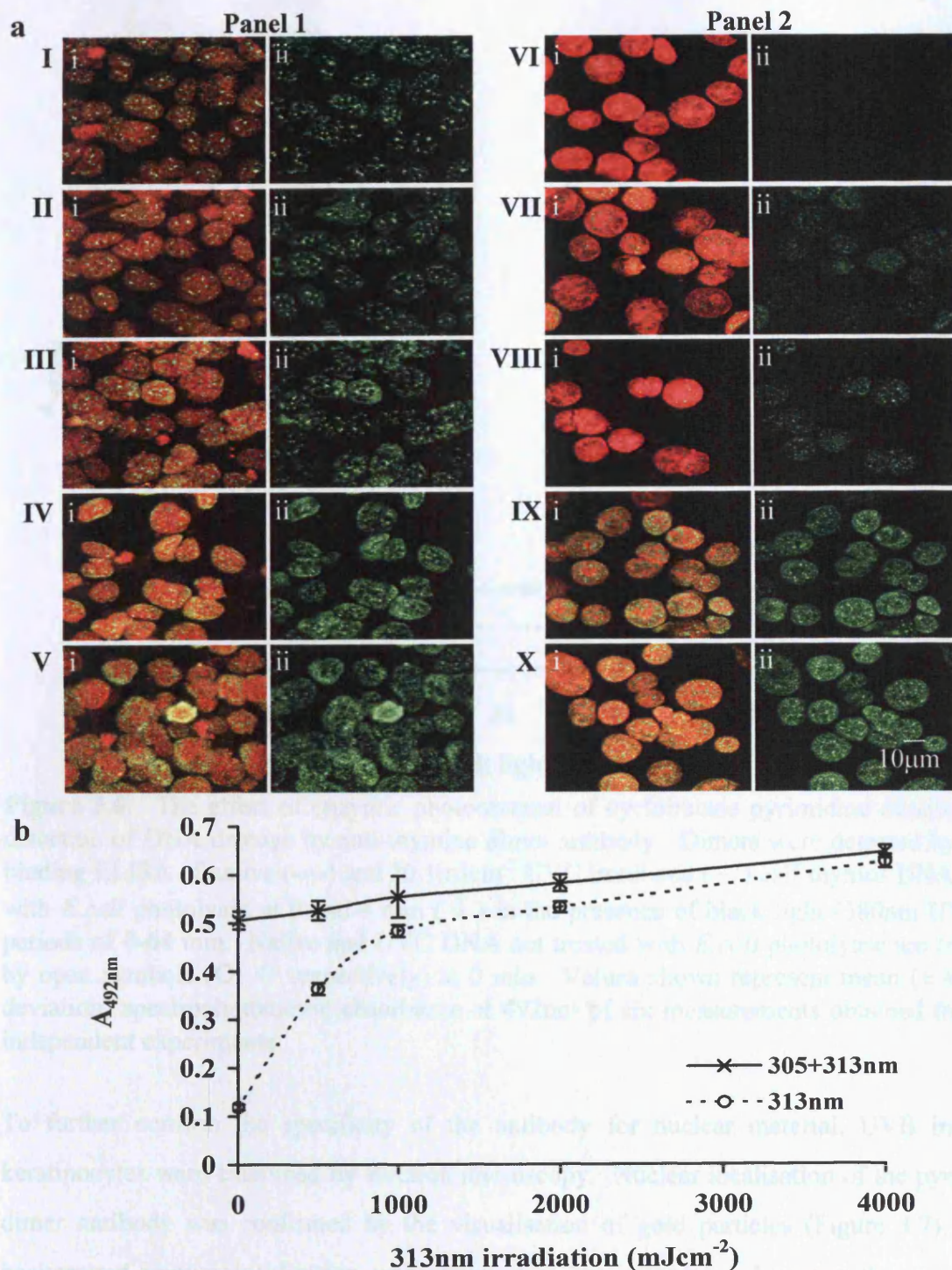


**Figure 3.5** The effect of photoisomerisation on the immunochemical detection of pyrimidine dimers. (a) immunocytochemical detection of pyrimidine dimers in transformed human keratinocytes after pretreatment (**Panel 1**) and no pretreatment (**Panel 2**) with  $25\text{mJcm}^{-2}$  305nm followed by doses of 313nm:  $0\text{mJcm}^{-2}$  (**I and VI**),  $500\text{mJcm}^{-2}$  (**II and VII**),  $1000\text{mJcm}^{-2}$  (**III and VIII**),  $2000\text{mJcm}^{-2}$  (**IV and IX**) and  $4000\text{mJcm}^{-2}$  (**V and X**). The presence of pyrimidine dimers was demonstrated by indirect immunofluorescence staining using an Alexa fluor™ 488 conjugated goat anti-rabbit IgG secondary antibody, in the presence (i) and absence (ii) of propidium iodide DNA counterstain. (b) ELISA detection of pyrimidine dimers in single-stranded calf thymus DNA with (—x—) and without (---o---) pretreatment with  $25\text{mJcm}^{-2}$  305nm UVB followed by doses of 313nm for described above transformed keratinocyte. Values shown represent mean ( $\pm$  standard deviation) spectrophotometric absorbance at 492nm of six measurements from two independent experiments.

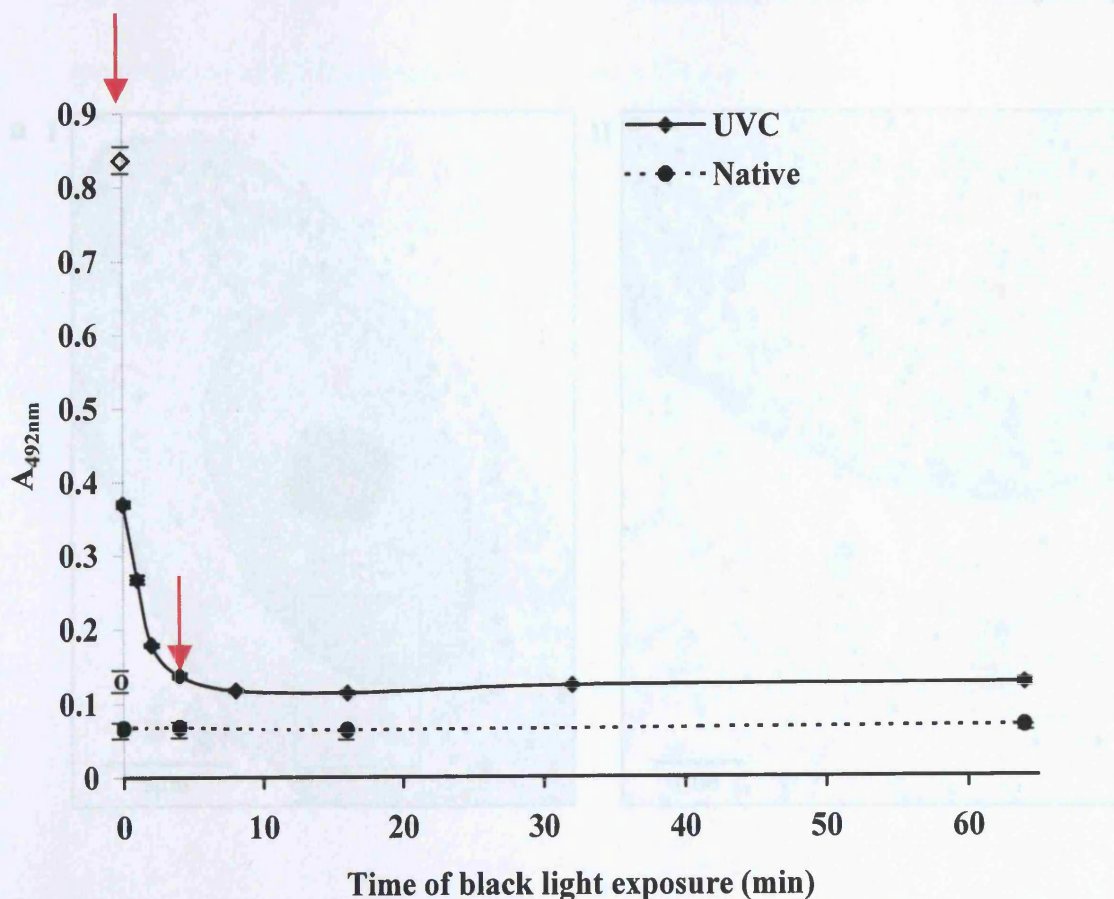


**Figure 3.6:** The effect of enzymic photoreversal of cyclobutane pyrimidine dimers on the detection of DNA damage by anti-thymine dimer antibody. Dimers were detected by direct-binding ELISA of native (----) and  $20.1\text{mJcm}^{-2}$  UVC irradiated (—) calf thymus DNA treated with *E.coli* photolyase at 0 and 4 min ( $\downarrow$ ) in the presence of black light (380nm UVA) for periods of 0-64 min. Native and UVC DNA not treated with *E.coli* photolyase are indicated by open symbols (O,  $\diamond$  respectively) at 0 min. Values shown represent mean ( $\pm$  standard deviation) spectrophotometric absorbance at 492nm of six measurements obtained from two independent experiments.

To further confirm the specificity of the antibody for nuclear material, UVB irradiated keratinocytes were examined by electron microscopy. Nuclear localisation of the pyrimidine dimer antibody was confirmed by the visualisation of gold particles (Figure 3.7). Some background immunolocalisation was observed in the cytoplasm, however the majority of staining was detected in the nucleus. These results were similar to those seen with confocal microscopy, specimens stained using the fluoronanogold secondary antibody demonstrated some background cytoplasmic staining (Figure 3.4c). Also, the alkaline fixation conditions and the permeabilisation steps resulted in some loss of cellular ultrastructure, such as the mitochondria. The granular region of the nucleolus (pars granulosa), the centre for RNA production, however showed no staining above background levels as anticipated. Similar staining profiles were observed in both NHEK and THEK following UVB irradiation (Figure 3.7a and b, respectively).

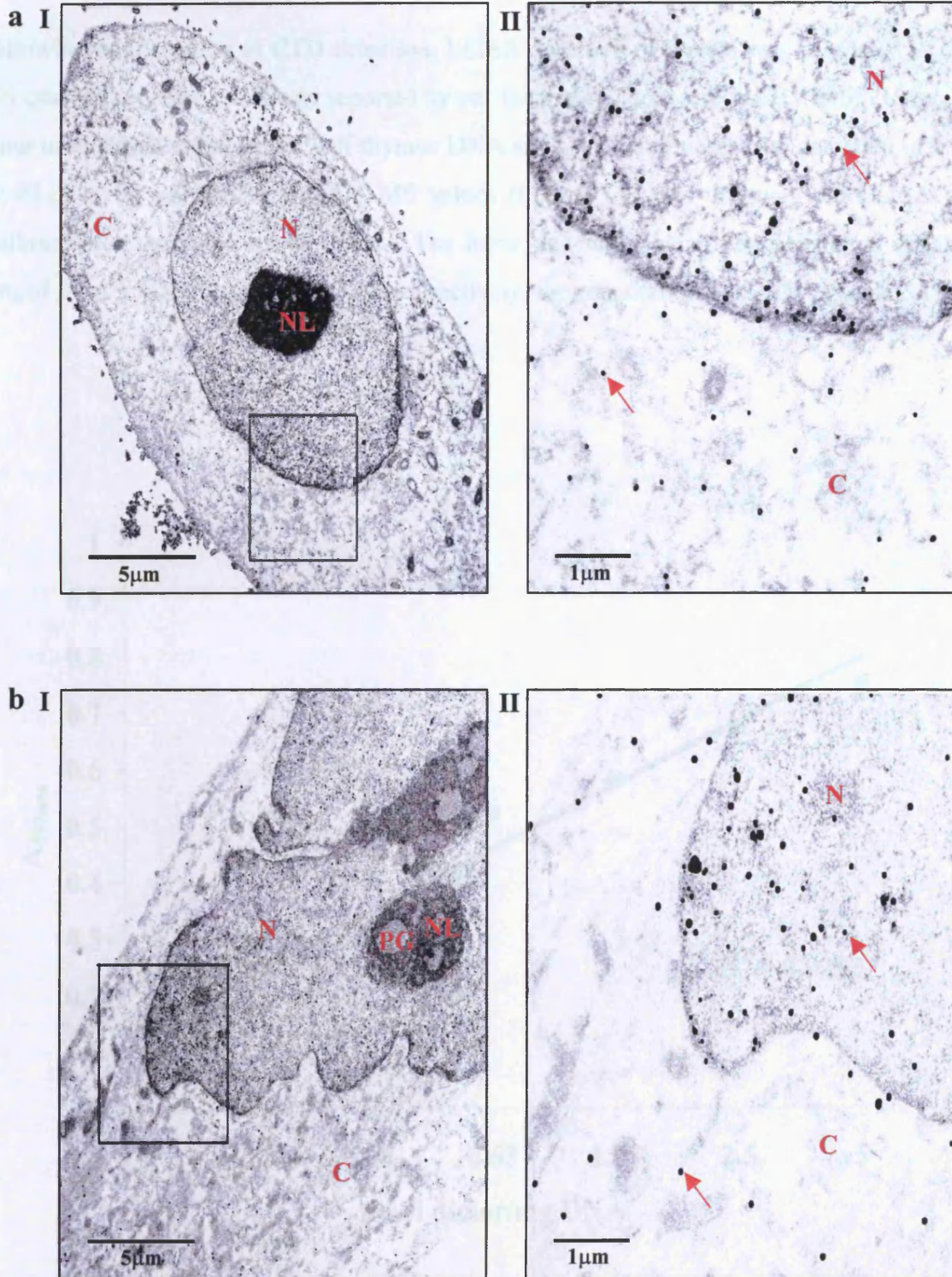


**Figure 3.7:** Ultrastructural localisation of the pyrimidine dimer antibody in NHEK (a) and THEK (b) cells irradiated with UVB. Electron micrographs show visualisation of pyrimidine dimers with nanogold conjugated goat anti-rabbit secondary antibody, appearing as black dots. Low magnification images (I) show the gross cellular infrastructure: the cytoplasm (C), nucleus (N), nucleolus (NL) and pars granulosa (PG). Higher magnification (II) shows the distribution of gold particles (as indicated by arrows) in the nucleus relative to the cytoplasm.

### 3.4.4 Quantitation of CTD formation in DNA by 305nm and 315nm UV

Following confirmation of CTD detection, ELISA detection of dimers was compared to GC-MS quantitation data previously reported by our laboratory (Podmore *et al.*, 1996). Using the same irradiation conditions for calf thymus DNA and UVC lamp described, detection of CTD by ELISA was correlated with GC-MS values (Figure 3.8). In this way the ELISA was calibrated for the detection of CTDs. The intra- and inter- batch coefficients of variation ranged from 3.9-5.1% and 12.1-17.5% respectively, for quantitation by ELISA (Table 3.1).

15	36.4	30.0	1.33	3.9	2.1
30	196.9	78.0	2.50	4.4	17.5
60	383.8	156.0	2.40	3.7	14.9

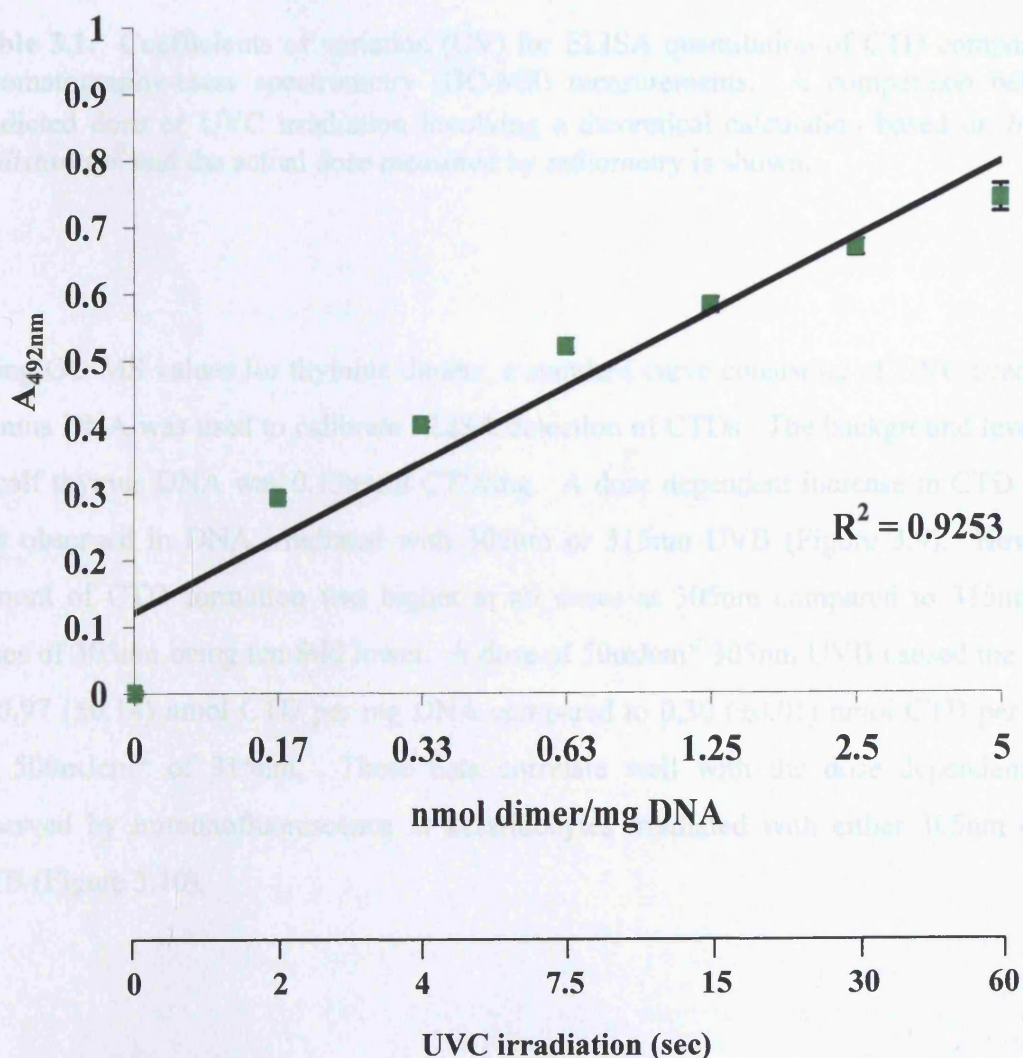


**Figure 3.8:** Comparison of CTD detection by ELISA with gas chromatography-mass spectrometry (GC-MS) values. All values represent background corrected mean ( $\pm$  standard deviation) spectrophotometric absorbance at 492nm.

UVC irradiation details			GC-MS quantitation	ELISA quantitation CV (%)	
Time (sec)	Theoretical dose (mJcm <sup>-2</sup> )	Actual dose (mJcm <sup>-2</sup> )	nmol CTD/mg DNA	Intra- (n=4)	Inter- (n=3)
0	0	0	0	5.0	15.8
7.5	49.2	19.5	0.63	4.9	12.1
15	98.4	39.0	1.25	3.9	12.1
30	196.9	78.0	2.50	4.4	17.5
60	393.8	156.0	5.00	5.1	14.9

**Table 3.1:** Coefficients of variation (CV) for ELISA quantitation of CTD compared to gas chromatography-mass spectrometry (GC-MS) measurements. A comparison between the predicted dose of UVC irradiation involving a theoretical calculation based on  $Intensity \propto 1/(distance)^2$  and the actual dose measured by radiometry is shown.

Using GC-MS values for thymine dimers, a standard curve consisting of UVC irradiated calf thymus DNA was used to calibrate ELISA detection of CTDs. The background level of CTD in calf thymus DNA was 0.13nmol CTD/mg. A dose dependent increase in CTD formation was observed in DNA irradiated with 305nm or 315nm UVB (Figure 3.9). However, the amount of CTD formation was higher at all doses at 305nm compared to 315nm, despite doses of 305nm being ten fold lower. A dose of 50mJcm<sup>-2</sup> 305nm UVB caused the formation of 0.97 (±0.14) nmol CTD per mg DNA compared to 0.30 (±0.01) nmol CTD per mg DNA for 500mJcm<sup>-2</sup> of 315nm. These data correlate well with the dose dependent increase observed by immunofluorescence in keratinocytes irradiated with either 305nm or 315nm UVB (Figure 3.10).

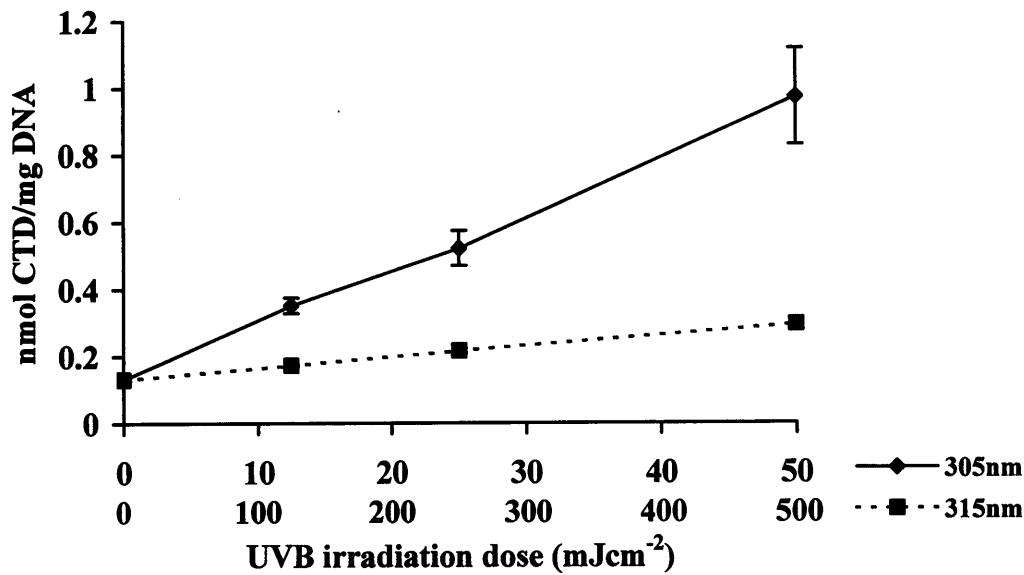


**Figure 3.9:** Quantitation of CTD by ELISA. Dimers detected in calf thymus DNA irradiated with 12.5, 25 and 50mJcm<sup>-2</sup> of 305nm (—), or 125, 250 and 500mJcm<sup>-2</sup> 315nm (----) UVB. Values shown represent mean (± standard deviation) nmol CTD/mg DNA of three measurements.

### 3.4.5 Comparison of CTD formation in cultured keratinocytes following 305nm and 315nm irradiation

NHEK and THEK cultured on chambered slides were irradiated with 305nm or 315nm UVB. Cells were stained for CTD following 50:50%(v/v) acetone:methanol fixation (see section 3.4.2) and confocal images taken. A clear distinction in the amount of nuclear CTD was observed, with irradiations at 305nm generating significantly more dimers compared to irradiations at 315nm (Figure 3.10a). Little dimer was observed in transformed keratinocytes with 25mJcm<sup>-2</sup> 315nm whilst clear punctate nuclear staining was observed with the same dose at 305nm (Figure 3.10a IV and II respectively). Some nuclear staining was observed with 250mJcm<sup>-2</sup> 315nm (Figure 3.10a V) but significantly lower compared to 25mJcm<sup>-2</sup> 305nm or 250mJcm<sup>-2</sup> 305nm (Figure 3.10a II and III). Similar results were obtained with NHEK cells (Figure 3.10b); only a small amount of staining was observed with 315nm UVB compared to cells irradiated with 305nm with a tenth of the dose.

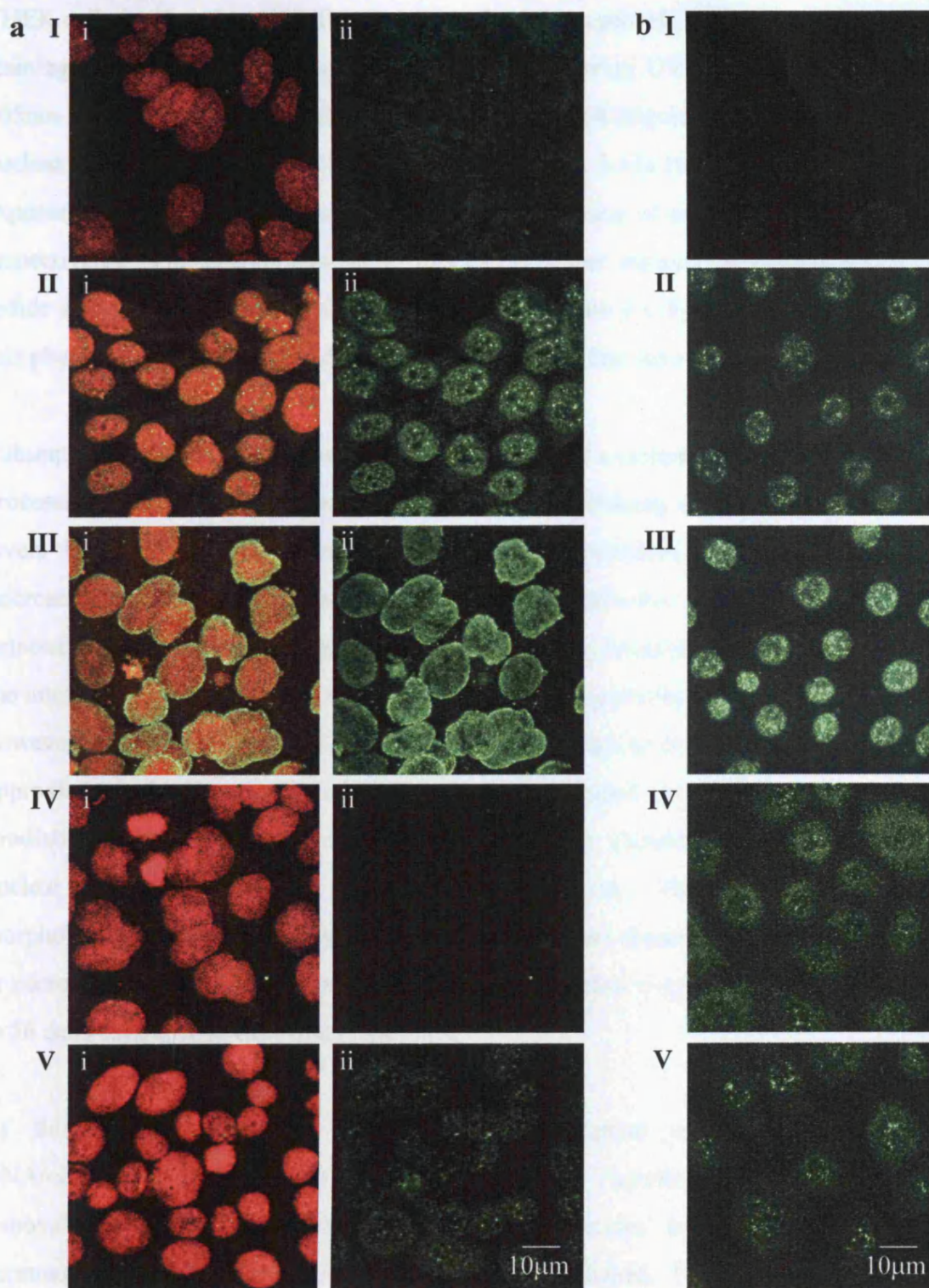


**Figure 3.10:** Immunofluorescence comparison of CTD formation with 305nm and 315nm UVB irradiation. CTD in: (a) THEK cells following sham irradiation (I) and doses of  $25\text{mJcm}^{-2}$  305nm (II),  $250\text{mJcm}^{-2}$  305nm (III),  $25\text{mJcm}^{-2}$  315nm (IV) and  $250\text{mJcm}^{-2}$  315nm (V). The presence of CTDs was demonstrated by indirect immunofluorescence using an Alexa fluor<sup>TM</sup> 488 conjugated goat anti-rabbit IgG secondary antibody, in the presence (i) and absence (ii) of propidium iodide DNA counterstain; (b) NHEK cells following sham irradiation (I) and doses of  $25\text{mJcm}^{-2}$  305nm (II),  $50\text{mJcm}^{-2}$  305nm (III),  $250\text{mJcm}^{-2}$  315nm (IV) and  $500\text{mJcm}^{-2}$  315nm (V).

#### **3.4.6 Immunofluorescence investigation of repair kinetics of pyrimidine dimers**

THEK cells irradiated with UVB were assessed for the repair of CTD by immunofluorescence staining and confocal microscopy. Immediately following UV irradiations with  $25\text{mJcm}^{-2}$  305nm UVB clear punctate nuclear staining was observed (Figure 3.11a II). Disappearance of nuclear staining for CTD was observed by 12hr (Figure 3.11a III), at 12 and 24hr post UVB exposure extra-nuclear DNA was detected in the cytoplasm of cells (Figure 3.11a III and IV respectively). On closer examination this extra-nuclear staining of DNA with propidium iodide was accompanied by dual staining for CTD (Figure 3.11b). Generally cells displaying this phenomenon exhibited 1-3 defined areas of extranuclear staining.

Subsequent immunoelectron microscopy studies showed a comparable repair profile for CTD processing, with most nuclei demonstrating no distinct staining difference above background levels by 12hr post UVB exposure (personal communications Dr Dinsdale, electron microscopy analyst). Unlike confocal microscopy, no definitive extra-nuclear DNA could be detected in the cytoplasm of irradiated cells at any of the timepoints analysed, perhaps due to the immunostaining parameters which would tend to compromise fine structure. Interestingly however, in routine electron microscopy preparations nuclear evaginations were observed in approximately 11.5% cells (in a total of 61 cells) examined at 24hr following 305nm UVB irradiation (Figure 3.12). Ultrastructurally this cellular phenomenon was accompanied by nuclear envelope swelling but only at the 'blebbing' site. The remainder of the cellular morphology appeared essentially 'normal' with no distinct characteristics typical of apoptosis or necrosis. At 0, 6 and 12hr post UVB exposure no nuclear evaginations were detected in 54 to 56 cells examined at each timepoint.

At this point the paucity of data in the literature on processing of excised DNA/oligonucleotides in human cells became apparent. Therefore, in order to investigate the removal of CTD in the form 'excised repair oligonucleotides' from UVB irradiated cultured keratinocytes, a competition ELISA approach was established. Firstly, a suitable solid phase antigen and competitor were investigated (Figure 3.13). A comparison of UVC irradiated calf thymus DNA versus UVC irradiated THEK DNA as competitor against a solid phase antigen consisting of UVC irradiated DNA was initially performed. Both DNA sources produced similar inhibition profiles demonstrating little difference in the antigen and ability of antibody to recognise the adducts formed (Figure 3.13a). Secondly competitors irradiated with 7.5-120sec UVC were compared; for all UVC irradiated DNA preparations a dose dependent inhibition of antibody binding to solid phase antigen was evident (Figure 3.13b). Non-

irradiated DNA displayed poor inhibition, even at high concentrations of DNA. Furthermore, calculated IC50 values for each competitor clearly displayed a dose dependent inhibition (Figure 3.13b).

Further to these experiments, in order to confirm the potential measurement of nucleotide excision repair products by competition ELISA, the inhibition of CTD antibody binding to a UVC irradiated solid phase antigen was compared using 120sec UVC irradiated calf thymus DNA and a synthetic 30mer oligonucleotide containing a single CTD (Figure 3.13c). Although the oligonucleotide yielded a more consistent inhibition curve, perhaps due to better solution homogeneity of the smaller nucleic acids, the competitors displayed similar profiles of inhibition and therefore confirmed a competition ELISA approach to measure potential excised oligonucleotides.

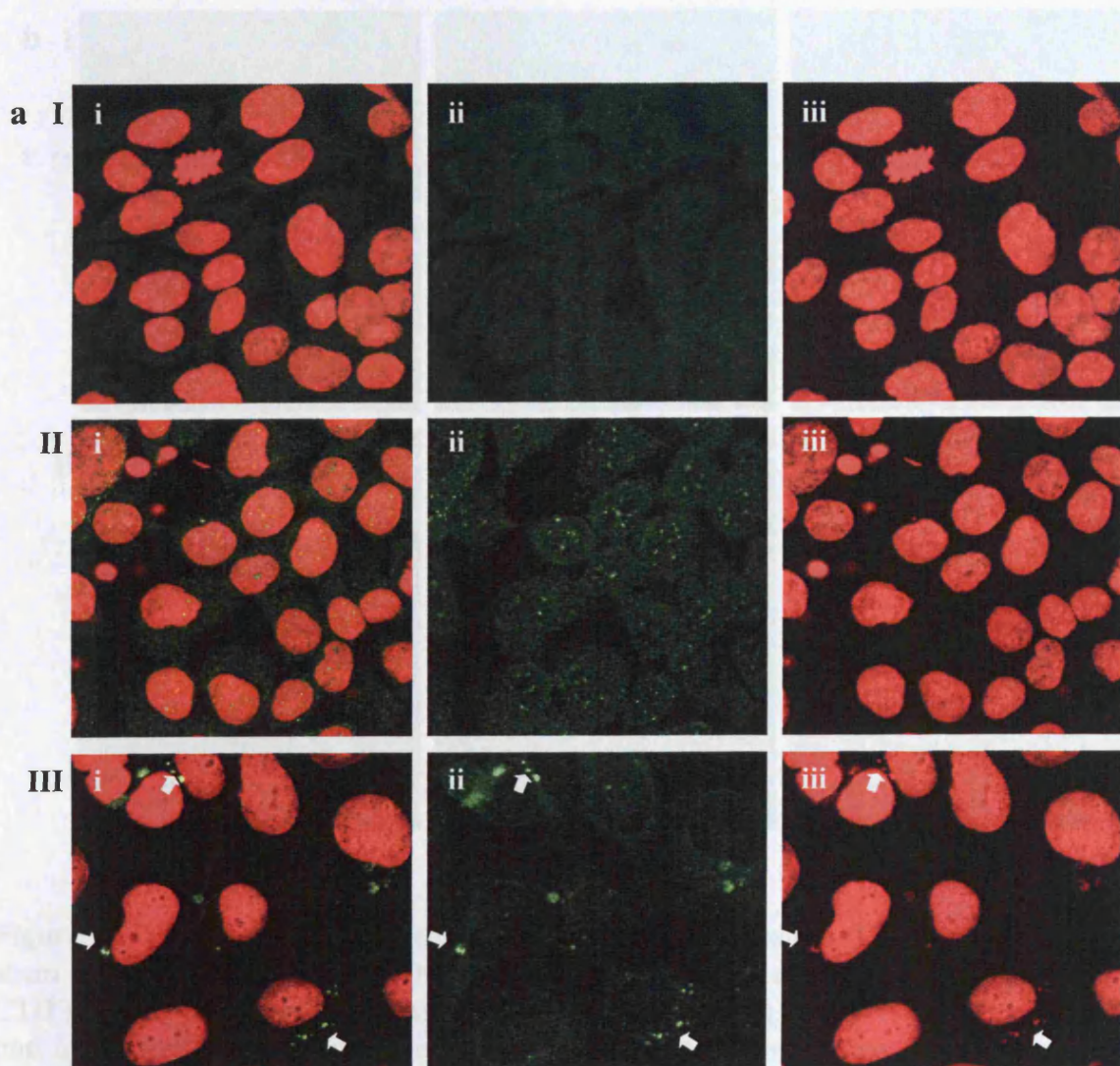


*Figure continued...*

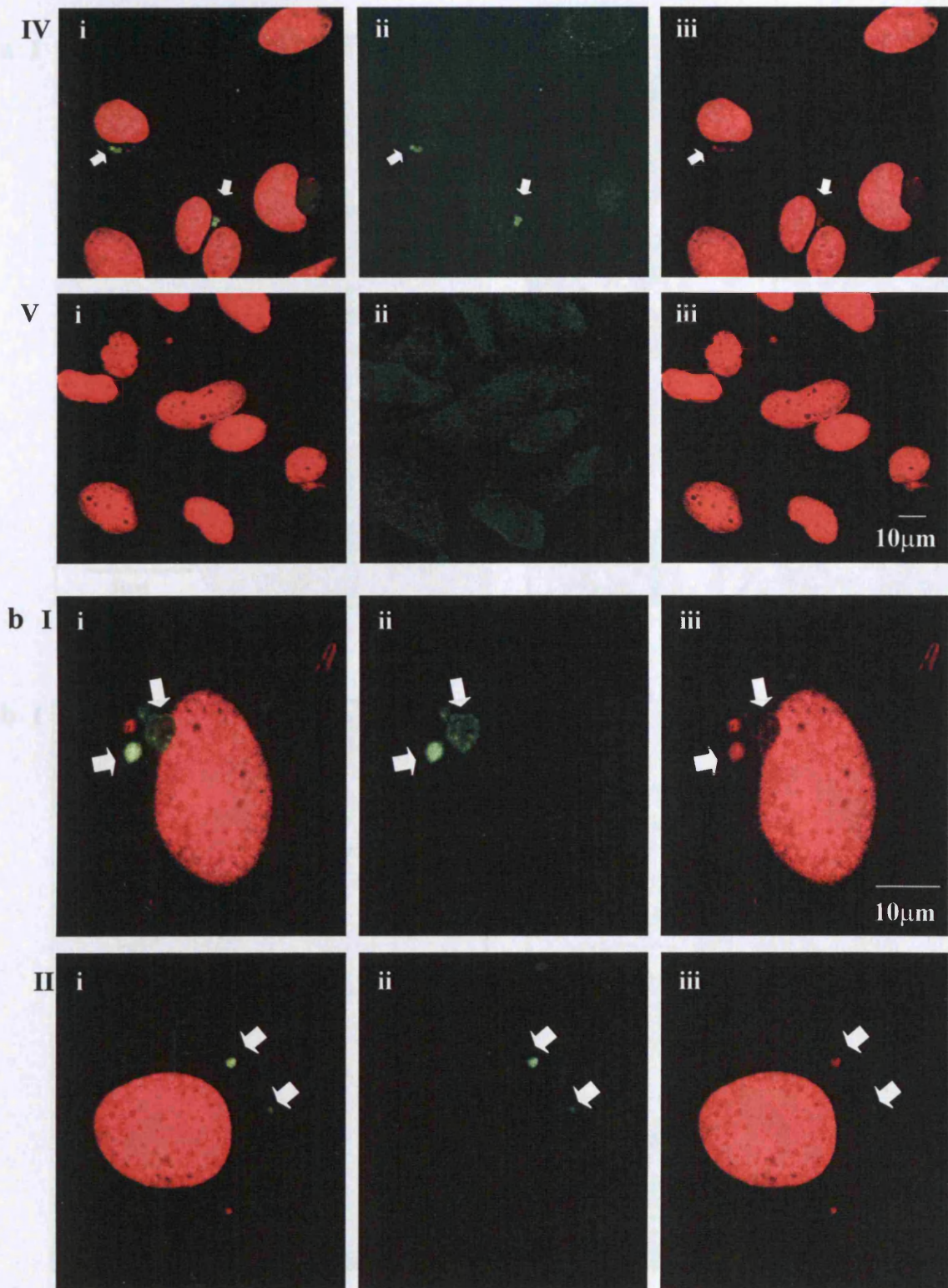


**Figure 3.11:** Immunofluorescence investigation of CTD repair in THEK cells. Cells were sham (**I**) or UVB irradiated at 305nm with a non-toxic dose of  $25\text{mJcm}^{-2}$  (**II**). Removal of CTD's in UVB irradiated cells was assessed by fixing at 0 (**II**), 12 (**III**), 24 (**IV**) and 48hr (**V**) post irradiation (**a**). The presence of CTDs was demonstrated by indirect immunofluorescence using an Alexa fluor<sup>TM</sup> 488 conjugated goat anti-rabbit IgG secondary antibody, in the presence (**i**) and absence (**ii**) of propidium iodide DNA counterstain; (**iii**) shows the DNA counter stain alone. Enlarged images of two cells demonstrating extra nuclear material typically observed only in cells at 12 (**I**) and 24hr (**II**) post UVB treatment (**b**).

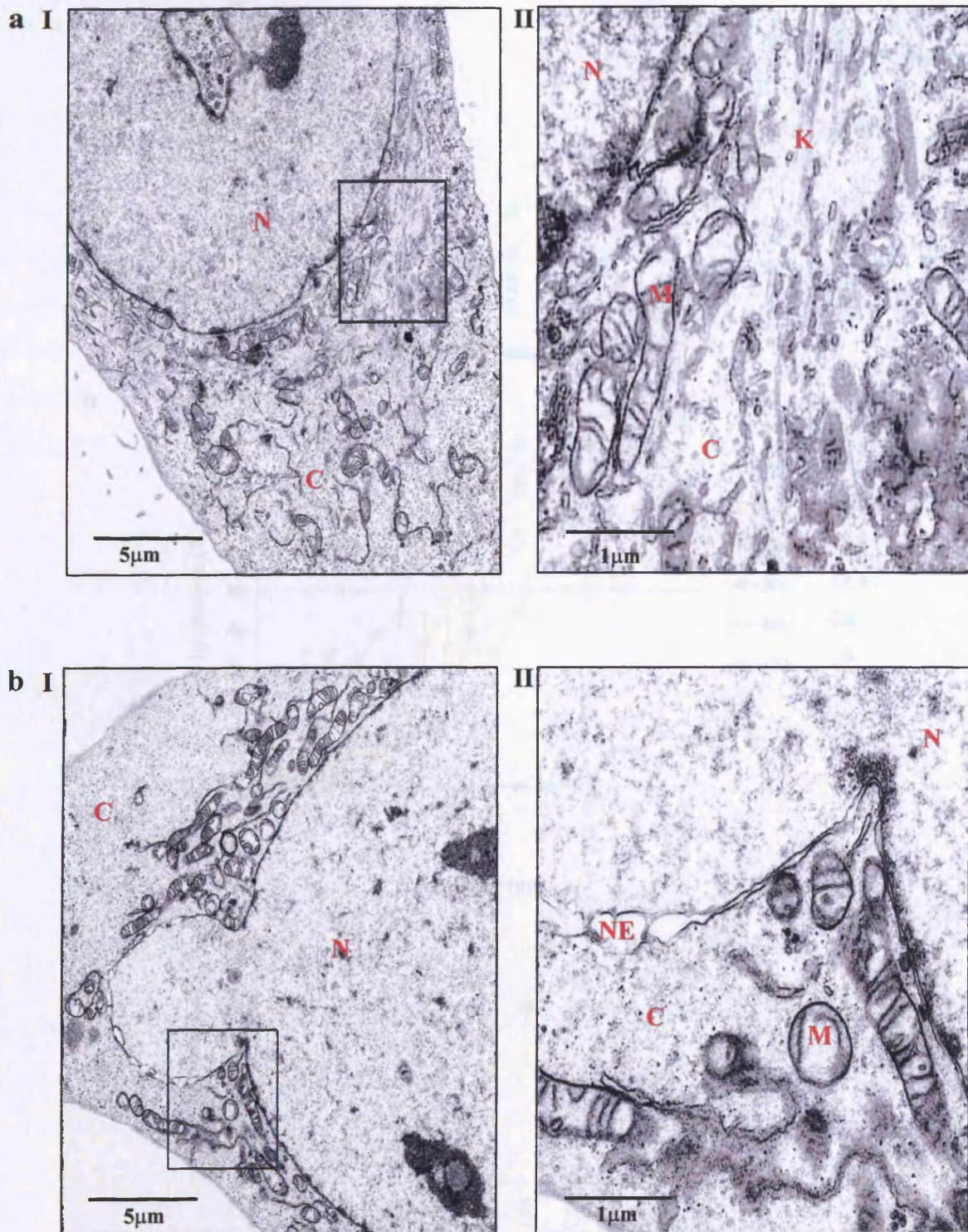


**Figure 3.12:** Changes in ultrastructure of THEK cells following UVB irradiation. Cells were sham (a) or UVB irradiated at 305nm with a non-toxic dose of  $25\text{mJcm}^{-2}$  (b). Following 24hr incubation post irradiation, cells were fixed in 2%(v/v) glutaraldehyde and post-fixed in 1%(w/v) osmium tetroxide, both prepared in 0.1M sodium cacodylate buffer (pH 7.3), then dehydrated and embedded in Epoxy resin for routine electron microscopy. Electron micrographs show changes in nuclear morphology at low magnification (I) and high magnification (II) of boxed area in (I): cytokeratins (K), cytoplasm (C), mitochondria (M), nucleus (N) and nuclear envelope (NE).

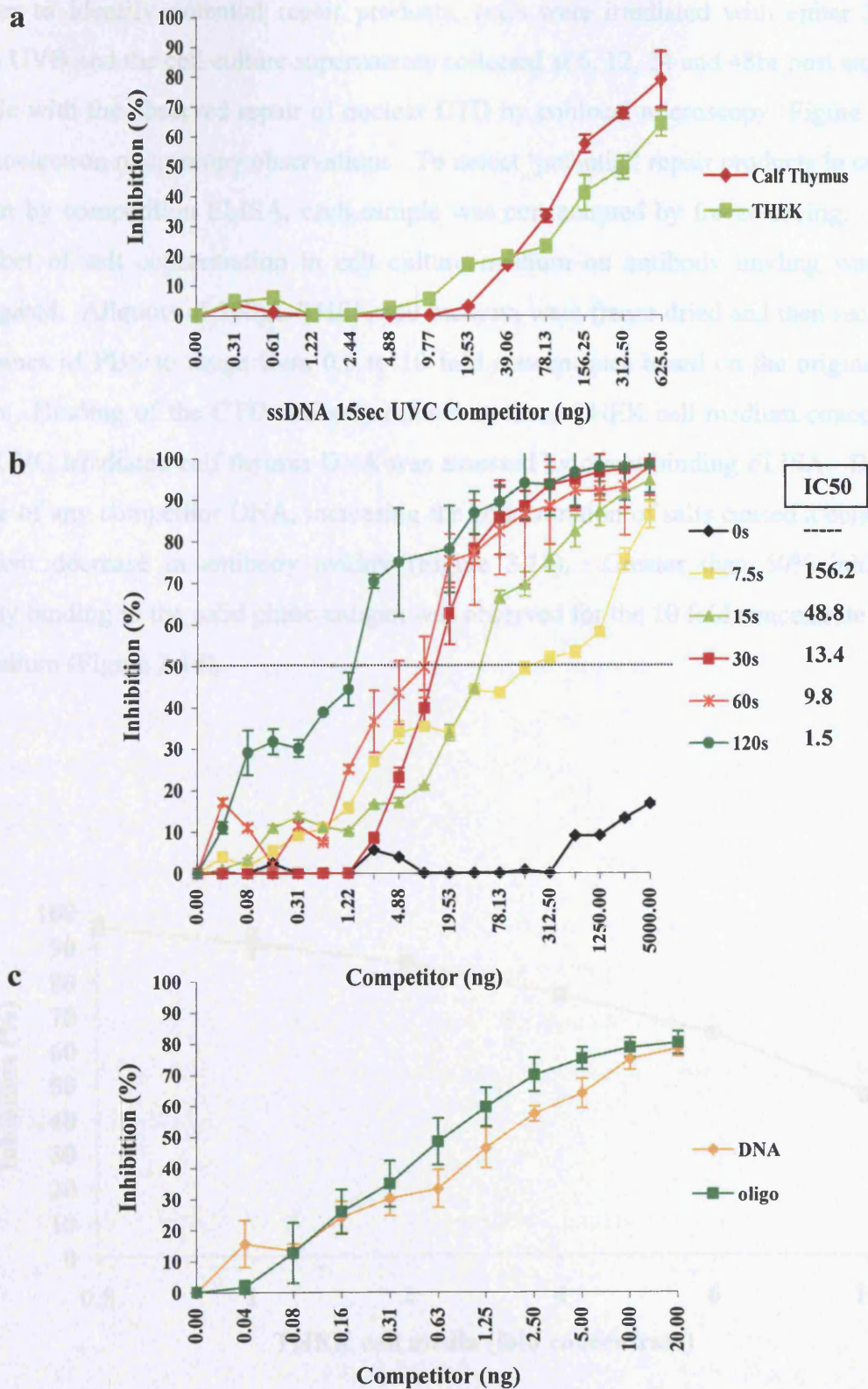


**Figure 3.13:** Optimisation of CTD competition ELISA using single-stranded 7.5sec UVC irradiated calf thymus DNA as solid phase antigen. A comparison of calf thymus DNA and DNA from THEK cells as competitors, both irradiated for 15sec with UVC (a), the differences in competition by calf thymus DNA irradiated with various UVC doses, ranging 0-120sec in irradiation time (b), and a comparison in competition of 120sec UVC irradiated calf thymus DNA with an oligonucleotide (30 nucleotides in length) containing a single CTD (c). The data represent the mean ( $\pm$  standard deviation) of the percentage inhibition of antibody binding calculated from three independent spectrophotometric absorbance readings at 492nm.

In order to identify potential repair products, cells were irradiated with either 305nm or 315nm UVB and the cell culture supernatants collected at 6, 12, 24 and 48hr post exposure, to coincide with the observed repair of nuclear CTD by confocal microscopy (Figure 3.11) and immunoelectron microscopy observations. To detect 'potential' repair products in cell culture medium by competition ELISA, each sample was concentrated by freeze-drying. Therefore the effect of salt concentration in cell culture medium on antibody binding was initially investigated. Aliquots of 300 $\mu$ L THEK cell medium were freeze dried and then reconstituted in volumes of PBS to range from 0.5 to 10 fold concentrates based on the original starting volume. Binding of the CTD antibody diluted in these THEK cell medium concentrates to 60sec UVC irradiated calf thymus DNA was assessed by direct-binding ELISA. Despite the absence of any competitor DNA, increasing the concentration of salts caused a concentration dependent decrease in antibody avidity (Figure 3.14). Greater than 50% inhibition of antibody binding to the solid phase antigen was observed for the 10 fold concentrate of THEK cell medium (Figure 3.14).

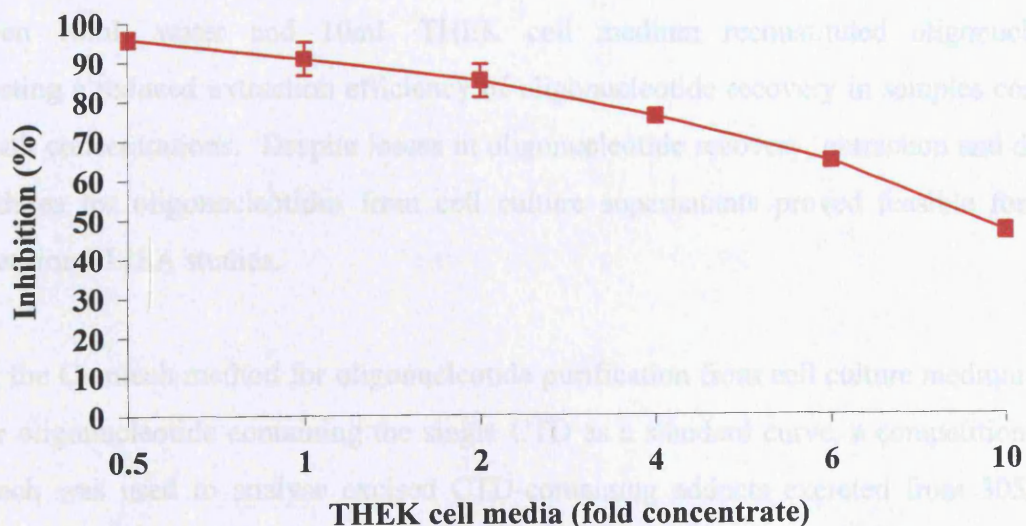


**Figure 3.14:** A direct-binding ELISA assessment of cell culture medium salt concentration on the binding of the CTD antibody to UVC treated DNA. Aliquots of 300 $\mu$ L THEK cell medium were freeze-dried and reconstituted in volumes PBS to range from 0.5 to 10 fold concentrates based on the original starting volume. Binding of CTD antibody, diluted in these THEK cell medium concentrates, to 60sec UVC irradiated calf thymus DNA was assessed. The data represent the mean ( $\pm$  standard deviation) of the percentage inhibition of antibody binding calculated from three independent spectrophotometric absorbance readings at 492nm.

To overcome any false positive competition ELISA data resulting from variations in salt concentration from cell culture medium, purification and desalting methods were investigated. Experiments used freeze-dried aliquots of 200µg 30mer oligonucleotide containing a single CTD. These were reconstituted in 200µL water. Reconstituted oligonucleotides for extraction were refreeze-dried and then extracted using a Clontech extraction kit or by a traditional sodium acetate/ethanol precipitation method. Both extraction techniques successfully isolated oligonucleotides to similar degrees of efficiency, with the Clontech procedure for extraction proving to be marginally better (Figure 3.15a). However, oligonucleotides from both techniques of extraction demonstrated some losses when compared with the no extraction (and no second freeze–drying step) control.

To further investigate the extent of oligonucleotide loss through freeze-drying procedures and the efficiency of desalting a larger volume of THEK cell medium, 200µg 30mer oligonucleotide containing a single CTD were reconstituted in 200µL or 10mL water, or 10mL THEK cell medium. Reconstituted oligonucleotides were subjected to a second freeze-drying step and then extracted using the Clontech kit. Some losses in oligonucleotide recovery were observed in samples reconstituted in 10mL of water when compared to oligonucleotides reconstituted in 200µL water (Figure 3.15b). Further losses were noted between 10mL water and 10mL THEK cell medium reconstituted oligonucleotides, suggesting a reduced extraction efficiency of oligonucleotide recovery in samples containing high salt concentrations. Despite losses in oligonucleotide recovery, extraction and desalting procedures for oligonucleotides from cell culture supernatants proved feasible for further competition ELISA studies.

Using the Clontech method for oligonucleotide purification from cell culture medium and the 30mer oligonucleotide containing the single CTD as a standard curve, a competition ELISA approach was used to analyse excised CTD-containing adducts excreted from 305nm and 315nm UVB irradiated transformed keratinocytes. Cell culture medium samples were collected over a 48hr period post irradiation, then purified and analysed by competition ELISA. Data revealed little difference in the percentage inhibition detected by competition ELISA in medium extracts from both irradiated and non-irradiated cells (Figure 3.16). Samples collected at 48hr demonstrated some increase in inhibition and possible release of excised repair oligonucleotides, however only in THEK cells irradiated with 315nm UVB. Further studies are required to validate these findings.

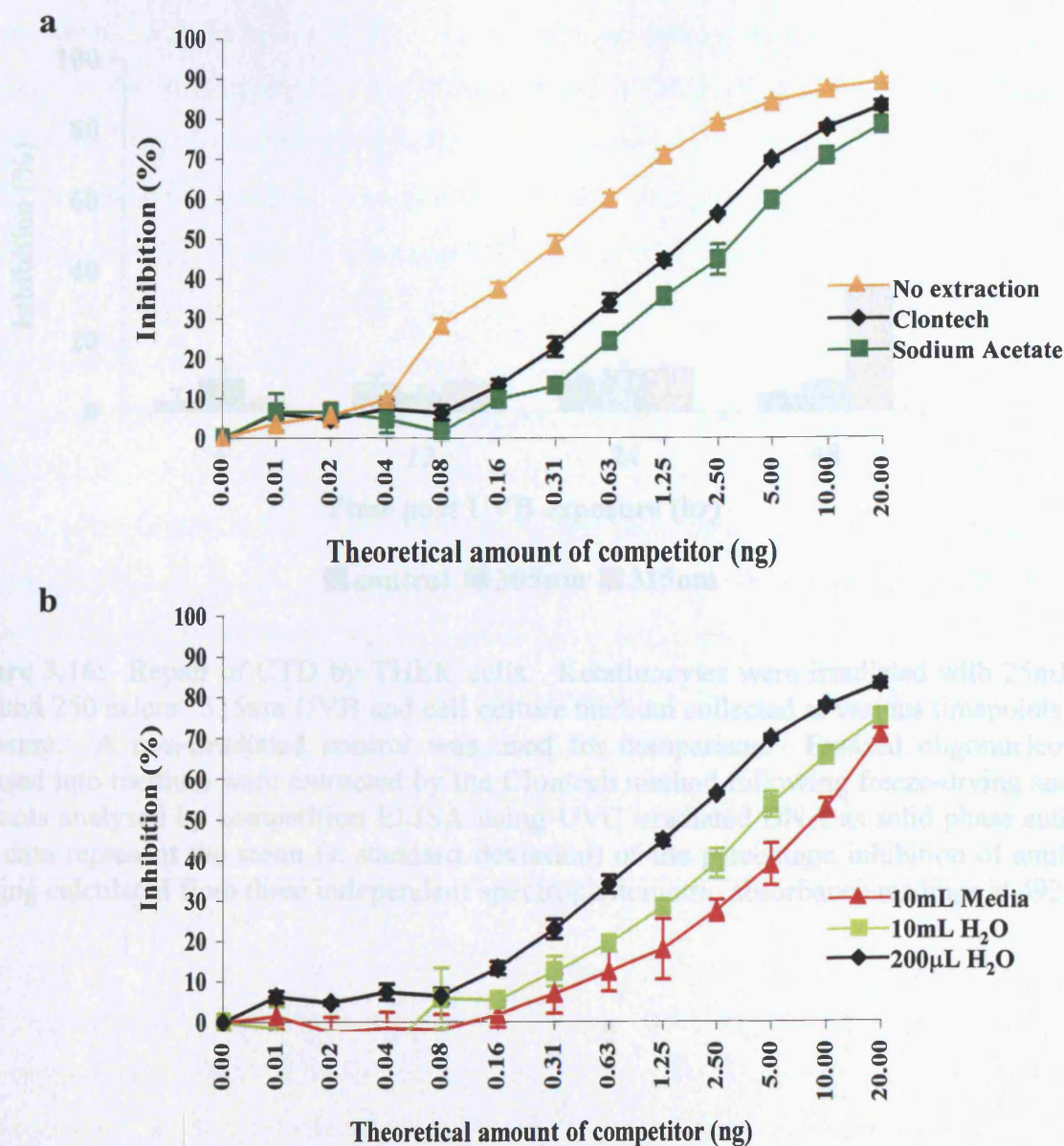


**Figure 3.15:** A competition ELISA comparison of desalting and purification procedures for repair oligonucleotides. Inhibition of binding of the CTD antibody to UVC treated DNA as solid phase antigen was used as a measure of oligonucleotide extraction efficiency. To compare extraction, freeze-dried aliquots of 200µg 30mer oligonucleotide containing a single thymine dimer were reconstituted in 200µL water, then refreeze-dried and extracted using a Clontech kit or by a standard sodium acetate/ethanol procedure (**a**). To account for loss of oligonucleotide during the second freeze-drying cycle and extraction technique, one aliquot of oligonucleotides was simply reconstituted in 200µL and analysed (no extraction). The potential extraction of oligonucleotides in varying volumes of THEK cell medium was examined in oligonucleotides reconstituted in 200µL or 10mL water, or 10mL THEK cell medium, and then desalted and extracted with the Clontech kit (**b**). The data represent the mean ( $\pm$  standard deviation) of the percentage inhibition of antibody binding calculated from three spectrophotometric absorbance readings at 492nm taken from one of two representative experiments.

## 3.5 DISCUSSION

The research described in this chapter was aimed at comparing direct DNA damage and repair induced by narrow band irradiations at 305nm and 315nm. Both wavelengths were biologically relevant wavelengths in terms of environmental UV exposure and phototherapy. The potency of each wavelength was assessed in *in vitro* repair models by immunological quantification of pyrimidine dimers.

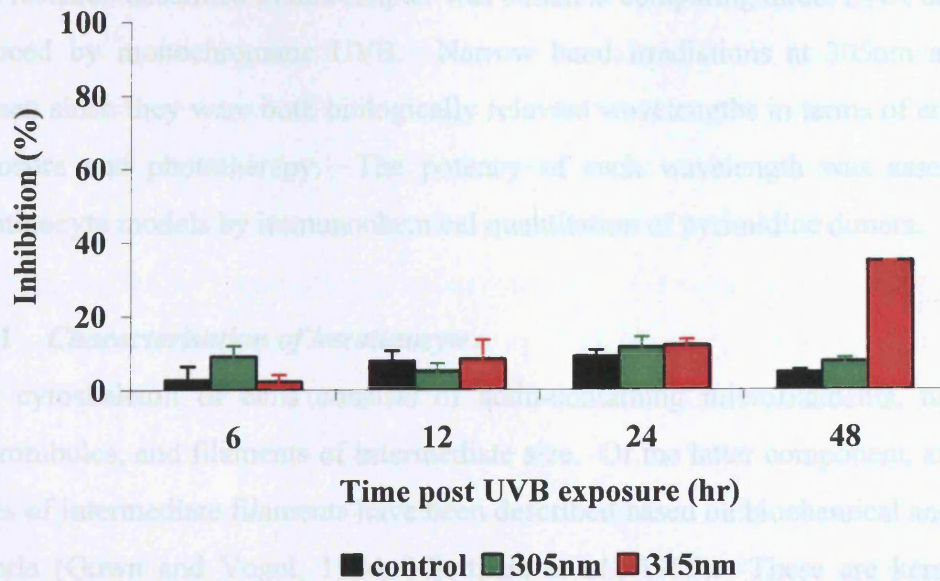
## 3.5.1 Cytotoxicity of narrow band irradiation

The cytotoxicity of UVB irradiation was assessed using immunofluorescence, tubulin-containing microtubules, and filaments of keratin filaments. On the latter arrangement, at least five major types of intermediate filament have been identified based on biochemical and immunological criteria (Cawin and Vogel, 1987). These are keratin-like proteins

(cytokeratins) characteristic of epithelial cells, vimentin filaments in mesenchymal cells, and desmin filaments in muscle cells. Cultured keratinocytes chosen as the *in vitro* model for these studies represent the predominant cell type in the epidermal layer of the skin. NHOK and THEK cells grown in *in vitro* conditions appear to take on "crazy paving" style morphology and grow in a monolayer of clusters. Both primary and transformed cells can be classified by their cytokeratin staining profile. Cytokeratins comprise 19 polypeptides with molecular weights ranging 38-70kDa and exist as heteropolymers of type I and II cytokeratin proteins (Moll *et al.*, 1992). Six co-expressed cytokeratins define basic epithelial phenotypes: simple epithelia co-express cytokeratins 5 and 18 (K5+K18) and complex stratified epithelia co-express one primary cytokeratin 5 and 14 pair (K5+14) and have other differentiation-specific pairs (K1+K10, K3+K11, K6+K16) and K3+K12 (Pincus *et al.*, 1990).

The expression of K14 and the co-expression of K5+18 were examined in both keratinocyte models used in this study. Both NHOK and THEK cells displayed positive staining for K14 indicating both cell lines were basal epithelia in origin. The staining pattern was less uniform in transformed keratinocytes compared to that observed in primary keratinocytes. Recently

The repair of CTD by THEK cells. Keratinocytes were irradiated with 25mJcm<sup>-2</sup> 305 and 250 mJcm<sup>-2</sup> 315nm UVB and cell culture medium collected at various timepoints post exposure. A non-irradiated control was used for comparison. Excised oligonucleotides released into medium were extracted by the Clontech method following freeze-drying and the amounts analysed by competition ELISA using UVC irradiated DNA as solid phase antigen. The data represent the mean ( $\pm$  standard deviation) of the percentage inhibition of antibody binding calculated from three independent spectrophotometric absorbance readings at 492nm.



### **3.5 DISCUSSION**

The research described in this chapter was aimed at comparing direct DNA damage and repair induced by monochromatic UVB. Narrow band irradiations at 305nm and 315nm were chosen since they were both biologically relevant wavelengths in terms of environmental UV exposure and phototherapy. The potency of each wavelength was assessed in *in vitro* keratinocyte models by immunochemical quantitation of pyrimidine dimers.

#### **3.5.1 Characterisation of keratinocytes**

The cytoskeleton of cells consists of actin-containing microfilaments, tubulin-containing microtubules, and filaments of intermediate size. Of the latter component, at least five major types of intermediate filaments have been described based on biochemical and immunological criteria (Gown and Vogel, 1984; Miettinen *et al.*, 1985). These are keratin-like proteins (“cytokeratins”) characteristic of epithelial cells, vimentin filaments in mesenchymally derived cells, desmin filaments typical of myogenic cells, neurofilaments that occur in neuronal cells and glial filaments of astrocytes. Detection of specific cytoskeletal components is used to characterise different types of cells within tissues; similarly changes in cytoskeletal components typical during cell transformation and tumour development provide invaluable tool for histodiagnosis (Fuchs and Cleveland, 1998; McLean and Lane, 1995).

Cultured keratinocytes chosen as the *in vitro* model for these studies represent the predominant cell type in the epidermal layer of the skin. NHEK and THEK cells grown in *in vitro* conditions appear to take on ‘crazy paving’ style morphology and grow in a monolayer of clusters. Both primary and transformed cells can be classified by their cytokeratin staining profile. Cytokeratins comprise 19 polypeptides with molecular weights ranging 38-70kDa and exist as heteropolymers of type I and II cytokeratin proteins (Moll *et al.*, 1982). Six co-expressed cytokeratins define basic epithelial phenotypes: simple epithelia co-express cytokeratins 8 and 18 (K8+K18) and complex stratified epithelia co-express one primary cytokeratin 5 and 14 pair (K5+14) and four other differentiation-specific pairs (K1+K10, K4+K13, K6+K16 and K3+K12; Purkis *et al.*, 1990).

The expression of K14 and the co-expression of K8+18 were examined in both keratinocyte models used in this study. Both NHEK and THEK cells displayed positive staining for K14 indicating both cell lines were basal epithelia in origin. The staining pattern was less uniform in transformed keratinocytes compared to that observed in primary keratinocytes. Recently

divided transformed keratinocytes were positive for K14 whilst those cells with a more mature cellular morphology, seen with generally larger nuclei, were negative. Co-expression of K8+18 was observed in THEK cells only. Collectively, these cytokeratin profiles demonstrate that both primary and transformed keratinocyte cell lines are basal epithelial cells in origin, and expression of K8+18 appears to be typical of immortal cell lines (Moll *et al.*, 1982). The loss of K14 in 'mature' transformed cells possibly indicates a loss of some basic keratinocyte phenotypes (personal communications Prof I Leigh, London Hospital Medical College, London). Further studies examining other cytokeratins such as K5 that is present in both epidermis and basal cell epitheliomas (Purkis *et al.*, 1990), may be used to further confirm the keratinocyte phenotype in these 'mature' transformed cells.

Both basal epithelial cells that comprise stratified epithelia and simple epithelial cells require the contact with the basal lamina, however simple epithelia have one luminal surface whilst those of stratified epithelia have no free surface. The expression of K8+K18 observed in THEK cells, typical of simple epithelia, appears to be essential for continued growth since expression of these cytokeratins is lacking in NHEK cells that have only a limited growth potential in culture (approximately 11 population doublings). Cytokeratin staining profiles provide a useful approach in defining distinct basal cell phenotypes and highlighting complexities of immortal cell lines. The differences observed here between primary and transformed keratinocytes demonstrate an important consideration whilst assessing cellular properties and capabilities of cell model systems.

### **3.5.2 Immunofluorescence detection of pyrimidine dimers**

In order to detect pyrimidine dimers a polyclonal antibody raised against UVC irradiated DNA was used. However full characterisation was not available so part of the aim was to complete the characterisation for this study. Studies by Umlas *et al.*, 1985 describe the relative formation of -TT- to -CT-/-TC- dimers in defined DNA sequences was approximately 2:1 respectively. The main epitope for this antiserum was previously described as dimerized adjacent thymines with either a 5' or 3' pyrimidine (Herbert *et al.*, 1994<sup>2</sup>), but the structural distinction between cyclobutane pyrimidine dimer (CPD) and 6-4 photoproduct (and its corresponding Dewar isomer) was not known. Based on photoisomerisation experiments involving irradiations at 305nm UVB followed by 313nm UVB, and treatment of UVC irradiated DNA with *E.coli* photolyase, it was concluded by both immunofluorescence and ELISA that the rabbit antiserum had strong reactivity for cyclobutane thymine dimers (CTD) as opposed to 6-4 photoproduct.

Immunochemical staining both in cells and tissues further confirmed the specificity of the rabbit antiserum to UV damaged DNA. In particular electron microscopy conclusively established the localisation of the antibody to nuclear material following UVB exposure of cultured keratinocytes. Some cytoplasmic staining was also observed, possibly as a result of mitochondrial DNA; however due to the high pH of the fixative required to assist unmasking of the antigen some definition of the ultrastructure was characteristically lost.

### **3.5.3 Genotoxicity of 305 and 315nm UVB**

Irradiations with 305 or 315nm UVB generated a dose-dependent increase in CTD formation both in human keratinocytes in culture as well as calf thymus DNA in solution. This comparison has not been reported in the literature previously. Both ELISA in isolated DNA and confocal microscopy *in situ* were performed since these approaches were complementary as ELISA provided a relatively easy means of quantitation of CTD and immunofluorescence allowed localisation of CTD to the nucleus. No difference in the rate of CTD formation was observed between THEK and NHEK cells as well as between THEK DNA and calf thymus DNA. Calibration of ELISA experiments with GC-MS quantitation data of CTD formation in UVC irradiated calf thymus DNA, showed that 305nm UVB generated in the region of 0.35-0.97nmol CTD/mg DNA following irradiation doses of 12.5-50mJcm<sup>-2</sup>, whilst irradiations with ten fold higher doses of 315nm UVB generated 0.17-0.30nmol CTD/mg of DNA; the shorter wavelength therefore proving more genotoxic.

The energies used with 305nm UVB relate to quoted MEDs at 300nm UVB (full width half maximum bandwidth of 5nm) as described by Young *et al.* (1998). However when monitoring thymine dimer removal in cultured keratinocytes it was noted that 25mJcm<sup>-2</sup> of 305nm UVB lead to approximately 50% cytotoxicity in experiments described in this chapter. This highlights one of the limitations of *in vitro* experiments, that is whilst some *in vivo* experiments base irradiation doses on MED's, these doses are far too cytotoxic for some aspects of *in vitro* experimentation. In this study assessment of DNA damage was performed immediately following irradiation, so prior to significant cytotoxicity and loss of cells and DNA. However when determining repair kinetics the contribution of cell death must be taken into consideration. Irradiations with 250mJcm<sup>-2</sup> 315nm UVB appeared less cytotoxic to cells in culture, however such doses related to only about a tenth of a MED reported for 320nm UVB (full width half maximum bandwidth of 10nm, Young *et al.* 1998).

#### **3.5.4 Repair processing of pyrimidine dimers**

The differing potencies of 305nm and 315nm monochromatic UVB in generating CTD was clearly demonstrated by ELISA and confocal microscopy. The repair processing of these dimers was assessed by confocal and electron microscopy in cultures of transformed keratinocytes. Both methods revealed a gradual loss of nuclear staining during the first 12hr post irradiation with either 305nm or 315nm UVB. Interestingly confocal microscopy demonstrated detection of extra-nuclear DNA material in the cytoplasm of transformed cells at 12 and 24hr post UVB exposure. Such observations were not reproduced by electron microscopy, possibly as a result of the sensitivity of the secondary antibody or the fixation conditions. The original cell preparations for confocal microscopy were fixed in a mixture of acetone and methanol, which may have assisted in precipitating or unmasking the damaged DNA in the cytoplasm. In order to examine similar UVB irradiated cells by electron microscopy, cells were required to be fixed with paraformaldehyde, however to allow access of the pyrimidine dimer antibody to the damaged DNA, the pH of fixation was adjusted to pH10 to assist unmasking. These alkaline conditions and permeabilization steps clearly affected the ultrastructural details, as seen by the loss of mitochondrial morphology, for example. However the use of an aldehyde-based fixative appeared to prevent the detection of any extra-nuclear DNA by both electron and confocal microscopy. In addition to the differences in fixation, the use of a FITC-conjugated fluoronanogold secondary antibody to detect bound CTD antibody demonstrated by immunofluorescence reduced nuclear staining compared to cells stained using the Alexa fluor™ 488 conjugated secondary antibody. This reduced sensitivity of fluoronanogold secondary antibody and possibly the excessive cross-linking of the formaldehyde fixative, may have contributed to the lack of extra-nuclear DNA in the cytoplasm of cells by electron microscopy.

Despite the differences in the observation of extra-nuclear DNA following UV irradiation, both confocal and electron microscopy revealed similar CTD repair kinetics, with nuclear staining disappearing by 12hr post UVB irradiation. Eveno and co-workers (1995) describe such repair timescales in SV40 transformed human skin fibroblasts. They reported using densitometry analyses of immunoslotblots approximately 50-75% of CPD are repaired by 6hr and over 80% by 24hr post  $15\text{Jm}^{-2}$  UVC irradiation. Similarly, earlier immunoslotblot studies by Wani and co-workers (1987), showed 40-50% of CPD being repaired by 24hr in human skin fibroblasts following much lower exposures to UVC ( $0.5\text{-}5\text{ Jm}^{-2}$ ). It is therefore possible that the staining post 12hr in cultured keratinocytes in this current study may be undetected due to the limits of detection by the antibody for CTDs. In particular the potency of the initial

dose of UVB irradiation was much weaker than the UVC doses described in these papers, as well as the differences in the nature of immunostaining, *i.e.* immunoslotblots with extracted DNA versus immunocytochemistry involving masking effects of cellular architecture. It is also possible that the recruitment of proteins during repair events such as adduct recognition may result in the loss of the antibody's ability to access and bind to the adduct. Interestingly the unusual nuclear evaginations observed by electron microscopy in routinely fixed keratinocytes post 24hr UVB exposure could be a natural morphological feature of repair. Further investigations are required to define whether these cellular changes are related to DNA repair processing, cell division defects, dying phenotype, or are purely artefacts of cells in culture. Discussions with experts in keratinocyte ultrastructure suggested that such evaginations had not been previously observed in either transformed or primary human keratinocytes (Prof RAJ Eady, Kings College, University of London, London).

The repair kinetics described here appear typical of cells in culture, however *in vivo* the removal of UV-induced DNA damaged appears to be at a slower rate. Immunohistochemical studies in monkey skin by Qin *et al.*, 1994 showed that with either 2000 Jm<sup>-2</sup> UVB (280-340nm) or 200 Jm<sup>-2</sup> UVC (254nm) irradiations, approximately 30% of CPDs were repaired within the first 24hr, followed by complete clearance by 72hr. In a recent immunohistochemical study by Katiyar *et al.* (2000) human skin exposed to 4 MED (exact dose unstated) UV (43% UVA, 54% UVB and 3% UVC), approximately 50% of CPDs were repaired by 3 days and levels comparable to non-irradiated skin were observed by 10 days post exposure. In earlier experiments by Young *et al.* (1996), similar repair kinetics were described both immunohistochemically and by the measure of unscheduled DNA synthesis.

The timescales described here refer to those established by immunostaining methods. There are however differences in the repair kinetics of pyrimidine dimers described using alternative experimental approaches. Previous reports assessing endonuclease-sensitive sites as a measure of repair activity described faster rates of repair; for example 40-50% of CPD were repaired within the first 1hr post damage (Eggset *et al.*, 1983; Reusch *et al.*, 1988 and Sutherland *et al.*, 1980). Subsequent papers using such measurements of endonuclease-sensitive sites, report on approximately 80% of CPD being removed by 24hr (Ruven *et al.*, 1993). Interestingly in a recent paper, reduced global genomic repair of CPD was reported in simian virus 40 (SV40) transformed human cells (Bowman *et al.*, 2000), since the large T antigen of SV40 binds to p53 protein and therefore modulates its function to activate excision

repair. Therefore the removal of CTD by THEK cells used in this study may be slower compared to NHEK cells; further work is required to confirm this.

In addition to the nature of the assay, other considerations to take into account whilst assessing the repair processing of pyrimidine dimers include the differences in the repair kinetics of different adducts. For example in cultured cells 6-4 photoproducts are preferentially and more efficiently removed compared to cyclobutane dimers, with 90% of 6-4 photoproducts being repaired within the first 6hr (Eveno *et al.*, 1995). Similarly in monkey skin the repair rate for 6-4 photoproduct was described to be much faster, with approximately 50% of the lesions being removed within the first 3hr and complete removal by 48hr post exposure (Qin *et al.*, 1994). These experiments reinforce the notion that the contrasting structural differences of these dimers (determined by NMR) influence damage recognition and thus repair activity (Kim *et al.*, 1995).

Another important consideration is the nature of the DNA damaged. It is widely accepted that damage existing on the transcribed strand of DNA is rapidly removed compared to damage existing on the non-transcribed strand (Ruven *et al.*, 1993). However, specific regions within a transcribed gene may be 'hotspots' of slow repair (Tornaletti and Pfeifer, 1994). To the contrary, a recent report by Zheng *et al.* (2001) demonstrates equal efficiency in the repair of either a transcriptionally active or a promoter-deleted gene containing CPD and other bulky lesions.

### **3.5.5 Pyrimidine dimers as biomarkers of DNA repair**

Excretion of pyrimidine dimers has been proposed as a biomarker of UV exposure (Cooke *et al.*, 2001; Le Curieux and Hemminki, 2001). Although the post excision events have been less well defined for UV induced lesions, Försti *et al.*, 1988 described the excretion of cis-diamminedichloroplatinum (II) DNA adducts in rat urine following i.p. injections of either the adduct alone  $\{cis-[Pt(NH_3)_2(dGpdG)]\}$  or DNA containing the  $\{cis-[Pt(NH_3)_2(dGpdG)]\}$ . The adduct alone was readily excreted in urine within 1-4 days post administration, however the DNA containing the adduct was excreted much more slowly, suggesting different excretion mechanisms and possible *in vivo* processing events. In this thesis, in order to measure excised UV adduct in the form of an oligonucleotide, a sensitive competition ELISA was successfully established using a synthetic oligonucleotide containing a CTD. However, following the *in vitro* irradiation of cultured keratinocytes with UVB, it was not possible to measure excised adduct in cell culture supernatants collected over 48hr using this competition ELISA

approach. This was possibly due to insufficient numbers of cells irradiated and/or more likely due to the inefficient extraction of low concentrations of dimer-containing oligonucleotides; or possibly even inadequate timecourse for sample collection. However if repair products are extensively degraded post excision, the detection and extraction of oligonucleotides containing adducts may not be viable with the antiserum used in this study.

Cooke *et al.* (2001) measured the excretion of pyrimidine dimers in urine using a competition ELISA approach. However in this current study, experiments investigating the freeze-drying of cell culture medium alone, revealed that without desalting the end product, antibody binding was greatly reduced. Such results would be interpreted as suggesting increased competition for the solid phase antigen, but in fact the salt content caused inadequate conditions for the antibody to bind efficiently. Perhaps the measurement of pyrimidine dimers in urine by a competition ELISA can be greatly affected by the salt concentration of urine within each specimen, which would prove naturally difficult to control for between individuals or even the time of day the specimen is collected. Although Cooke *et al.* (2001) correct for salt concentration by the measurement of creatinine, they assume the relationship between salt concentration and changes in inhibition is directly linear. That is, if the salt concentration is 2 fold higher compared to other samples, the value for inhibition is halved; however, the experiment describing the changes in antibody binding in response to increasing fold concentrates of THEK cell medium showed clearly that this is not a 1:1 relationship. Bearing in mind these experimental considerations and the larger standard deviations for samples, these authors go on to describe significant peak urinary thymine dimer levels at day 3 and days 9-11 post whole body irradiations of  $15\text{Jcm}^{-2}$  with UVA (320-405nm). The generation of dimers from this source was possibly due to the potency of the 313nm UVB spike they describe in the UV source used to irradiate human volunteers. This spike represented 0.5% of the total energy emitted, which in fact equates to approximately  $75\text{mJcm}^{-2}$ , which is sufficient to induce the significant number of dimers. In a report by Woollons *et al.* (1999), 75% of dimers detected in cultured human keratinocytes were generated by a lamp emitting only 0.8% UVB. This highlights the importance of understanding the relative contribution of specific wavelengths and their energetic output particularly in lamps that are used clinically as well as those used for tanning.

A recent paper by Le Curieux and Hemminki (2001) also describes the measurement of thymine dimers in urine; in this case using a  $^{32}\text{P}$ -postlabelling approach and HPLC separation with radiochemical detection. In this paper the authors photorevert the dimers with 254nm

UVC to their 'parental' thymines to allow <sup>32</sup>P-post labelling by T4 polynucleotide kinase and then assay the radiolabelled thymine dinucleotides following HPLC separation. In this study they describe the kinetics of thymine dimer excretion in two volunteers to peak 3 days post maximum daily exposure to Caribbean sun (exposure dose and UV spectrum undetermined). Similar urine samples (pre-photoreversion) have been analysed by LC-MS-MS and no dimers were detected (personal communication Dr JL Ravanat, CEA, Grenoble, France).

It therefore remains inconclusive whether thymine dimers can be detected in urine and can be used as a biomarker of UV exposure. In both pilot studies by Cooke *et al.* (2001) and Le Curieux and Hemminki (2001), the possible kinetics of thymine dimer presentation in urine may be as early as 18hr post UV exposure and may peak anywhere between 3 and 11 days post exposure. However if these observations are founded, this peak excretion of thymine dimer may certainly be governed by the source and dose of UV exposure, as well as the skin type and possibly the gender of the patients, amongst other variables. It is surprising that neither of these groups have attempted to establish their assays by the application of a cell culture model as described here.

Recent developments utilising HPLC-MS/MS have demonstrated the simultaneous detection of photoproducts generated in DNA following UV irradiation (Douki *et al.*, 2000; Douki and Cadet 2001). These studies have shown the relative yield of dimeric photoproducts at TT, CT, TC and CC sites, with each of these sites generating cyclobutane pyrimidine dimers, pyrimidine-(6-4)-photoproducts or the related Dewar valence isomer. The major lesion generated was the cyclobutane thymine dimer which was detected in 10 fold excess of its related 6-4 photoproduct. In addition the relative yield of photoproducts was reported to be similar for TT and TC adducts, however 10 and 5 times higher compared to CC and CT adducts, respectively. It is widely accepted that C→T and CC→TT are the signature mutations characteristic of UV exposure, interestingly the distribution of photoproducts within DNA of cells exposed to UVB reported by Douki and Cadet (2001) does not correlate to the UV mutational spectrum. The mechanism of mutagenesis by these 'low yield' photoproducts, including Dewar isomers, perhaps may relate to differences in recognition and efficiency of repair processing.

### **3.5.6 Conclusion**

This chapter investigated the immunochemical measurement of direct UV damage and repair processing. The main findings were:

- ❖ Characterisation of rabbit antiserum raised to UVC irradiated DNA confirmed detection of CTD.
- ❖ CTD were detected in DNA and in the nuclei of cultured keratinocytes or formalin-fixed paraffin embedded tissues following UVC irradiation or biologically relevant irradiations with discrete wavelengths of UVB.
- ❖ Distinct differences in CTD formation were shown following irradiation with 305nm or 315nm UVB of DNA and cultured keratinocytes. The shorter wavelength of UVB generating significantly higher levels of CTD with a tenth of dose of 315nm UVB.
- ❖ An assay to detect the potential CTD repair product in cell culture supernatants following UVB irradiation of cells was investigated. The repair processing of CTD or other pyrimidine dimer have yet to be proven.
- ❖ Ultrastructural analyses by electron microscopy revealed an interesting phenomenon in UVB irradiated THEK cells, where 10% of cells displayed nuclear evaginations. Further work to confirm these observations is required.

The use of a monochromatic source for UV experimentation allows a better understanding of the potency of wavelengths found in terrestrial UV. The contribution of specific wavebands to biological function/ dysfunction provides valuable insights into the influence of UV on human health. Establishing the balance between the genotoxic potential of UV and the therapeutic benefits is paramount for phototherapy and sunscreen efficacy. The work described in this chapter demonstrates a means by which *in vitro* experimentation involving the measurement of UV damage can be useful; by assessing the amount of CTD formation in DNA, the potency of a UV source can be governed. Ideally in the *in vitro* model the measurement of CTD formation in DNA extracted from cultured cells would be the ultimate calibration of experiments, however in relation to the application to *in vivo* experiments and phototherapy this would prove to be impractical.

In this study notionally small differences in wavelengths were observed to induce dramatically different levels of DNA damage in human keratinocytes in culture. In a recent editorial by Gasparro & Brown (2000), the need for more consideration of the type of UV source used for *in vitro* experimentation was described. They highlighted many problems

relating to the use of various types of unfiltered 'sunlamps', however suggested one inexpensive fluorescent lamp, the UVA-340 lamp, as an alternative to narrowband irradiations that could provide more 'meaningful' results. The use of *in vitro* models provide an ideal starting point for research without the need for ethics approval and exposure of individuals to genotoxic UV. Alternatively experiments may be performed in organ culture using normal human skin, obtained from for example breast reduction, and provided experimental parameters are well optimised the results generated via a relatively simple approach can be related to the situation *in vivo*.

## **CHAPTER FOUR**

### **CELLULAR OXIDATIVE STRESS INDUCED BY HYDROGEN PEROXIDE & THE UPTAKE OF ASCORBIC ACID**

## **4.0 CELLULAR OXIDATIVE STRESS INDUCED BY HYDROGEN PEROXIDE & THE UPTAKE OF ASCORBIC ACID**

### **4.1 INTRODUCTION**

Genotoxicity caused by terrestrial UV radiation is typically characterised by the formation of cyclobutane pyrimidine dimers and 6-4 photoproduct. These adducts are generated through the direct effects of the shorter wavelengths of the solar spectrum. Both UVB and UVA also cause damage to DNA through indirect mechanisms, involving photosensitisation and photoexcitation reactions of cellular constituents such as riboflavin, porphyrins, quinones and reduced nicotinamide co-factors (Imley and Linn, 1988; Stary and Sarasin, 2000). Such reactions lead to the generation of reactive oxygen species (ROS) and reactive nitrogen species (RNS), which can evoke an array of cellular modifications to DNA, proteins and lipids; and therefore ultimately influence gene expression changes and cellular homeostasis (Griffiths *et al.*, 1998).

The generation of these reactive species is not exclusive to UV irradiation but can also be synthesised by other external insults and/or endogenous physiological metabolism, such as chemical toxins, infection, inflammation, xenobiotic metabolism and mitochondrial electron transport chain (Ames 1989; Halliwell and Gutteridge 1999, Lindahl 1993). Both ROS and RNS have been implicated in pathogenesis and progression of many disease states and aging (DePinho, 2000; Finkel and Holbrook, 2000). ROS include the hydroxyl radical ( $\cdot\text{OH}$ ), singlet oxygen ( $^1\text{O}_2$ ), superoxide ( $\cdot\text{O}_2^-$ ) and hydrogen peroxide ( $\text{H}_2\text{O}_2$ ), the latter two also giving rise to hydroxyl radical via the reactions with metal ions. The genotoxic effects of ROS can be signified by the formation of a range of oxidative DNA damage adducts such as, thymine glycol (Cathcart *et al.*, 1984), 5-hydroxy-2'-cytosine (Wagner *et al.*, 1992), glyoxal-guanine (Murata-Kamiya *et al.*, 1995; Murata-Kamiya *et al.*, 1997) and 2-hydroxy-2'-deoxyadenosine (Kamiya and Kasai, 1995). One of the most studied DNA adducts, 7, 8-dihydro-8-oxo-2'-deoxyguanosine (8-oxodG), was first identified in 1984 by Kasai and Nishimura in experiments studying mutagens in glucose as a model for cooked foods. Since the discovery, mutagenesis experiments have revealed that this DNA adduct has the potential to induce mainly GC  $\rightarrow$  TA transversions (Cheng *et al.*, 1992; Grollman and Moriya, 1993), and therefore its importance in carcinogenesis and other human pathologies was highlighted (Kasai, 1997).

The accumulation of oxidative damage lesions has been associated with conditions such as diabetes (Shin *et al.*, 2001), Fanconi's anaemia (Degan *et al.*, 1995) as well as the ageing process (Kaneko *et al.*, 1997; Finkel and Holbrook, 2000) and certain neurodegenerative disorders (Alam *et al.*, 1997; Browne *et al.*, 1999; Mecocci *et al.*, 1994; Nunomura *et al.*, 1999). Various techniques have been utilised to demonstrate the influences and association of ROS damage in aetiology (Asami *et al.*, 1996; Asami *et al.*, 1997; Yamaguchi *et al.*, 1996). There are now several published methods allowing the sensitive detection and quantitation of 8-oxodG in DNA, these include high performance liquid chromatography with electrochemical detection (HPLC-ECD; Floyd *et al.*, 1986; Tagesson *et al.*, 1995) or with electrospray tandem mass spectrometry (HPLC-MSMS; Frelon *et al.*, 2000; Weimann *et al.*, 2001) and <sup>32</sup>P-post labelling techniques (Podmore *et al.*, 1997). Similarly, the base 8-oxoG can also be measured by HPLC-ECD (Herbert *et al.*, 1994<sup>1</sup>; Ravanat *et al.*, 1995) as well as gas chromatography with mass spectrometry (GC-MS; Dizdaroglu *et al.*, 2002).

Antibody based technology such as ELISA and immunohistochemistry with monoclonal antibodies (Hattori *et al.*, 1996; Toyokuni *et al.*, 1997) and avidin and its analogues (Struthers *et al.*, 1998) have claimed the detection of 8-oxodG in DNA as well as *in situ* in cells and tissues. In addition to these techniques, enzymic-based methods allow the detection of endogenous oxidative damage in nuclear DNA. Specific enzymes introduce strand breaks at the sites of damage, such as endonuclease III cleaves at sites of oxidised pyrimidines and formamidopyrimidine (fpg) at sites of ring-opened purines and 8-oxoG. The cleaved DNA can then be assessed by single-cell alkaline gel electrophoresis (the comet assay, Collins *et al.*, 1996), alkaline elution (Pflaum *et al.*, 1997) or by alkaline unwinding assays (Hartwig, *et al.*, 1996).

Many of the analytical techniques mentioned above require extraction procedures that can often cause artificial damage to DNA and lead to the generation of artefact. Complementary to these methods are fluorogenic, chemiluminescent or chromogenic probes, that specifically detect singlet oxygen, hydroxyl and superoxide radicals or general oxidative activity in live cells and tissues. For the latter, one particular compound dichlorodihydrofluorescein diacetate (H<sub>2</sub>DCFDA) has been widely utilised to demonstrate intracellular oxidative activity. This compound is readily internalised and is oxidised to its parent dye fluorescein by certain ROS. The fluorescence generated can then be detected and quantitated.

There are important defence systems against genotoxic damage such as cellular architecture where DNA is compartmentalised in the nucleus and protected by histones and polyamines, DNA repair mechanisms, as well as detoxification and antioxidant pathways. A major group of detoxification enzymes found in the endoplasmic reticulum is the glutathione-S-transferase (GST) multi-gene family; particular isoforms of GST determine a cell's response to a given insult (Hayes and Pulford., 1995). Studies with transgenic rats expressing the placental form of GST demonstrate a reduction of oxidative damage and inhibition of liver carcinogenesis (Nakae *et al.*, 1998). In humans there are distinct differences in isozyme expression, and heritable GST deficiencies have been associated with increased cancer risk, for example polymorphisms at the GST locus *GSTM3* and multiple cutaneous basal cell carcinoma (Yengi *et al.*, 1996). The importance of antioxidant systems in pathogenesis has also been demonstrated. For example, increases in oxidative damage in manganese SOD (MnSOD) knockout mice have been observed (Williams *et al.*, 1998) and genetic polymorphisms in MnSOD and low dietary intake of antioxidants lead to an increased risk of breast cancer (Ambrosone *et al.*, 1999). Similarly decreases in oxidative DNA damage are seen in response to the overexpression of copper/zinc SOD (Radak *et al.*, 1999) or catalase (Nilakantan *et al.*, 1998) in rodents.

In addition to these enzyme systems and natural intracellular antioxidants, dietary antioxidants are believed to play a role in the protection against ROS damage and possibly the prevention/progression of disease (Poulsen *et al.*, 2000). Dietary intervention trials with antioxidants such as vitamins C,  $\alpha$ -tocopherol (vitamin E),  $\beta$ -carotene, coenzyme Q and lycopene have been used to investigate correlations between supplementation and protection against disease (Loft and Poulsen, 2000). For example, the supplementation of women with a combination of vitamins C and E resulted in a reduced incidence of pre-eclampsia in those at high risk of the condition (Chappell *et al.*, 1999). Many studies combine epidemiological data and a measure of the efficacy of antioxidants, by assessing modulation of biomarkers such as oxidative DNA damage and repair activity (Loft and Poulsen, 2000). Such studies have demonstrated protective effects of antioxidants in individuals with nutritional deficiencies and/or increased basal oxidative stress levels (de la Asuncion *et al.*, 1998; Fraga *et al.*, 1991; Lee *et al.*, 1998). Nevertheless, further work at the *in vitro* level is required for the elucidation of cell signalling cascades and important gene expression pathways in response to antioxidants.

## 4.2 AIMS

The aim of this chapter is to establish methodologies to measure the generation of ROS and the effects of antioxidants in *in vitro* model systems. These investigations will provide the foundation for *in vitro* experiments examining the modulation of gene expression to two DNA repair enzymes involved in the base excision repair of 8-oxodG (Chapter 5). Cells will be treated with hydrogen peroxide a known inducer of ROS and the genotoxic potential will be assessed by the HPLC-ECD measurement of 8-oxodG formation in DNA, as well as immunochemical demonstration of the 8-oxodG *in situ*. General cellular ROS in response to hydrogen peroxide treatment will be measured by establishing a live-cell fluorogenic assay involving 5-(and-6)-chloromethyl-2',7'-dichlorodihydrofluorescein diacetate (CM-H<sub>2</sub>DCFDA), a derivative of H<sub>2</sub>DCFDA. In addition the effects of antioxidants on intracellular ROS will be examined by this assay in combination with the direct measure of internalisation and regeneration of ascorbic acid following the treatment with either ascorbic acid or dehydroascorbic acid respectively.

## 4.3 METHODS

### 4.3.1 *Measurement of 8-oxodG by HPLC-ECD.*

THEK ( $3 \times 10^6$ ) and CCRF ( $20 \times 10^6$ ) cells were serum starved for 48hr as described in section 2.3.1. Cells were treated with hydrogen peroxide at doses ranging from 0-800 $\mu$ M for 1hr at 37°C. THEK were trypsinised and both cell types were washed twice in PBS by centrifugation at 350g for 5min at 4°C. DNA was extracted by the 'sodium iodide method', quantitated spectrophotometrically (section 2.3.4.1) and 50 $\mu$ g digested (section 2.3.7.2). HPLC-ECD measurements of 8-oxodG and dG in DNA digests were carried out by Miss D. Chauhan (Division of Chemical Pathology, University of Leicester). Each sample was analysed in duplicate injections and the peak areas interpolated to a standard curve ranging 0, 0.5, 1, 5 and 10nM for 8-oxodG and for 5, 25, 50 and 100 $\mu$ M for dG, the internal measure of total DNA injected onto the HPLC (section 2.3.7.2).

### 4.3.2 *Immunochemical detection of ROS generated DNA adducts in cells and tissues*

The detection of ROS damage to DNA *in situ* was investigated using monoclonal antibodies to 8-oxodG and cytosine glyoxal. Immunohistochemical detection of oxidative DNA damage was optimised in formalin-fixed paraffin embedded tissues (section 2.3.3.6). Sections were incubated with primary antibodies at 10 $\mu$ g/mL of N45.1 antibody to 8-oxodG and 1 in 2 dilution of F3/9 unpurified cell culture supernatants to cytosine glyoxal. For the detection of 8-oxodG, sections were treated with 70mM sodium hydroxide in 70% (v/v) ethanol for 2min to assist denaturation of nuclear DNA (Hattori *et al.*, 1997; Toyokuni *et al.*, 1997) prior to blocking of non-specific sites. Controls for non-specific binding involved incubation of sections with IgGs for the N45.1 antibody or incubation with cell culture supernatants from non-secreting clones. Positive controls included the pre-treatment of tissue sections, involving the incubation of sections with a combination of 50-200 $\mu$ M hydrogen peroxide and ascorbic acid in UP water at 37°C for 1hr post dewaxing and rehydration steps.

To assess the formation of 8-oxodG in living cells, THEK cells were grown on chambered slides and treated with 10-1000 $\mu$ M hydrogen peroxide for 1hr (section 2.3.1). Immunocytochemistry for 8-oxodG with N45.1 was performed; briefly cells were fixed in ice-cold 50:50 (v/v) acetone:methanol, washed with PBS and blocked with NGS at 1 in 20 in PBS. Cells were incubated at 37°C for 1hr in primary antibody at 10 $\mu$ g/mL diluted in blocking solution. Following washes in PBS, cells were incubated with FITC conjugated goat

anti-mouse IgG secondary antibody at 1 in 50. Nuclei were counterstained with propidium iodide and fluorescence visualised by confocal microscopy (section 2.3.3.5).

#### **4.3.3 Measurement of endogenous ROS**

The use of CM-H<sub>2</sub>DCFDA to assess endogenous ROS generation was optimised. Initially, the cellular uptake conditions were optimised based on manufacturer's recommendations and on experiments reported by Ha *et al.* (1997), Nishikawa *et al.* (2000) and Xie *et al.* (1999). THEK cells were plated into 96-well plates and incubated at 37°C with 10µM CM-H<sub>2</sub>DCFDA in PBS for 15, 30 and 60min (section 2.3.2.3). Cells were then treated with 100 and 400µM hydrogen peroxide in PBS at 37°C and the fluorescence measured at 15, 30 and 60min post treatment using a Wallac Fluorescence Plate Reader with excitation and emission filters of 485nm and 535nm respectively (section 2.2.2). (The stock concentration of the hydrogen peroxide solution was determined by spectroscopy as described in Appendix II).

To minimise artificial cellular stress and detachment of THEK cells from plates caused by prolonged incubation of cells in PBS, alternative cell culture media were assessed for their background fluorescence levels. In addition, the plating efficiency and the variation in fluorescence measurements resulting from the growth pattern of both NHEK and THEK cells was investigated by Hoechst 33342 and propidium iodide staining in viable and fixed cells respectively (section 2.3.2.2). The optimal number of fluorescence scans, the scan area and the scan time per well were also investigated to reduce variability resulting from the non-uniform distribution of cells.

Following the optimisation of CM-H<sub>2</sub>DCFDA experimental conditions, THEK and/or NHEK cells were incubated at 37°C with 0, 50, 100, 200 and 400µM hydrogen peroxide, ascorbic acid or dehydroascorbic acid in PBS. At 15, 30 and 60min post treatment intracellular fluorescence generation was measured. The mean fluorescence calculated from 9 separate reads per well was used for subsequent statistical analysis (section 2.3.8).

#### **4.3.4 Cellular uptake and medium depletion of ascorbic acid and dehydroascorbic acid**

The stability of ascorbic acid in DMEM cell culture medium was initially assessed by the treatment of THEK cells with 0, 100 and 400µM ascorbic acid in either PBS or standard cell culture medium for THEK cells (section 2.3.1). Samples of medium or PBS were taken up to 4hr post incubation at 37°C. The ascorbic acid content was stabilised in metaphosphoric acid and analysed by HPLC with UV detection (section 2.3.7.1). Further to these experiments, the

stability of ascorbic acid in DMEM as well as RPMI medium was also assessed by capillary electrophoresis as described below.

To assess the uptake of ascorbic acid, THEK and CCRF cells were treated with 0, 100 and 400µM ascorbic acid or dehydroascorbic acid for up to 12hr. Dehydroascorbic acid is internalised at a more rapid rate compared to ascorbic acid and once internalised is converted to ascorbic acid. Cell culture samples and cell lysate preparations were prepared at 4, 8 and 12hr for CCRF cells and 4 and 12hr post incubation for THEK cells (section 2.3.6.3). The levels of ascorbic acid in each sample were assessed by capillary electrophoresis and the values normalised to the internal standard, isoascorbic acid (section 2.3.6.3).

## 4.4 RESULTS

### 4.4.1 Measurement of 8-oxodG

The genotoxic capacity of hydrogen peroxide was investigated by the measurement of 8-oxodG in DNA. THEK and CCRF cells were treated with hydrogen peroxide at doses ranging from 0-800 $\mu$ M for 1hr at 37°C. DNA was extracted and digested and analysed by HPLC-ECD for 8-oxodG and dG (Figure 4.1). The peak areas were integrated and the concentration of 8-oxodG calculated against a known standard curve. All 8-oxodG values were normalised to deoxyguanosine (dG), a measure of total DNA.

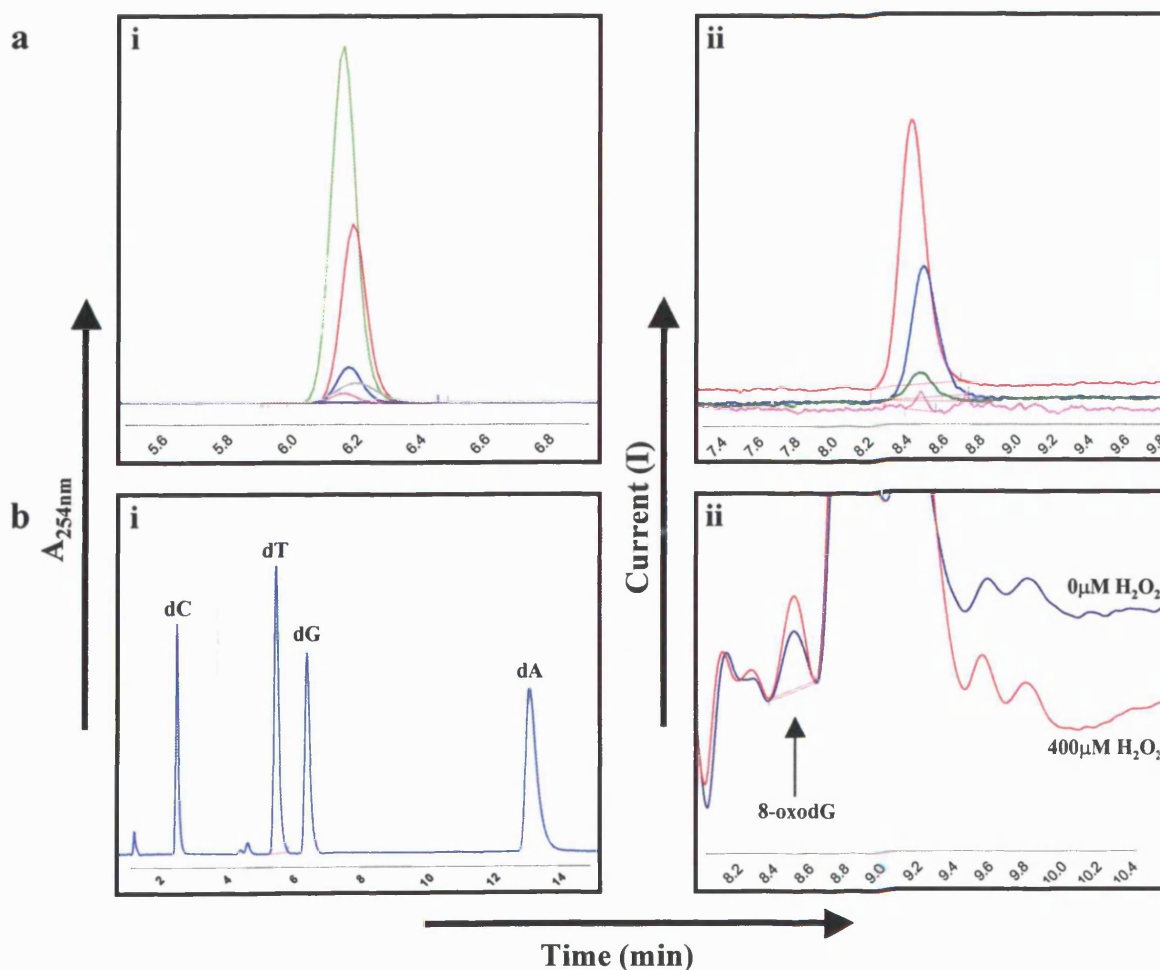


**Figure 4.1:** Representative HPLC chromatograms of (a) authentic standards: (i) 0-100 $\mu$ M deoxyguanosine (dG) detected at 254nm UV and (ii) 0-10nM 8-oxodG measured by electrochemical detection at 375mV. Example chromatograms of (b)(i) deoxynucleosides derived from enzymic hydrolysis of THEK DNA and (b)(ii) 8-oxodG detected in DNA derived from THEK cells treated with 0 and 100 $\mu$ M hydrogen peroxide as indicated.

In both THEK and CCRF a significant increase in 8-oxodG in DNA was observed in hydrogen peroxide treated cells (Figure 4.2). The data was expressed as the mean number of 8-oxodG adducts per 10<sup>5</sup> dG. The basal level of endogenous 8-oxodG was similar in both cell lines (mean  $\pm$  standard deviation: 2.0  $\pm$  0.4 and 1.8  $\pm$  0.2 8-oxodG per 10<sup>5</sup>dG in THEK and CCRF respectively). In THEK cells an approximate 1.5 and 1.8 fold increase in 8-oxodG formation was observed in cells treated with 400 and 800 $\mu$ M hydrogen peroxide, respectively. Similarly, in CCRF cells 8-oxodG formation increased by approximately 2-3 fold following 200-800 $\mu$ M hydrogen peroxide treatment. In both cell lines the formation of 8-oxodG following hydrogen peroxide treatment showed dose-dependent increases.

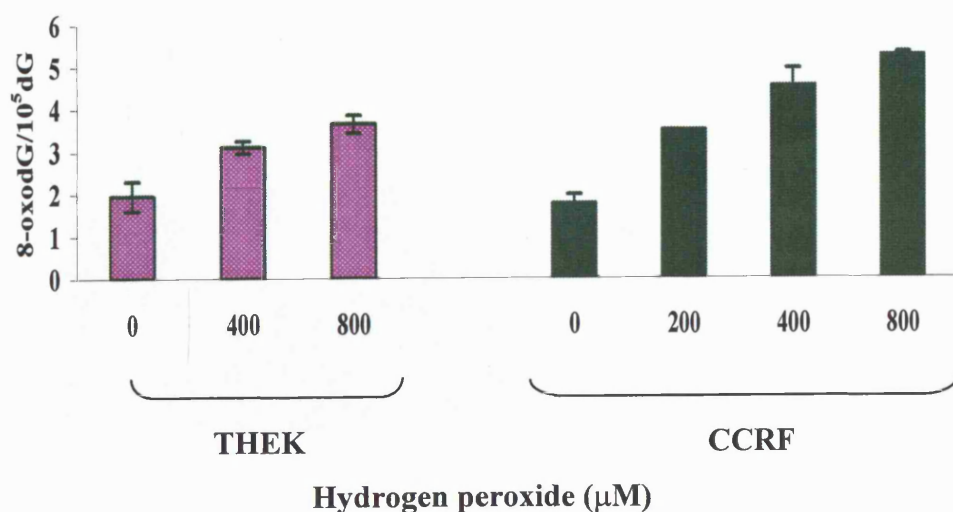


**Figure 4.2:** High performance liquid chromatography with electrochemical detection of 8-oxodG. THEK and CCRF cells were treated with 0-800 $\mu$ M hydrogen peroxide and DNA extracted by the sodium iodide method. The levels of 8-oxodG analysed and calculated against a known standard curve. The final values were normalised to the levels of deoxyguanosine (dG), a measure of total DNA, and expressed as the number of 8-oxodG per 10<sup>5</sup>dG. The data represent the mean ( $\pm$  standard deviation) of two measurements taken from one experiment.

#### **4.4.2 Immunocytochemical detection of ROS induced DNA damage**

Detection of ROS induced DNA damage was investigated *in situ*. The immunocytochemical demonstration of 8-oxodG with the monoclonal antibody N45.1 in THEK cells was successful (Figure 4.3). The distribution of staining appeared diffuse and not discrete within predicted DNA-containing cellular organelles, such as the nucleus or mitochondria, suggesting a degree of non-specific binding or detection of damaged RNA. Nevertheless, an increase in both cytoplasmic and nuclear staining was apparent in cells following non-cytotoxic hydrogen peroxide treatment.

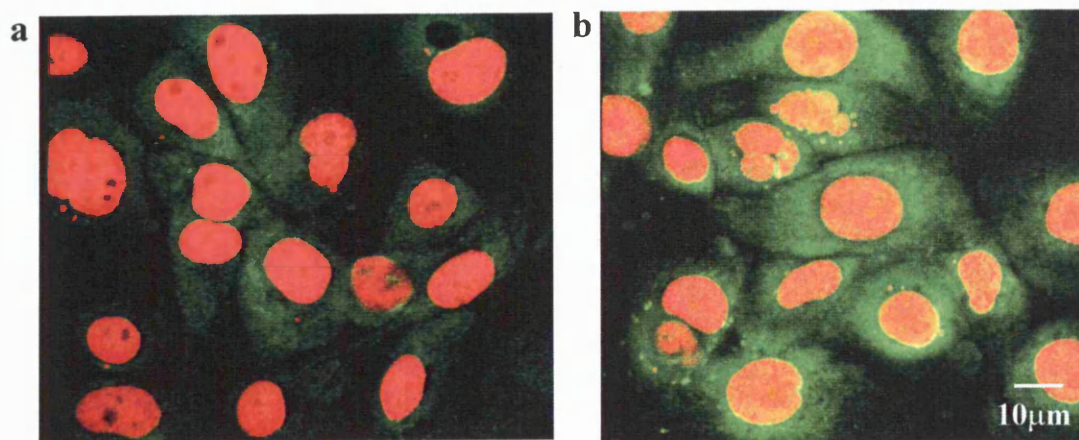


**Figure 4.3:** Immunocytochemical staining of 8-oxodG in mock-treated THEK cells (**a**) and cells treated with 100 μM hydrogen peroxide (**b**). Confocal images show immunocytochemical localisation of N45.1 primary antibody demonstrated by indirect fluorescence using a goat anti-mouse conjugated to FITC secondary antibody. The images represent the combined scans at 488nm for the FITC fluorochrome, seen as green fluorescence and 568nm for propidium iodide DNA counterstain, seen as red fluorescence.

Various skin tumours and tissues were probed for the presence of ROS-generated DNA adducts. No positive staining for 8-oxodG was seen with N45.1 except when tissues were pre-incubated with a hydrogen peroxide and ascorbic acid mixture *in vitro*, where a clear dose response was observed (Figure 4.4ai). The pattern of staining appeared both cytoplasmic and nuclear as observed in cultured cells, additionally the higher the concentration of hydrogen peroxide and ascorbic acid, the more nuclear the staining. Tumour tissues were investigated for potential increases in 8-oxodG levels and heterogeneity in distribution of damage. DNA damage was only detected in tumours post treatment with hydrogen peroxide and ascorbic acid *in vitro* (Figure 4.4aii).

Similar investigations were conducted with a monoclonal antibody to cytosine glyoxal (F3/9), an adduct typically generated through ROS damage. Positive nuclear staining in tissues pre-incubated with hydrogen peroxide and ascorbic acid *in vitro* was detected (Figure 4.4b), as seen with the N45.1 antibody. Overall little cytosine glyoxal could be detected in tumours and tumour surrounds in various skin cancers tested. However positive staining was observed in discrete cells within basal cell carcinoma specimens (Figure 4.4b). These cell types appeared morphologically characteristic of macrophage and/or dying cells.

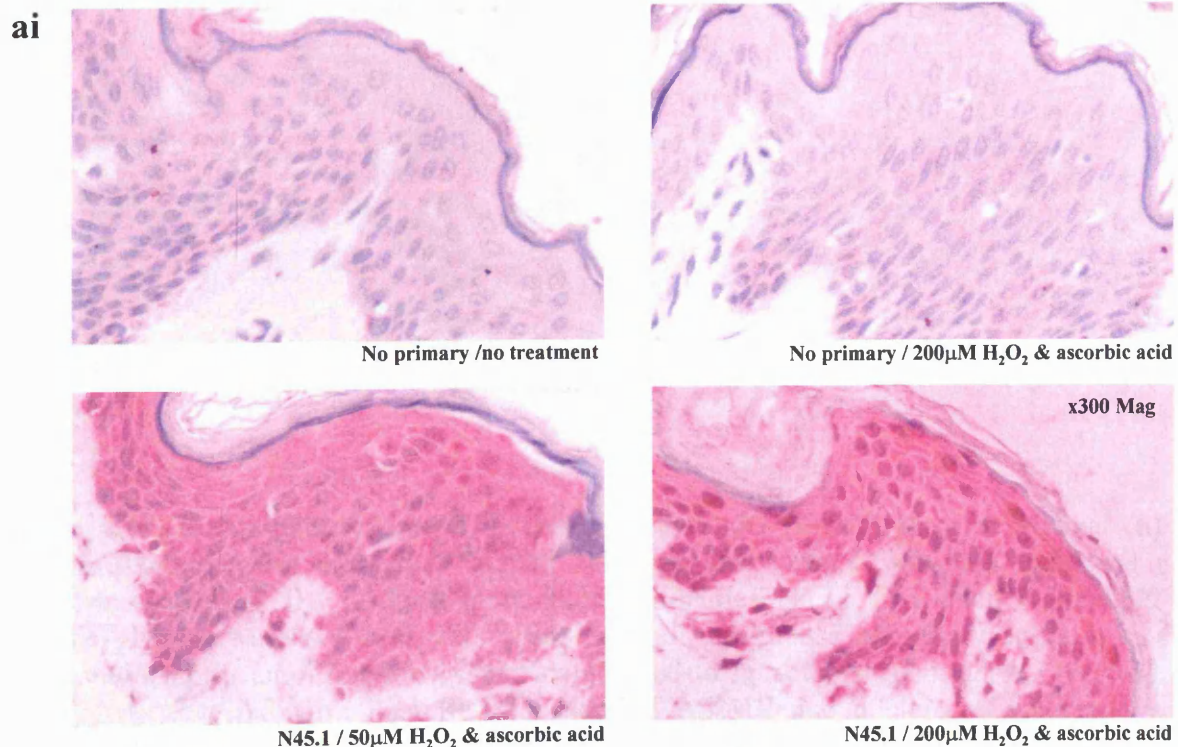


*Figure continued...*

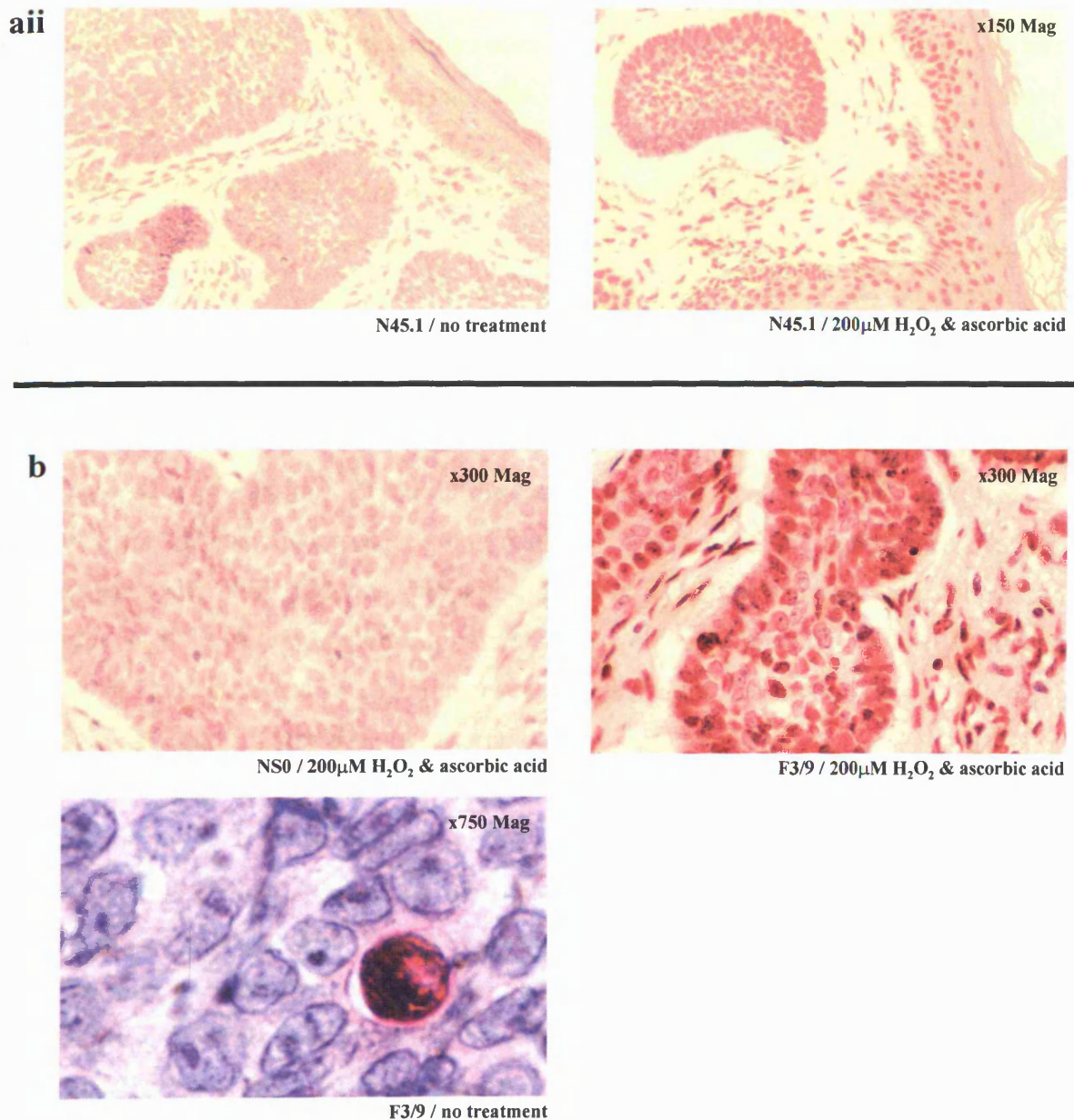


**Figure 4.4:** Immunohistochemical detection of 8-oxodG (**a**) and cytosine glyoxal (**b**) in formalin-fixed paraffin embedded human skin sections, normal skin (**ai**) and basal cell carcinomas (**a****ii** and **b**). Bound monoclonal antibodies N45.1 to 8-oxodG and F3/9 to cytosine glyoxal were detected with a biotinylated anti-mouse secondary antibody and a Streptavidin biotin amplification system conjugated to horseradish peroxidase. Peroxidase activity was detected with Fast Red TR-Naphthol AS-MX and nuclei counterstained with haematoxylin blue. Controls included: NS0, non-secreting supernatant for the cytosine glyoxal antibody and *in vitro* treatment of dewaxed and rehydrated sections in hydrogen peroxide and ascorbic acid both at 200 $\mu$ M, unless otherwise stated. Stained specimens were examined by light microscopy and photographed, magnifications as indicated.

### **4.4.3 Measurement of endogenous ROS**

In order to assess endogenous ROS generation in living cells a fluorogenic assay was established. CM-H<sub>2</sub>DCFDA was selected for its known stability in cells, however several parameters required optimisation: the duration of pre-loading of cells with CM-H<sub>2</sub>DCFDA, the concentration of hydrogen peroxide required to generate endogenous ROS as well as the exposure period of cells to hydrogen peroxide.

#### ***Optimisation of reproducibility of fluorescence measurements in keratinocytes***

Prior to the assessment of the effects of oxidants and antioxidants on intracellular ROS generation, the homogeneity of keratinocyte distribution in 96-well plates was investigated. Hoechst 33342 and propidium iodide staining of viable and fixed cells respectively was used to assess the plating/distribution of THEK and NHEK cells in 96-well plates (Table 4.1). However, in order to assess the distribution of the cells the optimal protocol for reading the wells required investigation. Based on the approximate area of each well in a 96 well plate (28 mm<sup>2</sup>), the Wallac fluorescence plate reader was programmed to conduct a number of readings per well, in the grid area with a displacement of 0.5mm between scan points. These data were used to determine the intra- and inter-well reproducibility in the detection of intracellular fluorescence as measured by excitation and emission filters of 355 and 460nm for Hoechst 33342, and 530 and 615nm for propidium iodide.

The variation in the distribution of keratinocytes as indicated by the coefficient of variation of intracellular fluorescence reading, was less than 8% (Table 4.1). The intra-well coefficient of variation range increased with increasing number of readings per well and the total area read; whilst the inter-well coefficient of variation decreased with increasing number of readings in both NHEK and THEK cells stained with Hoechst 33342. NHEK cells displayed an overall improved reproducibility in fluorescence measurements, with the inter-well coefficient of variation ranging from 2.0% to 2.7%. This coincides with the morphological appearances of these cells under light microscopy, where the growth pattern of NHEK cells appear more ordered compared to THEK cells. The intra- and inter-well coefficient of variation of THEK cells stained with either Hoechst 33342 or propidium iodide showed comparable values ranging from 4.5% to 6.9%. However the decrease in the inter-well coefficient of variation with increasing number of readings as seen in Hoechst 33342 stained cells, was not observed in propidium iodide stained THEK cells.

Overall the results indicate that for both types of keratinocytes grown in 96-well plates, despite growing in a non-uniform layer as observed by light microscopy, intracellular fluorescence can be monitored with excellent reproducibility. The optimal number of readings was determined as 9 per well, *i.e.* a 3x3 reading, as this offered intra- and inter-well reproducibility of readings at least as good as a 6x6 reading as well as a short length of time to complete the reading of a representative area in each well. One of the major considerations was to ensure that any given change in fluorescence readings from a series of treatment doses was not a result of the time taken to read the plate. To investigate this factor the wells were read in a different sequence order, *i.e.* from left to right or top to bottom, to check for any time-dependent changes and no trends were observed.

				Number of readings		
				1	3x3	6x6
<b>Approximate Scan Area (mm<sup>2</sup>)</b>					2.25	6.25
<b>Total Scan Time (sec) / Well</b>				1	9	36
<b>Fluorescent Compound</b>	<b>Keratinocyte Type</b>	<b>No of wells</b>	<b>Coefficient of Variation (CV)</b>			
<b>Hoechst 33342</b>	Transformed	15	Inter-well	6.7%	5.9%	4.5%
			Intra-well range		1.6-3.3%	2.2-6.4%
	Primary	20	Inter-well	2.7%	2.2%	2.0%
			Intra-well range		1.5-3.5%	2.9-4.1%
<b>Propidium Iodide</b>	Transformed	30	Inter-well	5.6%	6.9%	6.3%
			Intra-well range		2.4-5.9%	3.6-7.7%

**Table 4.1:** The assessment of homogeneity of THEK and NHEK cells growth in 96-well plates. The coefficient of intra- and inter well variation was determined by multiple fluorescent readings of cells stained with either Hoechst 33342 or propidium iodide. Fluorescence measurements were taken using excitation and emission filters of 355 and 460nm for Hoechst 33342 and 530 and 615nm for propidium iodide. Inter-well coefficient of variations were determined from 15, 20 or 30 independent wells, and the intra-well coefficient of variation range was determined from 9 or 36 readings taken per well from 15, 20 or 30 independent wells as stated. All calculated coefficient of variation values are described to 1 decimal place.

#### **Optimisation of CM-H<sub>2</sub>DCFDA uptake & hydrogen peroxide treatment conditions**

THEK cells were incubated with CM-H<sub>2</sub>DCFDA for periods of 15, 30 and 60min and subsequently washed and treated with 0, 100 and 400µM hydrogen peroxide. Fluorescence generation was monitored at 15, 30 and 60min post treatment by taking one reading per well from the top of the well, using excitation and emission filters of 485 and 535nm, respectively.

Fluorescence measurements were not taken beyond 60min as cells were noted to detach from the surface of the 96-well plates. Generally increasing doses of hydrogen peroxide caused an increase in fluorescence generation irrespective of conditions. However, maximum discrimination in endogenous ROS generation between control and treated cells was observed when cells were pre-loaded with CM-H<sub>2</sub>DCFDA for 15min (Figure 4.5). Fluorescence intensity increased in a dose dependent manner in cells treated with hydrogen peroxide throughout the 60min post treatment incubation. This observation was most apparent in cells pre-loaded with CM-H<sub>2</sub>DCFDA for 15 and 30min. Also, the increase in fluorescence measurements observed in control cells throughout treatment timecourse reflects endogenous ROS production generated under the described experimental conditions. Overall, these results demonstrate the optimal conditions for the measurement of endogenous ROS in transformed keratinocytes and also confirm the ROS generating capacity within cells of hydrogen peroxide applied extracellularly.

***Effect of cell culture medium & treatment reagents on background fluorescence measurements***

The treatment of cells in certain types of medium was assessed with the view to minimising cytotoxicity, cellular stress during treatment and preventing detachment of cells cultured in 96 well plates. Background fluorescence measurements were taken of various cell culture media selected because of their capacity to support THEK cell growth (Figure 4.6a). Fluorescence measurements of PBS were almost 8 fold lower than all other media tested. These results suggested certain aromatic compounds, such as tryptophan, tyrosine and others, present in DMEM and Ham's F12 (Appendix I) were possibly contributing to high background fluorescence. PBS was selected as treatment medium due to its low background fluorescence readings. All wells were subsequently read from the bottom to further minimise any interference of cell culture medium.

The reagents used to treat the cells were also assessed for any background interference to fluorescence (Figure 4.6b). The presence of hydrogen peroxide, ascorbic acid or dehydroascorbic acid at 400 $\mu$ M in PBS displayed no alteration to background fluorescence readings when compared to controls. Such results therefore allowed the immediate measurements of endogenous ROS activity post treatment without the need for any pre-washing of cells, and thus minimising cellular disruption.

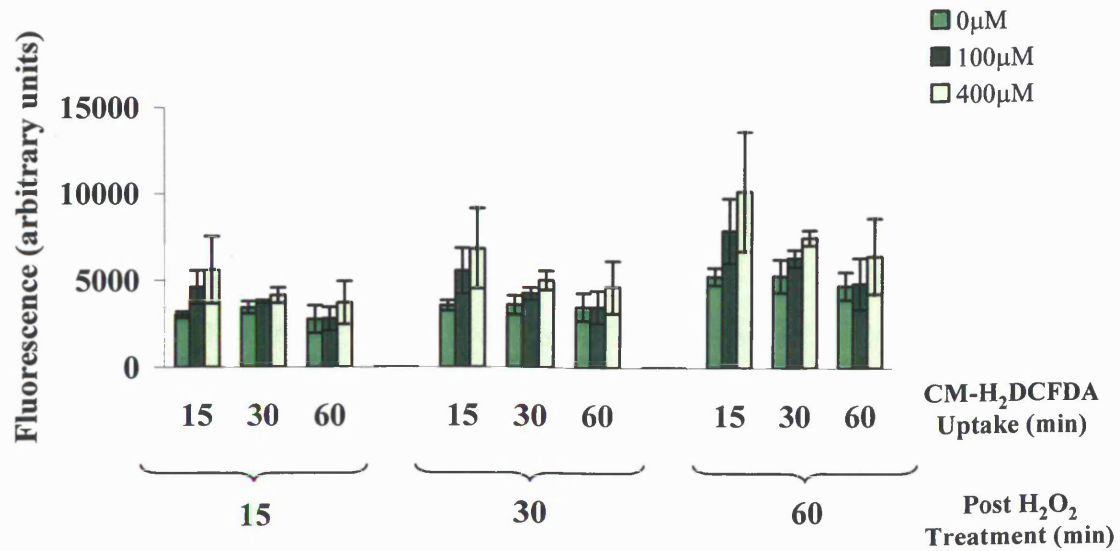


**Figure 4.5:** Optimisation of CM-H<sub>2</sub>DCFDA for the measurement of endogenous ROS in THEK cells. Cells were incubated with CM-H<sub>2</sub>DCFDA for 15, 30 and 60min prior to treatment with 0, 100 and 400μM hydrogen peroxide. Intracellular fluorescence was monitored for up to 60min using excitation and emission filters of 485nm and 535nm, as a measure of endogenous ROS generation post hydrogen peroxide treatment. The results are expressed as mean (±standard deviation) of 3 independent experiments, 1 reading per well.

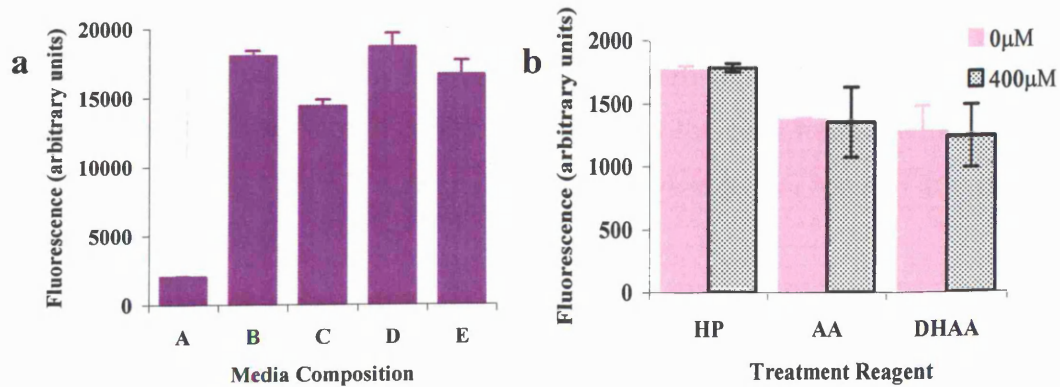


**Figure 4.6:** Background fluorescence measurements of cell culture medium alone (a) and treatment reagents alone (b) at excitation and emission of 485 and 535nm. The following abbreviations refer to: A= phosphate buffered saline (PBS), B= phenol-free Dulbecco's Minimal Essential Medium (DMEM), C= 75% phenol-free DMEM and 25% Hams F12, D= 0% foetal calf serum (FCS) THEK cell medium (75% DMEM and 25% Hams F12), F= 10% FCS THEK cell medium, HP= hydrogen peroxide in PBS, AA= ascorbic acid in PBS and DHAA= dehydroascorbic acid in PBS. The composition of cell culture medium is fully described in Appendix I. The results are expressed as the mean (±standard deviation) of 12 independent readings, 1 reading per well.

#### **4.4.4 Effects of hydrogen peroxide on intracellular ROS generation in keratinocytes**

NHEK cells were treated with 0, 50, 100, 200 and 400 $\mu$ M hydrogen peroxide and ROS generation was measured by the increase in intracellular fluorescence as a result of the internalisation of CM-H<sub>2</sub>DCFDA, cleavage of the diacetate groups, followed by the oxidation of CM-H<sub>2</sub>DCF. In cells loaded with CM-H<sub>2</sub>DCFDA but not treated with hydrogen peroxide, a time dependent increase in intracellular ROS was observed possibly reflecting endogenous ROS generation from for example the electron transport system within cells.

A dose dependent increase in intracellular ROS generation by hydrogen peroxide was observed in NHEK cells during a 60min timecourse (Figure 4.7a). The mean fluorescence intensity was significantly different ( $p < 0.01$ ) between control (mean  $\pm$  standard deviation at 15, 30 and 60 min post incubation: 3654.7  $\pm$  260.7; 4928.0  $\pm$  298.3 and 5906.1  $\pm$  352.1 respectively) and both 200 $\mu$ M (mean  $\pm$  standard deviation at 15, 30 and 60 min post incubation: 5830.0  $\pm$  877.2; 8667.2  $\pm$  1198.8 and 9401.0  $\pm$  2144.1 respectively) and 400 $\mu$ M (mean  $\pm$  standard deviation at 15, 30 and 60 min post incubation: 5699.3  $\pm$  1068.7; 8516.6  $\pm$  1562.6 and 9940.2  $\pm$  2034.2 respectively) hydrogen peroxide treated cells. Such significant differences were also observed between control (mean  $\pm$  standard deviation at 15 and 30 min post incubation: 3654.7  $\pm$  260.7 and 4928.0  $\pm$  298.3 respectively) and 50 $\mu$ M [mean  $\pm$  standard deviation at 15 ( $p < 0.05$ ) and 30 ( $p < 0.01$ ) min post incubation: 4385.5  $\pm$  382.5 and 6187.2  $\pm$  494.2 respectively], and between control and 100 $\mu$ M [mean  $\pm$  standard deviation at 15 and 30 min ( $p < 0.01$  for both) post incubation: 4517.7  $\pm$  646.6 and 6470.6  $\pm$  778.7 respectively] hydrogen peroxide treated cells. Other highly significant differences ( $p < 0.01$ ) in mean intracellular fluorescence were also observed between the cells treated with lower hydrogen peroxide doses (50 and 100 $\mu$ M) compared with the higher doses (200 and 400 $\mu$ M) at all three timepoints post treatment.

THEK cells treated with 0, 50, 100, 200 and 400 $\mu$ M hydrogen peroxide also showed a dose dependent increase in intracellular ROS generation as demonstrated by the increase in intracellular fluorescence detection (Figure 4.7b). Highly significant differences ( $p < 0.01$ , except  $p < 0.05$  between control and 200 $\mu$ M hydrogen peroxide treated cells at 60min) in mean fluorescence intensity were observed between control (mean  $\pm$  standard deviation at 15, 30 and 60min post incubation: 5654.8  $\pm$  746.1; 6034.2  $\pm$  947.6 and 8281.3  $\pm$  2395.8 respectively) and the cells treated with the higher concentrations of hydrogen peroxide, 200 $\mu$ M (mean  $\pm$  standard deviation at 15, 30 and 60min post incubation: 10340.8  $\pm$  2509.8; 11470.9  $\pm$  3709.3

and  $12255.2 \pm 4891.1$  respectively) and  $400\mu\text{M}$  (mean  $\pm$  standard deviation at 15, 30 and 60min post incubation:  $11703.5 \pm 3467.6$ ;  $14129.4 \pm 4460.6$  and  $15270.7 \pm 2129.3$  respectively) throughout the timecourse of treatment. Some significant difference ( $p < 0.05$ ) was observed between control (mean  $\pm$  standard deviation:  $5654.8 \pm 746.1$ ) and  $50\mu\text{M}$  (mean  $\pm$  standard deviation:  $8227.7 \pm 1865.9$ ) hydrogen peroxide treated cells at 15min. Similarly, significant differences ( $p < 0.01$ ) in mean fluorescence between control (mean  $\pm$  standard deviation at 15 and 30 min post incubation:  $5654.8 \pm 746.1$  and  $6034.2 \pm 947.6$  respectively) and cells treated with  $100\mu\text{M}$  hydrogen peroxide (mean  $\pm$  standard deviation at 15 and 30 min post incubation:  $9683.6 \pm 2464.4$  and  $10850.0 \pm 3501.5$  respectively) observed at both 15 and 30min post treatment.

During the 60min timecourse transformed keratinocytes demonstrated significant differences in mean fluorescence intensity between treatment doses of hydrogen peroxide. For example, significant differences ( $p < 0.01$  and  $p < 0.05$ ) were noted between  $50$  and  $400\mu\text{M}$ , and  $100$  and  $400\mu\text{M}$  hydrogen peroxide treated cells, respectively. Likewise, during the first 30min of the timecourse a significant difference ( $p < 0.05$ ) in mean fluorescence intensity was observed between cells treated with  $50\mu\text{M}$  hydrogen peroxide and cells treated with  $200\mu\text{M}$  hydrogen peroxide.

#### ***4.4.5 Effect of ascorbic acid & dehydroascorbic acid on intracellular ROS generation capacity in keratinocytes***

THEK cells treated with  $0$ ,  $50$ ,  $100$ ,  $200$  and  $400\mu\text{M}$  ascorbic acid demonstrated some unexpected changes in endogenous ROS activity (Figure 4.8a). After 15min incubation cell treated with  $200\mu\text{M}$  ascorbic acid (mean  $\pm$  standard deviation:  $4742.1 \pm 1075.6$ ) and  $400\mu\text{M}$  ascorbic acid (mean  $\pm$  standard deviation:  $4615.8 \pm 951.0$ ) demonstrated significantly ( $p < 0.01$ ) higher mean fluorescence compared to controls (mean  $\pm$  standard deviation:  $3335.8 \pm 409.0$ ) and the lower doses of ascorbic acid. Also a significant ( $p < 0.05$ ) difference between cells treated with  $50\mu\text{M}$  (mean  $\pm$  standard deviation:  $3885.7 \pm 308.4$ ) and  $200\mu\text{M}$  (mean  $\pm$  standard deviation:  $4742.1 \pm 1075.6$ ) ascorbic acid was observed. At 30min post treatment the only significant ( $p < 0.05$ ) difference was maintained between control (mean  $\pm$  standard deviation:  $4179.4 \pm 668.4$ ) and cells treated with  $200\mu\text{M}$  ascorbic acid (mean  $\pm$  standard deviation:  $5174.1 \pm 1259.1$ ). By 60min no significant difference in mean fluorescence was observed between control and treated samples.

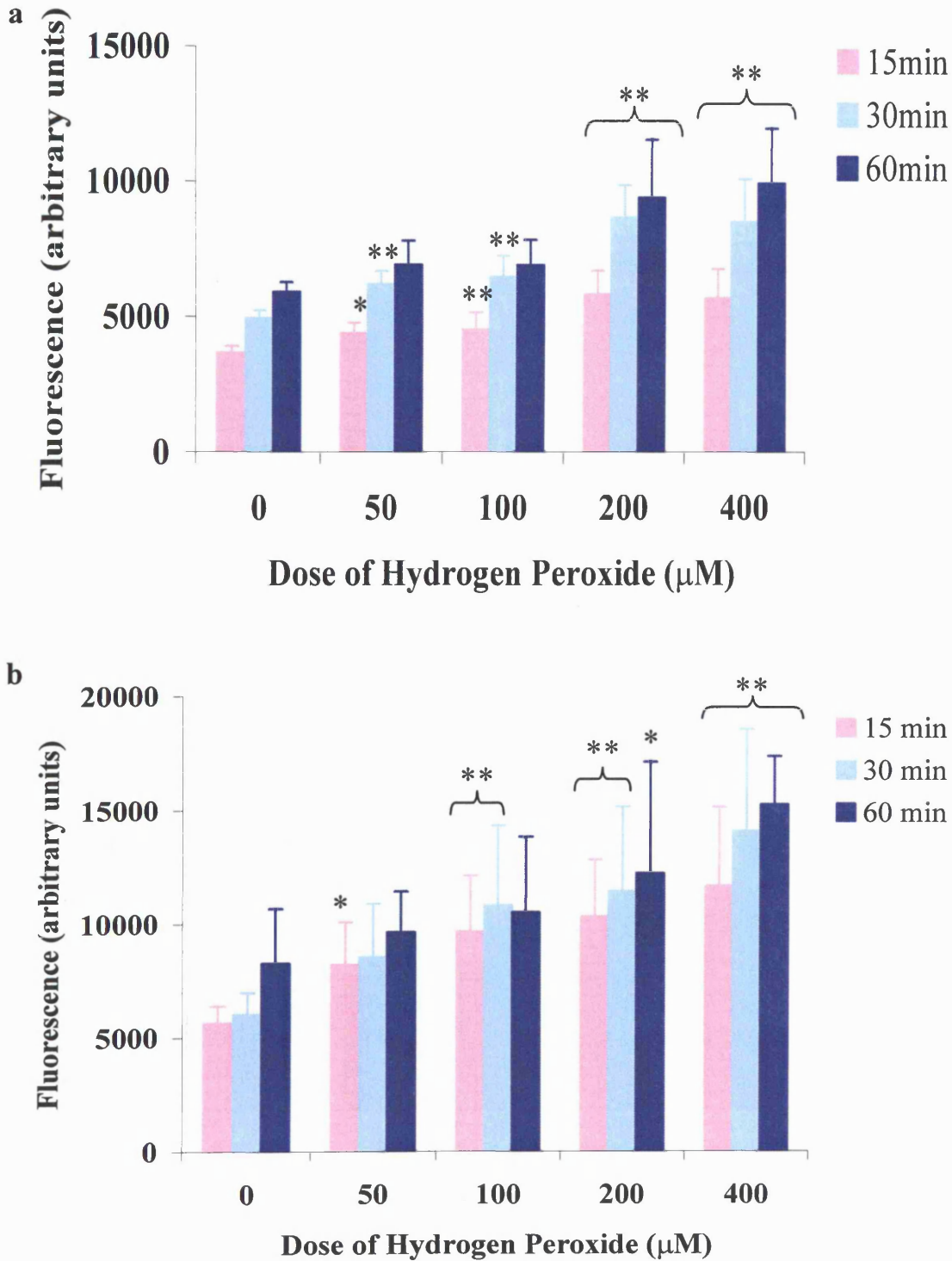


**Figure 4.7:** The effects of hydrogen peroxide on intracellular ROS activity in NHEK (a) and THEK cells (b). Cells were preloaded with CM-H<sub>2</sub>DCFDA for 15min, washed and then incubated for upto 60min with 0-400µM doses of hydrogen peroxide. The generation of ROS was measured as intracellular fluorescence resulting from the oxidation of CM-H<sub>2</sub>DCFDA to its parent fluorescent dye, using excitation and emission filters of 485 and 535nm respectively. Each data point represents the mean (± standard deviation) of 12 independent treatments, 9 readings per well. Means were compared using ANOVA and LSD post-test; statistically significant differences between control and treated samples are highlighted as \* and \*\*, representing p< 0.05 and p< 0.01 respectively.

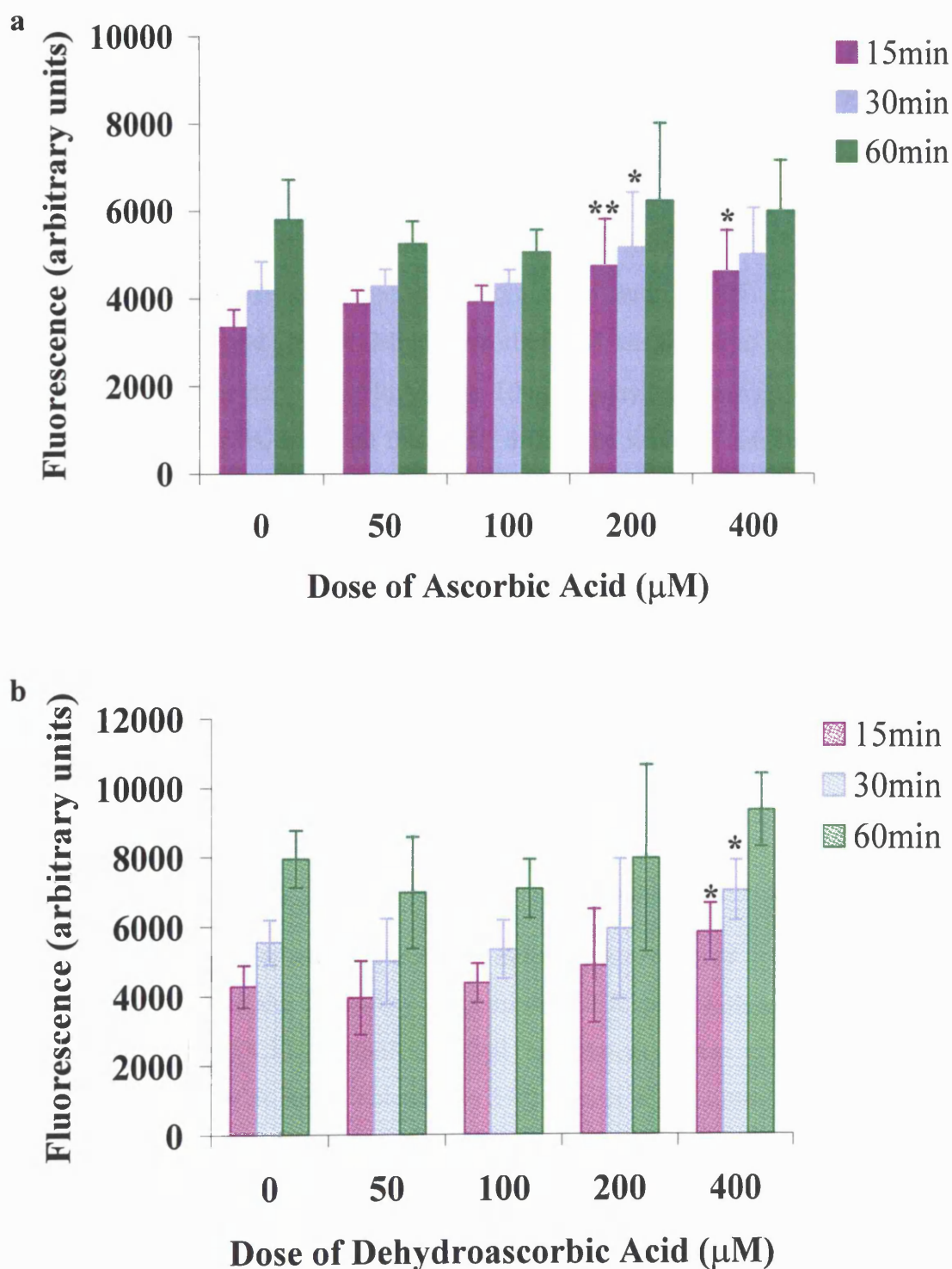


**Figure 4.8:** The effects of ascorbic acid (a) and dehydroascorbic acid (b) on intracellular ROS activity in THEK cells. Cells were preloaded with CM-H<sub>2</sub>DCFDA for 15min, washed and then incubated for 15, 30 and 60min with 0-400µM doses of either ascorbic acid or dehydroascorbic acid. The generation of ROS was measured as intracellular fluorescence resulting from the oxidation of CM-H<sub>2</sub>DCFDA, using excitation and emission filters of 485 and 535nm respectively. Each data point represents the mean ( $\pm$  standard deviation) of 6 independent treatments, 9 readings per well. Statistically significant differences between control and treated samples are highlighted as \* and \*\*, representing  $p < 0.05$  and  $p < 0.01$  respectively.

Changes in endogenous ROS activity were also noted in THEK treated with dehydroascorbic acid (Figure 5.8b). At 15 and 30min post treatment of cells with 400 $\mu$ M dehydroascorbic acid (mean  $\pm$  standard deviation at 15 and 30 min post incubation: 5828.8  $\pm$  829.8 and 7032.2  $\pm$  878.3 respectively) a significantly ( $p < 0.05$ ) higher mean fluorescence was observed compared to control cells (mean  $\pm$  standard deviation at 15 and 30 min post incubation: 4278.0  $\pm$  607.9 and 5550.5  $\pm$  642.3 respectively). Also at these timepoints a highly significant ( $p < 0.01$ ) difference in mean fluorescence intensity between cells treated with 400 $\mu$ M and 50 $\mu$ M dehydroascorbic acid, and a significant ( $p < 0.05$ ) difference between cells treated with 400 $\mu$ M and 100 $\mu$ M dehydroascorbic acid was observed. The mean fluorescence readings for cells treated with 50 $\mu$ M and 100 $\mu$ M dehydroascorbic acid were consistently lower than control cells, although this small difference was not statistically significant. For both ascorbic and dehydroascorbic acid treated cells no significant difference in mean fluorescence was observed between control and treated samples 60 min post incubation.

Overall, neither ascorbic acid nor dehydroascorbic acid demonstrated the ability to reduce intracellular ROS generation in THEK cells. Mean fluorescence intensity due to endogenous ROS increased in control and treated cells alike over the 60min timecourse, demonstrating that both ascorbic acid and dehydroascorbic acid were not acting as classical antioxidants in this system.

#### **4.4.6 Cellular uptake of ascorbic acid and dehydroascorbic acid**

In order to investigate the suitability of treating THEK cells with ascorbic acid in PBS or medium for CM-H<sub>2</sub>DCFDA studies, initial experiments were conducted involving the measurement of ascorbic acid depletion by HPLC over a 4hr timecourse. Cultures treated with either 100 or 400 $\mu$ M ascorbic acid in PBS demonstrated little reduction in extracellular ascorbic acid throughout the incubation, whilst cultures treated in medium demonstrated a two-fold reduction in extracellular ascorbic acid by 4hr. (Figure 4.9). These data were confirmed by a more detailed study involving capillary electrophoresis investigating the depletion of ascorbic acid in medium and the uptake of either ascorbic acid or dehydroascorbic acid in two different types of cell cultures (see Figures 4.10 and 4.11). All further experiments were conducted in cell culture medium.

THEK cells were treated with 0 and 400  $\mu$ M ascorbic acid or dehydroascorbic acid to assess changes in ascorbic acid levels within cells and in medium. Intracellular and extracellular ascorbic acid levels were measured by capillary electrophoresis with isosorbic acid as internal standard, and all concentrations calculated from calibration curve containing the internal standard ranging from 0-1000  $\mu$ M ascorbic acid (Figure 4.10). Levels of ascorbic acid in THEK medium were below the limits of detection of the assay prior to treatment. Following the addition of 400  $\mu$ M ascorbic acid to medium, initial ascorbic acid concentrations (mean  $\pm$  standard deviation) were seen to significantly ( $p < 0.01$ ) decrease by 2 hr (mean  $\pm$  standard deviation: 520  $\mu$ M  $\pm$  11.4) and by 4 hr (mean  $\pm$  standard deviation: 123.7  $\mu$ M  $\pm$  10.3) compared to 0 hr (mean  $\pm$  standard deviation: 329.7  $\mu$ M  $\pm$  11.2) (Figure 4.11a). No ascorbic acid was detected in medium throughout the time course following treatment with dehydroascorbic acid.

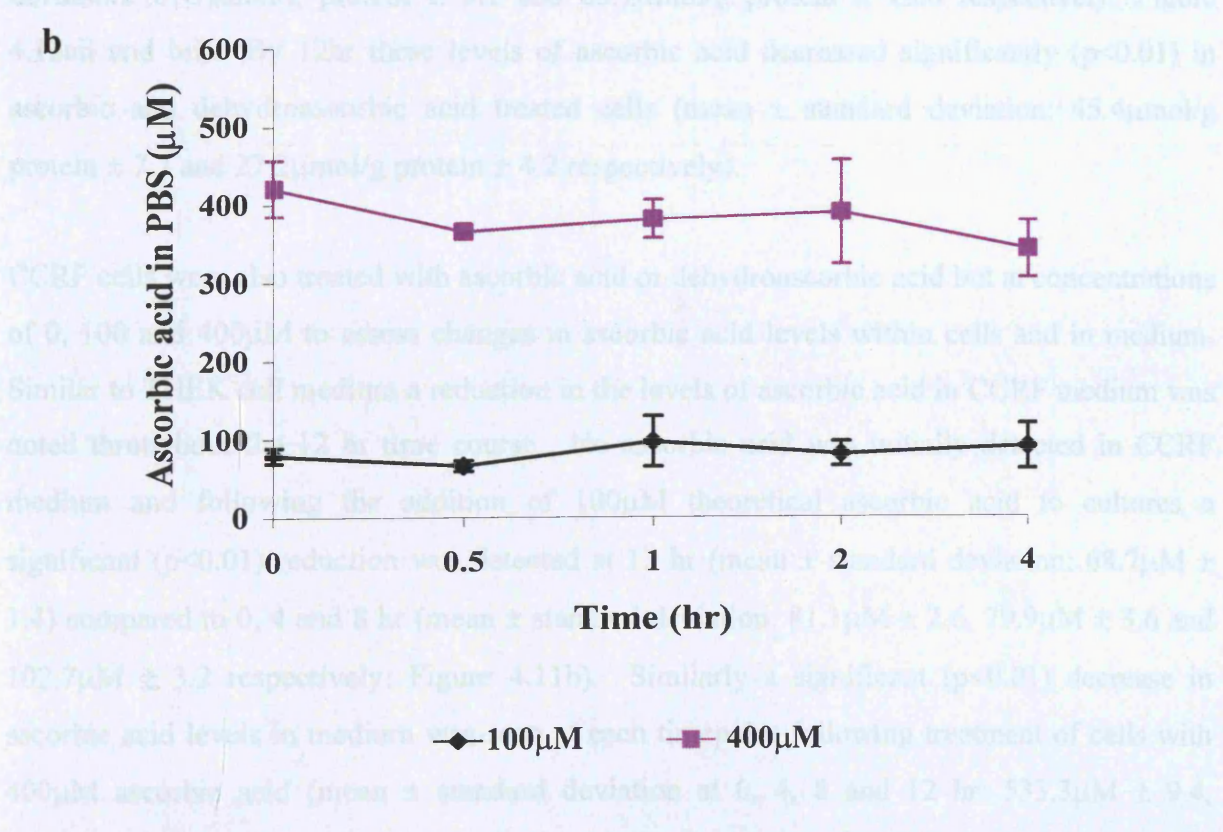
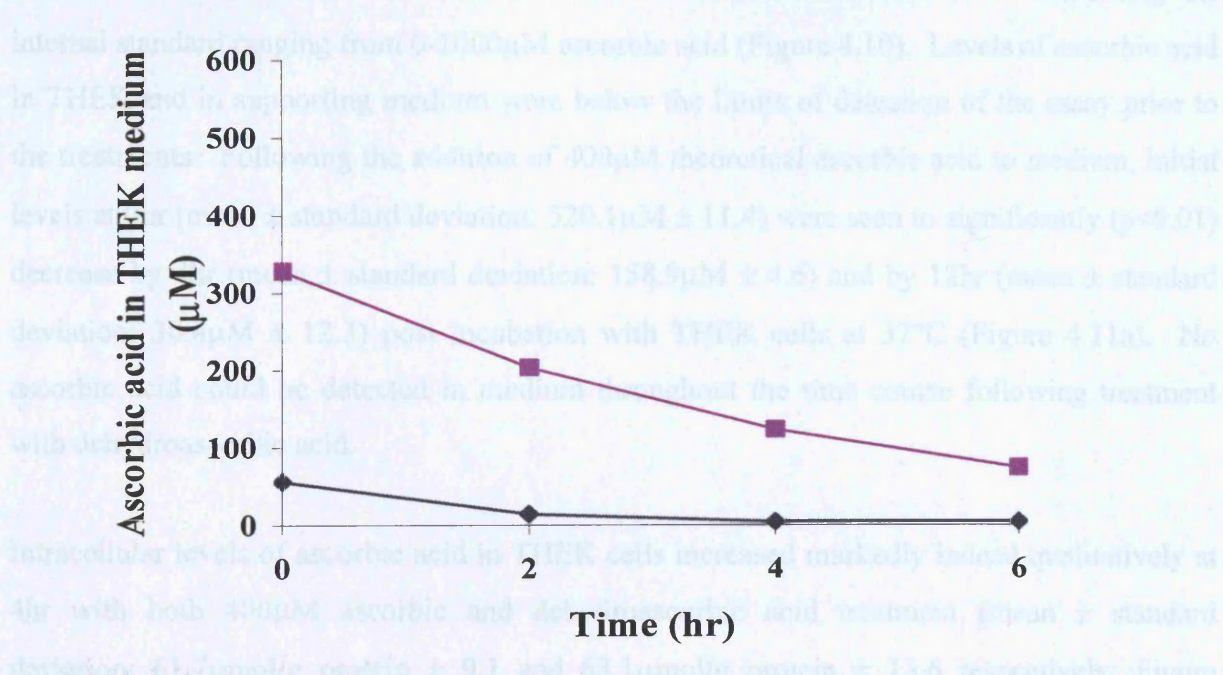


**Figure 4.9:** Extracellular ascorbic acid concentrations in cultures of transformed keratinocytes. Cells were treated with 0, 100 and 400  $\mu$ M ascorbic acid in THEK medium (a) or PBS (b). Samples were taken at each timepoint and the ascorbic acid stabilised with 10%(w/v) metaphosphoric acid prior to analysis by HPLC (see section 2.1.1.3). Each data point represents the mean ( $\pm$  standard deviation) of ascorbic acid concentrations from 2 (a) and 4 (b) independent experiments.

THEK cells were treated with 0 and 400 $\mu$ M ascorbic acid or dehydroascorbic acid to assess changes in ascorbic acid levels within cells and in medium. Intracellular and extracellular ascorbic acid levels were measured by capillary electrophoresis with isoascorbic acid as internal standard, and all concentrations calculated from calibration curve containing the internal standard ranging from 0-1000 $\mu$ M ascorbic acid (Figure 4.10). Levels of ascorbic acid in THEK and in supporting medium were below the limits of detection of the assay prior to the treatments. Following the addition of 400 $\mu$ M theoretical ascorbic acid to medium, initial levels at 0hr (mean  $\pm$  standard deviation: 520.1 $\mu$ M  $\pm$  11.4) were seen to significantly ( $p < 0.01$ ) decrease by 4hr (mean  $\pm$  standard deviation: 158.9 $\mu$ M  $\pm$  4.6) and by 12hr (mean  $\pm$  standard deviation: 30.4 $\mu$ M  $\pm$  12.3) post incubation with THEK cells at 37°C (Figure 4.11a). No ascorbic acid could be detected in medium throughout the time course following treatment with dehydroascorbic acid.

Intracellular levels of ascorbic acid in THEK cells increased markedly indeed qualitatively at 4hr with both 400 $\mu$ M ascorbic and dehydroascorbic acid treatment (mean  $\pm$  standard deviation: 61.7 $\mu$ mol/g protein  $\pm$  9.1 and 63.1 $\mu$ mol/g protein  $\pm$  13.6 respectively; Figure 4.12a<sub>ii</sub> and b<sub>ii</sub>). By 12hr these levels of ascorbic acid decreased significantly ( $p < 0.01$ ) in ascorbic and dehydroascorbic acid treated cells (mean  $\pm$  standard deviation: 45.4 $\mu$ mol/g protein  $\pm$  7.7 and 22.2 $\mu$ mol/g protein  $\pm$  4.2 respectively).

CCRF cells were also treated with ascorbic acid or dehydroascorbic acid but at concentrations of 0, 100 and 400 $\mu$ M to assess changes in ascorbic acid levels within cells and in medium. Similar to THEK cell medium a reduction in the levels of ascorbic acid in CCRF medium was noted throughout the 12 hr time course. No ascorbic acid was initially detected in CCRF medium and following the addition of 100 $\mu$ M theoretical ascorbic acid to cultures a significant ( $p < 0.01$ ) reduction was detected at 12 hr (mean  $\pm$  standard deviation: 68.7 $\mu$ M  $\pm$  1.4) compared to 0, 4 and 8 hr (mean  $\pm$  standard deviation: 81.1 $\mu$ M  $\pm$  2.6, 79.9 $\mu$ M  $\pm$  3.6 and 102.7 $\mu$ M  $\pm$  3.2 respectively; Figure 4.11b). Similarly a significant ( $p < 0.01$ ) decrease in ascorbic acid levels in medium was seen at each timepoint following treatment of cells with 400 $\mu$ M ascorbic acid (mean  $\pm$  standard deviation at 0, 4, 8 and 12 hr: 533.3 $\mu$ M  $\pm$  9.4, 458.9 $\mu$ M  $\pm$  8.8, 427.3 $\mu$ M  $\pm$  16.9 and 365.4 $\mu$ M  $\pm$  14.5 respectively). Also, as with THEK cells, no ascorbic acid could be detected in medium throughout the time course following treatment of cells with dehydroascorbic acid.

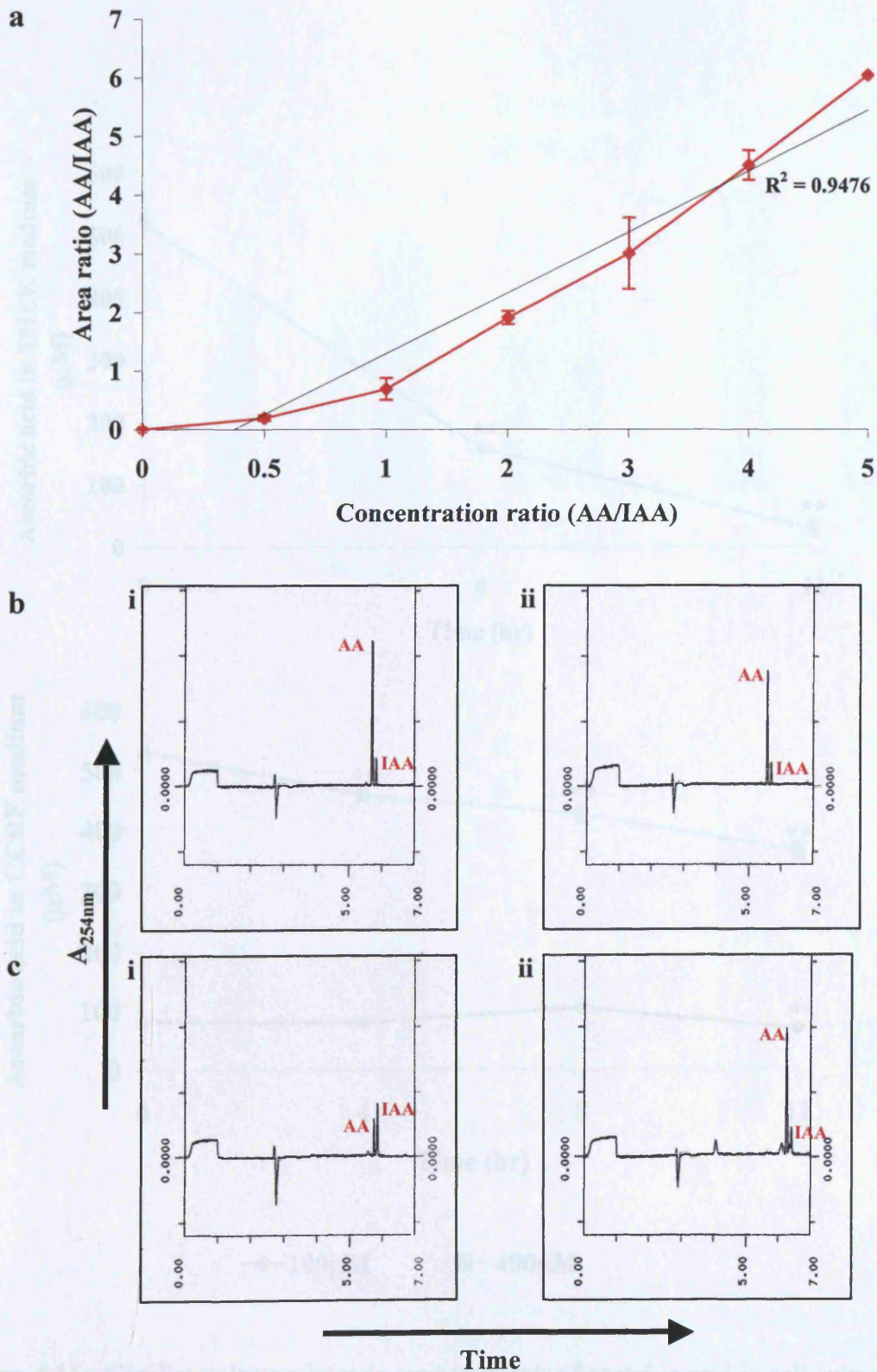
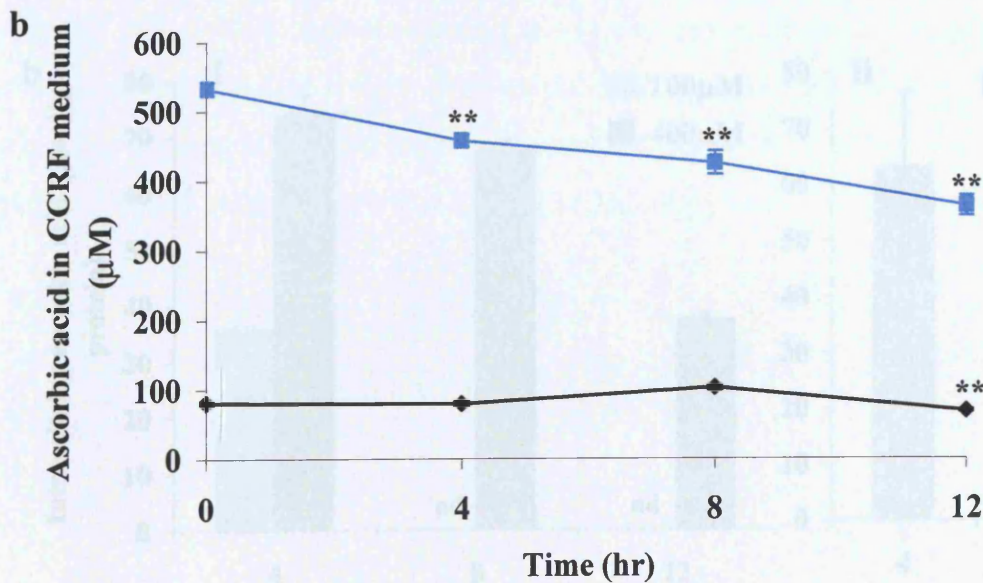
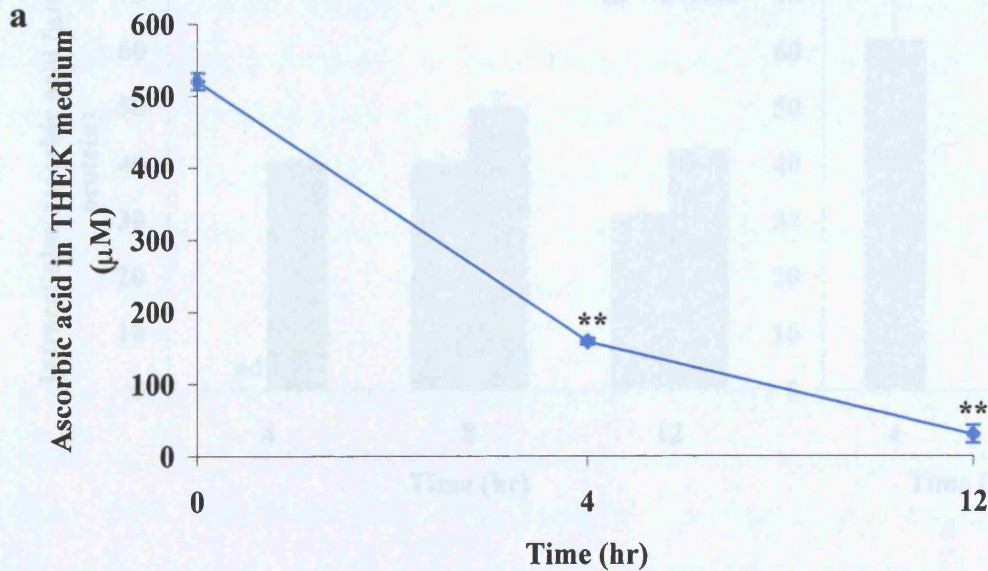


**Figure 4.10:** Typical calibration curve of ascorbic acid concentration (a) and representative capillary electropherograms of ascorbic acid (AA) with isoascorbic acid (IAA) internal standard detected in (b) cell culture medium and (c) intracellular extracts of transformed keratinocytes.



◆ 100µM      ■ 400µM

**Figure 4.11:** Capillary electrophoresis measurements of ascorbic acid in cell culture medium following supplementation of cell cultures with 0-400µM ascorbic acid (a) and THEK (a) and CCRF (b) cells. All measurements were normalised to an isoascorbic acid internal standard and final concentrations of ascorbic acid were calculated from standard curve standard ranging from 0-1000µM. Each data point represents the mean (± standard deviation) of 4 measurements. Statistically significant differences between 0hr and post incubation timepoints are highlighted as \*\* representing p< 0.01.

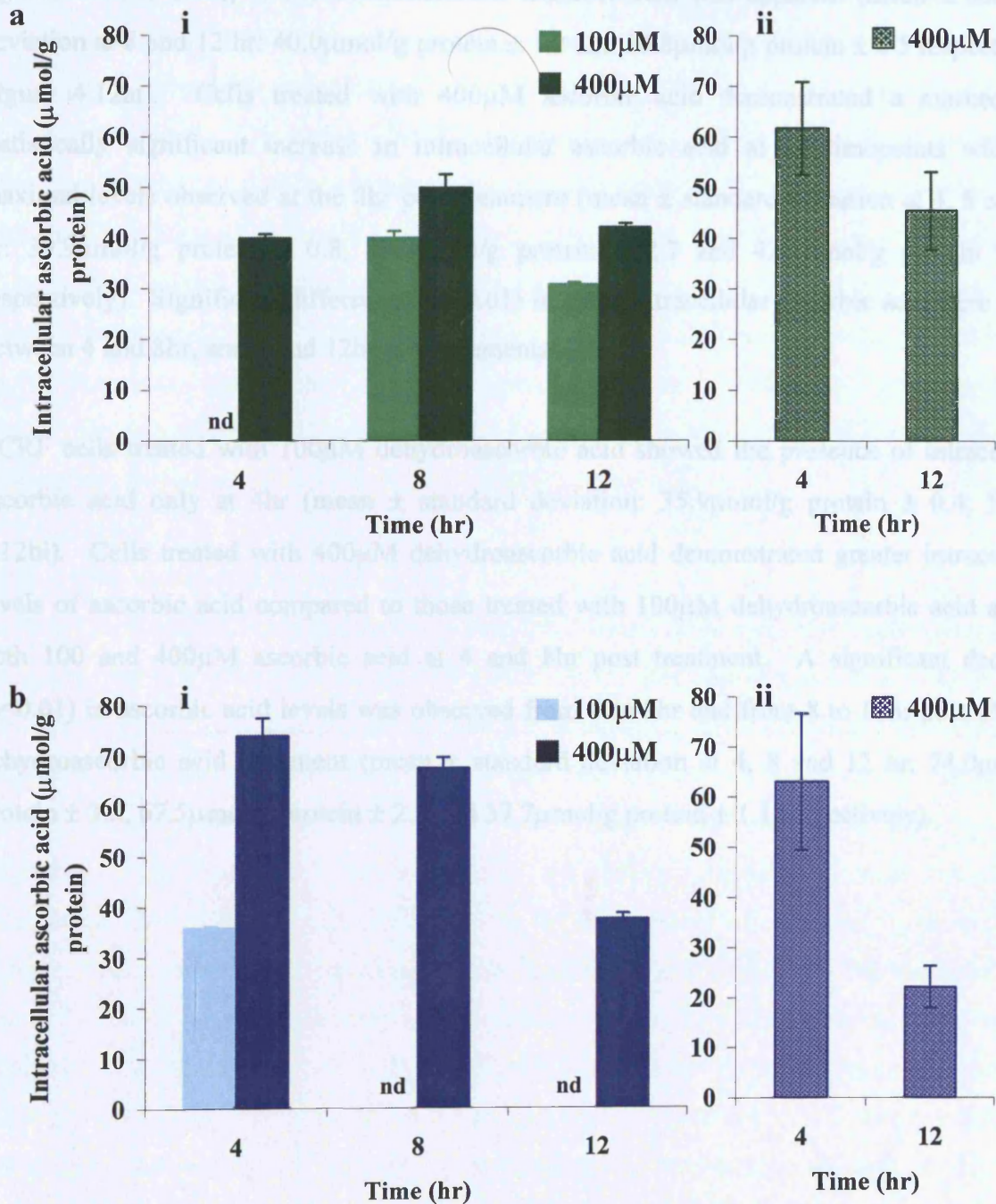


**Figure 4.12:** Capillary electrophoresis measurements of intracellular ascorbic acid following supplementation of cell cultures with 0-400µM ascorbic acid (a) or dehydroascorbic acid (b): CCRF (i) and THEK (ii) cells. All measurements were normalised to an isoascorbic acid internal standard and final concentrations of ascorbic acid were calculated from standard curve standard ranging from 0-1000µM. Each data point represents the mean (± standard deviation) of 4 measurements; **nd**: not detected/ascorbic acid levels below the limits of detection. Intracellular ascorbic acid at 0hr in both cell lines was at undetectable levels. All increases in intracellular levels of ascorbic acid post incubation represented were statistically significant ( $p < 0.01$ ) compared to basal levels.

Intracellular ascorbic acid was undetectable in CCRF cells prior to treatments with ascorbic acid or dehydroascorbic acid. Intracellular ascorbic acid in CCRF cells treated with 100 $\mu$ M ascorbic acid for 4hr were too low to be quantifiable, but at 8hr and 12hr post treatment a significant increase ( $p < 0.01$ ) in intracellular ascorbic acid was apparent (mean  $\pm$  standard deviation at 8 and 12 hr: 40.0 $\mu$ mol/g protein  $\pm$  1.3 and 30.8 $\mu$ mol/g protein  $\pm$  0.5 respectively, Figure 4.12ai). Cells treated with 400 $\mu$ M ascorbic acid demonstrated a marked and statistically significant increase in intracellular ascorbic acid at all timepoints with the maximal levels observed at the 8hr post treatment (mean  $\pm$  standard deviation at 4, 8 and 12 hr: 39.9 $\mu$ mol/g protein  $\pm$  0.8, 49.8 $\mu$ mol/g protein  $\pm$  2.7 and 42.1 $\mu$ mol/g protein  $\pm$  0.8 respectively). Significant differences ( $p < 0.01$ ) in mean intracellular ascorbic acid were noted between 4 and 8hr, and 8 and 12hr measurements.

CCRF cells treated with 100 $\mu$ M dehydroascorbic acid showed the presence of intracellular ascorbic acid only at 4hr (mean  $\pm$  standard deviation: 35.9 $\mu$ mol/g protein  $\pm$  0.4; Figure 4.12bi). Cells treated with 400 $\mu$ M dehydroascorbic acid demonstrated greater intracellular levels of ascorbic acid compared to those treated with 100 $\mu$ M dehydroascorbic acid and to both 100 and 400 $\mu$ M ascorbic acid at 4 and 8hr post treatment. A significant decrease ( $p < 0.01$ ) in ascorbic acid levels was observed from 4 to 8hr and from 8 to 12hr post 400 $\mu$ M dehydroascorbic acid treatment (mean  $\pm$  standard deviation at 4, 8 and 12 hr: 74.0 $\mu$ mol/g protein  $\pm$  3.5, 67.5 $\mu$ mol/g protein  $\pm$  2.2 and 37.7 $\mu$ mol/g protein  $\pm$  1.1 respectively).

## 4.5 DISCUSSION

The aim of this chapter was to establish *in vitro* cell model systems and assess the genotoxic potential of ROS and the efficacy of antioxidant treatments. To confirm the effectiveness of hydrogen peroxide at the induction of intracellular oxidation and genotoxicity, ROS was measured by the specific formation of 8-oxodG both in DNA and *in situ* by the investigation of antibody staining. To measure ROS generation directly in live cells a fluorogenic assay using a derivative of dichlorodihydrofluorescein diacetate (H<sub>2</sub>DCFDA) was optimised. In addition, the effects of antioxidants on cells in culture were confirmed by the direct measure of internalisation and regeneration of ascorbic acid following the treatment with ascorbic acid and dehydroascorbic acid respectively. These validation experiments provide the foundation for *in vitro* investigations into the modulation of cellular signalling and gene expression events. For this thesis these model systems will be used to assess two DNA repair enzymes important in the base excision repair of 8-oxodG (Chapter 5).

### 4.5.1 Measurement of 8-oxodG in DNA

Increases in 8-oxodG formation in DNA extracted from THEK and CCRF cells treated with hydrogen peroxide were demonstrated by HPLC-ECD. The basal level of 8-oxodG detected was approximately 2 adducts per 10<sup>5</sup> dG for both cell types, with levels doubling post treatment with hydrogen peroxide. Despite the clear differences in the amount of damage detected between treated and non treated cells, these basal levels were slightly higher compared to for example 0.33-0.9 8-oxodG per 10<sup>5</sup> dG reported in male and female lymphocyte DNA (Collins *et al.*, 1998). These differences may be explained by nature of the samples, that is culture cells may be subject to higher levels of oxidative stress compared to *in vivo* cells. However there are many considerations for the absolute measurement of 8-oxodG levels in extracted DNA. For example any inaccuracies with the spectrophotometric quantitation of DNA, hence the amount of DNA injected onto the HPLC was overcome by normalising the number of adducts to deoxyguanosine residues determined in the same chromatographic run. In addition, one important consideration was the generation of spurious damage during the extraction and digestion procedures; this was limited by the inclusion of desferrioxamine and the use of sodium iodide method of extraction (Helbock *et al.*, 1998; Wang *et al.*, 1994). DNA extraction methods have recently been assessed using LC-MS/MS and an 'internal standard' within cellular DNA comprising <sup>18</sup>O-labelled 8-oxodG (Ravanat *et al.*, 2002). Both the inclusion of desferrioxamine and the use of sodium iodide in DNA extraction were shown to be important in the minimisation of 8-oxodG in cellular DNA and in avoiding destruction of 8-oxodG during sample work-up.

The measurement of 8-oxodG has proved to be an invaluable marker of oxidative stress and potential genotoxicity. However, many previous studies report on varied and some falsely high levels of damage, therefore complicating interpretation and comparisons between other studies (Dizdaroglu *et al.*, 2002). There have been many improvements and considerations of the technical procedures over the past five years, with particular emphasis on the absolute measure of 8-oxodG and reduction in the inter-method and inter-laboratory variations (Collins *et al.*, 1997). Attempts to resolve these issues have been made by the establishment of the European Standards Committee on Oxidative DNA Damage (ESCODD, 2000; Lunec, 1998). The standardisation of 8-oxodG measurements will ultimately provide a more meaningful interpretation of data. Owing to the reported controversy about 8-oxodG levels it was therefore important in this thesis to confirm oxidative effects in *in vitro* models by other methods.

#### **4.5.2 Demonstration of 8-oxodG and cytosine glyoxal *in situ***

The analytical measurement of oxidation in DNA as a biomarker is useful, however some information is lost relating to tissue distribution and target sites *in vivo*. The application of antibodies specific for DNA adducts to pathological specimens can perhaps provide some insight. Since the earliest report of human cancer cell lines possessing the capacity of producing large amounts of hydrogen peroxide (Szatrowski and Nathan, 1991), many human tumours such as lung, breast, renal and colorectal cancers, have now been shown to have high levels of oxidative DNA damage compared with non-tumour tissues (Malins *et al.*, 1993; Okatmoto *et al.*, 1994, Olinski *et al.*, 1992). Two antibodies, one to 8-oxodG and the other to cytosine glyoxal, were applied to tissue specimens fixed in formaldehyde and embedded in paraffin wax. Little DNA damage was detected in human skin tumour specimens except with the anti-glyoxal antibody in discrete cells appearing typical of macrophages. The lack of DNA damage accumulation in tumour tissue and tumour surrounds may be interpreted as sufficient or effective DNA repair processes or that diseased tissues have enhanced protective mechanisms against ROS; but it is also possible that the antibodies are insufficiently sensitive to detect relatively low levels of oxidative damage. Interestingly however the pre-incubation of tissues with a combination of ascorbic acid and hydrogen peroxide appeared to yield a dose dependent increase in nuclear staining with both antibodies irrespective of the nature of the tissue. The precise mechanism of oxidative damage in this *in vitro* model requires further elucidation. However it may involve Fenton chemistry, where endogenous transition metal ions reduced by ascorbic acid react with hydrogen peroxide to yield hydroxyl radicals that ultimately damage DNA (Cai *et al.*, 2001).

THEK cells treated with hydrogen peroxide in culture displayed increases in 8-oxodG detected by immunocytochemistry. Non-specific binding of secondary antibody was evident in cells, despite the same secondary antibody being used for the cytokeratin studies described in chapter 3, suggesting this may be a direct result of the enhanced unmasking treatments and/or reduced blocking conditions. Recent work by Soultanakis and co-workers (2000) described an extended protocol for the detection of 8-oxodG in cultured cells with the same antibody, N45.1. Repetition of staining following this procedure did not significantly improve background staining problems.

The detection of ROS by immunochemical methods allows the distribution of damage within cells and heterogeneity between cell types in tissues to be identified, this information being lost by analytical procedures. However, antibodies do not detect all damage present in cells and tissues, and measurement of DNA damage is only semi quantitative at best. The major drawbacks with using antibody based technology to assess specific DNA adducts typical of ROS damage include specificity, sensitivity and reproducibility. Often, excessive unmasking techniques, as required by many DNA adducts antibodies can lead to increased non-specific binding, poor morphology and false positive results. The distribution and staining pattern of DNA adduct specific antibodies appear to vary in the literature. For example, the pattern of staining in nuclei can be described as discrete punctuate staining to more diffuse peripheral staining (Soultanakis *et al.*, 2000; Toyokuni *et al.*, 1999). Binding of any antibody to DNA adducts would therefore need to be validated by further techniques such as electron microscopy to ensure the location of antibody, hence adducts within the cells; this was successfully demonstrated in this thesis for the anti-CTD antibody (Chapter 3). Nevertheless, both the immunocytochemical and HPLC-ECD data for 8-oxodG provide evidence that the treatment of cultured cells with hydrogen peroxide generates oxidative stress leading to potential genotoxicity.

#### **4.5.3 Measurement of oxidative activity in living cells**

The intracellular generation of oxidative activity in live cells was assessed by a fluorescence-based assay involving CM-H<sub>2</sub>DCFDA, a derivative of H<sub>2</sub>DCFDA, selected for its improved retention in cells (Molecular Probes, [www.probes.com](http://www.probes.com)). CM-H<sub>2</sub>DCFDA is believed to passively diffuse into cells, where its acetate groups that assist cell permeation, are cleaved by intracellular esterases. The chloromethyl group reacts with intracellular glutathione and other thiols to maintain the subsequent fluorescent oxidation product within the cells (Molecular Probes, [www.probes.com](http://www.probes.com)). The generation of the fluorescent compound dichlorofluorescein through the oxidation of CM-H<sub>2</sub>DCFDA is believed to involve the combination of hydrogen

peroxide with a peroxidase or an iron or copper complex (Gray Laboratory Cancer Research Trust Report, [www.graylab.ac.uk/lab/report2000/report2000.html](http://www.graylab.ac.uk/lab/report2000/report2000.html)). Superoxide and its disproportion product, hydrogen peroxide, do not directly oxidise CM-H<sub>2</sub>DCFDA. Therefore any increases in dichlorofluorescein generation cannot confirm increased rates of superoxide and/or hydrogen peroxide production. Increases may even reflect decreased superoxide radical generation but increases in hydroxyl radical formation through the catalysed decomposition of hydrogen peroxide (Gray Laboratory Cancer Research Trust Report, [www.graylab.ac.uk/lab/report2000/report2000.html](http://www.graylab.ac.uk/lab/report2000/report2000.html)).

The detection of oxidative activity in cultured cells was successfully achieved with CM-H<sub>2</sub>DCFDA. The 96-well plate assay developed here, allowed the efficient and reproducible analysis of cells treated under a variety of conditions. The variation in fluorescence measurements owing to the heterogenous growth of cells within each well was overcome by the multiple measurements taken within each well. In addition any interference of the cell culture medium and/or treatment reagents on the fluorescence measurements was successfully addressed. The treatment of both THEK and NHEK cells with a range of hydrogen peroxide concentration showed a dose dependent increase in oxidative activity. Most of the changes observed were significantly different between controls and treated cells, as well as between different doses. The greatest differences in these fluorescence measurements were observed in readings taken in the first 30min post treatment, possibly suggesting saturation of fluorescence generation with the higher doses of hydrogen peroxide or the degradation of the CM-H<sub>2</sub>DCF. Nevertheless the treatment of cells in culture with hydrogen peroxide clearly resulted in increases in intracellular oxidative activity, further supporting the observed increases in 8-oxodG detected by HPLC-ECD and immunocytochemistry following similar treatments with hydrogen peroxide.

Whilst hydrogen peroxide might be expected to generate an oxidative environment in cells, antioxidants might be expected to do the opposite. Ascorbic acid was investigated in terms of its potential to affect DNA damage levels and potentially modulate DNA repair mechanisms in cells and tissues (Rehman *et al.*, 1998; Podmore *et al.* 1998). THEK cells treated with various doses of either ascorbic acid or dehydroascorbic acid demonstrated some modulation in intracellular oxidative activity. At the higher concentrations the levels of fluorescence generation increased compared to controls, however these differences were not observed beyond 30min incubation. These early changes may have resulted from membrane potential effects since the uptake of ascorbic acid and dehydroascorbic acid did not coincide with ROS generation. Particularly, the measurement of extracellular ascorbic acid following the

incubation of cells in PBS, revealed little depletion in ascorbic acid with time; unlike the rapid depletion observed with DMEM or RPMI medium. Interestingly neither ascorbic acid nor dehydroascorbic acid had the capacity to decrease basal intracellular oxidative activity in THEK cells during the period of treatment monitored. Perhaps the pre-incubation of cells with ascorbic acid or dehydroascorbic acid prior to the addition of CM-H<sub>2</sub>DCFDA may have resulted in the reduction of basal oxidative stress or potential protection from subsequent hydrogen peroxide treatments. Similarly any 'prooxidant' effects of ascorbic acid, particularly at high doses, may be demonstrated by pre-treating cells with either ascorbic or dehydroascorbic acid for periods long enough to ensure internalisation or regeneration of ascorbic acid.

The many forms of reactive oxygen as well as reactive nitrogen present in the intracellular compartment complicate the use of fluorogenic compounds to assay oxidative activity in living cells. In order to discriminate between these species, specific blocking agents or enzymes can be used, for example the addition of an arginine analogue, N<sup>G</sup>-methyl-L-arginine can block the effects of nitric oxide (Klatt *et al.*, 1994; Olken *et al.*, 1994; Rivier and Shen 1994). All treatments of CM-H<sub>2</sub>DCFDA-loaded cells were conducted in PBS as opposed to cell culture medium, owing to high background fluorescence measurements of medium. Therefore to minimise the potential cytotoxic effects of cells in PBS, all measurements were taken within one hour. In order to measure long-term changes in oxidative activity, cells would have to be treated prior to the loading of CM-H<sub>2</sub>DCFDA. In doing so the changes may show the status of oxidative activity at the time of other measurements of cellular change. Despite this, the increases in oxidative activity following the treatment of THEK cells with hydrogen peroxide in PBS, was mirrored by the increases of 8-oxodG formation in cells treated with hydrogen peroxide in medium, as determined by HPLC-ECD analyses of DNA and by immunocytochemistry.

#### **4.5.4 Stability of ascorbic acid in cell culture medium**

The stability of ascorbic acid in cell culture medium was investigated by both HPLC and CE measurements. Initial HPLC measurements of extracellular ascorbic acid revealed a notable depletion in the levels of ascorbic acid following incubation in DMEM compared to PBS where levels remained relatively constant during the 4hr of incubation at 37°C. The approximate 2-3 fold depletion of ascorbic acid in DMEM observed in the first 4hr was reproduced by CE analysis in separate experiments. The measurement of ascorbic acid in PBS was not repeated by CE analysis since the morphological appearance of the THEK cells was altered and signs of cytotoxicity were apparent by 4hr, and therefore the treatment of

cells in PBS for long periods was abandoned. Instead, ascorbic acid was measured in the medium on cultured cells.. Interestingly some reduction in ascorbic acid was noted in RPMI medium of CCRF cells throughout the timecourse, however the degree of reduction was substantially less than that observed in DMEM medium. In both DMEM and RPMI medium the level of ascorbic acid was undetectable prior to the addition of ascorbic acid.

Muller *et al.*, 1997 suggested treatment of cells with antioxidants in DMEM medium appeared to be unsuitable due to the presence of various transition metal ions such as iron and copper. Many *in vitro* studies have demonstrated pro-oxidant properties of ascorbic acid through its ability to reduce transition metal ions, which in turn can lead to further oxidation reactions and the production of ROS (Cai *et al.*, 2001). Therefore interpreting the cellular changes evoked by ascorbic acid requires careful consideration in an *in vitro* system. For this reason CCRF cells were chosen as an alternative model as the cells maintained in RPMI medium, a basal medium relatively free of transition metal ions (Appendix I). Also, this cell line was clinically relevant since measuring 8-oxodG levels in lymphocyte DNA as a non-invasive biomarker has been applied in many dietary intervention studies. In addition, this cell line proved more manageable with the large cell numbers required for certain assays.

#### **4.5.5 Internalisation and/or regeneration of ascorbic acid**

The extracellular measurement of ascorbic acid in culture medium was complemented with the measurement of ascorbic acid in the cells. Both CCRF and THEK cells were treated with ascorbic acid or dehydroascorbic acid and the intracellular levels of ascorbic acid determined by CE. Owing to the low UV absorbance, dehydroascorbic acid could not be efficiently measured alongside ascorbic acid in these experiments. Prior to the treatment with either reagent the basal levels of ascorbic acid were beyond the limits of detection of the assay; by 4hr post incubation the levels had dramatically increased in both cell types. In cells treated with high non-toxic doses of ascorbic acid the levels of intracellular ascorbic acid were sustained throughout the 12hr timecourse. However cells treated with 100µM ascorbic acid demonstrated a longer lag phase, as seen in CCRF cells. Interestingly, the intracellular levels of ascorbic acid following 100µM or 400µM dehydroascorbic acid treatment were maximal at 4hr suggesting a more rapid uptake mechanism compared to ascorbic acid. After 4hr a gradual reduction or a total depletion in intracellular ascorbic acid was observed during the 12hr timecourse in cells treated with dehydroascorbic acid. Due to large numbers of cells required for these measurements further timepoints were not included, however it was probable that the maximal levels of intracellular ascorbic acid following dehydroascorbic acid treatment may have been detected between 0 and 4hr post incubation. These results clearly

demonstrate the capacity of both cell types to internalise or regenerate ascorbic acid irrespective of cell culture medium. However, the differences in the rate of extracellular ascorbic acid depletion may be a result of the transition metal ions in DMEM or more efficiency of uptake by THEK cells compared to CCRF cells.

Ascorbic acid is reported to be internalised by certain cells through sodium-dependent ascorbic acid transporters (Tsukaguchi *et al.*, 1999), whilst dehydroascorbic acid is transported via facilitative glucose transport (Rumsey *et al.*, 2000; Vera *et al.*, 1993; Welch *et al.*, 1995). Once dehydroascorbic acid is internalised it is rapidly reduced to ascorbate in an enzymic (Park and Levine, 1996; Wells and Xu, 1994) or non-enzymic manner involving reduced glutathione (Vera *et al.*, 1995; Winkler *et al.*, 1994). The uptake mechanism for dehydroascorbic acid is reported to be much faster (approximately 10 fold) compared to ascorbic acid (Lutsenko *et al.*, 2002; Welch *et al.*, 1995). Interestingly Lutsenko and co-workers (2002) also demonstrated that pre-loading cells with ascorbic acid reduced the mutations induced by hydrogen peroxide treatments. Both cell types investigated in this chapter displayed efficient uptake of both ascorbic acid and dehydroascorbic acid and therefore these antioxidant conditions may have important anti-mutator activities, such as through the stimulation of DNA repair enzymes.

#### **4.5.6 Conclusion**

The aim of this chapter was to establish *in vitro* cell model systems in order to investigate the effects of ROS and antioxidants by confirming the efficacy of the treatment reagents. The main findings were:

- ❖ Endogenous ROS generation was successfully detected in live cells by a fluorogenic assay and genotoxic damage detected by immunochemistry and HPLC in fixed cells or extracted DNA.
- ❖ Treatment of cells with hydrogen peroxide caused increases in intracellular ROS and genotoxicity, demonstrated by the detection of 8-oxodG in DNA.
- ❖ The kinetics of uptake and regeneration of ascorbic acid following treatment with ascorbic acid or dehydroascorbic acid was demonstrated in both THEK and CCRF by the intracellular increase in ascorbic acid and/or the depletion of extracellular ascorbic acid.
- ❖ Ascorbic acid and dehydroascorbic acid caused a transient increase in intracellular ROS. Further studies to relate the kinetics of ascorbic acid uptake with intracellular ROS generation are required.
- ❖ The measures of oxidative stress and antioxidants in these *in vitro* cell models validate the efficacy of the experimental/ treatment conditions and provide the foundation for the work described in chapter 5.

**CHAPTER FIVE**

**THE EXPRESSION OF BASE EXCISION REPAIR ENZYMES  
SPECIFIC FOR THE REMOVAL OF 8-OXOGUANINE  
LESIONS**

## **5.0 THE EXPRESSION OF BASE EXCISION REPAIR ENZYMES SPECIFIC FOR THE REMOVAL OF 8-OXOGUANINE LESIONS**

### **5.1 INTRODUCTION**

The genetic stability of cells requires efficient repair mechanisms for direct and indirect UV-induced DNA damage. Both solar UVA and UVB have the capacity to generate reactive oxygen species and generate adducts characteristic of indirect UV damage. One such well-studied DNA adduct 7,8-dihydro-8-oxo-2'-deoxyguanosine (8-oxodG; Kasai, 1997), has been shown to display mutagenic potential by inducing GC→TA transversions (Michaels *et al.*, 1992; Thomas *et al.*, 1996). This adduct is repaired predominantly via the base excision repair (BER; section 1.2.1) pathway but other pathways, such as the nucleotide excision repair system, may also play a role (Jaiswal *et al.*, 1998; Reardon *et al.*, 1997).

In humans, BER of 8-oxodG appears to primarily involve two enzymes: 7,8-dihydro-8-oxoguanine (8-oxoG) DNA glycosylase (hOGG1) and an apurinic/apyrimidinic endonuclease (hAPE) (Dianov *et al.*, 1998). Although hOGG1 has dual glycosylase and AP lyase (class I endonucleases) enzyme activities, the removal of 8-oxodG is initiated by the glycosidic cleavage of the oxidized base involving a transient covalent enzyme-DNA interaction involving Lys249 residue (Bruner *et al.*, 2000; Nash *et al.*, 1996). The resulting abasic (AP) site in DNA can block DNA replication or can lead to mutagenesis, and therefore is eliminated by the action of class II endonucleases that cleave the phosphodiester bond 5' to the AP site (Figure 5.1). Recent *in vitro* studies have described that hOGG1 and hAPE act in tandem and the rate-limiting step of the AP lyase of hOGG1 can be bypassed by hAPE, which causes the displacement of hOGG1 thus freeing the enzyme for subsequent reactions (Hill *et al.*, 2001; Vidal *et al.*, 2001). In addition, Saitoh *et al.* (2001) showed AP lyase activity of a GST-hOGG1 protein was increased by the addition of hAPE enzyme.

In *Escherichia coli* three DNA repair enzymes have been associated with the prevention of potential mutations stemming from 8-oxodG lesions: Mut M protein (Fpg protein) excises 8-oxoG [as well as imidazole ring-opened forms of guanine 2,6-diamino-4-hydroxy-5-formamidopyrimidine (FapyGua) and adenine 4,6-diamino-5-hydroxy-5-formamidopyrimidine (FapyAde)] from DNA (Boiteux *et al.*, 1992); Mut Y excises misincorporated adenine opposite 8-oxoG during DNA replication (Michaels *et al.*, 1992) and Mut T protein, an 8-oxodGTPase that can block 8-oxodG misincorporation and prevent

potential AT→CG transversions (Maki and Sekiguchi, 1992). Michaels *et al.* (1992) also demonstrated, inactivation of *fpg* (*mut M*) and *mutY* (*micA*) genes leads to a strong GC→TA mutator phenotype in *E. coli*. Cloning of the *Saccharomyces cerevisiae* *OGG1* gene by functional complementation revealed some functional homology to *E. coli* Mut M protein (van der Kemp, *et al.*, 1996) and similar accumulation of GC→TA transversions in *OGG1*-deficient strains (Thomas *et al.*, 1996). A second *S. cerevisiae* 8-oxodG glycosylase (*OGG2*), described by Nash *et al.* (1996), displayed preferential substrate specificity for 8-oxodG paired opposite guanine as opposed to cytosine, as in the case of *OGG1*.

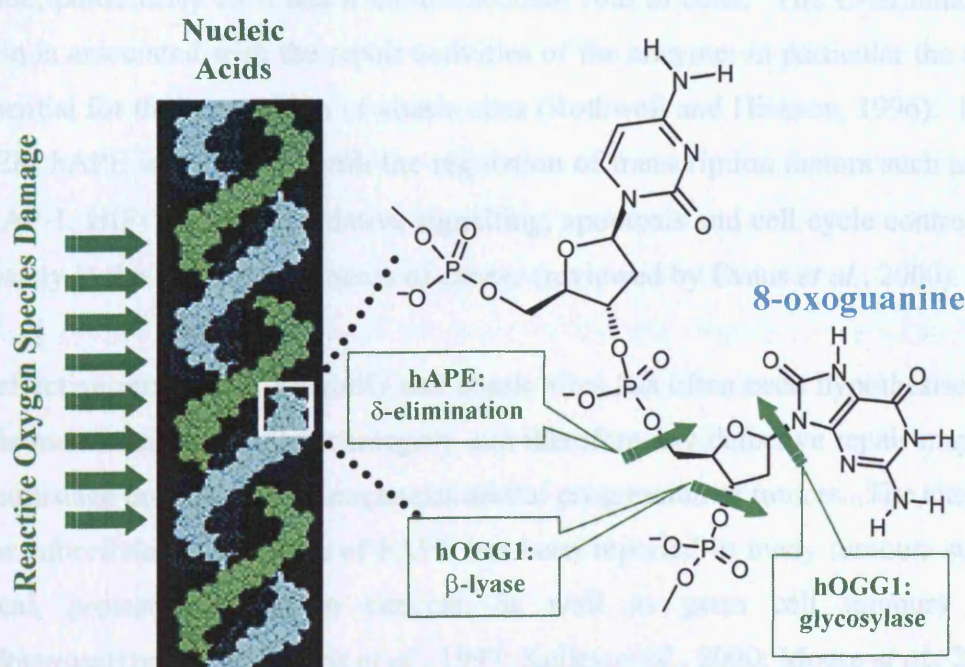


**Figure 5.1:** The interaction of hOGG1 & hAPE: their enzymatic potentials in the repair of the oxidative lesion 8-oxoguanine.

Cloning of mammalian *OGG1* genes revealed that both the mouse protein (Boiteux *et al.*, 1998), and the human protein (Arai *et al.*, 1997; Radicella *et al.*, 1997; Roldán-Arjona *et al.*, 1997; Rosenquist *et al.*, 1997) shared 38% amino acid homology to the yeast *OGG1* protein as well as similar preferential substrate specificity. Several isoforms of *hOGG1* transcripts have been described resulting from alternative splicing of the *hOGG1* gene localised on chromosome 3p25 (Aburatani *et al.*, 1997; Kohno *et al.*, 1998; Nishioka *et al.*, 1999, Radicella *et al.*, 1997). Two major isoforms have the same substrate specificity but have been shown to target either the nucleus or mitochondria;  $\alpha$ -hOGG1 contains a nuclear targeting signal at the C-terminus (translated from exon7), whilst  $\beta$ -hOGG1, lacking exon 7, localises to the mitochondria. Each isoform of hOGG1 may have specific intracellular localisation as

well as distinct functions. Hazra *et al.*, (1998) reported a second human 8-oxodG DNA glycosylase (hOGG2), that preferentially targets 8-oxodG incorporated through 8-oxodGTP opposite an adenine residue in DNA. This base pairing demonstrates a higher mutagenic potency compared to 8-oxoG paired opposite to cytosine (Le Page *et al.*, 1998).

In humans one major AP endonuclease (hAPE) was cloned through functional and sequence homology to *E coli* exonuclease III (Demple *et al.*, 1991; Robson and Hickson, 1991). *hAPE* is localised on chromosome 14q 11.2-12 (Robson *et al.*, 1992) and the 36 kDa monomer protein is often referred to as APE, HAP-1, APEX or Ref-1. Much more is known about this enzyme, particularly as it has a multifunctional role in cells. The C-terminal region of the protein is associated with the repair activities of the enzyme; in particular the asparagine 212 is essential for the recognition of abasic sites (Rothwell and Hickson, 1996). Besides its role in BER, hAPE is associated with the regulation of transcription factors such as CREB, ATF, p53, AP-1, HIF-1 $\alpha$ , HLF, oxidative signalling, apoptosis and cell cycle control and therefore ultimately in the multistage process of cancer (reviewed by Evans *et al.*, 2000).

The effective removal of 8-oxodG and abasic sites has often been hypothesised to be crucial for the maintenance of cellular integrity and therefore any defective repair may play a role in the multistage process of carcinogenesis and/or progression of tumors. The altered expression and/or subcellular localisation of hAPE has been reported in many tumours such as ovarian, cervical, prostate and colon cancers, as well as germ cell tumours and pediatric rhabdomyosarcomas (Kakolyris *et al.*, 1997; Kelley *et al.*, 2000; Moore *et al.*, 2000; Thomson *et al.*, 2001; Xu *et al.*, 1997). Similarly, the dysfunction of hAPE has been associated with neurodegenerative disease and aging (Mitra, 1999).

Several studies demonstrate high levels of 8-oxodG in tumours of the lung, kidney and the colon compared to tissues of 'normal'/non-cancerous equivalents (Kondo *et al.*, 2000; Okamoto *et al.*, 1994; Oliva *et al.*, 1997). Interestingly, hOGG1 is located on chromosome 3p25, the 3p region of the chromosome commonly shown by cytogenetic and molecular analyses to be associated with loss of heterozygosity and deletions in many major human cancers. A recent study by Audebert *et al.* (2000) demonstrates somatic missense mutations in the *hOGG1* gene in 4 of 99 human kidney clear cell carcinomas examined. Similarly, Chevillard *et al.* (1998) showed single base substitution in *hOGG1* gene in 2 of 25 small cell lung cancer and 1 of 15 kidney carcinomas examined; and Wikman *et al.* (2000) demonstrated the significance of loss of heterozygosity in lung tumourigenesis.

## 5.2 AIMS

Both *hOGG1* and *hAPE* gene products are ubiquitously expressed at low levels in all tissues, however both enzymes have been suggested to respond to conditions of oxidative stress. For example, studies by Lee *et al.*, 1996 showed a dose- and time-dependent increase in 8-oxodG glycosylase activity in rat kidney extracts following exposure to potassium bromate. Similarly, Tsurudome *et al.* (1999) described a reduction in 8-oxodG repair activity in rat lung extracts following an initial exposure to diesel exhaust particles. This activity recovered by day 5 and coincided with an increase in *OGG1* mRNA. Recently, Saitoh *et al.* (2001) demonstrated changes in *hAPE* protein expression and *OGG1* protein activity in HeLa cells following severe oxidative stress with hypochlorous acid treatment.

In addition to the possible response of *hOGG1* and *hAPE* to oxidative stress, both genes have potential antioxidant response elements (ARE) within their promoter sequences, suggesting they may be redox sensitive genes. Further to this observation, studies have shown that supplementation of human volunteers with 500mg/day vitamin C significantly reduced the levels of 8-oxodG in peripheral blood lymphocyte DNA, suggesting possible modulation of *hOGG1* and *hAPE* expression and/or activity (Rehman *et al.*, 1998; Podmore *et al.* 1998). The aim of this chapter is to study the mechanism for the apparent modulation of BER activity in humans *in vitro* models. This will include establishing methodologies to investigate gene, protein and enzyme activity levels of both *hOGG1* and *hAPE* and responses to either ROS or antioxidant stimuli.

## **5.3 METHODS**

### **5.3.1 Cell Culture and Treatment**

THEK cells were cultured in petri dishes and serum starved at 70% confluence. CCRF cells were serum starved at  $1 \times 10^6$ /mL cell density (section 2.3.1). Cells were treated with filter sterilised hydrogen peroxide, ascorbic acid or dehydroascorbic acid at doses of 0, 50, 100, 200 and 400 $\mu$ M in serum deficient medium. Cells were incubated at 37°C for periods ranging between 0 and 24hr and then washed twice in PBS prior to collection of either RNA (section 2.3.4.2) or cell lysates (section 2.3.4.4).

### **5.3.2 Measurement of cytotoxicity and cellular synchrony**

Cytotoxicity induced by hydrogen peroxide, ascorbic acid and dehydroascorbic acid treatments was determined by Trypan Blue exclusion in both THEK and CCRF cells (section 2.3.2.1). Triplicate measurements were taken at 4, 8 and 12hr post treatment, and the results expressed as the mean and standard deviation of percentage viability. The efficiency of serum starvation to arrest cell proliferation and promote cellular quiescence prior to studies examining modulation of gene and protein expression was performed by cell cycle analysis by flow cytometry of fixed cells stained with propidium iodide (section 2.3.2.2).

### **5.3.3 Measurement of transcription factor activation**

THEK cells were treated with various doses of either hydrogen peroxide or ascorbic acid and nuclear protein extracted following the method described by Staal *et al.* (1990) (section 2.3.4.5). Protein concentrations were determined (sections 2.3.4.4) and 4 $\mu$ g of nuclear extract incubated with  $^{32}$ P-end labelled double stranded oligonucleotide containing a consensus AP-1 site (section 2.3.5.2). Controls included 16nM 12- O-tetradecanoylphorbol 13-acetate (TPA) treated extracts as positive control, and incubation of extracts with competitor and non-competitor DNA to confirm band shift. Samples were resolved on a 4% non-denaturing polyacrylamide gel and AP-1 gel shift bands were visualised by autoradiography (section 2.3.6.2). Results were quantified by densitometry and expressed as fold increase from control levels.

### **5.3.4 Measurement of hOGG1 and hAPE gene expression**

#### *Isolation of RNA and RT-PCR*

Total RNA was extracted (section 2.3.4.2) and the purity and concentration assessed spectrophotometrically. Optimal RT-PCR conditions (section 2.3.5.1) were initially established by assessing a range of MgCl<sub>2</sub> concentrations (0.5-3 $\mu$ M), annealing temperatures (between 51-61°C) and PCR cycle numbers (20-40 cycles), for all three sets of primers ( $\beta$ -

actin, hOGG1 and hAPE). Primers designed to hOGG1 and hAPE mRNA were originally based on cDNA sequences since, at the time the full genomic sequences for hOGG1 and complete intron-exon boundaries for the hAPE genomic sequences were unavailable. Genomic DNA contamination during RT-PCR can be effectively controlled for if primers to a gene anneal to two separate exons. To assess whether the hOGG1 and hAPE primers could amplify an intron region (as with the  $\beta$ -actin primers), PCR of genomic DNA prepared by the Pronase method (section 2.3.4.1) was performed. Further validation of RT-PCR conditions involved the sequencing RT-PCR products extracted from gels (section 2.3.4.3).

PCR products from treatment experiments were resolved in duplicate on 1.5% (w/v) agarose gels containing ethidium bromide, visualised under UV light and images captured on Polaroid film (section 2.3.6.1). Photographic negatives were used for semi-quantitative densitometry measurements (section 2.2.6). The measurements of *hOGG1* and *hAPE* mRNA expression were normalised to  *$\beta$ -actin* levels (a measure of total RNA), and the mean and standard deviation calculated for two separate values obtained from three independent experiments for each cell type (except where stated, section 2.3.8).

#### *Sequencing of hOGG1 and hAPE PCR products*

To confirm the specificity of all three sets of primers, PCR products were prepared for sequencing. All residual dNTPs and enzymes were removed by standard sodium acetate/ethanol precipitation, and then quantified using  $\lambda$  DNA standards on agarose gels (section 2.3.4.3). The remainder of the protocol was kindly performed by the Protein and Nucleic Acids Chemistry Laboratory (PNAACL, University of Leicester) involving further extraction of 40ng of template by Centriscap columns and analysis using a 377 ABI sequencer.

### **5.3.5 Measurement of hOGG1 and hAPE protein expression**

#### *Production and characterisation of hOGG1 antibody*

Anti-hOGG1 peptide antibody was produced according to Harza *et al.* (1998) (section 2.3.3.1). Polyclonal antiserum production was monitored in test bleeds during the immunisation protocol by ELISA employing hOGG1 peptide as antigen (section 2.3.3.3). IgG fractions were purified from both pre-immune and immune serum (section 2.3.3.2) and antibody specificity was tested against whole cell extracts from THEK and CCRF cells and purified hOGG1 protein by Western blotting (section 2.3.3.4). Further validation experiments involved pre-incubation of IgG fractions with an excess of either peptide or purified protein (a gift from Dr S Boiteux, Fontenay aux Roses, France) to assess inhibition of antibody binding.

### *hAPE and hOGG1 Western blotting*

Whole cells extracts were collected following treatment of THEK and CCRF cells with hydrogen peroxide, ascorbic acid or dehydroascorbic acid and assayed for protein content (sections 2.3.4.4 and 2.3.4.5). Proteins were resolved on a 12% SDS PAGE gel and blotted onto PVDF membrane (section 2.3.3.4). Ponceau S staining prior to immunochemical detection was used routinely to assess efficiency of protein transfer. Optimal primary and secondary antibody concentrations were investigated for  $\beta$ -actin, hAPE and hOGG1 protein detection.

### *hAPE and hOGG1 immunocytochemistry*

The application of hAPE and hOGG1 antibodies to examine cellular localisation and expression of these proteins was investigated in THEK cells. Cells were fixed in either 50:50(v:v) acetone: methanol, methanol alone or 4% (w/v) formaldehyde (pH 7.4). Optimal blocking, primary and secondary antibody concentrations were also investigated and the nuclei counterstained with propidium iodide (section 2.3.3.5). For co-localisation studies, mitochondria were visualised by pre-loading live cells with a fluorescent mitochondrial stain prior to fixation with formaldehyde. This involved incubation of cells with 500nM MitoTracker<sup>®</sup> CMXRos in culture medium for 15min at 37°C. Nuclei were also counterstained with Hoechst 33258, emitting blue fluorescence (section 2.3.3.5).

### **5.3.6 Measurement of combined hOGG1 and hAPE enzyme activity**

Both a biotinylated and non-biotinylated double-stranded 21-22mer oligonucleotide substrate for hOGG1 and hAPE enzyme activity were prepared (section 2.3.5.3). The efficiency of annealing and the preparation of these double-stranded oligonucleotide substrates were verified by Metaphor<sup>®</sup> agarose electrophoresis (section 2.3.6.1). Cell lysates obtained from treatment experiments of CCRFs with hydrogen peroxide were incubated for 2hr at 37°C with either control or 8-oxodG-containing double-stranded oligonucleotide substrate. Other controls included a 0hr incubation of the oligonucleotide substrates with cell lysates. Biotinylated or non-biotinylated oligonucleotides were extracted from the lysate mix by Streptavidin coated Dynabeads<sup>®</sup> or by a standard sodium acetate/ ethanol extraction, respectively (section 2.3.4.3). Extracted oligonucleotides were resolved by either denaturing-PAGE (section 2.3.6.2) or capillary electrophoresis (section 2.3.6.3). Repair activity was expressed as percentage of conversion of oligonucleotide substrate into the 11-12mer repair product.

## 5.4 RESULTS

### 5.4.1 Cytotoxicity, cell cycle analyses & transcriptional activity of *in vitro* models

Cellular cytotoxicity was measured by Trypan Blue exclusion in THEK and CCRF cells following treatment with 0, 100 and 400 $\mu$ M hydrogen peroxide, ascorbic acid and dehydroascorbic acid (Figure 5.2). Triplicate measurements were taken at 4, 8 and 12hr post treatment and expressed as the mean and standard deviation of percentage viability. No obvious effect on cellular viability was seen for both cell types, with all measurements ranging between 85-100% viability, for any of the doses and at any of the timepoints for all three treatments.

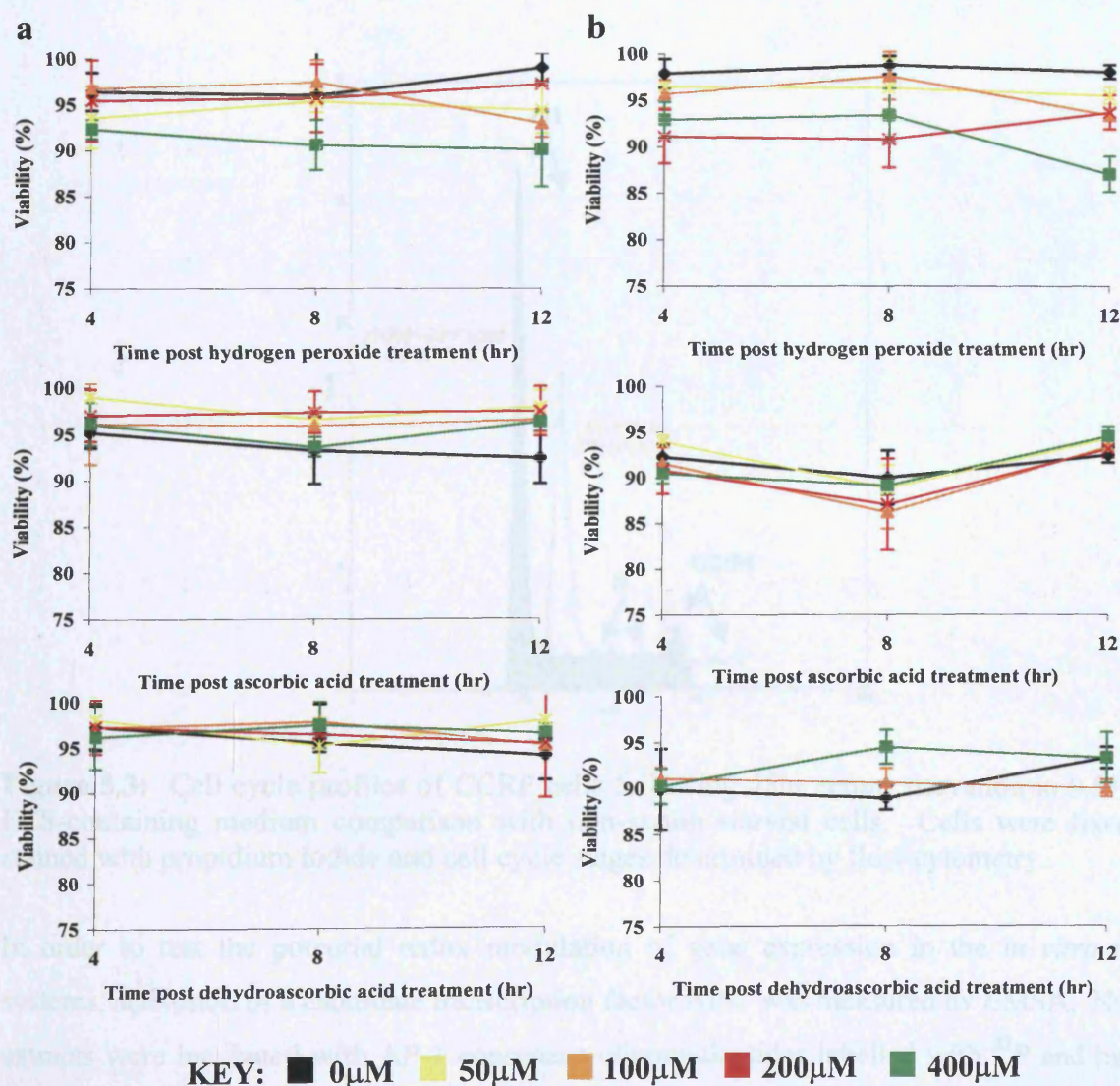


**Figure 5.2:** Effects of hydrogen peroxide, ascorbic acid and dehydroascorbic acid on cytotoxicity in CCRF (a) and THEK (b) cells. Cells were treated with 0-400 $\mu$ M hydrogen peroxide, ascorbic acid or dehydroascorbic acid for 4, 8 and 12hr at 37°C, and cellular viability was determined by Trypan Blue exclusion. The data represent the mean ( $\pm$  standard deviation) percentage viability determined by triplicate haemocytometry measurements.

To ensure cells were in resting phase prior to treatment, the efficiency of serum starvation was also measured by flow cytometry. CCRF cells were serum starved for 24 and 48hr in 0.5%(v/v) FCS-containing medium, cells were then fixed and stained with propidium iodide to measure DNA content and thus cell cycle status (Figure 5.3). At 48hr most cells were in G1 and S phase and cells in G2/M had decreased compared to non-serum-starved controls (Figure 5.3). Prior to each experiment, CCRF cells were also counted pre- and post- serum starvation to assess for quiescence. To ensure THEK cells were in stationary phase, cells were trypsinised and counted before and after serum-starvation. For subsequent experiments cells were monitored by microscopy. THEK cells were serum starved at 60-70% confluence for 48hr and re-assessed to ensure cells had not reached confluence and undergone any gross morphological change prior to each treatment.

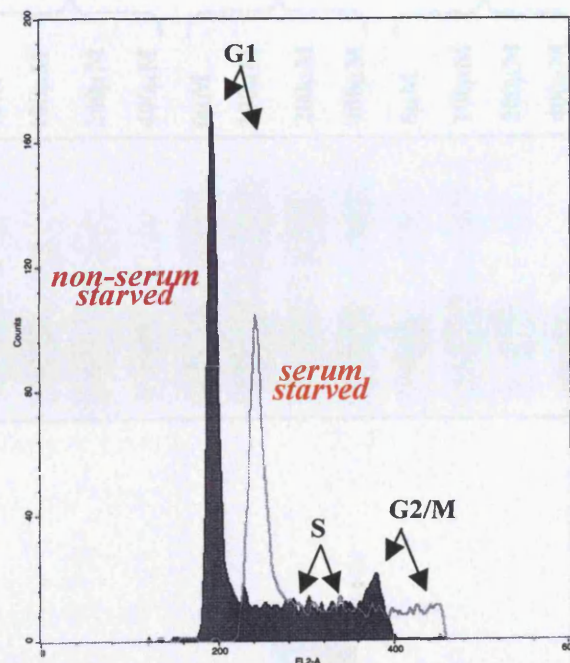


**Figure 5.3:** Cell cycle profiles of CCRF cells following 48hr serum starvation in 0.5%(v/v) FCS-containing medium comparison with non-serum starved cells. Cells were fixed and stained with propidium iodide and cell cycle stages determined by flow cytometry.

In order to test the potential redox modulation of gene expression in the *in vitro* model systems, activation of a candidate transcription factor AP-1 was measured by EMSA. Nuclear extracts were incubated with AP-1 consensus oligonucleotides labelled with  $^{32}\text{P}$  and binding of proteins measured as a band shift on autoradiographs following separation on non-denaturing PAGE. Positive controls included a nuclear extracts from cells treated with TPA, a known activator of AP-1 binding. Other experimental controls included incubation of nuclear extracts in the presence of non-radiolabelled DNA as competitor, or with a radiolabelled non-specific oligonucleotide as non-competitor. Activation of AP-1 binding in

CCRF nuclear extracts was previously demonstrated following treatment of cells with 10-250 $\mu$ M ascorbic acid for 2-4hr; a two fold increase in AP-1 binding was observed with 50 and 100 $\mu$ M ascorbic acid at 3-4hr (personal communication Dr K Holloway, Division of Chemical Pathology, University of Leicester). Treatments of THEK cells with 0, 100, 200 and 400 $\mu$ M ascorbic acid demonstrated a similar pattern of AP-1 binding activity to that seen with CCRF cells. AP-1 DNA binding activity was enhanced at 2hr with doses of 100 and 200 $\mu$ M ascorbic acid (Figure 5.4), with maximum DNA binding activity observed in cells treated with 100 $\mu$ M ascorbic acid. At 1 and 4hr post treatment with ascorbic acid, AP-1 activity was reduced compared to controls in a dose responsive manner.

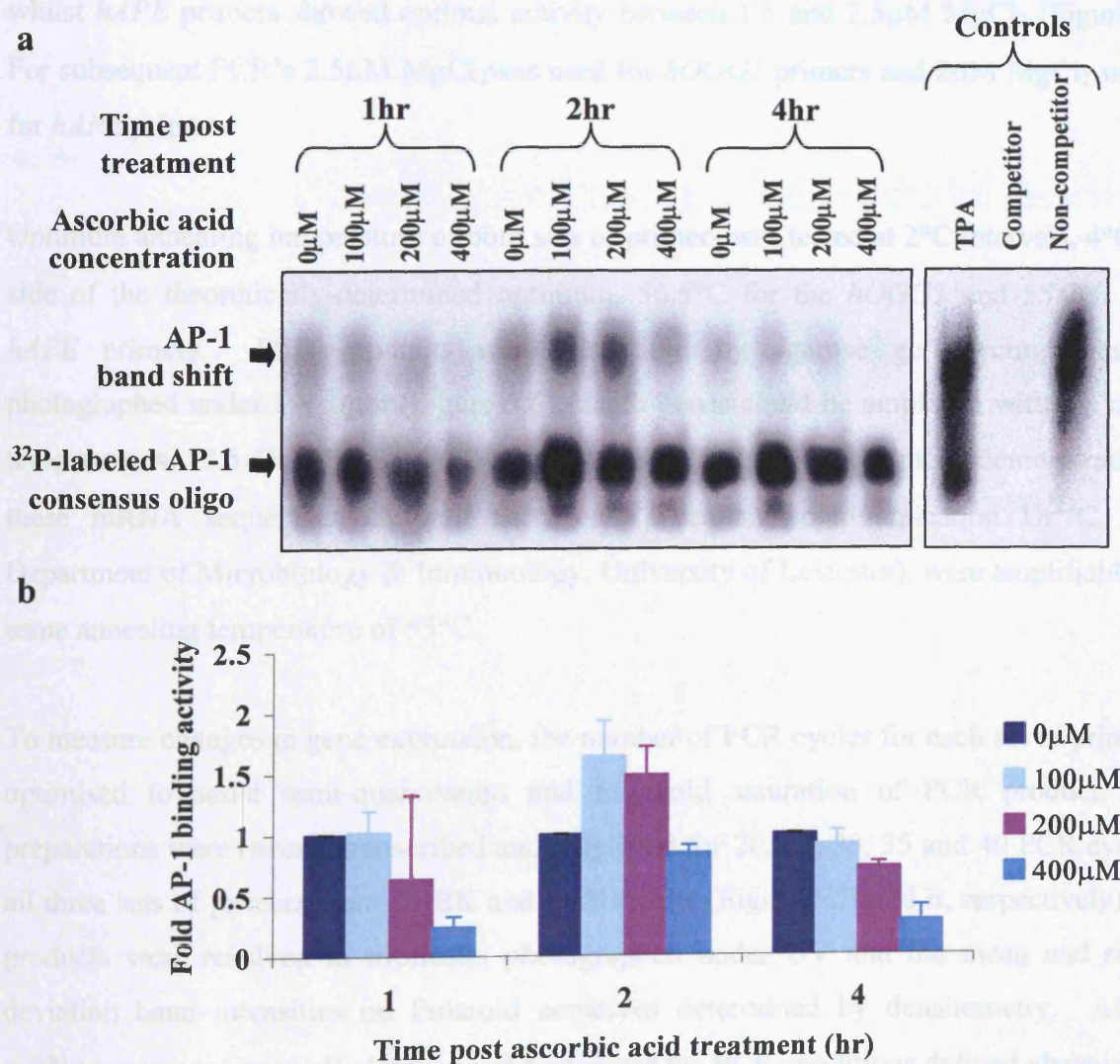


**Figure 5.4:** Electrophoretic mobility shift assay measuring AP-1 DNA binding activity in THEK nuclear extracts of cells treated with 0, 100, 200 and 400 $\mu$ M ascorbic acid. Nuclear extracts were collected at 1, 2 and 4hr post treatment and 4 $\mu$ g protein incubated with  $^{32}$ P-labelled AP-1 consensus sequences. The samples were resolved on a 4% non-denaturing polyacrylamide gel and AP-1 gel shift bands were visualized by autoradiography (a). Samples collected from one treatment were assayed in duplicate and the band shifts were analysed by densitometry and expressed as mean ( $\pm$  standard deviation) fold increase of AP-1 binding activity relative to control levels (b).

#### **5.4.2 Optimisation of *hOGG1* and *hAPE* mRNA expression measurements**

The successful amplification of *hOGG1* and *hAPE* mRNA required the initial optimisation of magnesium chloride concentration in the PCR mixture. The binding efficiency of both sets of primers to the template cDNA was tested with 0.5, 1, 1.5, 2, 2.5 and 3  $\mu\text{M}$   $\text{MgCl}_2$ . RNA was extracted from control and 400  $\mu\text{M}$  hydrogen peroxide treated THEK cells, reverse transcribed and amplified for 40 cycles under the conditions described in section 2.3.5.1. PCR products were resolved on agarose gels containing ethidium bromide and visualised under UV. The predicted PCR product sizes for *hOGG1* and *hAPE* primers were 263 and 251bp respectively. *hOGG1* primers performed optimally at concentrations of 2.5 and 3  $\mu\text{M}$   $\text{MgCl}_2$  (Figure 5.5a), whilst *hAPE* primers showed optimal activity between 1.5 and 2.5  $\mu\text{M}$   $\text{MgCl}_2$  (Figure 5.5b). For subsequent PCR's 2.5  $\mu\text{M}$   $\text{MgCl}_2$  was used for *hOGG1* primers and 2  $\mu\text{M}$   $\text{MgCl}_2$  was used for *hAPE* primers.

Optimum annealing temperature of both sets of primers was tested at 2°C intervals, 4°C either side of the theoretically-determined optimum, 56.5°C for the *hOGG1* and 55.9°C for the *hAPE* primers. PCR products were visualised by agarose gel electrophoresis and photographed under UV light (Figure 5.6). Both genes could be amplified within a range of temperatures, 52.5-58.5°C for *hOGG1* and 51.9-57.9°C for *hAPE* primers; demonstrating that these mRNA sequences, as well as  $\beta$ -actin (personal communication Dr C Hewitt, Department of Microbiology & Immunology, University of Leicester), were amplifiable at the same annealing temperature of 55°C.

To measure changes in gene expression, the number of PCR cycles for each set of primer was optimised to assist semi-quantitation and to avoid saturation of PCR product. RNA preparations were reverse transcribed and amplified for 20, 25, 30, 35 and 40 PCR cycles for all three sets of primers from THEK and CCRF cells (Figure 5.7i and ii, respectively). PCR products were resolved in triplicate, photographed under UV and the mean and standard deviation band intensities on Polaroid negatives determined by densitometry. All three mRNA sequences were efficiently amplified under the PCR conditions defined above;  $\beta$ -actin was easily visible on the gels by 20 PCR cycles, whilst *hAPE* and *hOGG1* were detected after 25 and 30 PCR cycles, respectively (Figure 5.7 a, c, and b, respectively). Saturation of  $\beta$ -actin was observed after 30 PCR cycles, similar to previous observations of 33 PCR cycles (personal communication Dr C Hewitt); and saturation of both *hOGG1* and *hAPE* was not clearly detected in the 40 amplification cycles studied (Figure 5.7d).

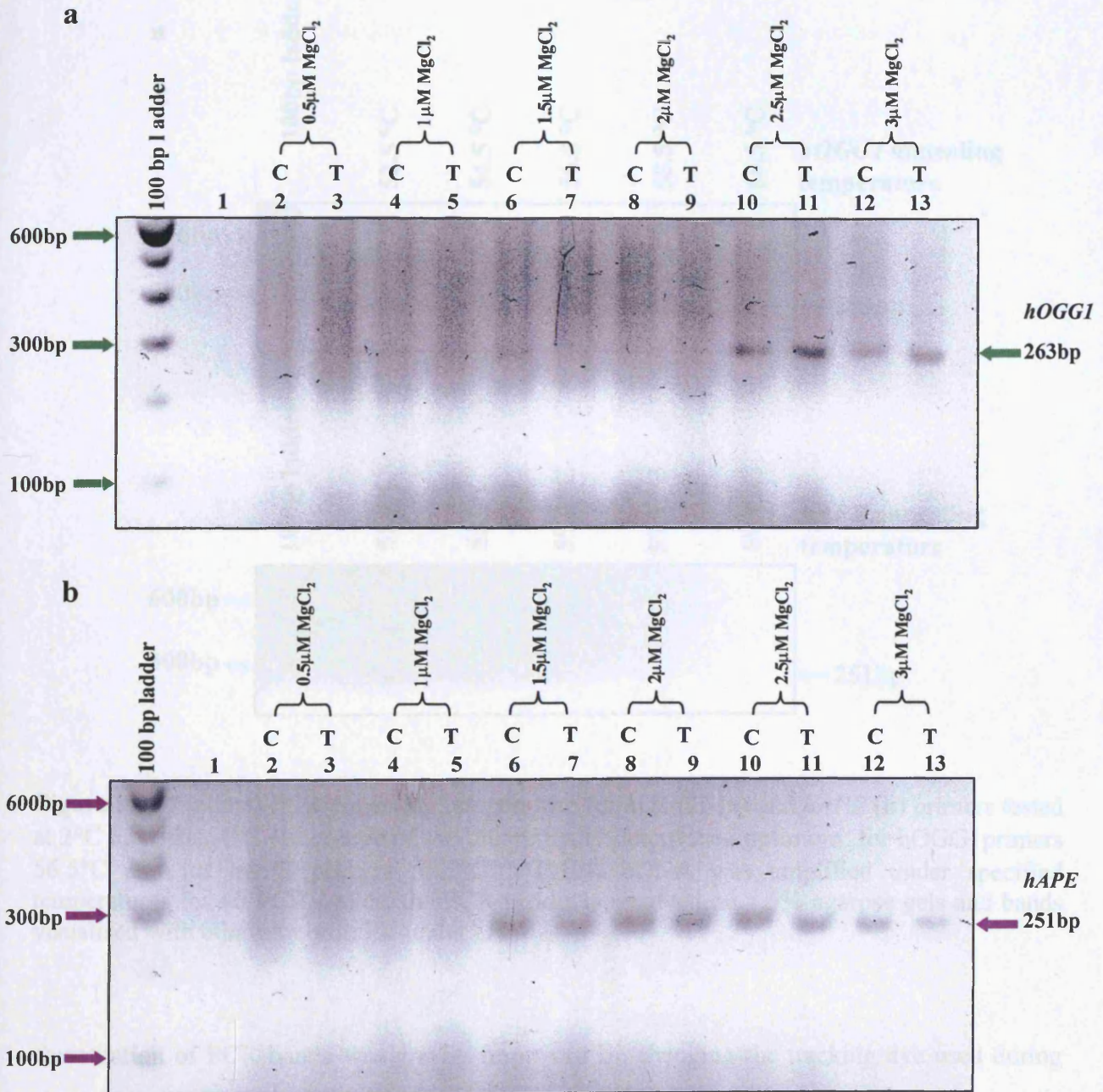


**Figure 5.5:** Optimisation of MgCl<sub>2</sub> concentration for *hOGG1* and *hAPE* PCR. Concentrations of 0.5, 1, 1.5, 2, 2.5 and 3 μM MgCl<sub>2</sub> were tested on cDNA prepared from control (C) and 100 μM hydrogen peroxide treated (T) THEK cells. PCR products were resolved on 1.5% agarose gels and bands visualised with ethidium bromide under UV. Optimal MgCl<sub>2</sub> for *hOGG1* primers (a): lane 1, negative control; lanes 2 & 3, 0.5 μM MgCl<sub>2</sub>; lanes 4 & 5 1 μM MgCl<sub>2</sub>; lanes 6 & 7, 1.5 μM MgCl<sub>2</sub>; lanes 8 & 9, 2 μM MgCl<sub>2</sub>; lanes 10 & 11, 2.5 μM MgCl<sub>2</sub>; lanes 12 & 13, 3 μM MgCl<sub>2</sub>. Similarly, the optimal MgCl<sub>2</sub> with *hAPE* primers (b): lane 1, negative control; lanes 2 & 3, 0.5 μM MgCl<sub>2</sub>; lanes 4 & 5 1 μM MgCl<sub>2</sub>; lanes 6 & 7, 1.5 μM MgCl<sub>2</sub>; lanes 8 & 9, 2 μM MgCl<sub>2</sub>; lanes 10 & 11, 2.5 μM MgCl<sub>2</sub>; lanes 12 & 13, 3 μM MgCl<sub>2</sub>.

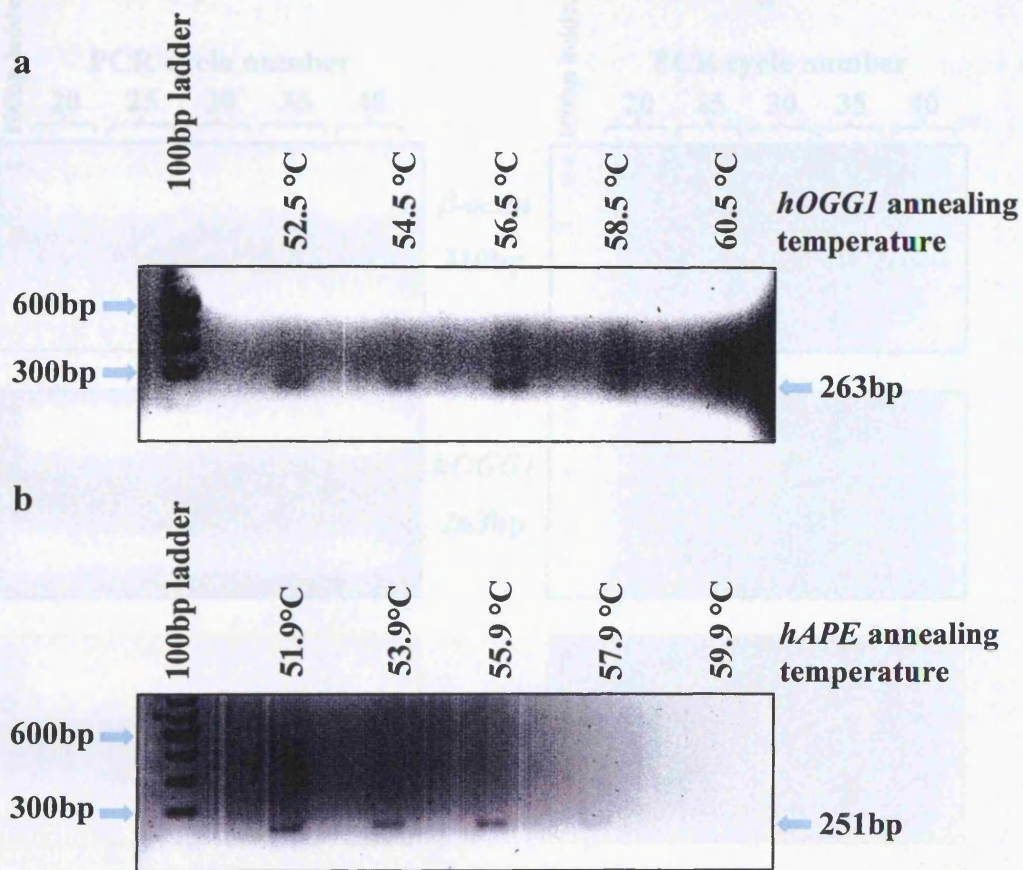


**Figure 5.6:** Optimal PCR annealing temperature for *hOGG1* (a) and *hAPE* (b) primers tested at 2°C intervals, 4°C either side of the theoretically determined optimum: for *hOGG1* primers 56.5°C and for *hAPE* primers 55.9°C. THEK cDNA was amplified under specified temperatures for 40 PCR cycles, the PCR products resolved on 1.5% agarose gels and bands visualised with ethidium bromide under UV.

Quantitation of PCR bands was greatly improved by changing the tracking dye used during electrophoresis. Both *hOGG1* and *hAPE* PCR products were seen very close to the bromophenol blue dye front (Figure 5.7i), therefore interfering with densitometry measurements. Changing the tracking dye to Orange G (7-Hydroxy-8-phenylazo-1,3-naphthalenedisulfonic acid) eliminated this problem (Figure 5.7ii). Overall, both THEK and CCRF RNA preparations displayed similar PCR amplification patterns for all three genes, with the *hOGG1* gene demonstrating lower abundance in comparison to both the  *$\beta$ -actin* and *hAPE* genes. Combining these observations, 30 PCR cycles were chosen for sufficient amplification without saturation, for subsequent gene expression studies. This data together with the annealing temperature data facilitated the amplification of all three sets of primers with same PCR cycling conditions, and therefore minimizing further experimental variations.

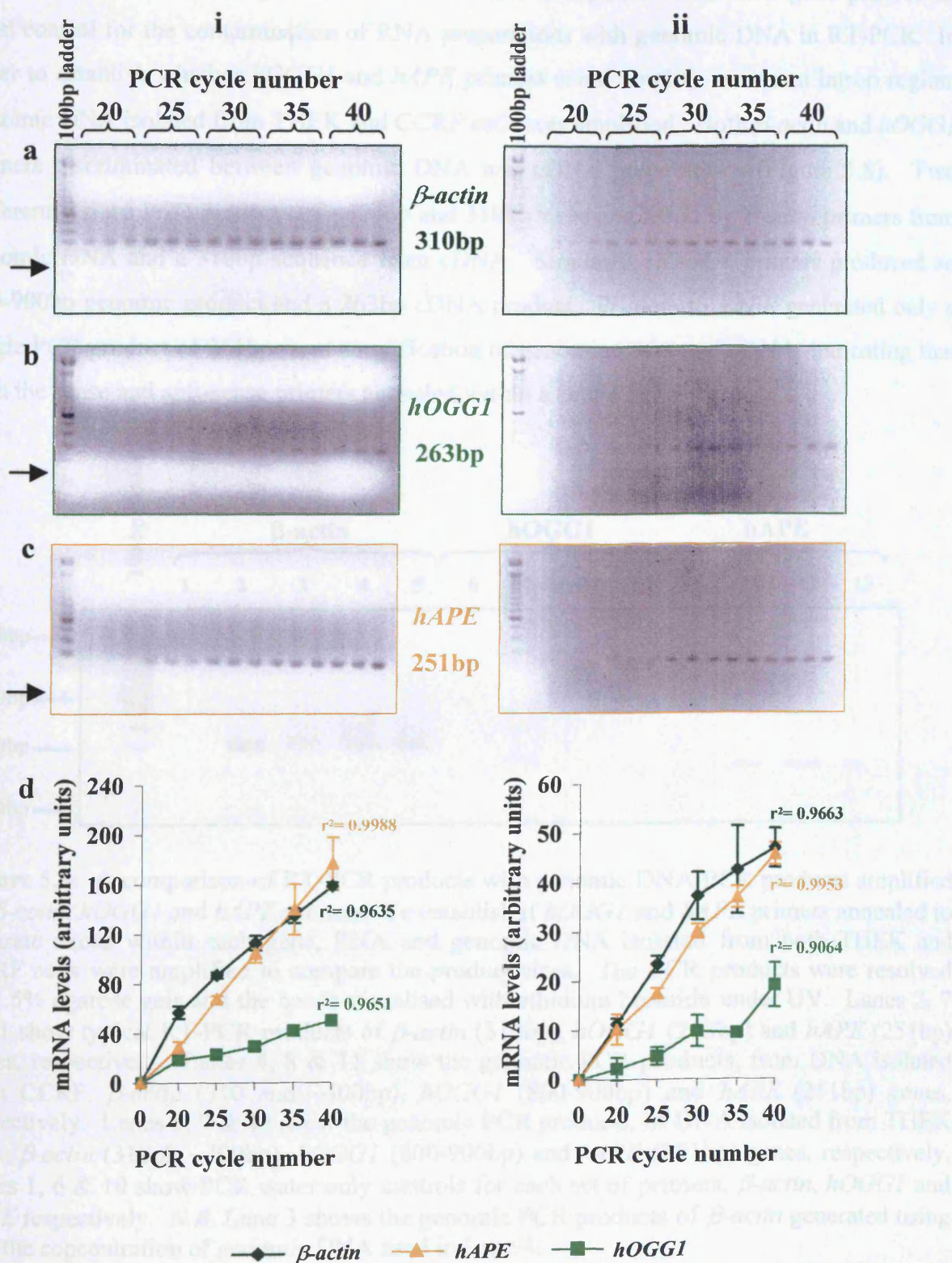


**Figure 5.7:** Optimal PCR cycle number for  $\beta$ -actin (a), hOGG1 (b) and hAPE (c) to study gene expression changes. THEK cDNA (i) and CCRF cDNA (ii) was amplified for 20-40 PCR cycles and the products resolved on a 1.5% agarose gels and bands visualised with ethidium bromide under UV. The graphs (d) illustrate the mean ( $\pm$  standard deviation) relative band intensity determined by densitometry measurements from three separate experiments. *N.B.*  $\blacktriangleright$  indicates the migration of bromophenol blue.

Sense and anti-sense PCR primers that anneal to two separate exons of a gene provide an ideal control for the contamination of RNA preparations with genomic DNA in RT-PCR. In order to establish whether *hOGG1* and *hAPE* primers could amplify across an intron region, genomic DNA isolated from THEK and CCRF cells was amplified. Both  $\beta$ -actin and *hOGG1* primers discriminated between genomic DNA and cDNA preparations (Figure 5.8). Two differently sized PCR products of ~400bp and 310bp were amplified by  $\beta$ -actin primers from genomic DNA and a 310bp sequence from cDNA. Similarly, *hOGG1* primers produced an 800-900bp genomic product and a 263bp cDNA product. Primers to *hAPE* generated only a single PCR product of 251bp from amplification of genomic DNA and cDNA, indicating that both the sense and anti-sense primers annealed within a single exon region.

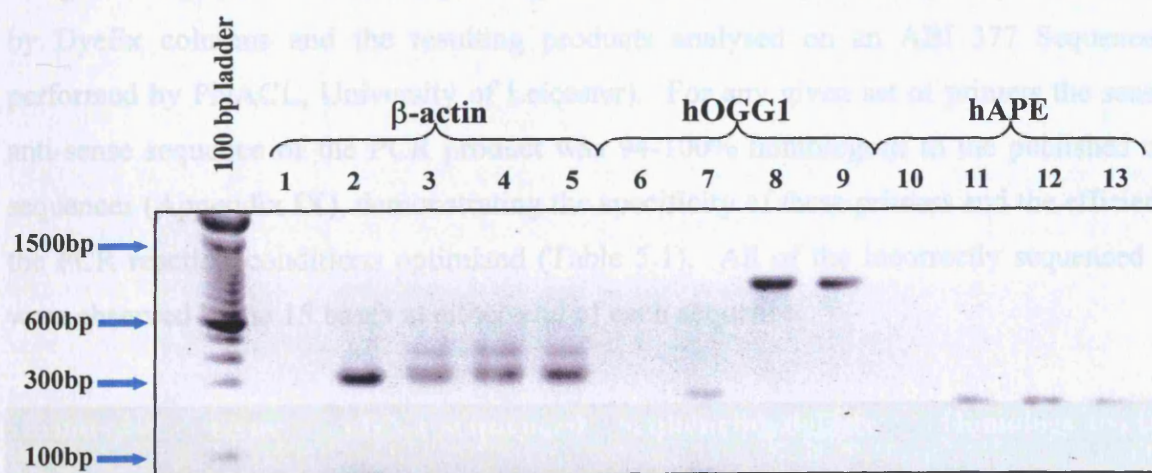


**Figure 5.8:** A comparison of RT-PCR products with genomic DNA PCR products amplified by  $\beta$ -actin, *hOGG1* and *hAPE* primers. To establish if *hOGG1* and *hAPE* primers annealed to separate exons within each gene, RNA and genomic DNA isolated from both THEK and CCRF cells were amplified to compare the product sizes. The PCR products were resolved on 1.5% agarose gels and the bands visualised with ethidium bromide under UV. Lanes 2, 7 & 11 show typical RT-PCR products of  $\beta$ -actin (310bp), *hOGG1* (263bp) and *hAPE* (251bp) genes, respectively. Lanes 4, 8 & 11 show the genomic PCR products, from DNA isolated from CCRF,  $\beta$ -actin (310 and ~400bp), *hOGG1* (800-900bp) and *hAPE* (251bp) genes, respectively. Lanes 5, 9 & 13 show the genomic PCR products, of DNA isolated from THEK cells,  $\beta$ -actin (310 & ~400bp), *hOGG1* (800-900bp) and *hAPE* (251bp) genes, respectively. Lanes 1, 6 & 10 show PCR water only controls for each set of primers,  $\beta$ -actin, *hOGG1* and *hAPE* respectively. *N.B.* Lane 3 shows the genomic PCR products of  $\beta$ -actin generated using half the concentration of genomic DNA used in Lane 4.

Following the submission of the *hOGG1* genomic sequence (Accession No. AJ131341.1, Feb 1999, Radicella *et al.*) the sense and anti-sense primers used in this thesis were confirmed to anneal to exons 2 and 3 respectively, and the predicted genomic PCR product was approximately 841bp (Appendix VII). Similarly, further sequence information submitted (Accession No M92444.1, Jul 1999, Zhao *et al.*) for the *hAPE* genomic sequence confirmed that both primers annealed within exon 5 (Appendix VII). In summary, provided the same

preparation of cDNA is used for all three sets of primers during RT-PCR, both  $\beta$ -actin and *hOGG1* primers could suitably control for any genomic DNA contamination and hence validate hAPE mRNA data.

#### 5.4.3 Validation of *hOGG1* and *hAPE* mRNA expression measurements

The specificity of  $\beta$ -actin, *hOGG1* and *hAPE* primers was confirmed by sequencing the PCR products from each primer set. The amplified products were gel extracted and purified of residual dNTP's and enzymes. Following quantitation, each preparation and its respective primers were analysed by automated sequencing. Cycle sequencing reactions were performed using ABI BigDye terminator sequencing chemistry, unincorporated dye terminators removed by DyeEx columns and the resulting products analysed on an ABI 377 Sequencer (all performed by PNAACL, University of Leicester). For any given set of primers the sense and anti-sense sequence of the PCR product was 94-100% homologous to the published cDNA sequences (Appendix IX), demonstrating the specificity of these primers and the efficiency of the PCR reaction conditions optimized (Table 5.1). All of the incorrectly sequenced bases were observed in the 15 bases at either-end of each sequence.

Primer	Gene	cDNA sequenced region (5' → 3')	Sequencing details	Homology to cDNA sequence (%)
Sense	$\beta$ -actin	936→1217	2 misincorporations	99.2%
Anti-sense	$\beta$ -actin	908→1190	3 misincorporations	98.9%
Sense	<i>hOGG1</i>	522→753	4 misincorporations 2 insertions	97.4%
Anti-sense	<i>hOGG1</i>	491→731	6 misincorporations 1 insertion	97.1%
Sense	<i>hAPE</i>	872→1099	10 misincorporations 1 insertion 1 deletion	94.7%
Anti-sense	<i>hAPE</i>	848→1079	10 misincorporation	95.7%

**Table 5.1:** Automated sequencing data of  $\beta$ -actin, *hOGG1* and *hAPE* RT-PCR products. Amplified PCR products were purified and the sense and anti-sense sequences determined by automated sequencing involving cycle sequencing reactions by ABI BigDye terminator sequencing chemistry, unincorporated dye terminators removed by DyeEx columns and the resultant products analysed on an ABI 377 Sequencer. The sequenced data (Appendix IX) was compared to published cDNA sequences (Appendix VII) and the level of homology expressed as percentage of the total bases analysed.

#### 5.4.4 RT-PCR analysis of *hOGG1* and *hAPE* gene expression

##### *Effects of hydrogen peroxide on hOGG1 and hAPE gene expression*

The potential modulation of *hOGG1* and *hAPE* mRNA expression by hydrogen peroxide was investigated in THEK and CCRF cells. Serum starved cells were treated with 0-400 $\mu$ M hydrogen peroxide for periods between 1-12hrs at 37°C. Total RNA extracted from cells was assessed by RT-PCR for levels of *hOGG1* and *hAPE* mRNA expression. The amount of RNA was normalized to the constitutively expressed housekeeping gene  $\beta$ -actin, and the densitometry values represented as mean ( $\pm$  standard deviation) fold increase in mRNA levels from controls at each timepoint.

Overall both THEK and CCRF cells displayed little systematic modulation in *hOGG1* and *hAPE* mRNA expression following hydrogen peroxide treatment at any of the time points measured (Figure 5.9 a and b respectively). At 6hr post treatment of CCRF cells with 400 $\mu$ M hydrogen peroxide a 2.5-3 fold increase in *hOGG1* and *hAPE* mRNA from control levels was calculated, however this was as a direct result of obscured  $\beta$ -actin bands resulting in low densitometry readings. Similarly, some increase in *hOGG1* mRNA (approximately 2.5 fold) was observed in THEK cells during the first 4hr post treatment with 100 and 200 $\mu$ M hydrogen peroxide. The statistical significance of these changes could not be confirmed due to sample size (a further set of experiments was not performed due to funding restrictions). In any case these changes are borderline significant with respect to widely accepted fold increase in gene expression *eg.* 2 fold.

##### *Effects of ascorbic acid on hOGG1 and hAPE gene expression*

The levels of *hOGG1* and *hAPE* mRNA were determined following treatments of THEK and CCRF cells with 0-400 $\mu$ M ascorbic acid for periods between 1-12hr. Similar to treatments with hydrogen peroxide, no significant difference in *hOGG1* and *hAPE* expression was observed at any of the timepoints with any of the doses in both cell types (Figure 5.10a and b). In CCRF cells treated with 200 $\mu$ M ascorbic acid for 12hr, mRNA levels of *hAPE* were determined as 2 fold higher compared to controls, however this value must be viewed critically as it appeared to be inconsistent with the neighbouring doses and timepoints. Further confirmation could not be acquired due to limited resources, however the overall changes in gene expression with ascorbic acid treatment in both cell types were not above levels accepted as significant with respect to fold change.

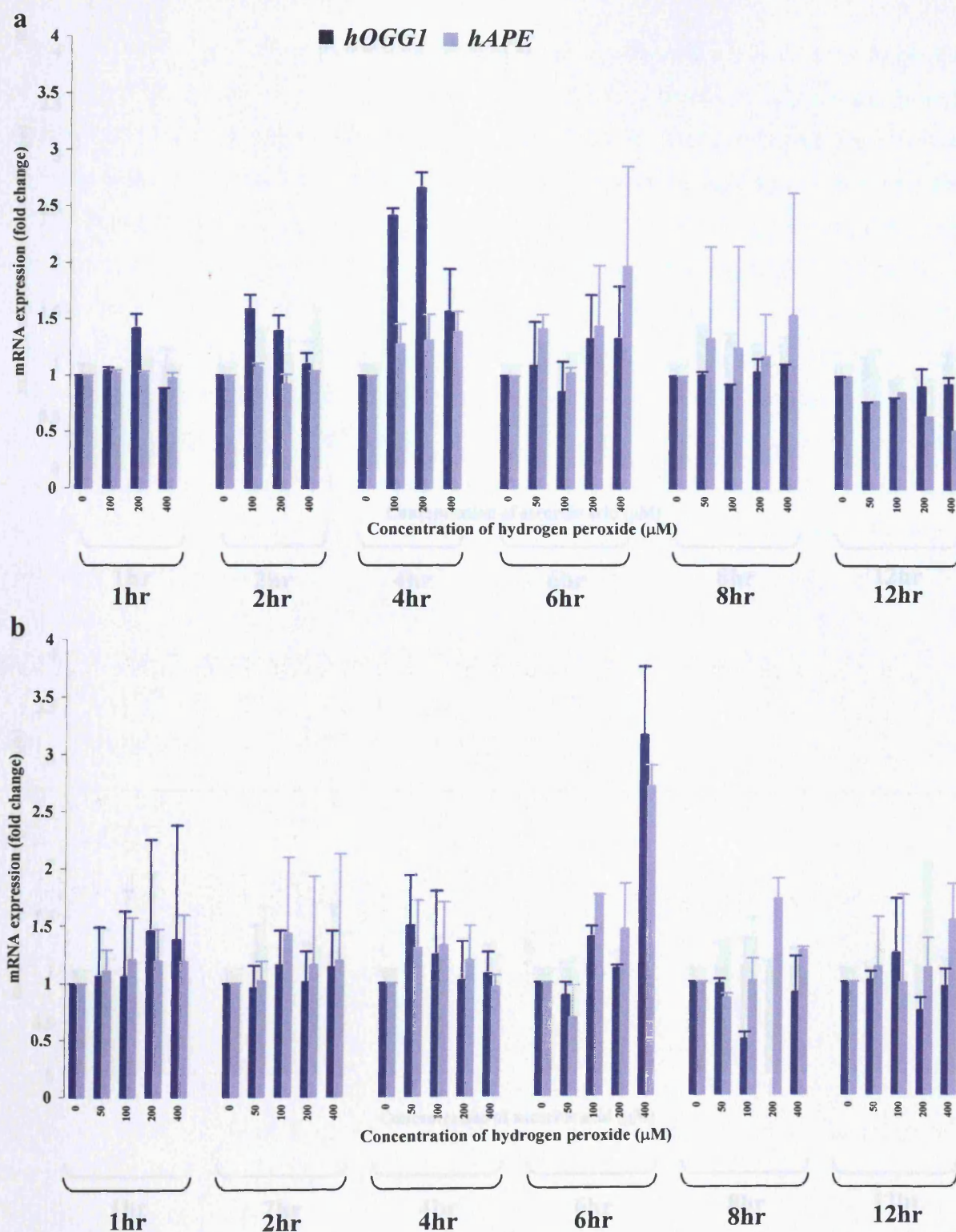


**Figure 5.9:** Effect of hydrogen peroxide on *hOGG1* and *hAPE* mRNA expression in THEK (a) and CCRF (b) cells. Cells were treated at 37°C with 0-400 μM hydrogen peroxide and total RNA extracted between 1-12hr. Levels of *hOGG1* and *hAPE* mRNA were assessed by RT-PCR and the products visualised by ethidium bromide under UV on 1.5% agarose gels. Densitometry values were normalized to levels of the constitutively expressed housekeeping gene,  $\beta$ -actin and modulation of mRNA is represented as the mean ( $\pm$  standard deviation) fold change from control levels at each timepoint. Each data point represents two independent measurements, except for timepoints 1, 2 and 4hr for CCRF RNA that represent three experiments.

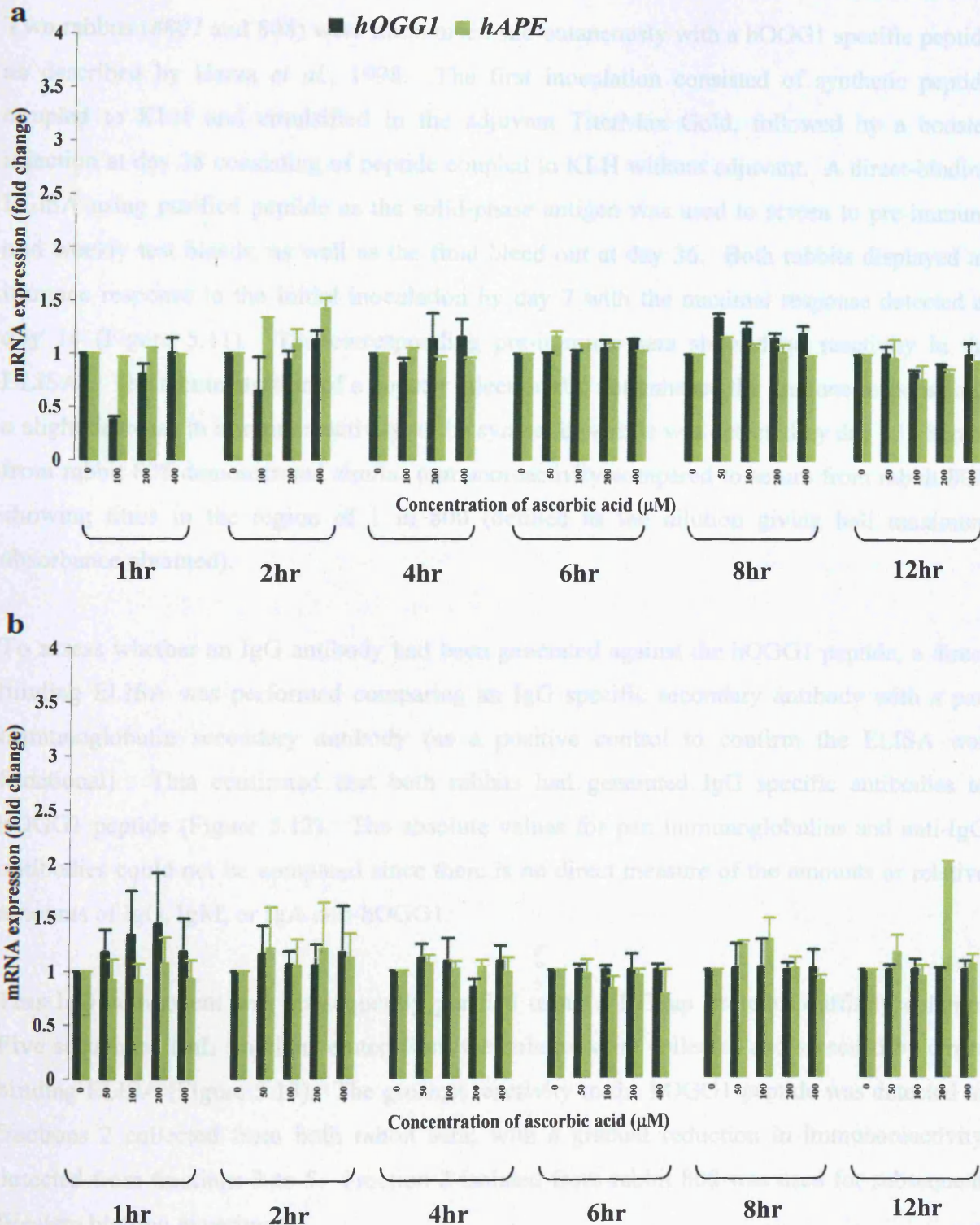


**Figure 5.10:** Effect of ascorbic acid on *hOGG1* and *hAPE* mRNA expression in THEK (a) and CCRF (b) cells. Cells were treated at 37°C with 0-400μM ascorbic acid and total RNA extracted between 1-12hr. Levels of *hOGG1* and *hAPE* mRNA were assessed by RT-PCR and the products visualised by ethidium bromide under UV on 1.5% agarose gels. Densitometry values were normalized to levels of the constitutively expressed housekeeping gene, *β-actin* and modulation of mRNA is represented as the mean ( $\pm$  standard deviation) fold change of control levels at each timepoint. Each data point represents two independent measurements, except for timepoints 1, 2 and 4hr for CCRF RNA that represent three experiments.

#### **5.4.5 Production of hOGG1 antibody**

Two rabbits (#807 and 808) were immunised sub-cutaneously with a hOGG1 specific peptide as described by Harza *et al.*, 1998. The first inoculation consisted of synthetic peptide coupled to KLH and emulsified in the adjuvant TiterMax Gold, followed by a booster injection at day 28 consisting of peptide coupled to KLH without adjuvant. A direct-binding ELISA using purified peptide as the solid-phase antigen was used to screen to pre-immune and weekly test bleeds, as well as the final bleed out at day 36. Both rabbits displayed an immune response to the initial inoculation by day 7 with the maximal response detected at day 14 (Figure 5.11). The corresponding pre-immune sera showed no reactivity in the ELISAs. The administration of a booster injection did not enhance the immune response and a slight decrease in immunoreactivity to the synthetic peptide was detected by day 35. Serum from rabbit 808 demonstrated similar immunoreactivity compared to serum from rabbit 807, showing titres in the region of 1 in 800 (defined as the dilution giving half maximum absorbance obtained).

To assess whether an IgG antibody had been generated against the hOGG1 peptide, a direct binding ELISA was performed comparing an IgG specific secondary antibody with a pan immunoglobulin secondary antibody (as a positive control to confirm the ELISA was functional). This confirmed that both rabbits had generated IgG specific antibodies to hOGG1 peptide (Figure 5.12). The absolute values for pan immunoglobulins and anti-IgG antibodies could not be compared since there is no direct measure of the amounts or relative amounts of IgG, IgM, or IgA anti-hOGG1.

This IgG component was subsequently purified using a HiTrap Protein G affinity column. Five sequential 1mL fractions eluted from the column were collected and screened by direct binding ELISA (Figure 5.13). The greatest reactivity to the hOGG1 peptide was detected in fractions 2 collected from both rabbit sera; with a gradual reduction in immunoreactivity detected from fractions 3 to 5. Fraction 2 isolated from rabbit 808 was used for subsequent Western blotting experiments.

#### **5.4.6 Investigation of hOGG1 antibody specificity**

In order to confirm the specificity of the anti-hOGG1 peptide antibody generated, Western blotting conditions were optimised using fraction 2 from both rabbits. Briefly, these conditions involved using 10% (w/v) milk in 0.1%(v/v) Tween 20 in TBS, primary IgG antibody from rabbit 807 at 1 in 750 and rabbit 808 at 1 in 1250, followed by HRP-conjugated anti-rabbit secondary antibody at 1 in 10,000 dilution. Both IgG fractions detected a protein of

approximately 38kDa in CCRF cell lysates, very similar to the theoretical weight of hOGG1 protein (38kDa).

Further confirmation of the anti-hOGG1 peptide antibody to denatured authentic hOGG1 was also performed. Firstly, to control for non-specific binding of the immune fraction, a similar IgG fraction was isolated from pre-immune test bleeds from each rabbit. The initial concentration of total protein in eluted pre-immune fractions was determined by the Bradford assay. To equalise the concentration of the IgG component in both the pre-immune and immune fractions, Coomassie staining of IgG fractions resolved by denaturing SDS-PAGE was performed (Figure 5.14). In both sera two bands were observed at 50-60kDa and 30-32kDa representing heavy and light chains of IgG respectively further confirming the presence and purity of IgG. The immunoglobulin light and heavy chain bands were quantitated by densitometry, the values used to equalise protein concentration in the two fractions. All subsequent Western blotting and immunocytochemical investigations were conducted with immune and pre-immune IgG isolated from rabbit 808.

To further validate the specificity of anti-hOGG1 peptide antibody, both pre-immune and immune IgG fractions were tested against purified hOGG1 protein (a kind gift from Dr S Boiteux, Fontenay aux Roses, France) and lysates (from both THEK and CCRF cells) resolved by denaturing SDS-PAGE. The concentration of purified hOGG1 protein was initially established by screening 50-600ng of protein per well; 400-600ng per well appeared optimal under the Western blotting conditions established. This amount of protein however was below the limits of detection of the Ponceau S stain, and therefore transfer of this protein onto PVDF membrane was assumed successful by assessing the transfer of adjacent THEK and CCRF cell lysates (Figure 5.15a). Incubation of the membrane with pre-immune IgG antibodies resulted in little detection of a 38kDa protein, whilst incubation with immune IgG antibodies resulted in clear detection of specific bands in the region of 38kDa. The detection of purified hOGG1 confirmed the successful development of an anti-hOGG1 peptide antibody. Also the immune fractions appeared to predominantly contain immunoglobulins specific to hOGG1, as seen by the lack of other non-specific bands.

A small difference in the molecular weight of purified hOGG1 protein and hOGG1 in cell lysates was observed (Figure 5.15b). These apparent differences were estimated by plotting the molecular weight of each standard against its mobility (a ratio of the migration of the bands and the dye front). The molecular weight of the purified hOGG1 and the cellular hOGG1 was estimated at 37.6kDa and 40.1kDa respectively. To further confirm these

differently sized proteins were genuinely hOGG1, the immune IgG fraction was pre-incubated with an excess of either protein or peptide. A clear reduction in detection of purified hOGG1 and hOGG1 in cell lysates was observed (Figure 5.15b). These validation experiments were conducted in parallel and the blots exposed to x-ray film following ECL simultaneously.

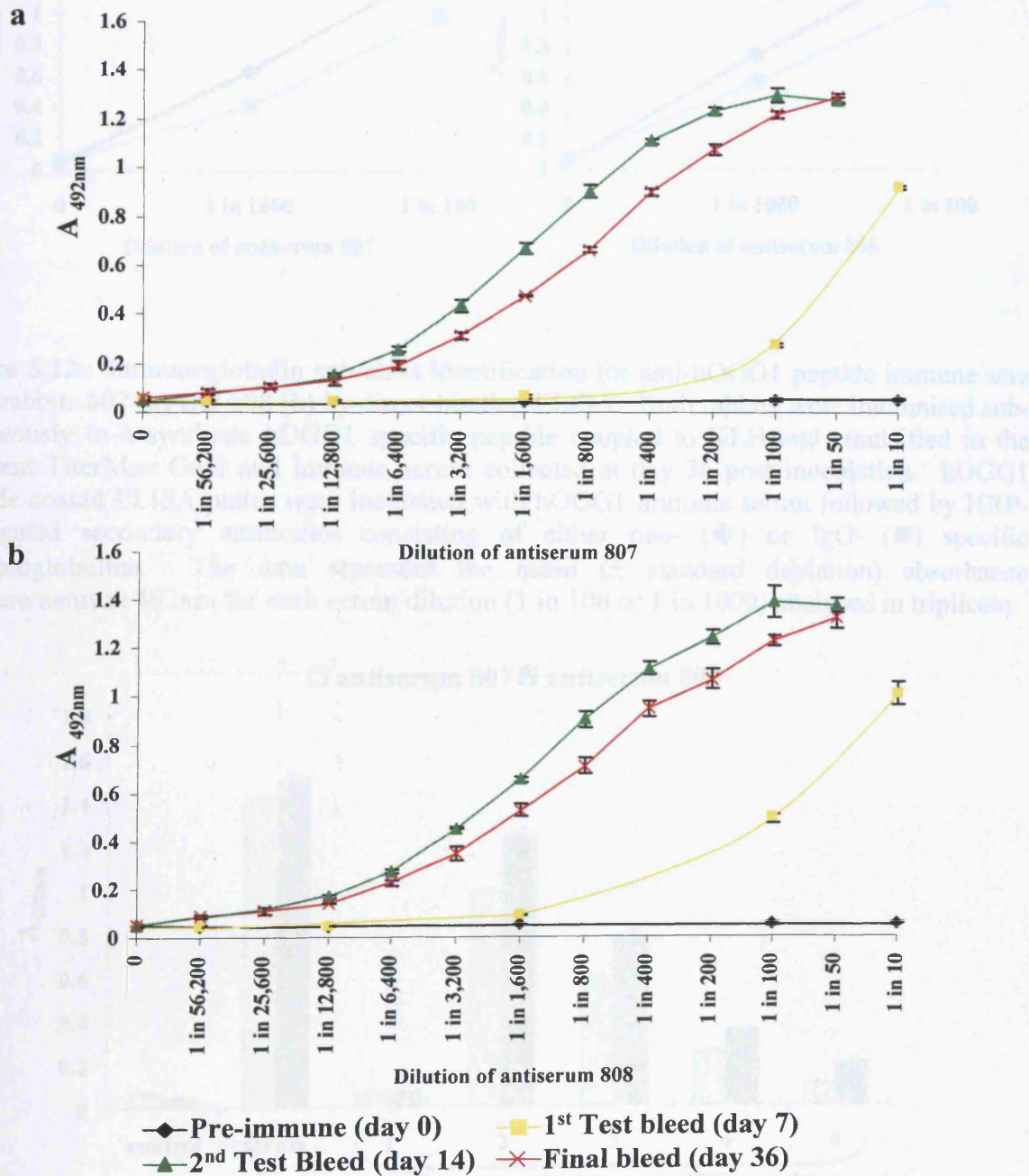


**Figure 5.11:** Direct-binding ELISA data of anti-hOGG1 peptide antibodies. Two rabbits (807 and 808) were immunised sub-cutaneously to a synthetic hOGG1 specific peptide coupled to KLH and then emulsified in the adjuvant TiterMax Gold. Final bleed out was conducted at day 36 following a booster injection of hOGG1 peptide at day 28. Sera from pre-immune and weekly test bleeds were analysed by ELISA using solid-phase peptide as antigen to assess antibody titre in each rabbit, 807 (a) and 808 (b). The data represent the mean ( $\pm$  standard deviation) spectrophotometric absorbance measurements at 492nm for each serum dilution assayed in triplicate.

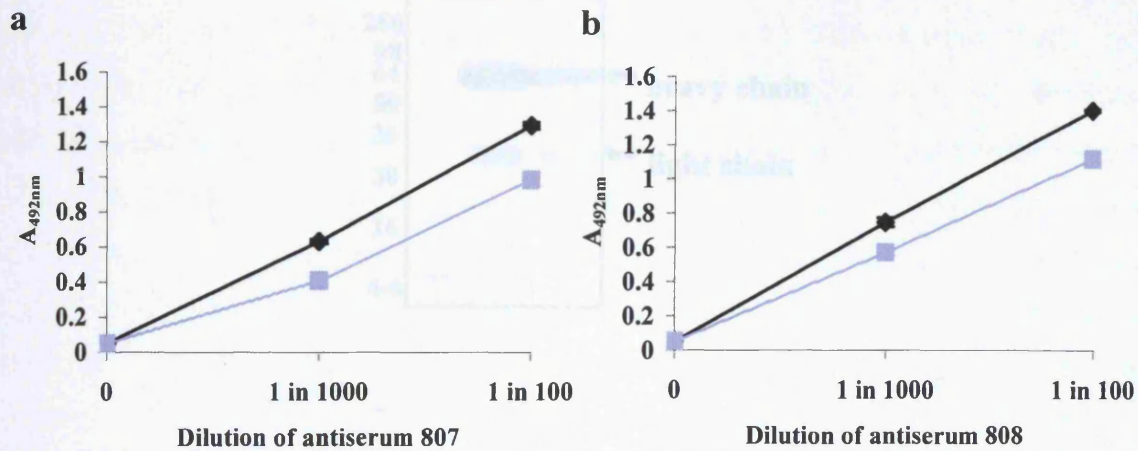


**Figure 5.12:** Immunoglobulin sub-class identification for anti-hOGG1 peptide immune sera from rabbits 807 (a) and 808 (b) by direct-binding ELISA. Both rabbits were immunised subcutaneously to a synthetic hOGG1 specific peptide coupled to KLH and emulsified in the adjuvant TiterMax Gold and immune serum collected at day 36 post inoculation. hOGG1 peptide coated ELISA plates were incubated with hOGG1 immune serum followed by HRP-conjugated secondary antibodies consisting of either pan- (◆) or IgG- (■) specific immunoglobulins. The data represent the mean ( $\pm$  standard deviation) absorbance measurements at 492nm for each serum dilution (1 in 100 or 1 in 1000) analysed in triplicate.

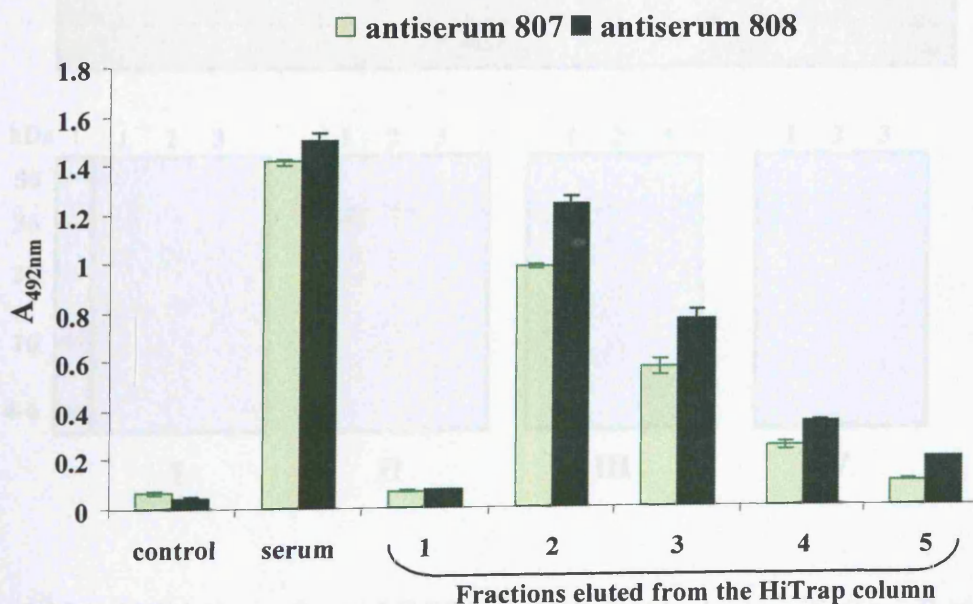


**Figure 5.13:** Isolation of IgG anti-hOGG1 peptide antibody from whole serum of rabbits 807 and 808. IgG-specific antibodies were purified from serum taken at day 36 post immunisation by HiTrap Protein G affinity columns. Five eluted fractions (1mL) were screened for IgG-specific anti-hOGG1 peptide antibody by direct binding ELISA with hOGG1 peptide as solid phase antigen. The data represent the mean ( $\pm$  standard deviation) of spectrophotometric absorbance measurements at 492nm for each fraction assayed in triplicate. Controls included incubations with non-affinity purified pre-immune serum (control) and immune serum (serum).

## 5.4.7 Western blotting analysis of changes in hOGG1 protein expression

The modulation of hOGG1 protein expression was investigated in THUK and CCRF cells following treatment with hydrogen peroxide. Serum starved cells were treated with 0-500µM hydrogen peroxide for 24 hours. Cells were harvested and lysates were collected and protein concentration adjusted to 1mg/ml. Samples were resolved by SDS-PAGE and transferred onto PVDF membrane. Non-specific sites were blocked and the membrane incubated with anti-hOGG1 peptide IgG antibody. Bound antibody was detected with HRP-conjugated anti-rabbit secondary antibody and visualised on x-ray film following incubation with ECL detection reagents. Ponceau S staining initially assessed transfer efficiency of protein onto PVDF membrane, however the amount of protein was normalized

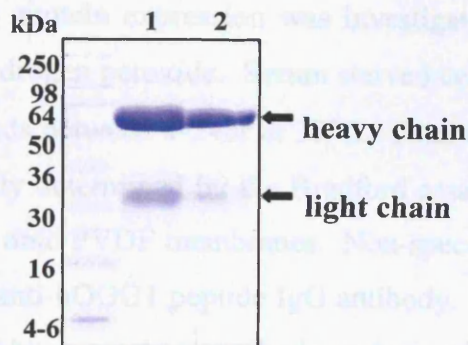


**Figure 5.14:** Coomassie blue stained IgG isolated from pre-immune serum (1) and hOGG1 peptide immune serum (2) from rabbit 808. IgG-specific antibodies were purified from serum by HiTrap Protein G affinity columns and resolved by denaturing SDS-PAGE. Immunoglobulin light and heavy chains were visualised by Coomassie staining and the relative intensities of bands quantitated by densitometry. The values assisted equalisation of IgG concentration in fractions isolated from pre-immune and immune serum.

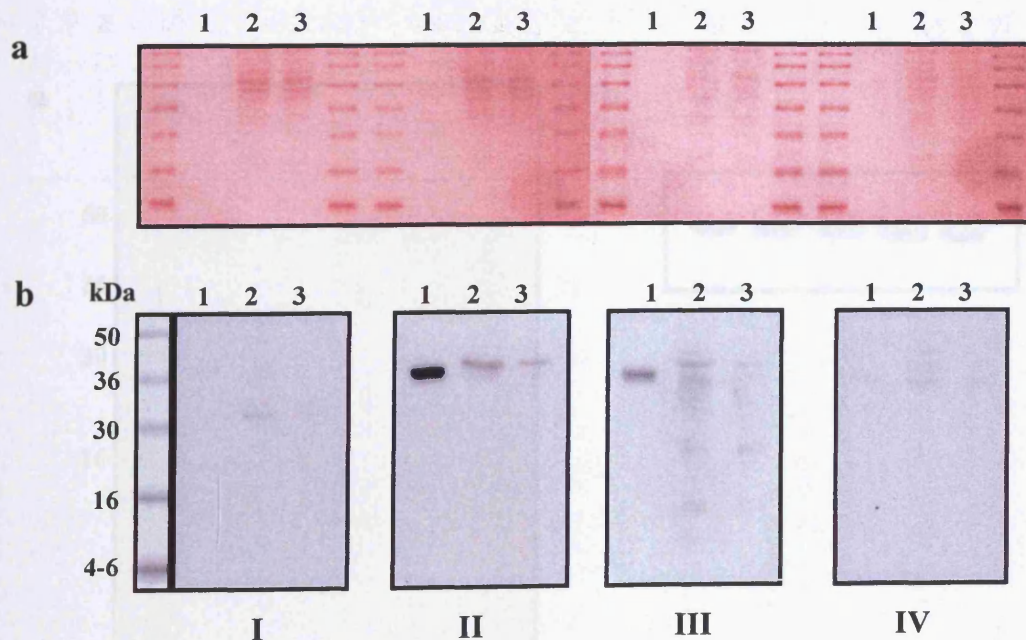


**Figure 5.15:** Validation of anti-hOGG1 peptide antibody specificity. Purified hOGG1 protein (lanes 1), and lysates of THEK (lanes 2) and CCRF (lanes 3) cells were resolved by SDS-PAGE and transferred onto PVDF membrane for Western blot analysis. Verification of protein transfer was established by Ponceau S staining (a). Non-specific sites were blocked and the blots incubated in either pre-immune IgG antibody (I), anti-hOGG1 peptide IgG antibody (II), anti-hOGG1 peptide IgG antibody pre-incubated with excess purified hOGG1 protein (III) or anti-hOGG1 peptide IgG antibody pre-incubated with excess hOGG1 peptide (IV). Bound antibody was detected by HRP-conjugated anti-rabbit secondary antibody and visualised on x-ray film following incubation with ECL detection reagents (b).

#### 5.4.7 Western blotting analysis of changes in hOGG1 protein expression

The modulation of hOGG1 protein expression was investigated in THEK and CCRF cells following treatment with hydrogen peroxide. Serum starved cells were treated with 0-400 $\mu$ M hydrogen peroxide for periods between 4-24hr at 37°C. Total cell lysates were collected and protein concentration initially determined by the Bradford assay. Samples were resolved by SDS-PAGE and transferred onto PVDF membranes. Non-specific sites were blocked and the membranes incubated with anti-hOGG1 peptide IgG antibody. Bound antibody was detected by HRP-conjugated anti-rabbit secondary antibody and visualised on x-ray film following incubation with ECL detection reagents. Ponceau S staining initially assessed transfer efficiency of protein onto PVDF membrane, however the amount of protein was normalized by the detection of the constitutively expressed protein  $\beta$ -actin after membrane stripping of anti-hOGG1 peptide antibody (Figure 5.16). Measurement of  $\beta$ -actin proved to be an accurate guide for protein levels loaded onto SDS-gels, and therefore was used to normalize hOGG1 protein levels detected (Figure 5.17).

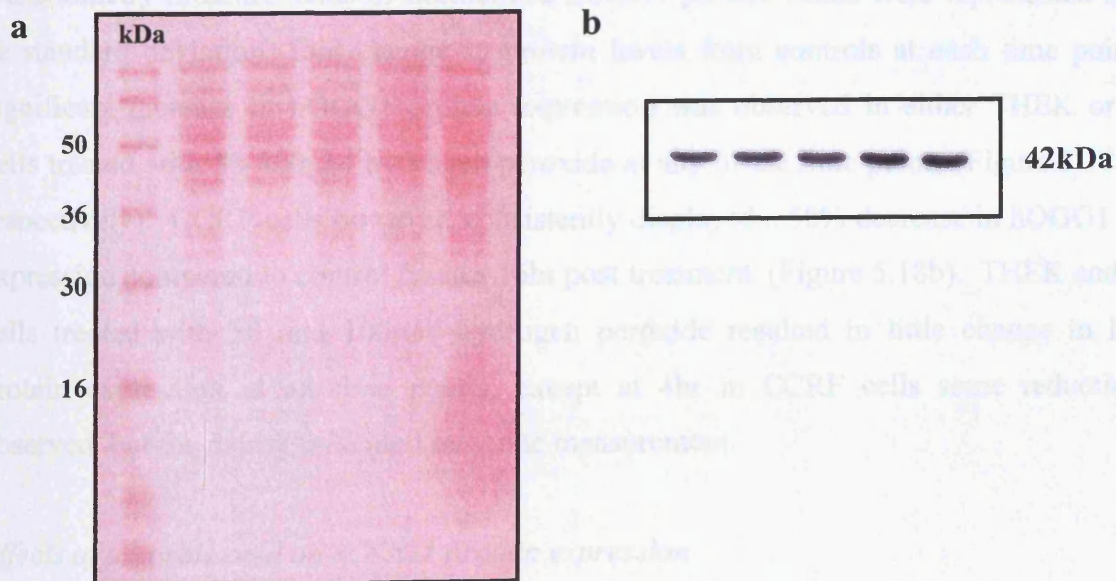


**Figure 5.16:** A comparison of protein levels determined by Ponceau S staining (a) followed by Western blot analysis of  $\beta$ -actin protein (b). Cell lysates were resolved by SDS-PAGE and transferred onto PVDF membrane for Western blot analysis. Protein transfer efficiency was assessed by incubation in 0.1%(v/v) Ponceau S stain in 5%(v/v) acetic acid. Ponceau S staining was removed in 0.1M NaOH and non-specific sites were blocked. Membranes were initially probed for hOGG1 protein and then stripped of primary and secondary antibodies. Membranes were re-blocked and then incubated with anti- $\beta$ -actin antibody and bound antibody was detected by HRP-conjugated anti-mouse secondary antibody and visualised on x-ray film following incubation with ECL detection reagents.

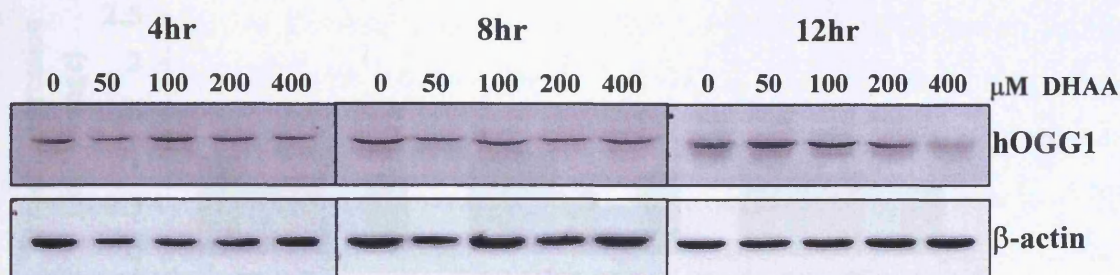


**Figure 5.17:** Western blot detection of hOGG1 and  $\beta$ -actin proteins in cell lysates. CCRF cells were treated with 0-400 $\mu$ M dehydroascorbic acid (DHAA) for 0-12hr, proteins were resolved by SDS-PAGE, blotted onto nitrocellulose membranes. Non-specific sites were blocked and the blots incubated with anti-hOGG1 peptide IgG antibody. Bound antibody was detected by HRP-conjugated anti-rabbit secondary antibody and visualised on x-ray film following incubation with ECL detection reagents. Membranes were stripped, re-blocked and probed with anti- $\beta$ -actin antibody to correct for protein loading differences. Bound anti- $\beta$ -actin antibody was detected by HRP-conjugated anti-mouse secondary antibody and visualised by ECL.

#### *Effects of hydrogen peroxide on hOGG1 protein expression*

Densitometry measurements of normalized hOGG1 protein bands were represented as mean ( $\pm$  standard deviation) fold change in protein levels from controls at each time point. No significant increase in hOGG1 protein expression was observed in either THEK or CCRF cells treated with 50-400 $\mu$ M hydrogen peroxide at any of the time points (Figure 5.18a and b respectively). CCRF cells however, consistently displayed a 50% decrease in hOGG1 protein expression compared to control lysates 16hr post treatment. (Figure 5.18b). THEK and CCRF cells treated with 50 and 100 $\mu$ M hydrogen peroxide resulted in little change in hOGG1 protein expression at all time points, except at 4hr in CCRF cells some reduction was observed, but the data represented only one measurement.

#### *Effects of ascorbic acid on hOGG1 protein expression*

A change in hOGG1 protein expression was also investigated in CCRF cells following the treatment of serum-starved cells with either ascorbic acid or dehydroascorbic acid at 0-400 $\mu$ M for periods between 4-24hr at 37°C. Cells treated with 50-200 $\mu$ M ascorbic acid showed a transient increase in hOGG1 protein expression; approximately 50% above controls levels, at 12 and 16hr post treatment (Figure 5.18c). Similar increases were also observed with CCRF cells treated with 50-400 $\mu$ M dehydroascorbic acid at 16hr (Figure 5.18d). At all other time points and doses of ascorbic or dehydroascorbic acid, little significant change in protein expression could be detected.

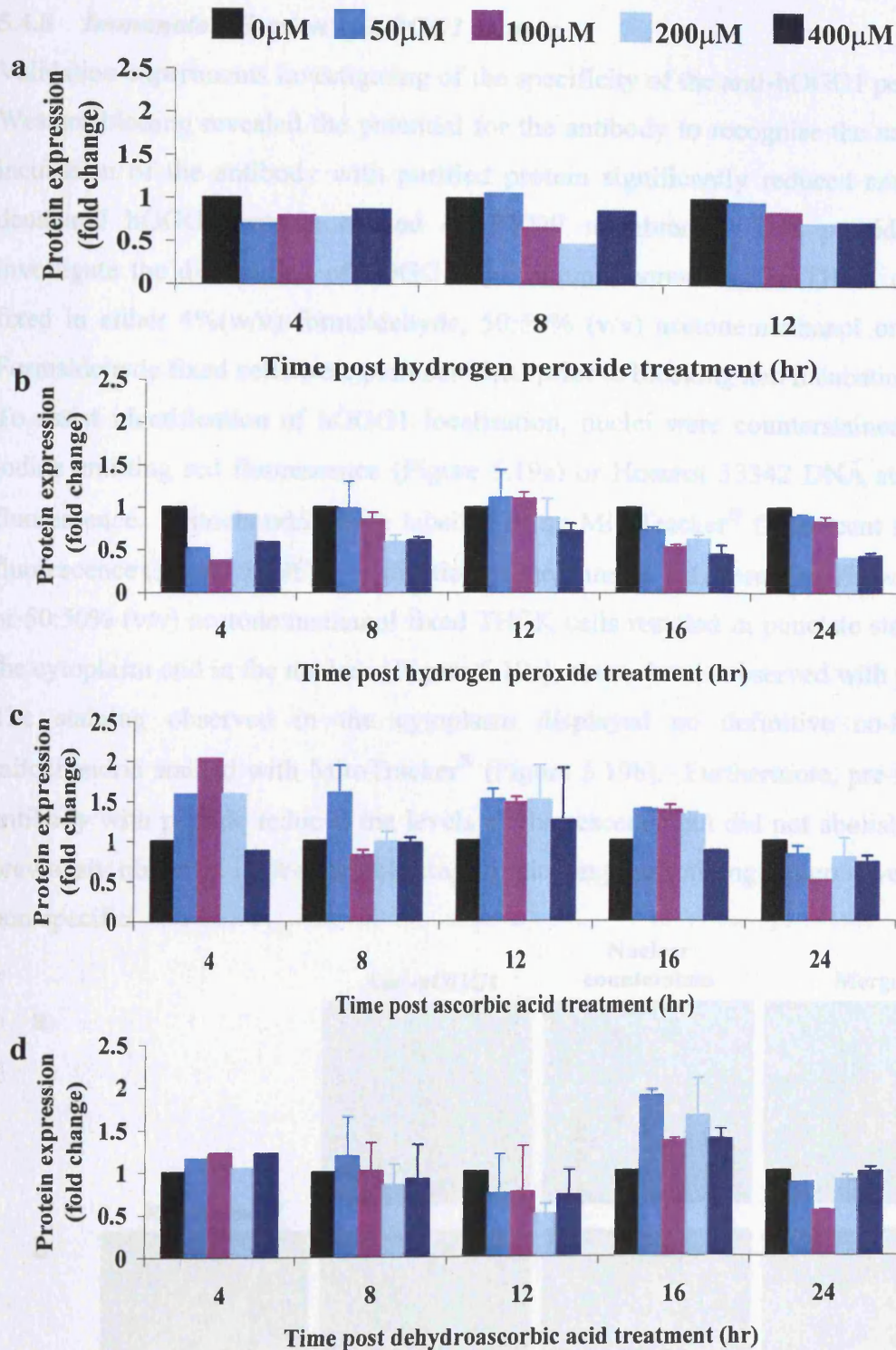


**Figure 5.18:** Western blot analysis of hOGG1 protein expression following hydrogen peroxide (a and b), ascorbic acid (c) and dehydroascorbic acid (d), in THEK (a) and CCRF (b, c and d) cells. Cell lysates were resolved by SDS-PAGE and transferred onto PVDF membrane for Western blot analysis. Non-specific sites were blocked and the blots incubated with anti-hOGG1 peptide IgG antibody. Bound antibody was detected by HRP-conjugated anti-rabbit secondary antibody and visualised on x-ray film following incubation with ECL detection reagents. Membranes were stripped and re-probed with anti- $\beta$ -actin antibody to correct for protein loading differences. The data expressed as mean ( $\pm$  standard deviation) fold change from control levels obtained from densitometer measurements. Each data point represents three independent measurements, except 4hr timepoints and for THEK data that represents one.

### 5.4.8 Immunolocalisation of hOGG1 protein

Validation experiments investigating of the specificity of the anti-hOGG1 peptide antibody by Western blotting revealed the potential for the antibody to recognise the native protein; pre-incubation of the antibody with purified protein significantly reduced antibody binding to denatured hOGG1 protein blotted on PVDF membrane. This provided the scope to investigate the distribution of hOGG1 by immunofluorescence in THEK cells. Cells were fixed in either 4%(w/v) formaldehyde, 50:50% (v/v) acetone:methanol or methanol alone. Formaldehyde fixed cells were permeabilised prior to blocking and incubations with antibody. To assist identification of hOGG1 localisation, nuclei were counterstained with propidium iodide emitting red fluorescence (Figure 5.19a) or Hoechst 33342 DNA stain emitting blue fluorescence. Mitochondria were labelled using MitoTracker<sup>®</sup> fluorescent stain emitting red fluorescence (Figure 5.19b). Application of the immune IgG serum to 4%(w/v) formaldehyde or 50:50% (v/v) acetone:methanol fixed THEK cells resulted in punctate staining throughout the cytoplasm and in the nucleus (Figure 5.19a), above levels observed with pre-immune IgG. The staining observed in the cytoplasm displayed no definitive co-localisation with mitochondria stained with MitoTracker<sup>®</sup> (Figure 5.19b). Furthermore, pre-incubation of the antibody with peptide reduced the levels of fluorescence but did not abolish staining (unlike previously observed in Western blotting), indicating the staining patterns were may be partly non-specific.

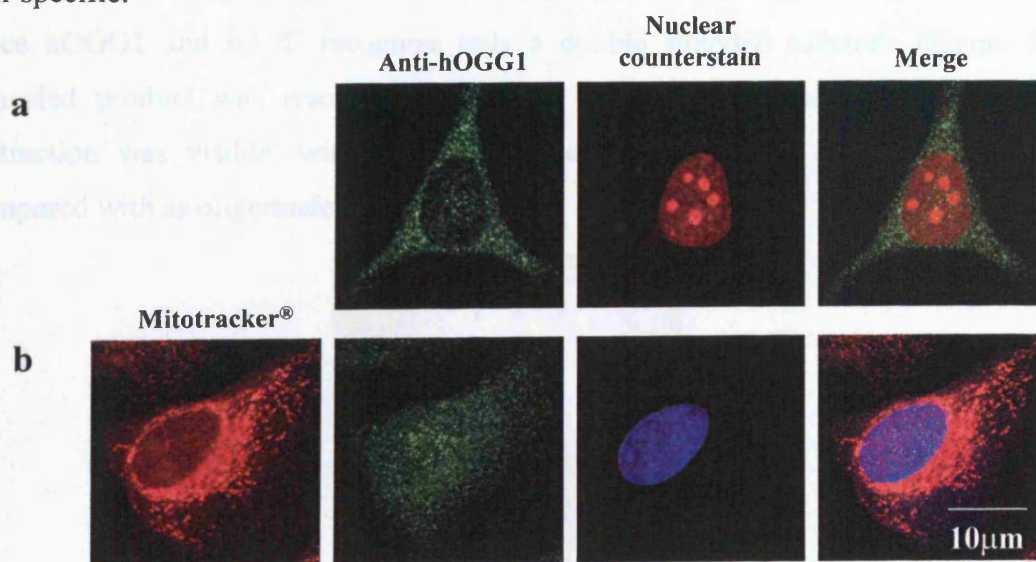


**Figure 5.19:** Immunofluorescence localisation of hOGG1 protein in THEK cells. Cells were fixed in 4%(w/v) formaldehyde in PBS, permeabilised and blocked with BSA. Cells were incubated with anti-hOGG1 peptide IgG-specific antibody and bound antibody was demonstrated by indirect immunofluorescence staining using an Alexa fluor<sup>™</sup> 488 conjugated goat anti-rabbit IgG secondary antibody emitting green fluorescence. Localisation of hOGG1 was assisted by counterstaining nuclei with either propidium iodide alone emitting red fluorescence (a) or Hoechst 33342 DNA stain emitting blue fluorescence together with mitochondria labelled with MitoTracker<sup>®</sup> stain emitting red fluorescence (b).

#### 5.4.8 Immunochemical detection of hAPE

Modulations in hAPE protein expression could not be successfully measured owing to optimisation problems with both Western blotting and immunocytochemical approaches. The following parameters were investigated for Western blotting: concentration of protein in cell lysates, blocking conditions, primary and secondary antibody concentrations; however no combination of these parameters proved successful. Similarly, for immunocytochemistry the fixation, blocking, and antibody conditions were unsuccessfully optimised. Combined, these results perhaps indicate the requirement of signal amplification or pre-purification of protein prior to Western blot analysis (these parameters were not investigated due to cost of hAPE antibody).

#### 5.4.9 Measurement of combined hOGG1 and hAPE enzyme activity

The enzymic repair activity of hOGG1 and hAPE was estimated by the ability of cell lysates to excise 8-oxodG from a double stranded oligonucleotide substrate. The actions of hOGG1 and hAPE would result in nicking of the oligonucleotide substrate and when extracted and denatured would result in the detection of a fragmented oligonucleotide, in this case a 11mer repair product (see appendix VIII for a figure describing the mechanism of the assay). Prior to the incubation of cell lysates with the oligonucleotide substrate, the preparation of the double-stranded oligonucleotide was initially verified by Metaphor<sup>®</sup> agarose electrophoresis since hOGG1 and hAPE recognise only a double stranded substrate (Figure 5.20). The annealed product was resolved alongside a single-stranded oligonucleotide, and a clear distinction was visible, with double-stranded oligonucleotide having a reduced mobility compared with ss oligonucleotides.

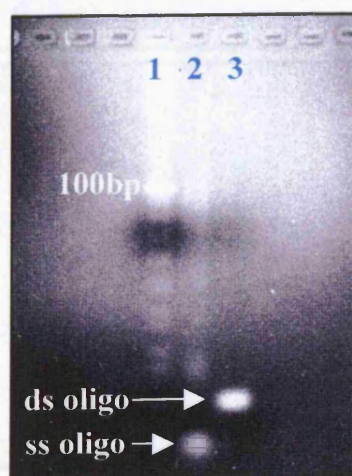


**Figure 5.20:** Metaphor<sup>®</sup> agarose electrophoresis verification of double-stranded repair oligonucleotide. Single-stranded repair oligonucleotides (ss oligo) designed to constitute a substrate for hOGG1 and hAPE enzymic cleavage were annealed. The efficiency of annealing was confirmed prior to incubation of the double-stranded substrate (ds oligo) with cell lysates: lane 1, a 10bp ladder; lane 2, ss oligo; and lane 3, ds oligo.

Resolution of small oligonucleotides, namely the single stranded oligonucleotide substrate (21mer) and repair product (11mer) required denaturing-PAGE. This approach successfully separated the 11 and 21mer oligonucleotides with sensitivities of 1pmol oligonucleotide per lane using FITC-labelled oligonucleotides (Figure 5.21a). Following incubation of the double-stranded substrate with cell lysates, 'repair' oligonucleotides were successfully extracted by a traditional sodium acetate and ethanol method. However problems were encountered with the loading of these samples, possibly as a result of residual salts and ethanol in the final preparation. To overcome this an alternative form of oligonucleotide extraction was adopted. This involved tagging the substrate with biotin and using Streptavidin conjugated magnetic Dynalbeads<sup>®</sup> to extract the oligonucleotides from the cell lysates. This assisted loading of the samples and partly improved electrophoresis, however the same resolution seen with the non-extracted 21 and 11mer size markers was not achieved (Figure 5.21b). Also due to the high urea content within the gels melting problems were encountered despite the chilled electrophoresis conditions, and therefore affecting overall reproducibility.

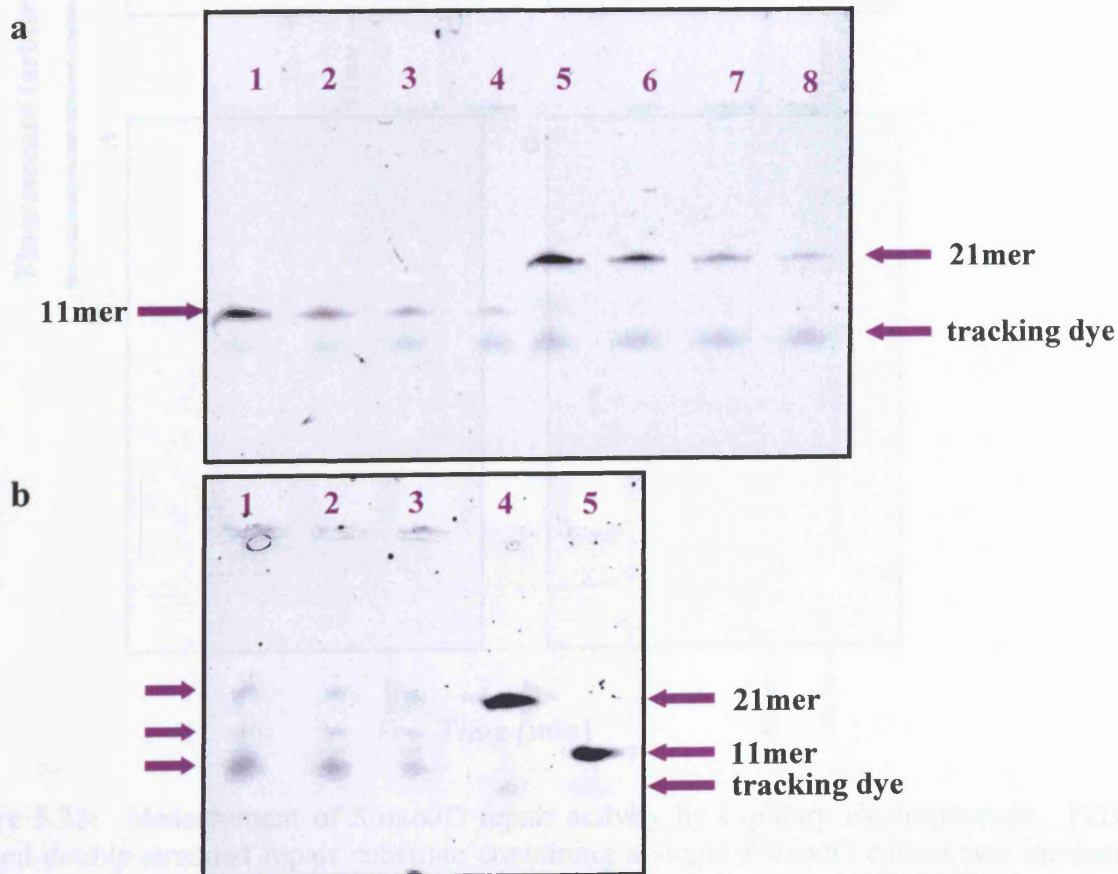


**Figure 5.21:** Detection of 11 and 21mer oligonucleotides by denaturing-polyacrylamide gel electrophoresis. (a) 11mer (lanes 1-4) and 21mer (lanes 5-8) FITC-labelled standards at 10pmol (lanes 1 & 5), 4pmol (lanes 2 & 6), 2pmol (lanes 3 & 7) and 1pmol (lanes 4 & 8). (b) Oligonucleotides recovered by triplicate magnetic bead extractions following incubation with cell lysate (lanes 1-3) and oligonucleotide standards, 21mer (lane 4) and 11mer (lane 5).

To overcome problems incurred by the denaturing PAGE approach, repair oligonucleotides were measured by capillary electrophoresis following Streptavidin conjugated magnetic Dynalbeads<sup>®</sup> extraction of oligonucleotides. Both the 21mer and 11mer single-stranded oligonucleotides could be clearly separated, allowing efficient and more sensitive quantitation of oligonucleotides (Figure 5.22). Repair activity was expressed as the percentage conversion of substrate oligonucleotide to cleaved product.

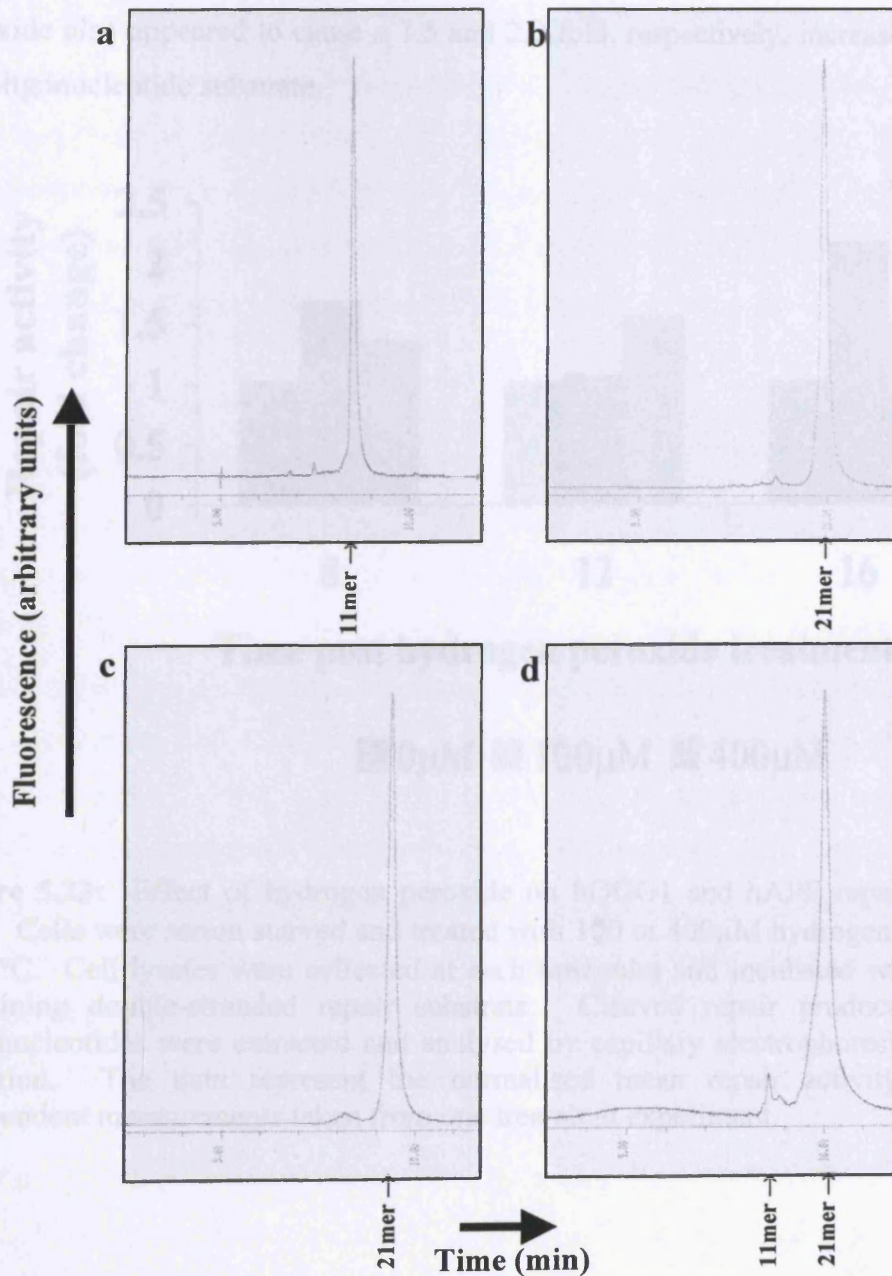


**Figure 5.22:** Measurement of 8-oxodG repair activity by capillary electrophoresis. FITC-labelled double-stranded repair substrate containing a single 8-oxodG adduct was incubated for 2hr at 37°C with CCRF cell lysates. Repair activity was assessed by fluorescence (Ex 488nm, Em 520nm) detection of oligonucleotides loaded under 0.5psi pressure at the cathodic end of the capillary over 10sec and separated under a constant voltage at 12kV in a gel-sieving matrix at 40°C. Typical electrophorograms of 11mer standard (a), 21mer standard (b) and extracted single-stranded oligonucleotides post incubation with 0 $\mu$ M (c) and 400 $\mu$ M (d) hydrogen peroxide lysate treated for 16hr.

*Effects of hydrogen peroxide on hOGG1 and hAPE repair activity.*

CCRF cells were treated with 0, 100 and 400 $\mu$ M hydrogen peroxide for periods of 8, 12 and 16 hr. Cells lysates were obtained and incubated with the double-stranded oligonucleotide substrate. Repair oligonucleotides were extracted using Streptavidin-coated magnetic beads and samples analysed by capillary electrophoresis. The high concentration of hydrogen peroxide caused a small increase in activity at all timepoints. At 8 and 16 hr 100 $\mu$ M hydrogen peroxide also appeared to cause a 1.5 and 2.0 fold, respectively, increase in activity towards the oligonucleotide substrate.

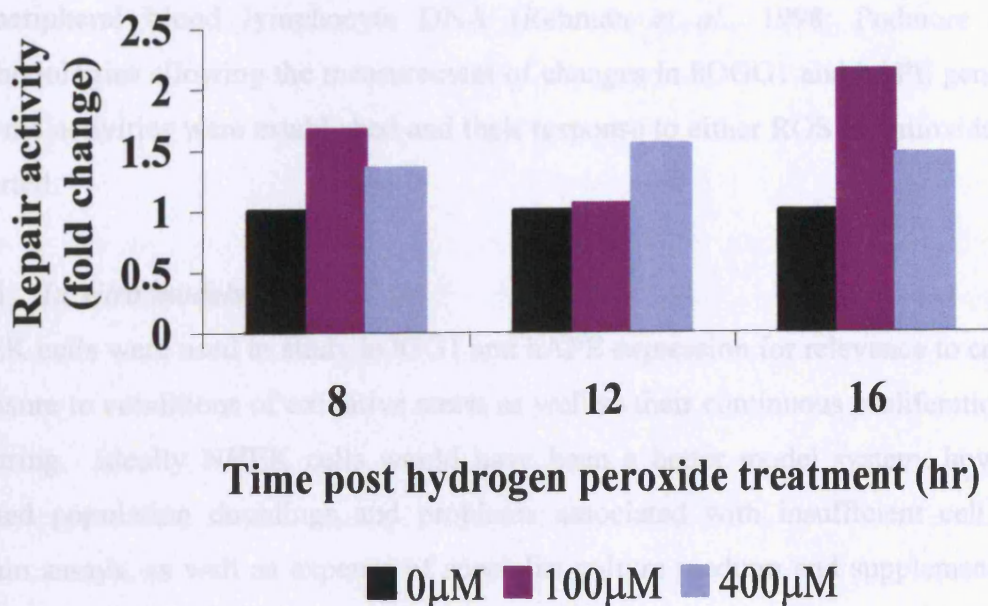


**Figure 5.23:** Effect of hydrogen peroxide on hOGG1 and hAPE repair activity in CCRF cells. Cells were serum starved and treated with 100 or 400 $\mu$ M hydrogen peroxide for 8-16 hr at 37°C. Cell lysates were collected at each timepoint and incubated with an 8-oxoguanine containing double-stranded repair substrate. Cleaved repair products and non-cleaved oligonucleotides were extracted and analysed by capillary electrophoresis with fluorescence detection. The data represent the normalised mean repair activity observed in two independent measurements taken from one treatment experiment.

## 5.5 DISCUSSION

The aim of the chapter was to investigate in human *in vitro* models the modulation of BER activity involving two key enzymes hOGG1 and hAPE, fundamental in the removal of the mutagenic lesion 8-oxodG. Both *hOGG1* and *hAPE* are ubiquitously expressed at low levels in all tissues, however both enzymes have been reported to respond to conditions of oxidative stress. In addition, recent evidence suggest that these enzymes may be sensitive to antioxidant conditions, since studies have shown, albeit controversially, that supplementation of human volunteers with 500mg/day vitamin C significantly reduced the levels of 8-oxodG in peripheral blood lymphocyte DNA (Rehman *et al.*, 1998; Podmore *et al* 1998). Methodologies allowing the measurement of changes in hOGG1 and hAPE gene, protein and enzyme activities were established and their response to either ROS or antioxidant stimuli are reported.

### 5.5.1 *In vitro* models

THEK cells were used to study hOGG1 and hAPE expression for relevance to cells constantly exposure to conditions of oxidative stress as well as their continuous proliferation and ease of culturing. Ideally NHEK cells would have been a better model system, however due the limited population doublings and problems associated with insufficient cell numbers for certain assays, as well as expense of specialist culture medium and supplements; these cells could not used. To overcome potential problems of high passage number masking gene expression changes and achieving sufficient cell numbers, CCRF cells were chosen for their low passage number and the ease in growing suspension cells to high cell densities. More importantly, these cells were of particular relevance as lymphocytes are often used as a non-invasive model system to assess oxidative burden and antioxidant intervention. Additionally, it was interesting to monitor the responses of two cell types stemming from different lineages.

Another advantage of using CCRF cells as opposed to THEK cells was based on the p53 status of these cell lines. The role of p53 is important since this tumour suppressor protein influences the cellular response to DNA damage and genomic aberrations. The activation of p53 through several phosphorylation sites can lead to cell cycle arrest, and DNA repair or apoptosis. Checkpoints in the cell cycle monitor DNA integrity and appropriate cell growth conditions at two stages, prior to replication (G1/S) and division (G2/M). DNA damage induces phosphorylation at Ser15 and Ser20 of p53, once activated p53 acts as transcriptional activator or repressor for other gene products. In addition, hAPE with its multifunctional properties, has the ability to interact with the carboxy terminus p53 to enhance DNA binding

of the transcription factor. The SV40 transformation in THEK cells may modulate the function of p53 and interfere with G1 arrest, since the large T antigen of SV40 has the capacity to bind to the p53 protein (Bowman *et al.*, 2001). Unlike THEK cells, CCRF cells were shown to possess wild type p53 status and therefore can readily arrest in G1 in response to DNA damage (personal communications Miss S Philips, Department of Pathology, University of Leicester). It is however equally important to investigate modulation of DNA repair in these immortal cells, despite differences in their p53 status, since firstly there are p53-independent pathways of cell cycle arrest at G2/M in response to DNA damage (Kohn, 1999). And secondly, such dysregulation/ or mutation of genes such as p53 have been described in tumours such as basal and squamous cell carcinomas (Burns *et al.*, 1993; Rady *et al.*, 1993), and therefore may provide important information in establishing cause and/or predict potential invasiveness of the certain cancers.

Prior to the investigation of the modulation of hOGG1 and hAPE expression and repair activity, the following parameters were established in the *in vitro* models: adequate serum starvation conditions, treatment doses causing the minimal toxicity, and sensitivity of cells to transcriptional activation. In order to reduce background levels of transcription and translation associated with cells undergoing rapid cell turnover, THEK and CCRF cells were serum starved. The concentration of serum in the culture medium was reduced to levels that could sustain the cells with healthy morphology and cause no adverse toxicity, as well as reduce the cell division rate to levels more relevant to the *in vivo* situation. THEK cells could withstand complete serum deprivation for up to 96hr, whilst CCRF cells required 0.5%(v/v) serum in the culture medium to sustain viability for up to 72hr. The effects of serum starvation on cells was monitored by Trypan Blue exclusion, and for CCRF cells, flow cytometry analysis of propidium iodide stained DNA clearly confirmed a reduction in the number of cells in the G2/M phase following 48hr serum starvation.

Further to the investigation of non-toxic serum starvation conditions, the ability of the cells to withstand treatments with hydrogen peroxide, ascorbic acid or dehydroascorbic acid was examined. In order to study the modulation of genes, toxic conditions can often mask the effects since many genes are non-specifically upregulated or downregulated following the triggering of cell death. Both cell types were treated with concentrations ranging 0-400µM of each reagent for up to 12hr. Cellular viability was assessed by Trypan Blue exclusion and both THEK and CCRF cells demonstrated no adverse cytotoxic effects on with any of the reagents at any given dose in the 12hr period studied. With minimal toxicity demonstrated by the cell lines following serum starvation and treatment with oxidant and antioxidant

conditions, the investigation of modulation of hOGG1 and hAPE expression in these *in vitro* systems was achievable.

To confirm these cell lines were sensitive to transcriptional activation following treatments that would modulate their redox status, activation of the transcription factor AP-1 was measured by EMSA. Both *hOGG1* and *hAPE* have potential AP-1 binding sites in the region upstream of the start sites (Appendix X) and therefore activation of AP-1 was deemed relevant. Studies in HeLa cells by Yao *et al.*, 1994 indicate that in general AP-1 activity is greatly enhanced by antioxidants compared to reducing agents such as hydrogen peroxide. Also, AP-1 DNA binding activity in response to antioxidants tends to be biphasic, with maximum induction after 45 min and 5 hr post treatment. CCRF cells following exposure to 100-250 $\mu$ M ascorbic acid for 3hr showed an increase in AP-1 binding activity, and with 10 $\mu$ g/mL cyclohexamide pre-treatment (for 15min) caused a 50% reduction in activity (personal communications Dr K Holloway, University of Leicester). Similar experiments were conducted with THEK cells to ensure they were also responsive to redox changes; particularly since the high passage number of THEK cells may have conferred adaptation of cells to oxidative stress and therefore may have affected the responsiveness to redox changes at the transcriptional level (Muller *et al.*, 1997). Despite the higher passage number of THEK, activation of AP-1 in response to 100-200 $\mu$ M ascorbic acid treatment for 2hr was comparable to the level of activation seen in CCRF cells treated under similar conditions. Both cell models were confirmed to be transcriptionally responsive to modulations in redox status.

### **5.5.2 *hOGG1* & *hAPE* mRNA expression**

The measurement of *hOGG1* and *hAPE* mRNA was successfully achieved by RT-PCR. Both genes as well as the constitutive marker,  $\beta$ -*actin* could be amplified under the same PCR cycling conditions. A multiplex PCR system for triple amplification of genes within one sample was not viable owing to the reduced magnesium chloride concentration required for optimal hAPE primer annealing. Also all three sets of primers generated PCR products of similar size and therefore resolution on agarose gels would have proved difficult. Sequencing data of PCR products further confirmed the specificity of the primers and the efficiency of the PCR conditions optimised.

The modulation of *hOGG1* and *hAPE* mRNA expression was investigated following the treatment of THEK and CCRF cells with non-toxic doses of hydrogen peroxide and ascorbic acid. The cells were treated over a period of 12hr and RNA collected at 1, 2, 4, 6, 8 and 12hr

post treatment. These timepoints were selected through evaluation of the literature and timescales reported for BER. Oxidative stress caused by hydrogen peroxide was clearly demonstrated in Chapter 4, however treatment of both THEK and CCRF with hydrogen peroxide at doses of 0-400 $\mu$ M had little effect on *hOGG1* and *hAPE* mRNA expression during 12hr treatment. Some transient increases in *hOGG1* and *hAPE* mRNA expression were observed however these appeared to be more experimental variations as opposed to systematic changes in response to dose or time of treatment. Also these small changes were not consistent between both cell models, although it is possible that modulation of *hOGG1* and *hAPE* mRNA expression may be cell specific.

In spite of the confirmed entry of ascorbic acid into the cells (see Chapter 4), no modulation of *hOGG1* and *hAPE* mRNA expression was evident during the 12hr studied. The lack of gene expression change was evident in both cell types. Overall, despite no statistical evaluation, the pattern of data quite clearly demonstrated no significant modulation in *hOGG1* and *hAPE* mRNA expression levels following either oxidant or antioxidant treatments in the *in vitro* models studied.

Recent structural and functional studies examining a 2.1kb genomic fragment, spanning promoter sequences upstream of the transcription start site and part of the first exon of *hOGG1* (Dhénaut *et al.*, 2000) showed several putative transcription factor binding sites including AP, GATA, SP1 and more interestingly a Nrf2/C-Ets1 site 29 base pairs upstream of the transcription site start. This Nrf2 site is associated with Jun proteins and has been shown to regulate antioxidant responses and induce genes encoding detoxifying enzymes. Despite these sites no putative TATA or CCAAT boxes were identified and the sequence was noted to be G and C rich and possess two candidate CpG islands. Functional studies with *OGG1* promoter-luciferase constructs showed the first 135bp upstream of the start site to be sufficient to drive transcription of the reporter gene.

Combining these results Dhénaut *et al.* (2000) conclude the *hOGG1* promoter displays strong characteristics of a classical housekeeping gene promoter. Interestingly the presence of CpG islands in the promoter suggests that transcription of the gene may be modulated by somatic *de novo* methylation as seen with the mismatch repair system being inactivated by methylation and causing genetic instability in colon cancer (Herman *et al.*, 1998). Similarly, somatic inactivation through hypermethylation is reported in the gene associated with Von Hippel-Lindau (VHL) disease; an autosomal dominant disorder predisposing to a variety of benign and malignant tumours such as renal cell carcinoma, retinal and CNS

hemangioblastomas, pheochromocytoma and pancreatic tumours (Prowse *et al.*, 1997). Interestingly, the VHL gene maps to the same chromosome region as hOGG1, chromosome 3p25.

In summary these studies support the lack of *hOGG1* gene expression changes observed in both THEK and CCRF cells in response to oxidative and antioxidative stimuli. In addition, Dhénaut *et al.*, 2000 also claimed that *hOGG1* expression is unaltered in HeLa cells treated with hydrogen peroxide or lipopolysaccharide (LPS), however this data was not shown in their paper. In a recent paper by Saitoh *et al.* (2001), RT-PCR of hOGG1 mRNA showed no alteration in HeLa S3 cells, following severe oxidative stress treatment with 2mM hypochlorous acid (HOCl) during 48hr treatment.

*hAPE* mRNA expression levels have been shown to increase in conditions generating ROS (Grösch *et al.*, 1998; Ramana *et al.*, 1998), hypoxia (Yao *et al.* 1994) and ischaemia (Gillardon *et al.* 1997). Ramana *et al.* (1998), showed by Northern blotting in HeLa S3 cells treated with low doses (130-850nM) of HOCl a 5-10 fold increase in hAPE mRNA expression after 10hr post treatment. The presentation of the data was unconvincing, since the quality of the Northern blots were poor with no semi-quantitative analysis or indication of repetition. Using similar techniques Grösch *et al.* (1998) showed a 2-3 fold increase in hAPE mRNA expression following 50µM NaOCl or 300µM hydrogen peroxide between 3-9hr post treatment in CHO cells. Although the quality of Northern blot analysis was much improved compared to Ramana *et al.* (1998), no evidence of repetition was apparent. Pre-treatment of cells with cyclohexamide or anisomycin inhibited the increase in mRNA following hydrogen peroxide treatment, suggesting *de novo* protein synthesis was required to elicit the response. Transfections with hAPE promoter-CAT constructs also showed transcriptional activation with both 100-500µM NaOCl and 300-700µM hydrogen peroxide (Grösch *et al.*, 1998).

In a study by Saitoh *et al.* (2001), a maximum 4-fold increase in hAPE mRNA expression was measured by RT-PCR in HeLa S3 cells following 5hr 2mM HOCl treatment. This increase declined by 24hr. No cell viability data was included in their study, and graphical presentation of fold induction of the gene was calculated by dividing the band intensity of HOCl-treated sample with the control sample, so no normalisation of a constitutively expressed marker was included. Furthermore none of the induction data reported included error bars and there was no mention of experimental repetition.

Other changes in hAPE gene expression have been reported using Northern blotting and/or *in situ* hybridisation techniques. Fung *et al.*, 1998 showed treatment of rat mesothelial cells with non-toxic concentrations of crocidolite asbestos, potentially increased APE mRNA, protein and DNA incision activity in both nuclei and mitochondria, 24-72 hr post exposure.

The functional basal promoter of hAPE (~300bp) is located on a CpG island, with a CCAAT box (Harrison *et al.*, 1995, Harrison *et al.*, 1997, Zhao *et al.*, 1992) and possibly a functional CREB binding site (Grösch and Kaina, 1999). Many other putative transcription factor-binding sites are found in this region, including Sp1, AP-1, upstream factor (USF) and ATF; however their effect on the basal levels of transcription requires further investigation. Approximately 3kb upstream of the basal promoter lies a negative regulatory element, containing one negative calcium-responsive element-A type (nCaRE-A) and two B-types sequences, nCaRE-B1 and nCaRE-B2 (Izumi *et al.*, 1996). Deletion analyses of these sequences indicate that the latter sequence may be important in the repression of hAPE expression and interestingly through the binding of hAPE itself to the element (Izumi *et al.*, 1996). In support of hAPE autoregulation, hAPE has been demonstrated to bind to nCaRE sites within the parathyroid hormone promoter (Okazaki *et al.*, 1994). It appears evident combining the information known for the hAPE promoter and negative regulatory element, that the expression of this gene may be sensitive to a multitude of transcription factor activities. Nevertheless the hAPE promoter appears to also contain many features typical of 'housekeeping' genes, such a CpG island, the lack of a TATA box and multiple transcription start sites (Akiyama *et al.*, 1994; Harrison *et al.*, 1995; Zhao *et al.*, 1992), further experiments are required to unravel the complexities regulating the expression of this gene.

### **5.5.3 hOGG1 & hAPE protein expression**

A polyclonal anti-hOGG1 antibody was successfully generated, using a peptide sequence described by Harza *et al.*, 1998. The peptide sequence represented amino acids 81-98 of hOGG1 and therefore the antibody had the potential reactivity to both nuclear and mitochondrial hOGG1, designated hOGG1 $\alpha$  and hOGG1 $\beta$  respectively. The IgG component was affinity purified from both immune and pre-immune sera for validation work and specificity was confirmed through Western blotting and the detection of a 38-40kDa protein in THEK and CCRF cell lysates, and in a purified hOGG1 protein preparation. The predicted weight of hOGG1 was 38kDa, however a small difference in molecular weight of purified hOGG1 and hOGG1 in cell lysates was observed. To confirm these differently sized proteins were hOGG1, pre-incubation of the antibody with either hOGG1 protein or peptide significantly reduced reactivity of the antibody to both the purified protein and the cell

lysates. The differences in hOGG1 protein may be explained by truncation of the hOGG1 protein during purification (as suggested by Dr S Boiteux, Fontenay aux Roses, France), or perhaps hOGG1 in cell lysates may be subject to post-translation modification such as phosphorylation, or other components within the lysate preparation may cause reduced mobility of the protein during electrophoresis.

The modulation of hOGG1 protein expression was measured in THEK and CCRF cells treated with 0-400 $\mu$ M hydrogen peroxide for periods up to 24hr. No increases in hOGG1 protein expression were observed throughout the timecourse for both cell types, however an approximate reduction of 50% in expression was consistently observed post 16hr in CCRF treated with 200 and 400 $\mu$ M hydrogen peroxide. This decrease may be due to turnover of the protein post repair events or may be explained by cytotoxicity, since viability was not assessed post 12hr. Saitoh *et al.* (2001) reported of little change in hOGG1 protein expression during a 48hr timecourse post HOCl treatment, although quality of their data may be questioned (see later discussion for hAPE protein expression).

CCRF cells treated with 0-400 $\mu$ M ascorbic acid or dehydroascorbic acid for periods up to 24hr displayed some small changes in protein expression. CCRF cells treated with 50-200 $\mu$ M ascorbic acid showed a transient increase in hOGG1 protein expression; approximately 50% above controls levels, at 12 and 16hr post treatment, similar to increases observed in cells treated with 50-400 $\mu$ M dehydroascorbic acid for 16hr. At all other time points and doses of ascorbic or dehydroascorbic acid, little significant change in protein expression could be detected. These increases in protein may be a direct result of the stimulation of hOGG1 mRNA through antioxidant signalling mechanisms. Interestingly, if such a mechanism is activated then one of the protective roles of antioxidants may involve the direct stimulation of DNA repair genes. Further work is required to validate these findings.

In order to study the cellular localisation of the hOGG1 and potential translocation events, the antibody and the pre-immune serum were applied to THEK cells. Initially, the reactivity of the immune serum was higher than the pre-immune or the secondary antibody only controls. However the distribution of staining prompted co-localisation studies with a mitochondrial stain. No significant co-localisation was observed with MitoTracker<sup>®</sup> and the anti-hOGG1 antibody. In addition, pre-incubation of the antibody with purified hOGG1 or peptide, did not reduced the degree of staining observed, suggesting another antibody with higher affinity for certain sub-cellular structure was masking the potential staining of the anti-hOGG1 antibody.

It was also possible that the anti-peptide antibody had little affinity for hOGG1 protein in its natural conformation and could only detect the denatured protein as in SDS-PAGE. Therefore further affinity purification of the IgG fraction with purified protein may not resolve this problem.

The detection of hAPE protein expression was not successfully achieved using a commercially available antibody. Part of the failure of the antibody may have arisen from the requirement of an amplification step to enhance the signal or insufficient or inappropriate antibody incubation periods. Although information in the methodologies is often sparse, previous papers report on successful staining with the same antibody using a Streptavidin biotin amplification procedure for histology sections and Western blotting (Duguid *et al.*, 1995; Roberston *et al.*, 1997; Xu *et al.*, 1997). Perhaps immunoprecipitation of the protein or an overexpression system was required for Western blot analysis of hAPE using this antibody.

Several studies claim hAPE protein expression may increase in response to ROS. Saitoh *et al.*, 2001 demonstrated a 4 fold increase in hAPE protein expression at 6-12hr following severe oxidative stress, however cells were treated with 2mM HOCl which would probably affect cell viability; no data was shown in this respect. Also their experiments involve measuring  $\alpha$ -tubulin as a constitutive marker to normalise data, however in their methods they describe detection of hAPE using 50 $\mu$ g of cell lysate and 20 $\mu$ g for  $\alpha$ -tubulin, indicating separate electrophoresis of samples. This therefore introduces separate loading and transfer errors and inaccuracies in the normalisation of image analysis data. Also no error bars were included in their representation of data. Similarly Grösch *et al.* (1998) presented a peak 4 fold increase in hAPE protein expression at 11 and 15hr post treatment with 50 $\mu$ M NaOCl and 300 $\mu$ M hydrogen peroxide respectively. However no constitutive marker was used during their Western blot analysis and therefore the levels were not normalised for the amount of total protein. Likewise Ramana *et al.*, 1998 reported 3-8 fold increase in hAPE protein expression following HOCl treatment with no normalisation of data or semi-quantitation.

There are many factors during Western blotting that can affect the overall outcome of protein expression studies. Firstly the use of the Bradford assay to determine protein concentration can only be regarded as a crude measure of protein, as variations in loading were clearly visible by Ponceau S staining of PVDF membranes following transfer. In order to correct for protein loading a constitutively expressed protein,  $\beta$ -actin was immunochemically detected. This proved to be a sensitive measure and more accurate measure of protein concentration on

membranes originally probed for hOGG1 expression. However, other factors could also affect the results, such as uneven transfer of proteins onto PDVF membranes, inadequate incubations with primary and secondary antibodies, as well as insufficient coverage with ECL reagent during detection. These factors can affect the overall results observed and therefore as with RT-PCR, sufficient repetitions are required to confirm any protein expression changes.

The measurement of gene expression by RT-PCR and protein expression by Western blotting can often prove difficult owing to the number of experimental parameters. Pipetting errors often significantly contribute to intra- and inter- sample variations observed in RT-PCR. Similarly the spectrophotometric determination of either RNA or protein concentrations often prove unreliable and the measurement of a constitutive marker is essential to normalise the data in Western blotting. However despite these considerations other technical variations in experimental conditions (*e.g.* new batch of enzyme or antibody) can also cause some alteration in expression measurements. It is therefore necessary to repeat experiments several times to reduce standard deviation in order to confirm small changes in gene or protein expression as being significant.

#### **5.5.4 *hOGG1* & *hAPE* enzyme activity**

Despite little significant change being observed with *hOGG1* and *hAPE* mRNA and protein expression following exposure of cells to oxidant and anti-oxidant conditions, modulation in the enzymatic activity could not be ruled out. The measurement of 8-oxoG glycosylase/AP lyase activities was previously described involving the incubation of cell free extracts with a 5' radiolabelled double-stranded oligonucleotide containing a single 8-oxoG residue (Chung *et al.*, 1991; Yamamoto *et al.*, 1992). The approach taken here was to follow the same experimental principal however utilising a non-radiolabelled oligonucleotide substrate (Appendix VIII). Some success was achieved with using denaturing-PAGE, however components in the cell extracts interfered with the electrophoresis and resolution of the bands. This was partly improved by the use of Dynabeads to extract biotinylated oligonucleotides from cell extracts, however problems with the gels melting during electrophoresis were difficult to control. To overcome these problems and improve sensitivity, a capillary electrophoresis approach was successfully undertaken allowing the clear separation of cleaved oligonucleotide and single-stranded substrate oligonucleotide and consequently, improved quantitation.

The preliminary experiments with CCRF cells treated with 100 and 400 $\mu$ M hydrogen peroxide for 16hr showed an unconfirmed increase of 1.5-2 fold in endonuclease nicking activity compared to control levels. This assay has the potential application for future experimentation, particularly as the measurement of enzyme activity is functionally more relevant than measuring mRNA or protein expression levels. Using similar approaches to measure endonuclease nicking activity, Tsurudome *et al.* (1999) reported decreases of 25% in repair activity in rat lung 2hr to 2 day post exposure to diesel exhaust particles. Whilst in rat kidney homogenates Lee *et al.* (1996) showed maximal increases in repair activity 6hr post treatment with potassium bromate and Yamaguchi *et al.* (1996) showed significant increases at 6-24hr post ferric nitrilotriacetate administration. Lin *et al.*, 2000 also reported increases in mOGG1 protein and enzyme activity following mouse forebrain ischaemia-reperfusion with no associated alteration in mRNA expression changes. Grösch *et al.* (1998) and Ramana *et al.* (1998) both reported on increases in the rate of hAPE activity in cells treated with hydrogen peroxide and HOCl respectively. Interestingly, the overexpression of OGG1 resulted in a several fold increase in enzyme activity and an accelerated repair rate of exogenously-induced damage, although with little effect on the spontaneous oxidative damage and mutation rates (Hollenbach *et al.*, 1999).

A genetic polymorphism in  $\alpha$ -hOGG1 (Ser326Cys) is frequently found in the human population; for example, in the Caucasian population the allele frequency is 75% for Ser<sup>326</sup> and 25% for Cys<sup>326</sup> (Janssen *et al.*, 2001). The significance of this polymorphism in relation to functional activity and cancer predisposition was examined. Kohno *et al.* (1998) demonstrated transfections of the two polymorphic forms of GST-fusion proteins into *mutMmutY* double mutant of *E. coli* resulted in hOGG1-Ser<sup>326</sup> showing stronger suppression of G:C  $\rightarrow$  T:A mutation rate, compared to hOGG1-Cys<sup>326</sup>. However, Shinmura *et al.*, (1997) and Dherin *et al.*, (1999) report on GST-constructs of  $\alpha$ -hOGG1-Ser<sup>326</sup> or  $\alpha$ -hOGG1-Cys<sup>326</sup> displaying similar rate constants for the cleavage of a 34mer DNA oligonucleotide containing 8-oxodG or FapyGua. And more recently Janseen *et al.* (2001) demonstrated DNA repair activity in cryopreserved human lymphocytes taken from a Caucasian population was unaltered by this genetic polymorphism; further supporting the findings of Dherin and coworkers and highlighting possible differences in enzyme expression/activity in the bacterial systems.

mechanism/s to maintain low endogenous mutation frequency. Nevertheless the association of DNA repair defects and cancer in humans has escalated in recent years, particularly since the identification of defects in the gene encoding the human homologue of MutS in hereditary non-polyposis colorectal cancer. In spite of the outcome of *ogg1*<sup>-/-</sup> knockout mice, the role of hOGG1 in human carcinogenesis and the interplay with other DNA repair enzymes will continue to be studied.

Unlike *ogg1*<sup>-/-</sup> knockouts, hAPE nullizygous demonstrate embryonic lethality (Xanthoudakis *et al.*, 1996), perhaps highlighting the significance of this multifunctional protein. There have been many reports of altered expression and/or subcellular localisation of hAPE in tumours such as cervical (Xu *et al.*, 1997), colon (Kakolyris *et al.*, 1997), ovarian (Moore *et al.*, 2000) and others. Also, mutations in *hAPE* have been reported in patients with amyotrophic lateral sclerosis (ALS) and familial ALS (Olkowski, 1998), suggesting defects in repair of abasic sites cause inhibition of DNA replication, affect viability, and ultimately lead to neuronal death typical of such neurodegenerative disorders. More work is required to elucidate the significance of this multifunctional protein in disease.

**CHAPTER SIX**

**GENERAL DISCUSSION & FUTURE WORK**

## 6.1 GENERAL DISCUSSION

The focus of this thesis was to establish suitable *in vitro* model systems in order to investigate DNA damage and repair mechanisms responding to pro- and anti-oxidants. Much of the research utilised cultured lymphoblastoma cells as well as primary and transformed keratinocytes as models. Changes to the intracellular environment were investigated following exposure to a ROS generating reagent. ROS-specific and UV-specific DNA lesions were detected by immunochemical and analytical techniques. Repair of DNA lesions was investigated by the disappearance of nuclear immunochemical staining with adduct specific antibodies. Also, specifically the modulation in gene and protein expression and enzymic activity of specific DNA repair enzymes was studied.

### 6.1.1 Characterisation of genotoxicity

The measurement of DNA damage provides a useful biomarker of potential genotoxic change within cells or tissues. The quantitation of damage can reflect the severity and dose of insult. Whatever the nature of an insult, be it due to environmental and chemical agents or endogenous perturbations, it can generate a range of DNA lesions that in turn can evoke an array of cellular events. In order to understand these cellular changes, *in vitro* models provide a convenient starting point. In this thesis DNA damage in cultured cells was generated by both chemical and physical treatment, namely hydrogen peroxide and UV irradiation respectively. Each insult generates an assortment of DNA damage characteristic of the nature of the damaging agent. For example irradiation with the shorter wavelengths of UV causes the formation of characteristic bulky lesions, cyclobutane pyrimidine dimers (CPD) and 6-4 photoproducts. The use of monochromatic UV showed differing levels of dimer formation. Irradiation with 305nm UVB caused a significantly much higher proportion of CPD compared to irradiations with 315nm in both cells and DNA. In addition to the formation of UV-specific DNA damage, UVB can also generate DNA damage via ROS. Both hydrogen peroxide and UVB can generate similar types of lesions; 8-oxodG is one such lesion. However the levels of 8-oxodG formation and potency of these insults require further investigation.

The use of antibody-based technology to detect DNA adducts allows the direct detection of specific lesions in DNA as well as the scope for identifying damage *in situ* and monitoring repair processing. Immunostaining techniques combined with confocal, light or electron microscopy used in this thesis allowed the identification of specific DNA lesions in relation to

the distribution within cellular compartments and/or particular cell types within a tissue. Characterisation of an antibody raised to UVC DNA indeed confirmed the detection of cyclobutane thymine dimers (CTD). CTD formation was shown to vary following irradiation with specific wavelengths of monochromatic UVB differing by 10nm. Immunofluorescence with confocal microscopy clearly showed the nuclear detection of CTD with further validation by electron microscopy. In theory the detection of ROS induced DNA damage may be similarly successful. The detection of ROS-induced damage in cultured cells was subject to problems of antibody specificity or unmasking techniques. Antibodies to oxidative lesions currently lack the requisite specificity. Some success in the recognition of 8-oxodG in keratinocytes exposed to increasing doses of hydrogen peroxide was observed despite some high background staining. Also both 8-oxodG and cytosine glyoxal antibodies bound to nuclear material in tissue sections following pre-treatment of specimens with hydrogen peroxide and ascorbic acid. The precise mechanism by which ROS damage is generated in this *in vitro* pre-treatment of formalin-fixed paraffin embedded tissues presents an interesting investigative challenge.

In addition to some technical parameters affecting the immunodetection of DNA damage *in situ*, immunostaining is semi-quantitative at best. The use of image analyses packages can assist semi-quantitation, however often not all the DNA damage is recognised by the antibody due to obstruction by cellular ultrastructure. Immunostaining is best complemented by the parallel detection of DNA damage in extracted DNA, such as by ELISA-based assays. Ideally the source of DNA is that extracted from treated cells, however in experiments involving monochromatic UV irradiation using an 8mm liquid light guide this was not possible due to the number of cells required for sufficient DNA isolation. Nevertheless, the detection of CTD *in situ* and in calf thymus DNA provided a clear illustration of dose responses following irradiation with 305nm and 315nm UVB. Also, the ELISA data allowed an unambiguous comparison of the potencies of each wavelength.

Improvements to the absolute quantitation of DNA damage can be addressed by analytical techniques such as HPLC, GC-MS and LC-MS-MS, but also, and perhaps more accurately, using 'enzymatic' procedures such as Comet, alkaline elution or alkaline unwinding assays coupled with specific DNA glycosylase, such as fpg for oxidative damage. For the chromatographic procedures using a damage-specific standard curve the actual number of adducts can be quantitated and related to the concentration of DNA or the content of a specific nucleotide. For the measurement of 8-oxodG, the levels were directly related to the total of deoxyguanosine measured within the same sample to account for variations in DNA

concentration pre-digestion. In both CCRF and THEK cells the measurement of 8-oxodG by HPLC-ECD showed a dose dependent increase following hydrogen peroxide treatment. There are however some technical considerations, one of the most important being the generation of artificial damage through sample processing; this was minimised amongst other measures by the inclusion of desferrioxamine in the DNA extraction solutions. Another issue is the reproducibility of measurement (inter- and intra- batch variations); the 8-oxodG HPLC-ECD data presented in this thesis required further analysis, however due to instrumentation problems repetitions were hindered. In any case the immunofluorescence data of 8-oxodG in THEK cells complemented the HPLC-ECD trend in 8-oxodG formation.

Although these analytical techniques lose the anatomical information of DNA damage *in situ*, they do complement immunochemical data. The trend in immunofluorescence detection of CTD in THEK cells was reaffirmed by the ELISA data of CTD formation in DNA following irradiation with 305nm and 315nm UVB. In addition to this, spectrophotometric absorbance values from ELISA measurements of CTD were compared to GC-MS quantitative data using UVC irradiated DNA (reproduced under the same conditions and with the same lamp as stated for the GC-MS experiments). This comparison provided an indication of the magnitude of damage generated by both 305nm and 315nm even though absolute values could not be determined in this thesis.

### **6.1.2 Modulation of BER enzymes specific for oxidative DNA damage**

#### *Intracellular prooxidant and antioxidant measurements*

The measure of global intracellular redox status provides a reflection of changes to lipids, proteins and DNA. Often the measurement of a single endpoint masks other changes occurring, therefore measuring intracellular oxidative activity highlights potential modifications to any of these components. In this thesis, a fluorescent 96-well plate live cell assay was successfully established using 5-(and-6)-chloromethyl-2',7'-dichlorodihydrofluorescein diacetate (CM-H<sub>2</sub>DCFDA). THEK cells were pre-loaded with this compound and treated for up to 1hr with hydrogen peroxide, ascorbic acid or dehydroascorbic acid. Oxidative activity was measured post-treatment by the generation of fluorescence through the oxidation of CM-H<sub>2</sub>DCFDA. The changes in intracellular oxidative activity measured following hydrogen peroxide further complemented data for 8-oxodG measured by HPLC-ECD and immunofluorescence. All three assays confirmed an increase in the generation of ROS or 8-oxodG following hydrogen peroxide treatments.

The CM-H<sub>2</sub>DCFDA assay could also have been extended to assess intracellular changes following UV irradiation and/or for long-term treatment effects. In particular the treatment of THEK cells with ascorbic acid and dehydroascorbic acid generated a small initial increase in oxidative activity with the higher treatment doses in the first 30min of incubation. Any sequestration of basal oxidative activity by ascorbic acid or dehydroascorbic acid may have been evident if cells had been pre-incubated with antioxidants prior to loading with CM-H<sub>2</sub>DCFDA. Such experiments may have also demonstrated any potential prooxidant effects of due to high intracellular levels of antioxidants. All treatments with hydrogen peroxide, ascorbic acid or dehydroascorbic acid of doses ranging 0-400 $\mu$ M were confirmed to be non-toxic to cells by measuring viability by the trypan blue exclusion test.

The assessment of live cell intracellular oxidative activity most certainly complements any measure of specific damage whether it be protein, lipid or DNA damage. The effects of a compound can also be assessed by measuring the compound itself or its by-product in cells. In this thesis the effects of ascorbic acid and dehydroascorbic acid were measured by intracellular or extracellular changes in ascorbic acid levels. Dehydroascorbic acid could not be measured directly due to the low UV absorbance, however the effects of dehydroascorbic acid was measured by the intracellular regeneration of ascorbic acid. In both cell models it was apparent that ascorbic acid and dehydroascorbic acid were actively internalised. The significant increases in intracellular ascorbic acid were detected in both THEK and CCRF cells; the regeneration of intracellular ascorbic acid following dehydroascorbic acid treatment being more efficient than the rate of ascorbic acid uptake. Interestingly, in THEK cell medium the levels of ascorbic acid significantly decreased at faster rate compared to CCRF cell culture medium during the 12hr studied. The rate of extracellular reduction in ascorbic acid was not proportional to the rate of intracellular increases, suggesting differing components in cell culture medium influencing the degradation of ascorbic acid.

Another important consideration is the sensitivity of a cell to DNA damage and the differing degrees of intracellular protection. For example, keratinocytes may have more elaborate protective mechanisms compared to lymphocytes *in vivo* as they are continuously exposed to environmental stresses. Cells in culture are also believed to adapt to high levels of oxidative stress and therefore may differ in relation to how they cope with an insult that causes an increase in oxidative stress or how they may have modified or elevated rates of repair.

*Expression of DNA repair enzymes*

For this thesis the focus was to establish an *in vitro* model system suitable to measure the expression of hOGG1 and hAPE base excision repair enzymes, key enzymes in the removal of 8-oxodG lesions. Having provided evidence for the generation of 8-oxodG adducts following hydrogen peroxide treatment of both THEK and CCRF cells, these treatment models were used to address potential modulation of gene and protein expression as well as an enzyme activity presumed to involve hOGG1 and hAPE. The changes in genes, protein and enzyme activity can often be independent of each other; for example mRNA expression can be affected by the half-life of the transcript and rate of translation, whilst protein levels may be sensitive to the intracellular environment and enzyme activity may be reliant on post-translational modifications such as phosphorylation events, translocation to different cellular compartments or other such events. It was therefore important to address modulation of hOGG1 and hAPE at all three levels of expression.

Prior to the investigation of gene expression of *hOGG1* and *hAPE* by reverse-transcription-polymerase chain reaction (RT-PCR) methods, the transcriptional activity of cells was established. Both DNA repair genes have potential candidate activator protein-1 (AP-1) binding sites in their promoter sequences, amongst many other transcriptional motifs. The activation of AP-1 is often associated with antioxidant stimuli, therefore transcriptional activation was investigated in cells following ascorbic acid treatment. In both cell types there was evidence of differences in transcription factor binding activity of AP-1 in nuclear extracts assessed by an electrophoretic shift assay. Although this did not confirm transcriptional activation of *hOGG1* and *hAPE* genes specifically, the measured AP-1 binding activity showed interestingly the potential of ascorbic acid to stimulate the expression of certain genes. However the changes in AP-1 binding activity could not be easily correlated to increases in intracellular ascorbic acid levels measured by capillary electrophoresis since insufficient timepoints were taken. In any case, treatments with the higher doses of ascorbic acid probably would have raised intracellular ascorbic acid before 4hr in both cell types, however lower doses may not have been detected due to the sensitivity of the measurements. Further investigations into the uptake of ascorbic acid and the identification of changes in gene expression using techniques such as microarray, may enhance our understanding of the effects of ascorbic acid in cells and provide information relating to more effective antioxidant therapies such as those aimed at reducing pre-eclampsia.

RT-PCR methods were successfully established to measure gene expression changes in *hOGG1* and *hAPE*. Having investigated potential modulation of cellular redox status, neither

hydrogen peroxide nor ascorbic acid treatment caused a change in *hOGG1* nor *hAPE* gene expression during a 12hr timecourse studied in both THEK and CCRF cells. Similarly, detection of hOGG1 protein expression by Western blotting also presented little change following different doses of hydrogen peroxide in both cells types. Interestingly, the treatment of CCRF cells with ascorbic acid or dehydroascorbic acid induced a transient increase in hOGG1 protein expression post 12hr. These increases were coupled directly with increases in intracellular ascorbic acid post ascorbic acid but not dehydroascorbic acid at the lower treatment doses. In summary, bearing in mind the parameters of variation owing to experimental procedure for both RT-PCR and Western blotting, it was concluded that hOGG1 gene and protein expression did not alter following hydrogen peroxide treatment. The expression of hAPE protein remained inconclusive owing to experimental difficulties, however *hAPE* gene expression was unaltered following treatment with either hydrogen peroxide or ascorbic acid.

Interestingly, the measurement of endonuclease nicking activity for an oligo substrate containing an 8-oxodG lesion revealed some potential differences in activity in cell extracts following treatment with hydrogen peroxide. These observations however require further investigation to confirm whether these changes were significant with respect to variations occurring through experimental technique. Nevertheless, the optimisation of two electrophoresis methods for the examination of excised oligos, enables the dual comparison and confirmation of data from both assays and therefore provides the potential application for future *in vitro* studies. In addition the incorporation of different adducts into the repair substrate can be utilised to study other enzyme systems within the same sample.

## **6.2 FUTURE WORK**

The following experiments and approaches would complement the data described in this thesis:

### **6.2.1 *Demonstration of genotoxicity***

The immunochemical detection of DNA lesions provides an excellent approach to appreciate the distribution and removal of damage in cell and tissues. The work presented in this thesis highlights the need for the development of antibodies with improved specificity and sensitivity for oxidative lesions such as 8-oxodG. The ELISA detection of lesions in extracted DNA from cells treated with damaging agents also provides a useful indication of the extent of disruption to DNA; this was demonstrated successfully with CTD formation following monochromatic UVB exposure. The same extracted DNA could be further analysed by ELISA for other DNA lesions; therefore building a detailed picture of DNA adduct spectra generated by one damaging agent.

The quantitation of DNA adducts by analytical procedures compliments semi-quantitative immunochemical data. In this thesis the HPLC-ECD detection of 8-oxodG in cells treated with hydrogen peroxide clearly showed an increase when compared to basal levels, however owing to technical difficulties at the time further repetitions are required to confirm these changes and levels of 8-oxodG detected; bearing in mind the considerations highlighted by ESCODD relating to the absolute measurement of 8-oxodG in DNA. Alternative to analytical procedures, the quantitation of low levels of DNA adducts maybe better approached by enzymatic assays discussed earlier and in chapter 4.

The measurement of DNA damage in conserved regions of genes that translate to functional protein regions may provide a more refined approach into the understanding of the mutational capacity of certain lesions with respect to cellular function. Nevertheless the successful establishment of the CM-H<sub>2</sub>DCFDA assay to measure general intracellular ROS provides a valuable assessment of the global cellular effects of a treatment. In addition to the further experiments previously discussed relating to the potential demonstration of antioxidant effects of ascorbic acid, this assay could be applied to other conditions, such as investigating the ROS generating capacity by specific wavelengths of monochromatic UV.

### **6.2.2 Modulation of DNA repair enzymes**

Owing to limitations of possibly the sensitivity and selectivity of the CTD antibody, removal of dimers and the reported timescales requires further investigation. The generation of a specific cyclobutane cytosine dimer antibody would provide a more interesting adduct to monitor, particularly with respect to its reported mutational capacity. Also the complementary measurement of enzymes important in GG-NER and/or TC-NER may yield interesting information regarding potential modulation and regulation. Another interesting aspect of the research presented in this thesis is processing of UV-specific damage. Electron microscopy data showing nuclear evaginations requires further investigation to confirm the relevance of this phenomenon in relation to UV damage and repair, possibly through the application of timelapse microscopy. Also the issues relating to the processing of the excised oligos and the potential expulsion from the cells, raised through the competition ELISA data, could be further investigated by microinjecting a tagged antibody specific to UV damage and monitoring the release and/or processing by timelapse microscopy.

RT-PCR and Western blotting approaches to assess the modulation of hOGG1 and hAPE proved successful. Perhaps future work assessing the modulation of DNA repair enzymes could encompass the interactions of multiple DNA repair pathways. Approaches such as ribonuclease protection assays (currently being utilised by Sam Phillips, Department of Pathology, University of Leicester) and microarray analysis allow the simultaneous detection of numerous mRNA transcripts and therefore provide more information relating to the interplay of DNA repair pathways. Any changes detected at the transcriptional levels could be investigated at the translation level. The measurement of repair activities of hOGG1 and hAPE using the endonuclease nicking assay required further validation to confirm the reported observations in this thesis. The assay could also be adopted to measure enzyme activities important in the removal of other DNA lesions including those typically removed by NER. In addition this assay could be further complimented with the measurement of released bases by techniques such as HPLC.

### **6.2.3 Review of model systems**

Cell lines provide a good starting point for most investigations as they are often simple to maintain and are non-invasive models; in addition they do not require ethics approval or the use of animals. However cell lines lack biochemical and physical interactions of neighbouring cells, some of differing phenotypes; in addition to the lack of an active blood flow system transporting essential nutrients, cytokines, by-products of metabolism etc.

Perhaps to achieve some of these interactions, studies using *ex vivo* tissue may provide more information before entering into more complex *in vivo* studies. The use of skin explants, taken from breast reduction operations for example, could be used to investigate the penetrance of monochromatic UVB and formation and clearance of specific DNA lesions in different cells type constituting the layers of skin. This would be particularly useful for gauging the potencies of narrowband UVB irradiations used in the treatment of various skin disorders, particularly for those patients (for example with skin type I) at high risk of developing malignancies.

Studying the accumulation/excretion of DNA damage adducts or the repair efficiency in cells may provide useful indicators of potential cancer progression and/or the development of certain disease states. In particular understanding the mechanism of genomic maintenance and the regulation of DNA repair genes may provide avenues for potential therapies. Certain inflammatory conditions such as systemic lupus erythematosus (SLE) and rheumatoid arthritis (RA) are reported to have increased levels of ROS adducts in their DNA, which may exacerbate the condition and lead to associated pathologies; patients may benefit from the enhancement of DNA repair systems and/or the intervention of effective antioxidant treatments. In addition patients defective in certain repair proteins may be assisted by a gene therapy approach and/or the enhancement of other compensatory DNA repair mechanisms.

**APPENDIX I**      **Composition of cell culture media:** Dulbecco's Modified Eagles Medium (DMEM) with Glutamax 1™, Ham's Nutrient Mixture F-12 (Ham's F12) with Glutamax 1™ and Roswell Park Memorial Institute medium (RPMI-1640) without glutamine (data from Gibco Life Technologies Catalogue 2001).

COMPONENT	DMEM (mg/L)	Ham's F12 (mg/L)	RPMI (mg/L)
<b>Inorganic Salts:</b>			
CaCl <sub>2</sub> (anhyd.)	264.00	44.00	
Ca(NO <sub>3</sub> ) <sub>2</sub> •4H <sub>2</sub> O			100.00
CuSO <sub>4</sub> •5H <sub>2</sub> O		0.0024	
Fe(NO <sub>3</sub> ) <sub>3</sub> •9H <sub>2</sub> O	0.10	0.83	
KCl	400.00	223.60	400.00
MgSO <sub>4</sub> •7H <sub>2</sub> O	200.00		100.00
MgCl <sub>2</sub> •6H <sub>2</sub> O		122.00	
NaCl	6400.00	7599.00	6000.00
NaHCO <sub>3</sub>	3700.00	1176.00	2000.00
Na <sub>2</sub> HPO <sub>4</sub> (anhyd.)		142.00	800.00
NaH <sub>2</sub> PO <sub>4</sub> •2H <sub>2</sub> O	141.00		
ZnSO <sub>4</sub> •7H <sub>2</sub> O		0.86	
<b>Other Components:</b>			
D-Glucose	1000.00	1802.00	2000.00
Glutathione (reduced)			1.00
Linoleic Acid		0.084	
DL-68 Thioctic Acid		0.20	
Phenol red	15.00	1.20	5.00
Putrescine 2HCl		0.161	
Sodium Pyruvate	110.00	110.00	
Hypoxanthine		4.00	
Thymidine		0.70	
<b>Amino Acids</b>			
L-Alanine		8.90	
L-Asparagine (Free base)		13.00	50.00
L-Arginine •HCl	84.00	211.00	240.00
L-Aspartic Acid		13.30	20.00
L-Cysteine	48.00		50.00
L-Cysteine HCl		36.00	
L-Glutamic Acid		14.70	20.00
L-Alanyl-L-Glutamine	862.00	217.00	

Glycine	30.00	7.50	10.00
L-Histidine (free base)			15.00
L-Histidine HCl•H <sub>2</sub> O	42.00	21.00	
L-Hydroxyproline			20.00
L-Isoleucine	105.00	4.00	50.00
L-Leucine	105.00	13.00	50.00
L-Lysine HCl	146.00	36.50	40.00
L-Methionine	30.00	4.50	15.00
L-Phenylalanine	66.00	5.00	15.00
L-Proline		34.50	20.00
L-Serine	42.00	10.50	30.00
L-Threonine	95.00	12.00	20.00
L-Tryptophan	16.00	2.00	5.00
L-Tyrosine	72.00	5.40	20.00
L-Valine	94.00	11.70	20.00
<b>Vitamin:</b>			
Biotin		0.0073	0.20
D-Ca Pantothenate	4.00	0.50	0.25
Choline Chloride	4.00	14.00	3.00
Folic Acid	4.00	1.30	1.00
i-Inositol	7.20	18.00	35.00
Nicotinamide	4.00	0.036	1.00
Para-aminobenzoic Acid			1.00
Pyridoxine HCl	4.00	0.06	1.00
Riboflavin	0.40	0.037	0.20
Thiamine HCl	4.00	0.30	1.00
Vitamin B <sub>12</sub>		1.40	0.005

**APPENDIX II      Spectrophotometric assessment of hydrogen peroxide molarity**

$$\text{Abs} = E \times C \times L$$

where Abs : Spectrophotometric absorbance

E:      extinction coefficient

C:      concentration (M)

L:      light path ( $\cong$  1cm)

The extinction coefficient of hydrogen peroxide are as follows:

@ 240nm:  $43.6\text{cm}^{-1}\text{M}^{-1}$

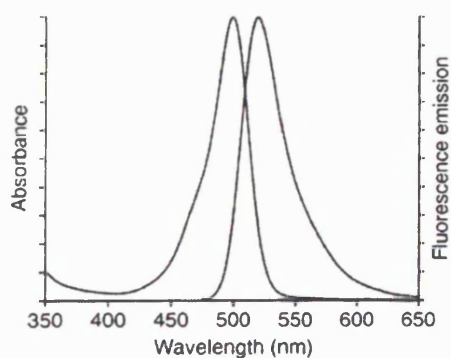
@ 230nm:  $72.4\text{cm}^{-1}\text{M}^{-1}$

The molar concentration of a 30% (w/w) hydrogen peroxide solution (Sigma) determined at both 230 and 240nm averaged 9.1M

## APPENDIX III Excitation and emission spectra of fluorochromes

(data from www.probes.com)

Fluorochrome	Excitation (nm)	Emission (nm)
Alexa fluor™ 488	494	517
CM-H <sub>2</sub> DCFDA	495	529
FITC	494	519
Hoechst 33258	352	461
Hoechst 33342	350	461
MitoTracker®	578	599
Propidium Iodide	535	617



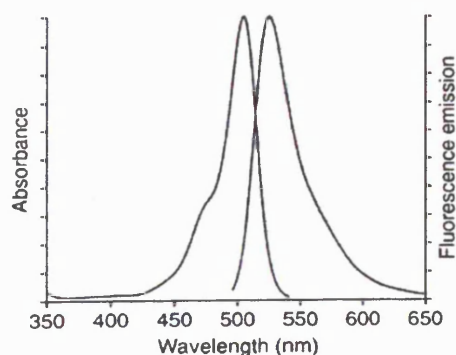
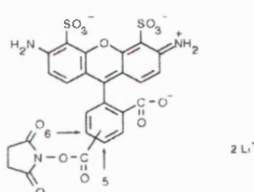
## Alexa Fluor® 488 Protein Labeling Kit

COMPONENT A: Alexa Fluor® 488 carboxylic acid, succinimidyl ester, dilithium salt

Molecular Formula: C<sub>25</sub>H<sub>15</sub>Li<sub>2</sub>N<sub>3</sub>O<sub>13</sub>S<sub>2</sub>

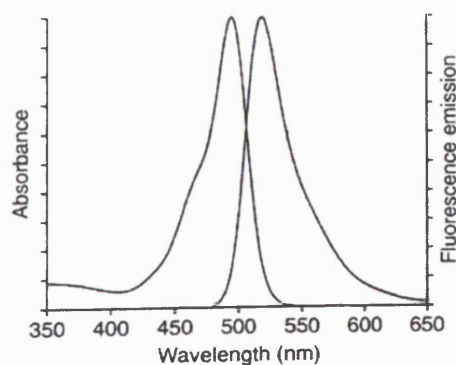
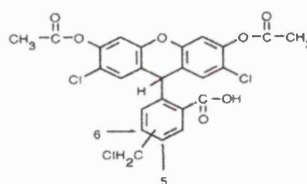
Molecular Weight: 643.41

CAS Number/Name: Not determined

5-(and-6)-chloromethyl-2',7'-dichlorodihydrofluorescein diacetate (CM-H<sub>2</sub>DCFDA)Molecular Formula: C<sub>25</sub>H<sub>17</sub>Cl<sub>3</sub>O<sub>7</sub>

Molecular Weight: 535.76

CAS Number/Name: Not determined



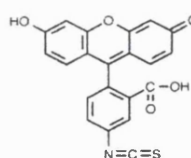
## FluoReporter® FITC Protein Labeling Kit

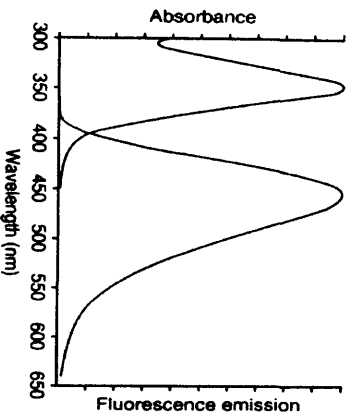
COMPONENT A: fluorescein-5-isothiocyanate, isomer I

Molecular Formula: C<sub>21</sub>H<sub>11</sub>NO<sub>5</sub>S

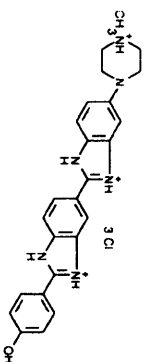
Molecular Weight: 389.38

CAS Number/Name: 3326-32-7 Spiro(isobenzofuran-1(3H),9'-(9H)xanthen)-3-one, 3',6'-dihydroxy-5-isothiocyanato-



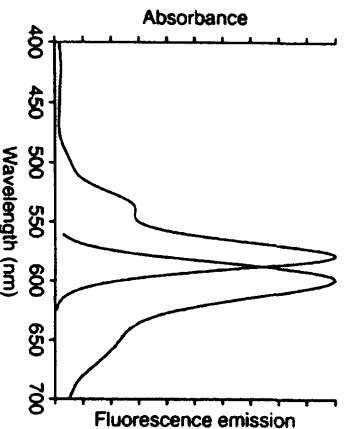
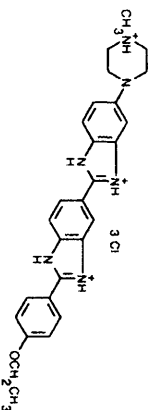
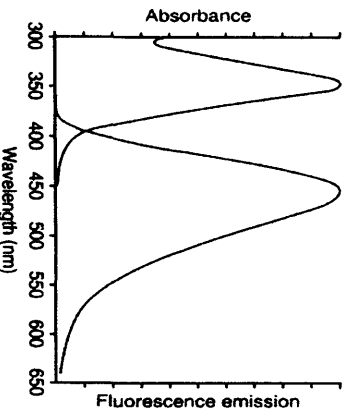


**Hoechst 33258 (bis-benzimidide)**  
**Ingredient A: Hoechst 33258, pentahydrate (bis-benzimidide)**  
**Molecular Formula:**  $C_{25}H_{27}Cl_3N_6O$   
**Molecular Weight:** 533.89  
**CAS Number/Name:** Not determined

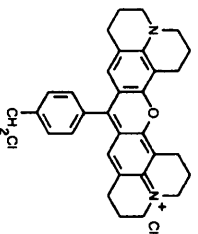


**Hoechst 33342**

**Ingredient A: Hoechst 33342, trihydrochloride, trihydrate**  
**Molecular Formula:**  $C_{27}H_{27}Cl_3N_6O$   
**Molecular Weight:** 567.99  
**CAS Number/Name:** Not determined

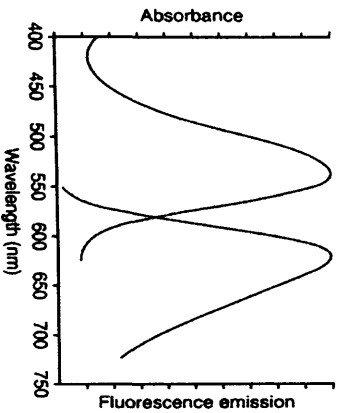
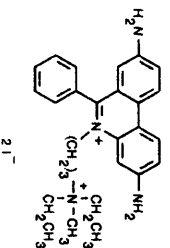


**MitoTracker@ Red CMXRos**  
**Molecular Formula:**  $C_{31}H_{32}Cl_2N_2O$   
**Molecular Weight:** 531.52  
**CAS Number/Name:** 167095-09-2 / 1H,5H,11H,15H-Xantheno[2,3,4-bj:5,6,7-i']diquinoliz-18-ium, 9-[4-(chloromethyl)phenyl]-2,3,6,7,12,13,16,17-octahydro-, chloride



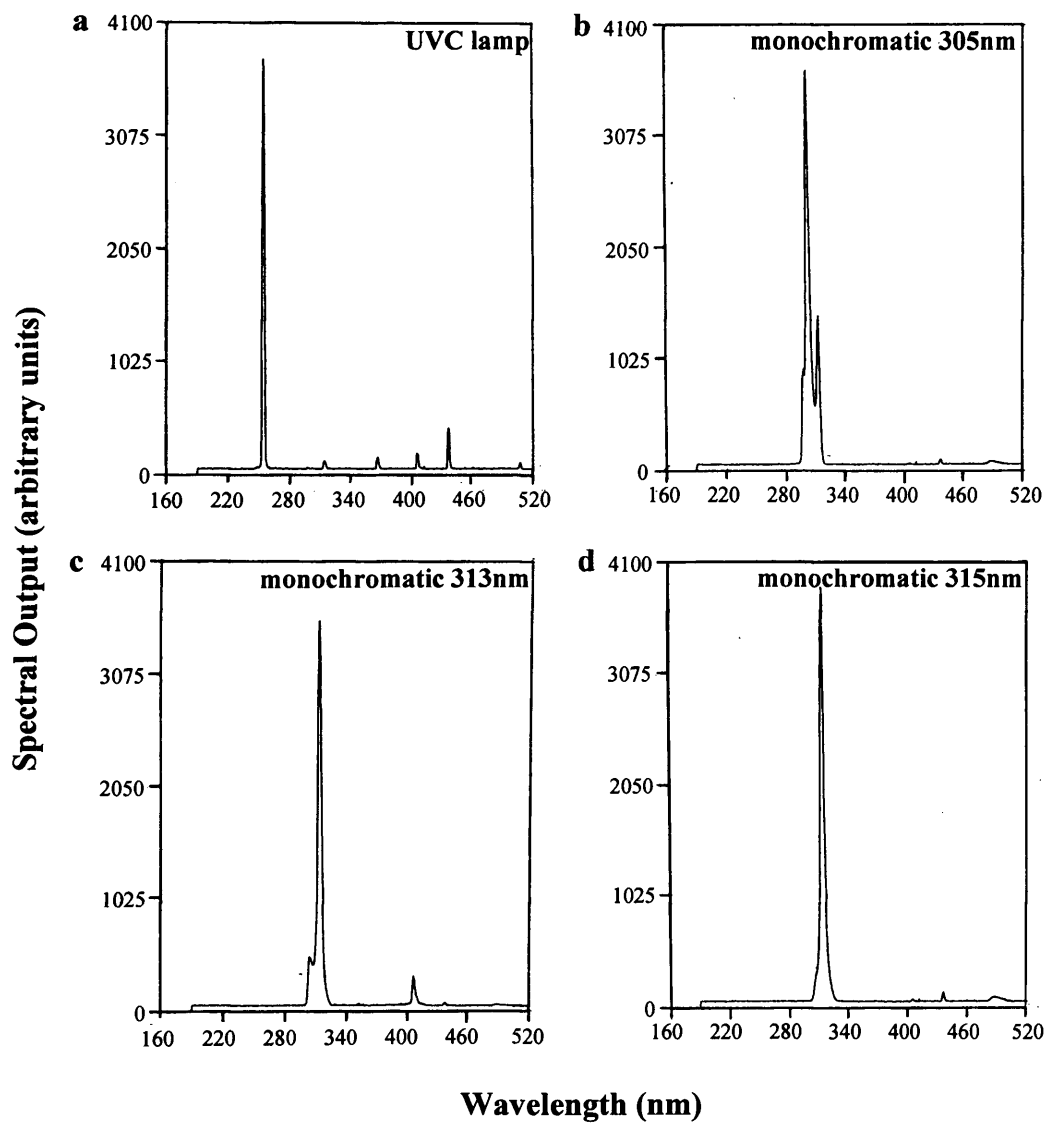
**propidium iodide**

**Molecular Formula:**  $C_{27}H_{34}I_2N_4$   
**Molecular Weight:** 668.4  
**CAS Number/Name:** 25535-16-4 Phenanthridinium, 3,8-diamino-5-[3-(diethylmethylammonio)propyl]-6-phenyl-, diiodide



**APPENDIX IV Emission spectra of UV sources: spectral output measured by a S2000 Fiber Optic Spectrometer with computerised Spectrawin 2000 software**

254nm UVC lamp (a) and monochromatic light with  $\pm 4.5\text{nm}$  bandwidth at 305nm (b), 313nm (c) and 315nm (d)



## APPENDIX V Calculation of UV dose and coefficient of variation of irradiation

### Calculation of UV dose

#### Conversions

$1 \text{kJm}^{-2} \equiv 0.1 \text{Jcm}^{-2}$  or  $100 \text{mJcm}^{-2}$  (accepted units for UVA and UVB exposure, respectively)

$1 \text{mWcm}^2 (4 \div 100)^2$

$1 \text{mJs}^{-1} \text{cm}^2$

#### Calculation of UV dose

$$\text{Dose (mJcm}^{-2}\text{)} = \text{Time (s)} \times \text{Energy output (mJs}^{-1}\text{cm}^2\text{)}$$

#### Theoretical calculation of 254nm UVC output

$$\text{Intensity} \propto \frac{1}{[\text{distance (r)}]^2}$$

Maximum output:  $10.5 \mu\text{Wcm}^2$  at 1M

At 4cm (height of the lamp):  $r^2 = (4 \div 100)^2$

$$\text{Intensity} = [1 \div (4 \div 100)^2] \times 10.5 = 6562.6 \mu\text{Wcm}^2 \equiv 6.5626 \text{mWcm}^2$$

**Radiometric coefficient of variation of monochromatic irradiation doses achieved with 8mm post-optic liquid light guide for cells in 8-well chambered slides and DNA in 24-well plates**

Irradiation $\lambda$	Coefficient of Variation (%)	
	8-well slides	24-well plates
305nm	5.43	10.45
313nm	3.89	10.64
315nm	5.13	10.75

## APPENDIX VI hOGG1 peptide synthesis

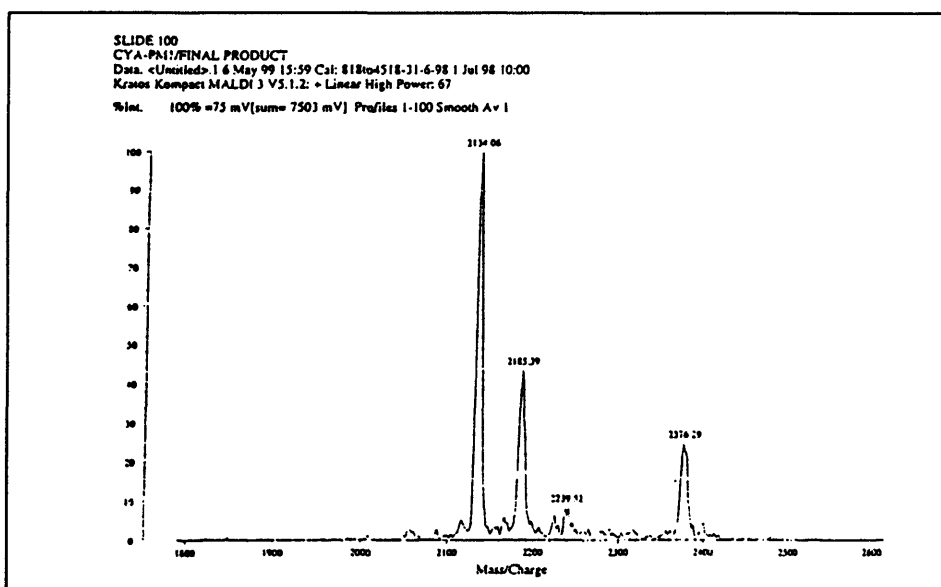
## Production of hOGG1 Synthetic Peptide.

A hOGG1 specific peptide was produced as described by Harza *et al.*, 1998 in order to facilitate polyclonal antibody production.

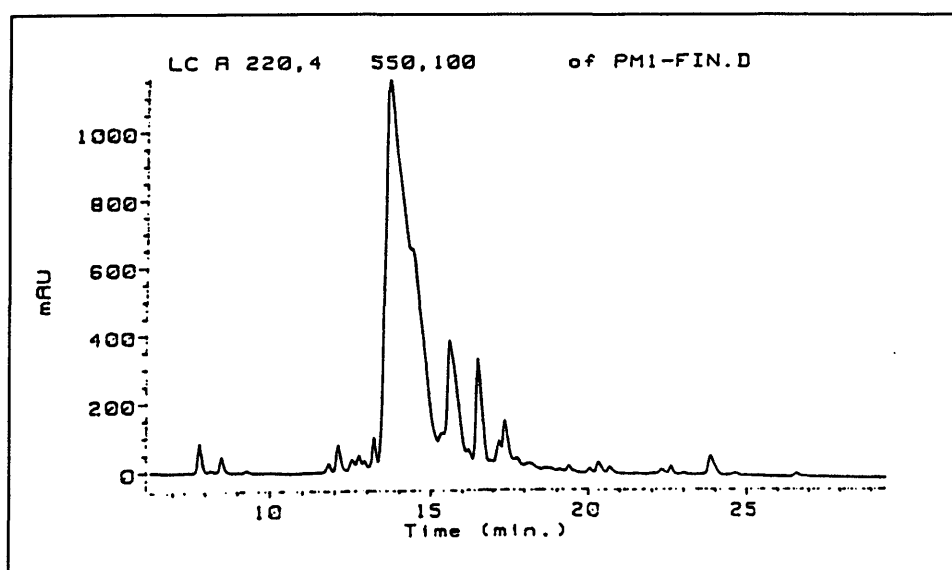
Synthetic peptide sequence: N-DKSQASRPTPDELEAVRKC-C

Estimated  $M_w$ : 2130.38

Actual  $M_w$  as determined by MALDI: 2134.06

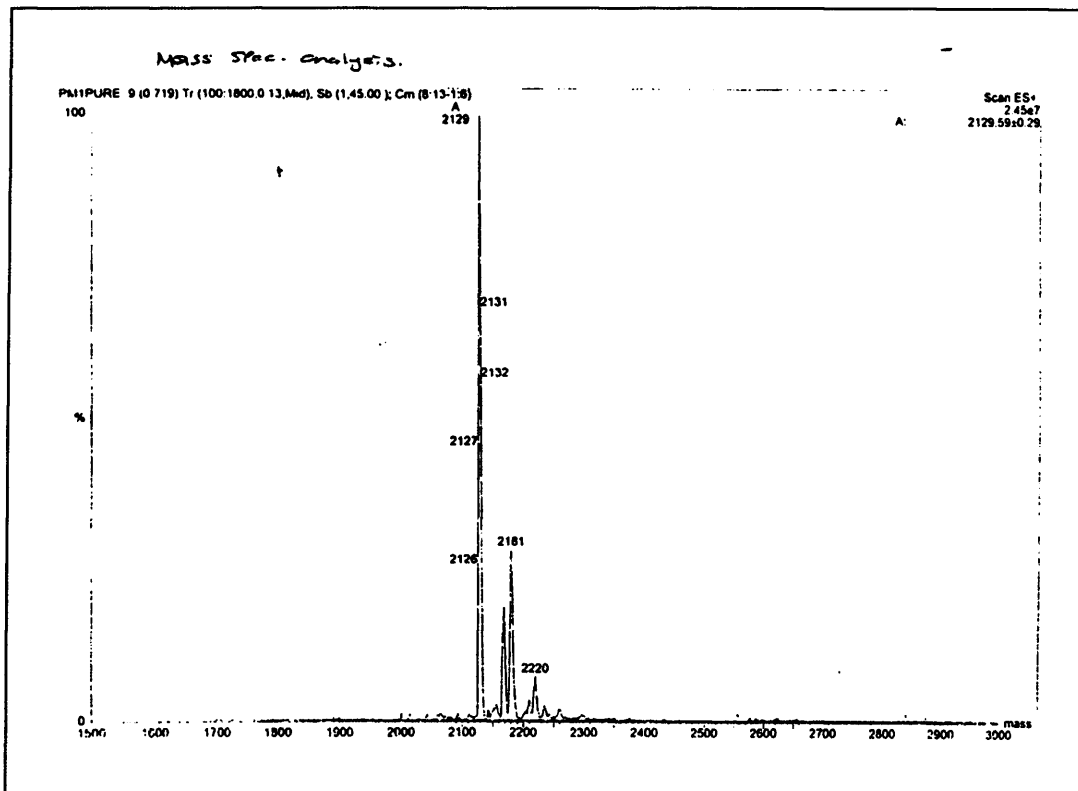
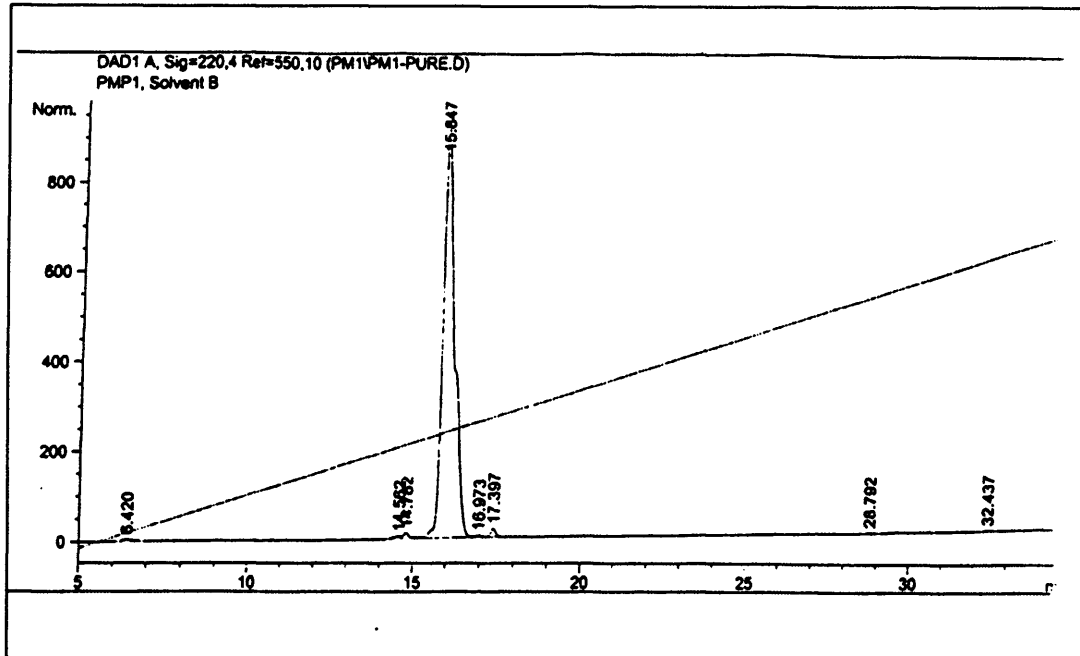


Peptide purity was also assessed by HPLC:



2mg of peptide was conjugated to 2mg maleimide activated Keyhole Limpet Hemocyanin (KLH). Conjugated peptide was quantified using the Bradford Assay.

\*To improve specificity of hOGG1 antibody screening, the synthetic hOGG1 peptide (used as solid phase antigen for ELISA) was further purified and assessed by HPLC:

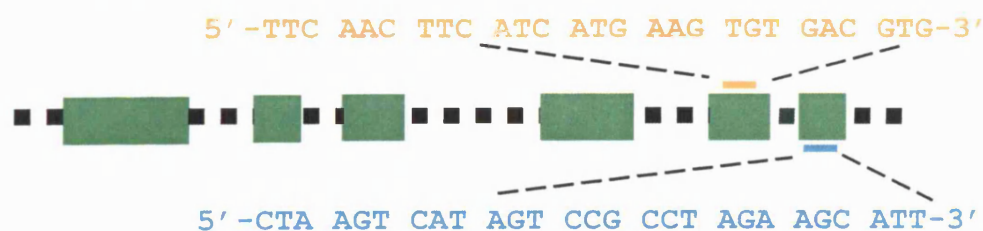


Purity was estimated at approximately 97% and  $M_w$  at 2129

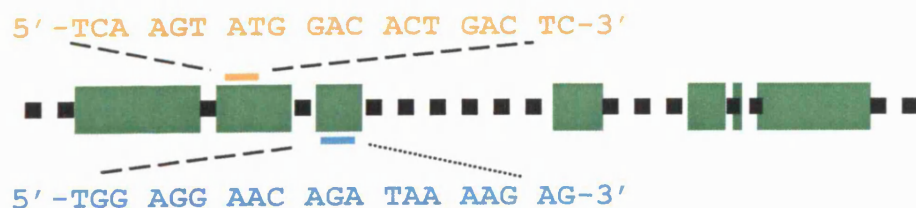
APPENDIX VII  $\beta$ -actin, hOGG1 and hAPE sequence information and primer positions

Gene	$\beta$ -actin	hOGG1	hAPE
Gene accession code	M10277	AJ131341	M92444
Gene sequence length	3646	9507bases	3046bases
Gene primer position 5' → 3': sense anti-sense	Exon 5 (2595→2621) Exon 6 (2990→3016)	Exon 2 (2972→2991) Exon 3 (3793→3812)	Exon 5 (2391→409) Exon 5(2623→2641)
Genomic PCR size	422bp	841bp	251bp
cDNA accession code	NM_001101	Y11731	X59764
cDNA sequence length	1793bases	1609bases	1437bases
cDNA primer position 5' → 3': sense anti-sense	908→934 1191→1217	491→519 734→753	848→866 1080→1098
RT-PCR size	310bp	263bp	251bp

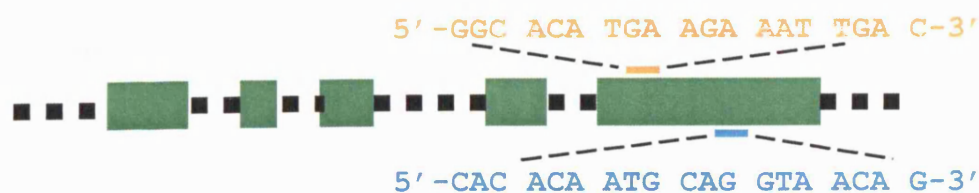
$\beta$ -actin : sense primer GC% 40.7,  $T_m$  56.6°C / anti-sense primer GC% 44.4,  $T_m$  58.1°C



hOGG1 : sense primer GC% 45.0,  $T_m$  49.6°C / anti-sense primer GC% 40.0,  $T_m$  47.6°C

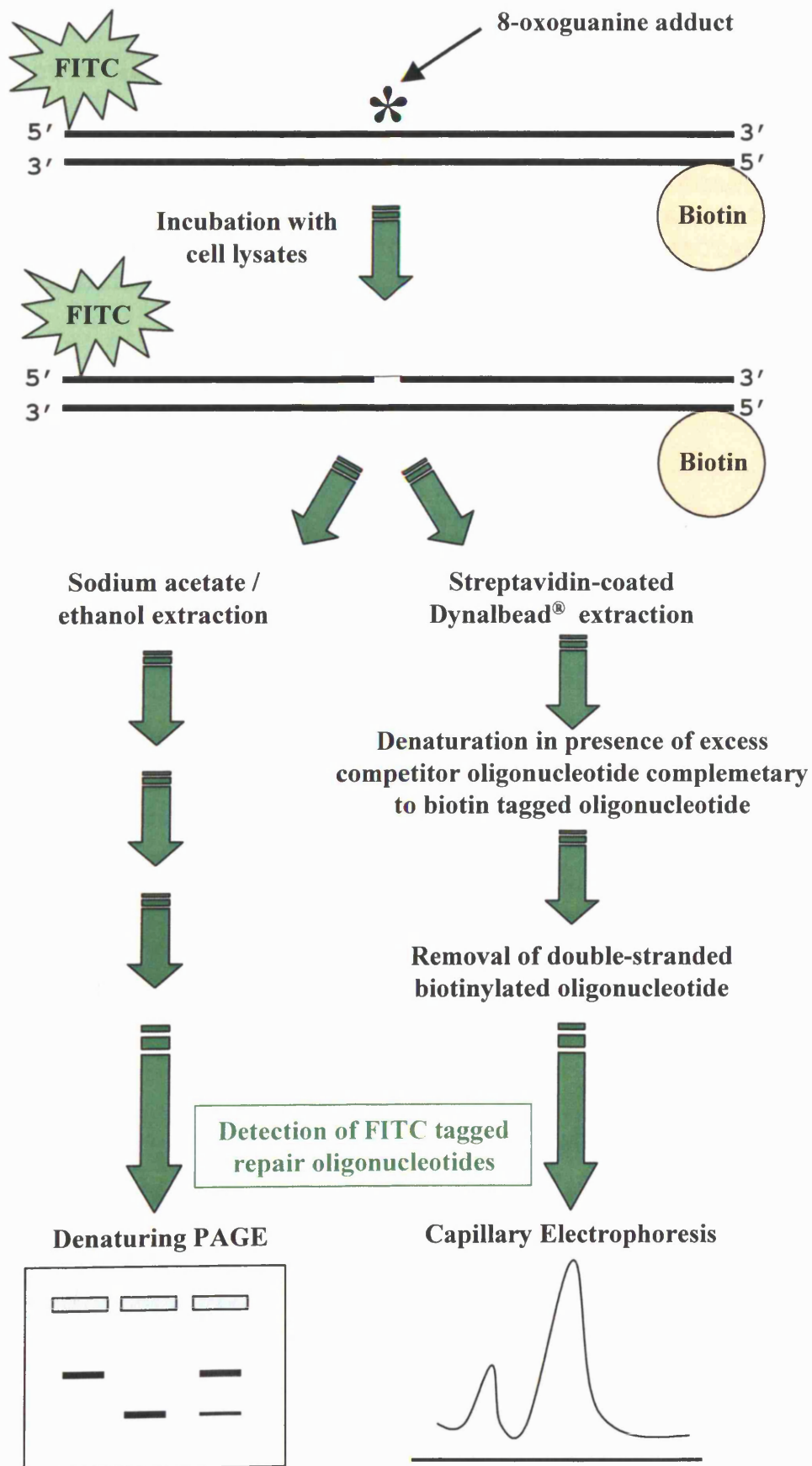


hAPE: sense primer GC% 42.1,  $T_m$  46.6°C / anti-sense primer GC% 47.4,  $T_m$  48.8°C



KEY: ■ Exons ■ ■ Introns — Primers

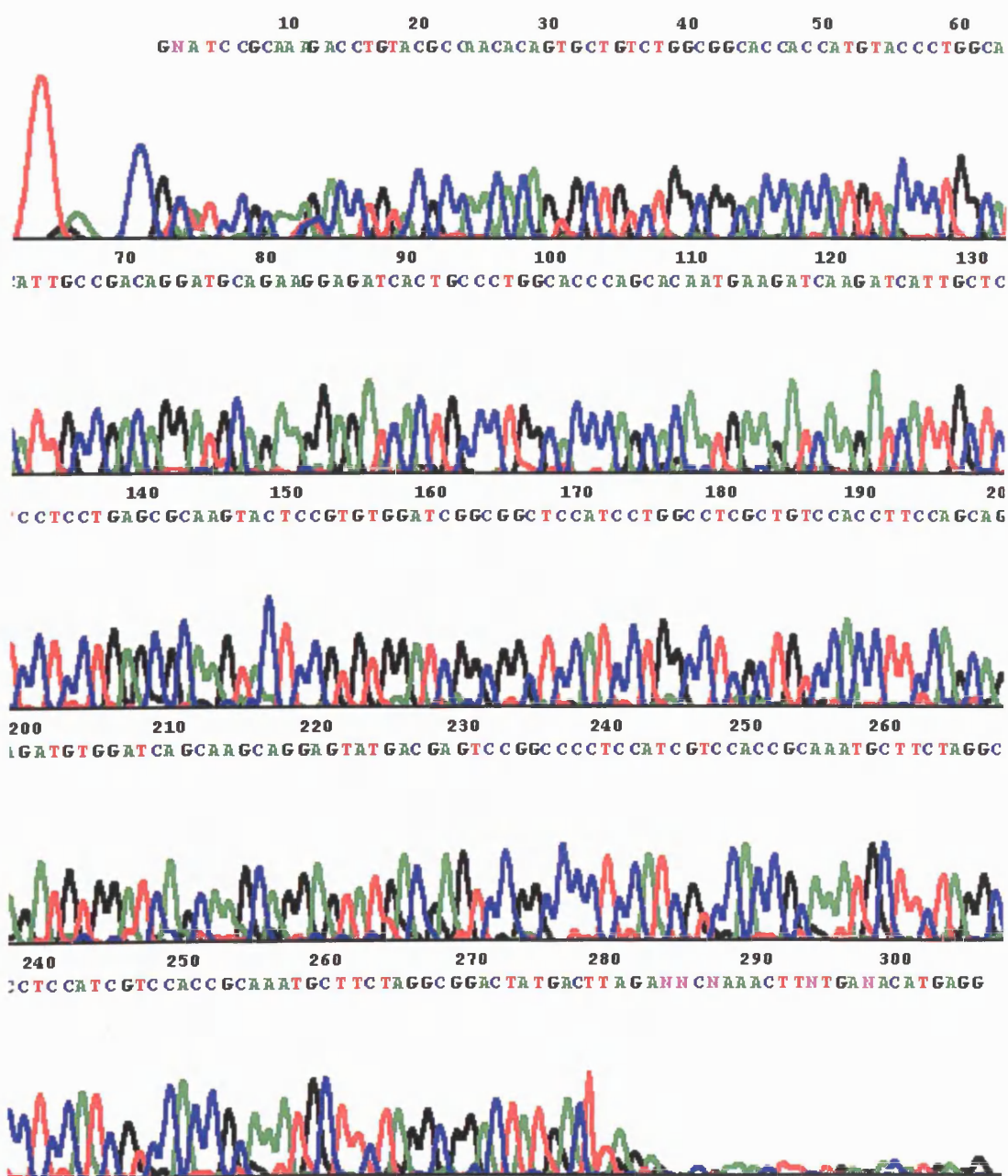
APPENDIX VIII Endonuclease nicking assay experimental approaches



APPENDIX IX  $\beta$ -actin, hOGG1 and hAPE PCR product sequencing data

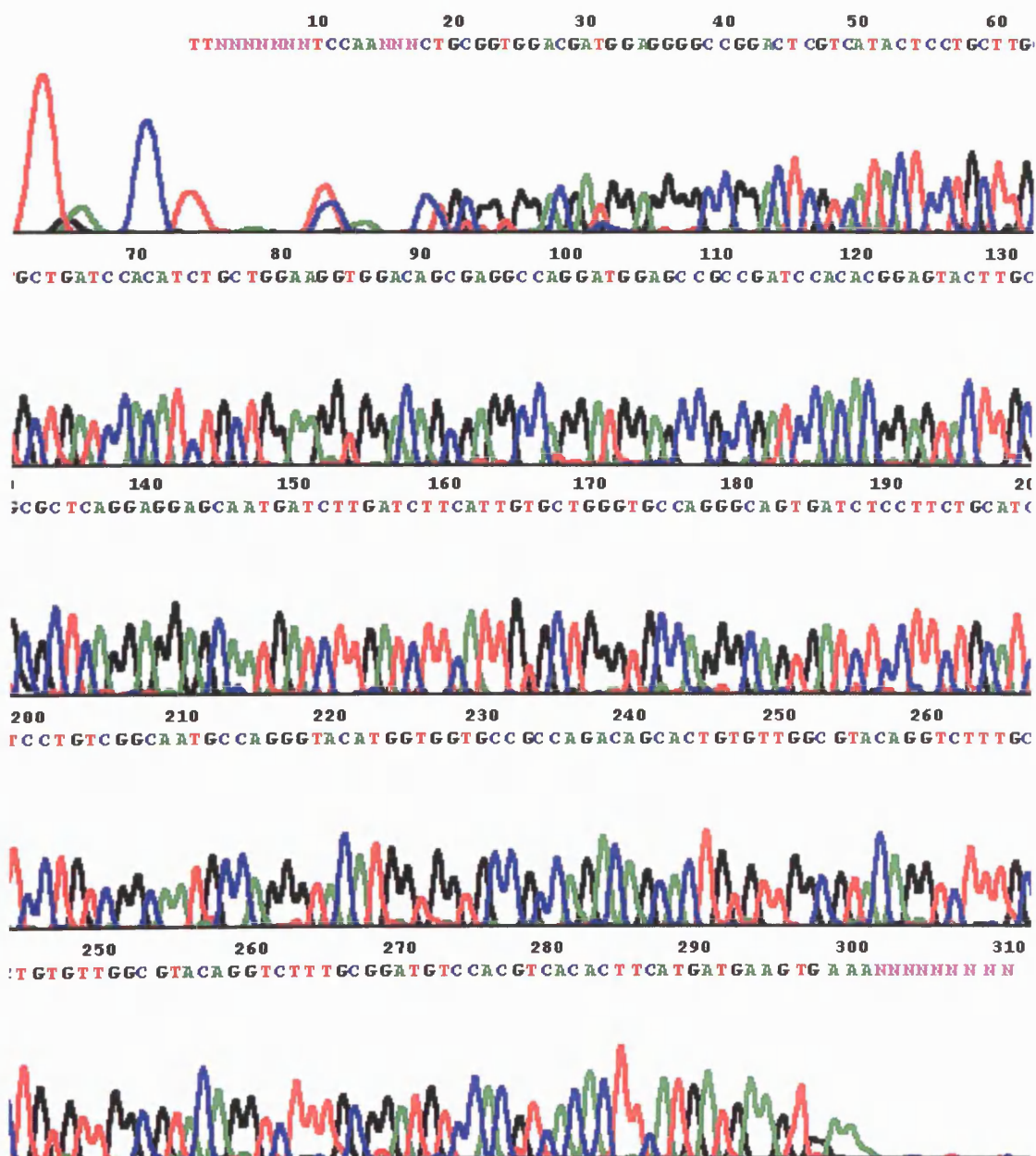
>ACTIN sense sequence exported from chromatogram file

GNATCCGCAAAGACCTGTACGCCAACACAGTGCTGTCTGGCGGCACCACCATGTACC  
 CTGGCATTGCCGACAGGATGCAGAAGGAGATCACTGCCCTGGCACCCAGCACAAATGA  
 AGATCAAGATCATTGCTCCTCCTGAGCGCAAGTACTCCGTGTGGATCGGCGGCTCCA  
 TCCTGGCCTCGCTGTCCACCTTCCAGCAGATGTGGATCAGCAAGCAGGAGTATGACG  
 AGTCCGGCCCCCTCCATCGTCCACCGCAAATGCTTCTAGGCGGACTATGACTTAGANN  
 CNAAACTTNTGANACATGAGG



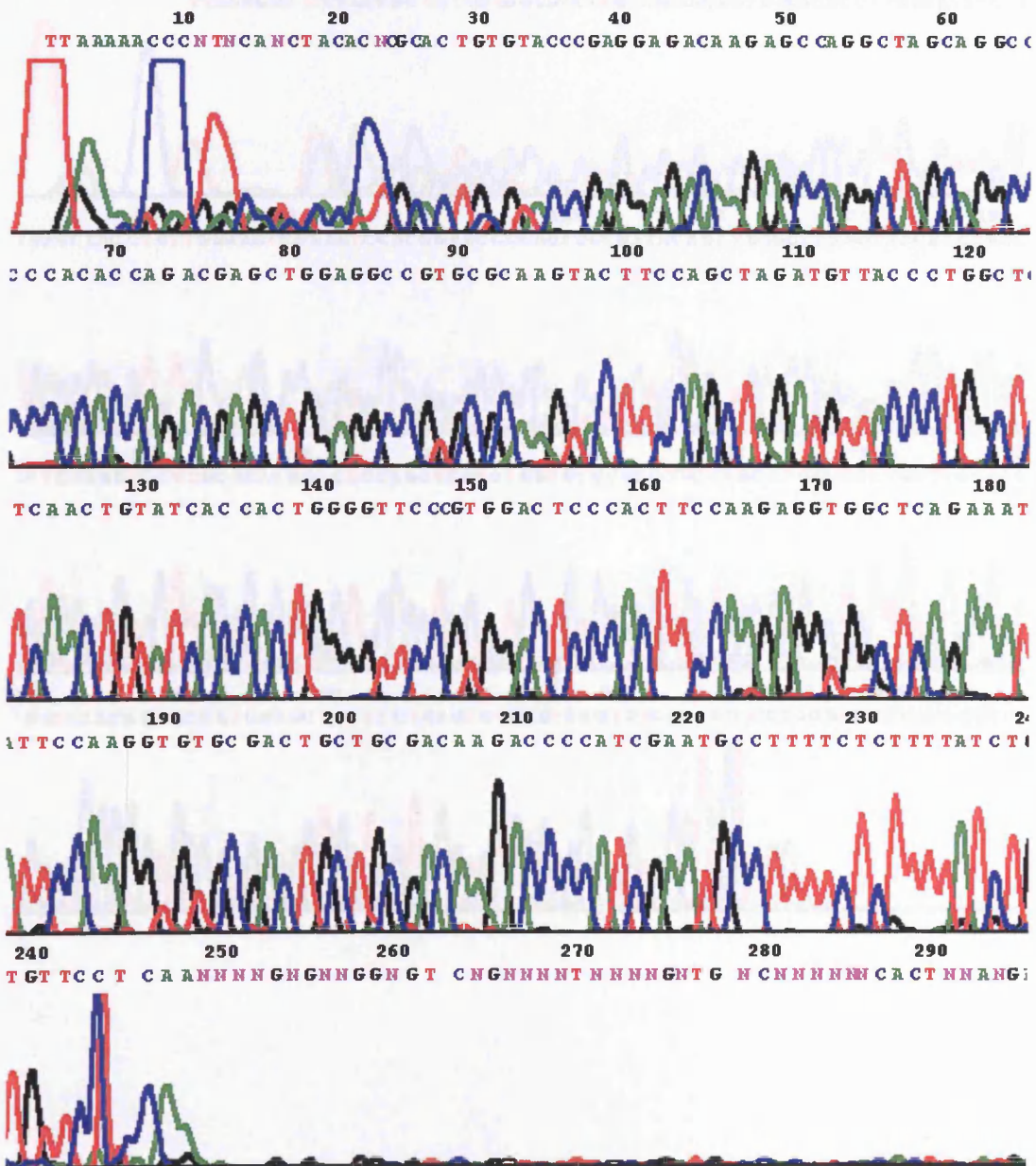
>ACTIN anti-sense sequence exported from chromatogram file

TTNNNNNNNTCCAANNCTGCGGTGGACGATGGAGGGGCCGGACTCGTCATACTCCT  
 GCTTGCTGATCCACATCTGCTGGAAGGTGGACAGCGAGGCCAGGATGGAGCCGCCGA  
 TCCACACGGAGTACTTGCCTCAGGAGGAGCAATGATCTTGATCTTCATTGTGCTGG  
 GTGCCAGGGCAGTGATCTCCTTCTGCATCCTGTCGGCAATGCCAGGGTACATGGTGG  
 TGCCGCCAGACAGCACTGTGTTGGCGTACAGGTCTTTGCGGATGTCCACGTACACT  
 TCATGATGAAGTGAAANNNNNNNNN



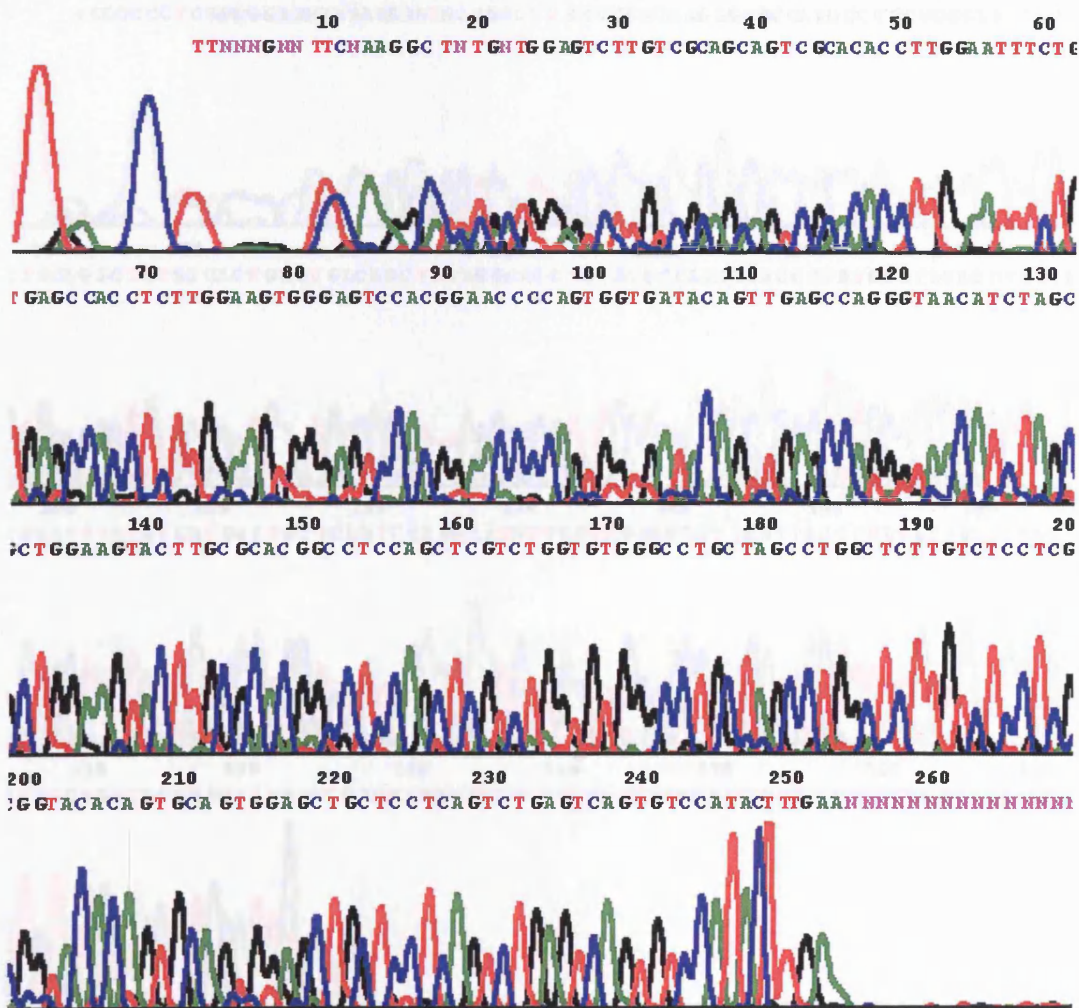
>hOGG1 sense sequence exported from chromatogram file

TTAAAAACCCNTNCANCTACACNCGCACTGTGTACCCGAGGAGACAAGAGCCAGGC  
 TAGCAGGCCACACCAGACGAGCTGGAGGCCGTGCGCAAGTACTTCCAGCTAGATG  
 TTACCCTGGCTCAACTGTATCACCCTGGGGTTCCCGTGGACTCCCCTTCCAAGA  
 GGTGGCTCAGAAATCCAAGGTGTGCGACTGCTGCGACAAGACCCCATCGAATGCC  
 TTTTCTCTTTTATCTGTTCCCTCAANNNGNGNNGGNGT CNGNNNTNNNNGNTGNC  
 NNNNNNCACTNNANGANGNANNNNNNNNNNNNNNNNNN



>hOGG1 anti-sense sequence exported from chromatogram file

TTNNNGNNTTCNAAGGCTNTGNTGGAGTCTTGTCGCAGCAGTCGCACACCTTGGAA  
 TTTCTGAGCCACCTCTTGGAAAGTGGGAGTCCACGGAACCCAGTGGTGATACAGTT  
 GAGCCAGGGTAACATCTAGCTGGAAGTACTTGCGCACGGCCTCCAGCTCGTCTGGT  
 GTGGGCCTGCTAGCCTGGCTCTTGTCCTCTCGGTACACAGTGCAGTGGAGCTGCTC  
 CTCAGTCTGAGTCAGTGTCCATACTTTGAANNNNNNNNNNNNNNNNNNNNNTNNNN  
 NANNNNNNNNNNNNNTNNNNNNNNNNNATNNC

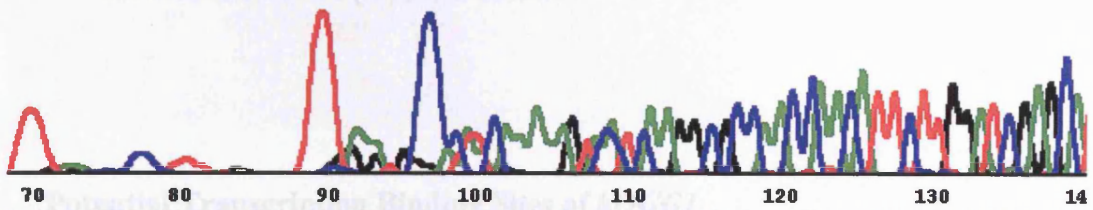




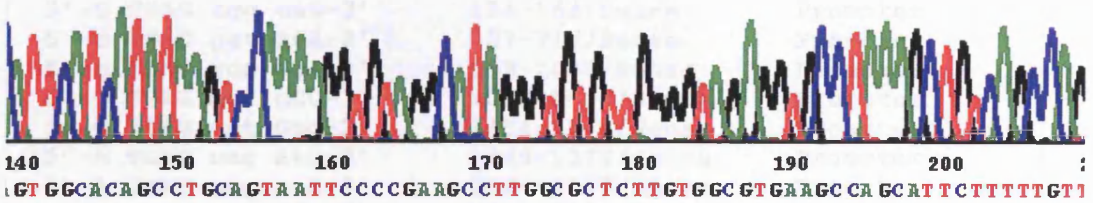
>hAPE anti-sense sequence exported from chromatogram file

CNTTTNNNNNNNTTTGAATGCCCCANCAAAAAGTAATCAAGGCGCCAACCAACATT  
 CTTGGATCGAGCATTTCATCATATAAGTCCAAAAGGTGTAGGCATAGGGTGTGTTGG  
 GGTAGAGGTGCCTAAAGCTGTCAGCCAGTGGCACAGCCTGCAGTAATCCCCGAAG  
 CTTGGCGCTCTTGTGGCGTGAAGCCAGCATTCTTTTTGTTCCCCTTGGGGTTGCG  
 AAGGTCAATTTCTTCATTGCCANNNGNCNNNNCTTTNNGNACCNTTNNCNGNNA  
 NACCNTGNNNGGNCNNNNNNNNANNTNAATNAC

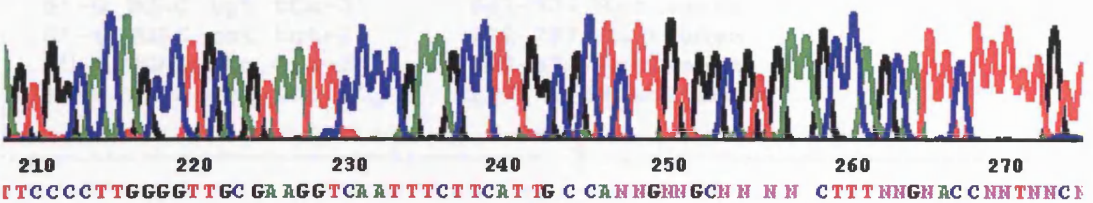
10 20 30 40 50 60 ;  
 CNTTTNNNNNNNTTTGAATGCCCCANCAAAAAGTAATCAAGGCGCCAACCAACATT



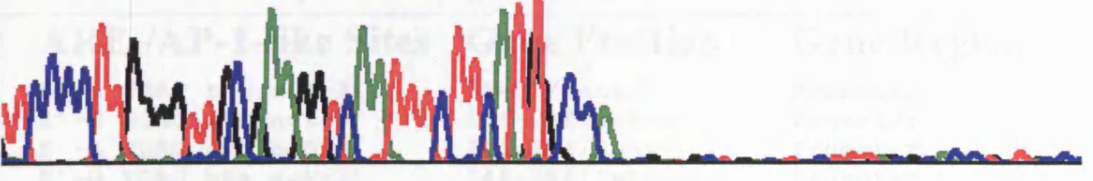
ATTTCATCATATAAGTCCAAAAGGTGTAGGCATAGGGTGTGTTGGGGTAGAGGTGCCTAAGGCTGTCAAGCCAG



GTGGCACAGCCTGCAATTTCCCGAAGCCTTGGCGCTCTTGTGGCGTGAAGCCAGCCTTCTTTTGT



TTCCCCTTGGGGTTGCAGAGGTCAATTTCTTCATTCGCAANNNGNCHNNCTTTNNGNACCNTTNNC



Gene	Gene Position	Gene Region
1	100-110	100-110
2	120-130	120-130
3	140-150	140-150
4	160-170	160-170
5	180-190	180-190
6	200-210	200-210
7	220-230	220-230
8	240-250	240-250
9	260-270	260-270
10	280-290	280-290
11	300-310	300-310
12	320-330	320-330
13	340-350	340-350
14	360-370	360-370
15	380-390	380-390
16	400-410	400-410
17	420-430	420-430
18	440-450	440-450
19	460-470	460-470
20	480-490	480-490
21	500-510	500-510
22	520-530	520-530
23	540-550	540-550
24	560-570	560-570
25	580-590	580-590
26	600-610	600-610
27	620-630	620-630
28	640-650	640-650
29	660-670	660-670
30	680-690	680-690
31	700-710	700-710
32	720-730	720-730
33	740-750	740-750
34	760-770	760-770
35	780-790	780-790
36	800-810	800-810
37	820-830	820-830
38	840-850	840-850
39	860-870	860-870
40	880-890	880-890
41	900-910	900-910
42	920-930	920-930
43	940-950	940-950
44	960-970	960-970
45	980-990	980-990
46	1000-1010	1000-1010
47	1020-1030	1020-1030
48	1040-1050	1040-1050
49	1060-1070	1060-1070
50	1080-1090	1080-1090
51	1100-1110	1100-1110
52	1120-1130	1120-1130
53	1140-1150	1140-1150
54	1160-1170	1160-1170
55	1180-1190	1180-1190
56	1200-1210	1200-1210
57	1220-1230	1220-1230
58	1240-1250	1240-1250
59	1260-1270	1260-1270
60	1280-1290	1280-1290
61	1300-1310	1300-1310
62	1320-1330	1320-1330
63	1340-1350	1340-1350
64	1360-1370	1360-1370
65	1380-1390	1380-1390
66	1400-1410	1400-1410
67	1420-1430	1420-1430
68	1440-1450	1440-1450
69	1460-1470	1460-1470
70	1480-1490	1480-1490
71	1500-1510	1500-1510
72	1520-1530	1520-1530
73	1540-1550	1540-1550
74	1560-1570	1560-1570
75	1580-1590	1580-1590
76	1600-1610	1600-1610
77	1620-1630	1620-1630
78	1640-1650	1640-1650
79	1660-1670	1660-1670
80	1680-1690	1680-1690
81	1700-1710	1700-1710
82	1720-1730	1720-1730
83	1740-1750	1740-1750
84	1760-1770	1760-1770
85	1780-1790	1780-1790
86	1800-1810	1800-1810
87	1820-1830	1820-1830
88	1840-1850	1840-1850
89	1860-1870	1860-1870
90	1880-1890	1880-1890
91	1900-1910	1900-1910
92	1920-1930	1920-1930
93	1940-1950	1940-1950
94	1960-1970	1960-1970
95	1980-1990	1980-1990
96	2000-2010	2000-2010
97	2020-2030	2020-2030
98	2040-2050	2040-2050
99	2060-2070	2060-2070
100	2080-2090	2080-2090
101	2100-2110	2100-2110
102	2120-2130	2120-2130
103	2140-2150	2140-2150
104	2160-2170	2160-2170
105	2180-2190	2180-2190
106	2200-2210	2200-2210
107	2220-2230	2220-2230
108	2240-2250	2240-2250
109	2260-2270	2260-2270
110	2280-2290	2280-2290
111	2300-2310	2300-2310
112	2320-2330	2320-2330
113	2340-2350	2340-2350
114	2360-2370	2360-2370
115	2380-2390	2380-2390
116	2400-2410	2400-2410
117	2420-2430	2420-2430
118	2440-2450	2440-2450
119	2460-2470	2460-2470
120	2480-2490	2480-2490
121	2500-2510	2500-2510
122	2520-2530	2520-2530
123	2540-2550	2540-2550
124	2560-2570	2560-2570
125	2580-2590	2580-2590
126	2600-2610	2600-2610
127	2620-2630	2620-2630
128	2640-2650	2640-2650
129	2660-2670	2660-2670
130	2680-2690	2680-2690
131	2700-2710	2700-2710
132	2720-2730	2720-2730
133	2740-2750	2740-2750
134	2760-2770	2760-2770
135	2780-2790	2780-2790
136	2800-2810	2800-2810
137	2820-2830	2820-2830
138	2840-2850	2840-2850
139	2860-2870	2860-2870
140	2880-2890	2880-2890
141	2900-2910	2900-2910
142	2920-2930	2920-2930
143	2940-2950	2940-2950
144	2960-2970	2960-2970
145	2980-2990	2980-2990
146	3000-3010	3000-3010
147	3020-3030	3020-3030
148	3040-3050	3040-3050
149	3060-3070	3060-3070
150	3080-3090	3080-3090
151	3100-3110	3100-3110
152	3120-3130	3120-3130
153	3140-3150	3140-3150
154	3160-3170	3160-3170
155	3180-3190	3180-3190
156	3200-3210	3200-3210
157	3220-3230	3220-3230
158	3240-3250	3240-3250
159	3260-3270	3260-3270
160	3280-3290	3280-3290
161	3300-3310	3300-3310
162	3320-3330	3320-3330
163	3340-3350	3340-3350
164	3360-3370	3360-3370
165	3380-3390	3380-3390
166	3400-3410	3400-3410
167	3420-3430	3420-3430
168	3440-3450	3440-3450
169	3460-3470	3460-3470
170	3480-3490	3480-3490
171	3500-3510	3500-3510
172	3520-3530	3520-3530
173	3540-3550	3540-3550
174	3560-3570	3560-3570
175	3580-3590	3580-3590
176	3600-3610	3600-3610
177	3620-3630	3620-3630
178	3640-3650	3640-3650
179	3660-3670	3660-3670
180	3680-3690	3680-3690
181	3700-3710	3700-3710
182	3720-3730	3720-3730
183	3740-3750	3740-3750
184	3760-3770	3760-3770
185	3780-3790	3780-3790
186	3800-3810	3800-3810
187	3820-3830	3820-3830
188	3840-3850	3840-3850
189	3860-3870	3860-3870
190	3880-3890	3880-3890
191	3900-3910	3900-3910
192	3920-3930	3920-3930
193	3940-3950	3940-3950
194	3960-3970	3960-3970
195	3980-3990	3980-3990
196	4000-4010	4000-4010
197	4020-4030	4020-4030
198	4040-4050	4040-4050
199	4060-4070	4060-4070
200	4080-4090	4080-4090
201	4100-4110	4100-4110
202	4120-4130	4120-4130
203	4140-4150	4140-4150
204	4160-4170	4160-4170
205	4180-4190	4180-4190
206	4200-4210	4200-4210
207	4220-4230	4220-4230
208	4240-4250	4240-4250
209	4260-4270	4260-4270
210	4280-4290	4280-4290
211	4300-4310	4300-4310
212	4320-4330	4320-4330
213	4340-4350	4340-4350
214	4360-4370	4360-4370
215	4380-4390	4380-4390
216	4400-4410	4400-4410
217	4420-4430	4420-4430
218	4440-4450	4440-4450
219	4460-4470	4460-4470
220	4480-4490	4480-4490
221	4500-4510	4500-4510
222	4520-4530	4520-4530
223	4540-4550	4540-4550
224	4560-4570	4560-4570
225	4580-4590	4580-4590
226	4600-4610	4600-4610
227	4620-4630	4620-4630
228	4640-4650	4640-4650
229	4660-4670	4660-4670
230	4680-4690	4680-4690
231	4700-4710	4700-4710
232	4720-4730	4720-4730
233	4740-4750	4740-4750
234	4760-4770	4760-4770
235	4780-4790	4780-4790
236	4800-4810	4800-4810
237	4820-4830	4820-4830
238	4840-4850	4840-4850
239	4860-4870	4860-4870
240	4880-4890	4880-4890
241	4900-4910	4900-4910
242	4920-4930	4920-4930
243	4940-4950	4940-4950
244	4960-4970	4960-4970
245	4980-4990	4980-4990
246	5000-5010	5000-5010
247	5020-5030	5020-5030
248	5040-5050	5040-5050
249	5060-5070	5060-5070
250	5080-5090	5080-5090
251	5100-5110	

**APPENDIX X Potential ARE and AP-1 transcription factor binding sites of *hOGG1* and *hAPE***

**Consensus Sequences**

• **Antioxidant Responsive Elements (ARE's)**

G TGAC NNN GCA  
 A ...T ... ..G  
 . ...G ... ..

• **Activator Protein (AP)-1 Elements**

TGAC TCA  
 ...G .A.

**Potential Transcription Binding Sites of *hOGG1***

<b>ARE /AP-1-like Sites</b>	<b>Gene Position</b>	<b>Gene Region</b>
5' -G TGAG tgg caG-3'	154-164/Sense	Promoter
5' -c TGAC ggt aCA-3'	727-737/Sense	Promoter
5' -c TGAG gca GgA-3'	990-1000/Sense	Promoter
5' -G TGAG act cCG-3'	1076-1086/Sense	Promoter
5' -G TGAG aat Ggc-3'	1154-1164/Sense	Promoter
5' -A TGAG cag atG-3'	1369-1379/Sense	Promoter
5' -A TGAC ccg caA-3'	2084-2094/Sense	Exon 1
5' -G TGAC tga GCc-3'*	2410-2420/Sense	Intron 1
5' -G TGAC tgt tCc-3'	642-632/Antisense	
5' -t TGAC cct tgt-3'	772-762/Antisense	
5' -t TGAC ctc GtG-3'	882-872/Antisense	
5' -c TGAG gca GCc-3'*	1278-1268/Antisense	

**Potential Transcription Binding Sites of *hAPE***

<b>ARE /AP-1-like Sites</b>	<b>Gene Position</b>	<b>Gene Region</b>
5' -c TGAC tcc aCA-3'	71-81/Sense	Promoter
5' -G TGAC gtt aat-3'	196-206/Sense	Promoter
5' -A TGAG act cgG-3'	224-234/Sense	Promoter
5' -G TGAC gta agt-3'	344-354/Sense	Promoter
5' -G TGAC cag Gtc-3'	946-956/Sense	Exon 1
5' -t TGAG tca GgA-3'*	1096-1106/Sense	Exon 1
5' -A TGAT cta Gtt-3'	1173-1183/Sense	Intron 1
5' -G TGAC gcg GtA-3'	1368-1378/Sense	Exon 2
5' -A TGAC aaa GaG-3'	1714-1724/Sense	Exon 3
5' -c TGAC att GCG-3'*	490-480/Antisense	
5' -G TGAC act Gac-3'	776-766/Antisense	
5' -G TGAC gga Gac-3'	884-874/Antisense	
5' -G TGAT cag agG-3'	945-935/Antisense	
5' -c TGAC tca agc-3'*	1106-1096/Antisense	

\* Strong candidate sites

**APPENDIX XI Publications & communications arising from this thesis**

**Papers**

- Griffiths HR, Mistry P, Herbert KE and Lunec J (1998). Molecular and cellular effects of ultraviolet light-induced genotoxicity. *Crit Rev Clin Lab Sci.* **35 (3):** 189-237
- Mistry P and Herbert KE. Terrestrial UVB wavelength dependent formation of cyclobutane pyrimidine dimers: distribution in cultured keratinocytes and quantitation in DNA. *submitted for publication*
- Mistry P and Herbert KE. Modulation of hOGG1 DNA repair enzyme in human cultured cells in response to pro-oxidant and antioxidant challenge. *submitted for publication*

**Published abstracts**

- Herbert KE and Mistry P (2001). The effect of ascorbic acid and dehydroascorbic acid uptake on a base excision repair pathway for oxidative DNA damage in human cells. *Free Radical Biol Med.* **31:** 260

**Oral presentation**

- Mistry P, Herbert KE and Lunec J. Redox regulation of base excision repair genes in eukaryotes. Society for Free Radical Research, Liverpool, UK (2000).

## REFERENCES

- Aburatani H, Hippo Y, Ishida T, Takashima R, Matsuba C, Kodama T, Takao M, Yasui A, Yamamoto K, Asano M, Fukasawa K, Yshinari T, Inoue H, Ohtsuka E and Nishimura S (1997). Cloning and characterisation of mammalian 8-hydroxyguanine-specific glycosylase/apurinic, apyrimidinic lyase, a functional mutM homologue. *Cancer Res.* **57**: 2151-2156
- Ahmad SI, Hanaoka F and Kirk SH (2002). Molecular biology of Fanconi anaemia– an old problem, a new insight. *Bioessays.* **24**: 439-448
- Ahmed FE, Setlow RB, Grist E and Setlow N (1993). DNA damage, photorepair, and survival in fish and human cells exposed to UV radiation. *Environ. Mol. Mut.* **22**: 18-25
- Ahmed NU, Ueda M, Nikaido O, Osawa T and Ichihashi M (1999). High levels of 8-hydroxy-2'-deoxyguanosine appear in normal human epidermis after a single dose of ultraviolet radiation. *Br J Dermatol.* **140**: 226-231
- Akiyama K, Seki S, Oshida T and Yoshida MC (1994). Structure, promoter analysis and chromosomal assignment of the human APEX gene. *Biochem Biophys Acta.* **1219**: 15-25
- Alam ZI, Jenner A, Daniel SE, Lees AJ, Cairns N, Marsden CD, Jenner P and Halliwell B (1997). Oxidative damage to DNA in the Parkinsonism brain: an apparent selective increase in 8-hydroxyguanine levels in substantia nigra. *J Neurochem.* **69**: 1196-1203
- Ambrosone CB, Freudenheim JL, Thompson PA, Bowman E, Vena LE, Marshall JR, Graham S, Laughlin R, Nemoto T and Shields PG (1999). Manganese superoxide dismutase (MnSOD) genetic polymorphism, dietary antioxidants and risk of breast cancer. *Cancer Res.* **59**: 602-606
- Ames (1989). Endogenous DNA damage related to cancer and aging. *Mutat Res.* **214**: 41-46
- Anderson CT and Friedberg EC (1980). The presence of nuclear and mitochondrial uracil DNA glycosylase in extracts of human KB cells. *Nucleic Acids Res.* **8**: 875-888
- Anderson ME (1998). Glutathione: an overview of biosynthesis and modulation. *Chemico-Biological Interactions.* **111-112**: 1-14
- Angus B, Purvis J, Stock D, Westley BR, Samson AC, Routledge EG, Carpenter FH and Horne CH (1987). NCL-5D3: a new monoclonal antibody recognizing low molecular weight cytokeratins effective for immunohistochemistry using fixed paraffin-embedded tissue. *J Pathol.* **153**: 377-384
- Arai K, Morishita K, Shinmura K, Kohno T, Kim S-R, Nohmi T, Taniwaki M, Ohwada S and Yokota J (1997). Cloning of a human homolog of the yeast *OGG1* gene that is involved in the repair of oxidative DNA damage. *Oncogene.* **14**: 2857-2861
- Araújo SJ and Wood RD (1999). Protein complexes in nucleotide excision repair. *Mutat Res.* **435**: 23-33
- Arlett CF and Green MH (1993). Ultraviolet: the dark side of the sun. *MRC News.* Spring 1993: 34-36

- Asami S, Hirano T, Yamaguchi R, Tomioka Y, Itoh H and Kasai H (1996). Increase of a type of oxidative DNA damage, 8-hydroxyguanine, and its repair activity in human leukocytes by cigarette smoking. *Cancer Res.* **56**: 2546-2549
- Asami S, Manabe H, Miyake J, Tsurudome Y, Hirano T, Yamaguchi R, Itoh H, and Kasai H (1997). Cigarette smoking induces an increase in oxidative DNA damage, 8-hydroxydeoxyguanosine, in a central site of the human lung. *Carcinogenesis.* **18**: 1763-1766
- Aspinwall R, Rothwell DG, Roldan-Arjona T, Aspinwall R, Rothwell DG, Roldan-Arjona T, Anselmino C, Ward CJ, Cheadle JP, Sampson JR, Lindahl T, Harris PC and Hickson ID (1997). Cloning and characterization of a functional human homologue of *Escherichia coli* endonuclease III. *Proc Natl Acad Sci USA.* **94**: 109-114
- Audebert M, Chevillard S, Levalois C, Gyapay G, Vieillefond A, Klijanienko J, Vielh P, El Naggar AK, Oubard S, Boiteux S and Radicella JP (2000). Alterations of the DNA repair gene *OGG1* in human clear cell carcinomas of the kidney. *Cancer Res.* **60**: 4740-4744
- Balajee AS, May A, Dianova I and Bohr VA (1998). Efficient PCNA complex formation is dependent upon both transcription coupled repair and genome overall repair. *Mutat Res.* **409**: 135-146
- Barzilay G, Walker LJ, Rothwell DG and Hickson ID (1996). Role of the HAP1 protein in repair of oxidative DNA damage and regulation of transcription factors. *Br J Cancer. Suppl 27*: S145-150
- Beal MF, Hyman BT and Koroshetz W (1993). Do defects in mitochondrial energy metabolism underlie the pathology of neurodegenerative diseases? *Trends Neurosci.* **16**: 125-131
- Bessho T, Sancar A, Thompson LH and Thelen MP (1997). Reconstitution of human excision nuclease with recombinant XPF-ERCC1 complex. *J Biol Chem.* **272**: 3833-3837
- Bessho T, Tano K, Kasai H, Ohtsuka E and Nishimura S (1993). Evidence for two DNA repair enzymes for 8-hydroxyguanine (7,8-dihydro-8-oxoguanine) in human cells. *J Biol Chem.* **268**: 19416-19421
- Bodak N, Queille S, Avril MF, Bouadjar B, Drougard, Sarasin A and Daya-Grosjean L (1999). High levels of patched gene mutations in basal cell carcinomas from xeroderma pigmentosum patients. *Proc Natl Acad Sci USA.* **96**: 5117-5122
- Bohr VA (1995). DNA repair fine structure and its relations to genomic instability. *Carcinogenesis.* **16**: 2885-2892
- Bohr VA and Anson M (1995). DNA damage, mutation and fine structure DNA repair in aging. *Mutat Res.* **338**: 25-34
- Bohr VA, Smith CA, Okumoto DS and Hanawalt PC (1985). DNA repair in an active gene: removal of pyrimidine dimers from DHFR gene of CHO cells is much more efficient than in the genome overall. *Cell.* **40**: 359-369
- Boiteux S, Dherin C, Reille F, Apiou F, Dutrillaux and Radicella JP (1998). Excision repair of 8-hydroxyguanine in mammalian cells: the mouse OGG1 protein as a model. *Free Radical Res.* **29**: 487-497

- Boiteux S, Galewski E, Laval J and Dizdaroglu M (1992). The substrate specificity of the *Escherichia coli* Fpg protein (Formamidopyrimidine-DNA glycosylase): Excision of purine lesions in DNA produced by ionising radiation or photosensitization. *Biochemistry*. **31**: 106-110
- Boiteux S and Radicella JP (2000). The human *OGG1* gene: structure, functions and its implication in the process of carcinogenesis. *Arch Biochem Biophys*. **377**: 1-8
- Bowman KK, Sicard DM, Ford JM and Hanawalt PC (2000). Reduced global genomic repair of ultraviolet light-induced cyclobutane pyrimidine dimers in simian virus 40-transformed human cells. *Mol Carcinog*. **29**: 17-24
- Bradford MM (1976). A rapid and sensitive method for the quantitation of microgram quantities of protein utilizing the principle of protein-dye binding. *Anal. Biochem*. **72**: 248-254
- Bray TM, Ho E and Levy MA (1998). Glutathione, sulphur amino acids and chemical detoxification. In: Ioannides C, ed. *Nutrition and Chemical Toxicity*. Wiley and Sons, New York. pp183-200
- Brookman KW, Lamerdin JE, Thelen MP, Hwang M, Reardon JT, Sancar A, Zhou ZQ, Walter CA, Parris CN and Thompson LH (1996). ERCC4 (XPF) encodes a human nucleotide excision repair protein with eukaryotic recombination homologs. *Mol Cell Biol*. **16**: 6553-6562
- Broughton BC, Thompsom AF, Harcourt SA, Vermeulen W, Hoeijmakers JHJ, Botta E, Stefanini M, King MD, Weber CA, Cole J, Arlett CF and Lehmann AR (1995). Molecular and cellular analysis of the DNA repair defect in a patient with xeroderma pigmentosum complementation group D who has the clinical features of xeroderma pigmentosum and Cockayne syndrome. *Am J Hum Genet*. **56**: 167-174
- Browne SE, Ferrante RJ and Beal MF (1999). Oxidative stress in Huntingdon's disease. *Brain Pathology*. **9**: 147-163
- Bruner SD, Norman DP, and Verdine GL (2000). Structural basis for recognition and repair of the endogenous mutagen 8-oxoguanine in DNA. *Nature*. **403**: 859-866
- Burns JE, Baird MC, Clark LJ, Burns PA, Edington K, Chapman C, Mitchell R, Robertson G, Soutar D and Parkinson EK (1993). Gene mutations and increased levels of p53 protein in human squamous cell carcinomas and their cell lines. *Br J Cancer*. **67**: 1274-1284
- Cadet J, Anselmino C, Douki T and Voituriez L (1992). Photochemistry of nucleic acids in cells. *Photochem. Photobiol*. **15**: 277-298
- Cai L, Koropatnick J and Cherin MG (2001). Roles of vitamin C in radiation-induced DNA damage in presence and absence of copper. *Chem Biol Interact*. **137**: 75-88
- Camplejohn RS (1996). DNA damage and repair in melanoma and non-melanoma skin cancer. *Cancer Surveys*. **26**: 193-206
- Carell T (1995). Sunlight induced DNA lesions. Lesion structure, mutation characteristics and repair. *Chimia*. **49**: 365-373

- Cathcart R, Schwiers E, Saul RL and Ames BN (1984). Thymine glycol and thymidine glycol in human and rat urine. A possible assay for oxidative stress. *Proc Natl Acad Sci USA*. **81**: 5633-5637
- Chappell LC, Seed PT, Briley AL, Kelley FJ, Lee R, Hunt BJ, Parmar K, Bewlwy SJ, Shennan AH, Steer PJ and Poston L (1999). Effect of anti-oxidants on the occurrence of pre-eclampsia in women with increased risk: a randomised trial. *Lancet*. **354**: 810-816
- Chen YT, Dubrow R, Zheng T, Barnhill RL, Fine J and Berwick M (1998). Sunlamp use and the risk of cutaneous malignant melanoma: a population-based case-control study in Connecticut, USA. *Int J Epidemiol*. **27**: 758-765
- Cheng KC, Cahill DS, Kasai H, Nishimura S and Loeb LA (1992). 8-Hydroxyguanine an abundant form of oxidative DNA damage causes G→T and A→C substitutions. *J Biol Chem*. **267**: 166-172
- Chevillard S, Radicella JP, Levalois C, Lebeau J, Poupon M-F, Oudard S, Dutrillaux B and Boiteux S (1998). Mutations in *OGG1*, a gene involved in the repair of oxidative DNA damage, are found in human lung and kidney tumours. *Oncogene*. **16**: 3083-3086
- Choi J-Y, Kim H-S, Kang H-K, Lee D-W, Choi E-M and Chung M-H (1999). Thermolabile 8-hydroxyguanine DNA glycosylase with low activity in senescence-accelerated mice due to a single-base mutation. *Free Radical Biol Med*. **27**: 848-854
- Chuang TY, Heinrich LA, Schultz MD, Reizner GT, Kumm RC and Cripps DJ (1992). PUVA and skin cancer. A historical cohort study on 492 patients. *J Am Acad Dermatol*. **26**: 173-177
- Chung MH, Kasai H, Jones DS, Inoue H, Ishikawa H, Ohsuka E, Hori T and Nishimura S (1991). An endonuclease activity of *Escherichia coli* that specifically removes 8-hydroxyguanine residues from DNA. *Mutat Res*. **254**: 1-12
- Clark C, Dawe RS, Evans AT, Lowe G and Ferguson J (2000). Narrowband TL-01 phototherapy for patch-stage mycosis fungoides. *Arch Dermatol*. **136**: 748-752
- Clawson GA, Benedict CM, Kelley MR and Weisz J (1997). Focal nuclear hepatocyte response to oxidative damage following low dose thioacetamide intoxication. *Carcinogenesis*. **18**: 1663-1668
- Clayton DT, Doda JN and Friedberg EC (1974). The absence of a pyrimidine dimer repair mechanism in mammalian mitochondria. *Proc Natl Acad Sci USA*. **71**: 2777-2781
- Cleaver JE (1968). Defective repair replication of DNA in xeroderma pigmentosum. *Nature*. **218**: 652-656
- Cleaver JE and Kraemer KH (1989). Xeroderma Pigmentosum. In: Scriver CR, Beaudet AL, Sly WS, Valle D, eds. *Metabolic basis of inherited disease*. McGraw-Hill, New York. pp 2949-2971
- Clingen PH, Arlett CF, Roza L, Mori T, Nikaido O, Green MH (1995). Induction of cyclobutane pyrimidine dimers, pyrimidine(6-4)pyrimidone photoproducts, and Dewar valence isomers by natural sunlight in normal human mononuclear cells. *Cancer Res*. **55**: 2245-2248

- Codonier AM and Fuchs RPP (1999). Replication of damaged DNA: molecular defect in xeroderma pigmentosum variant cells. *Mutat Res.* **435**: 111-119
- Collins AR (1999). Oxidative DNA damage, antioxidants, and cancer. *BioEssays.* **21**: 238-246
- Collins AR, Cadet J, Epe B and Gedik C (1997). Problems in the measurement of 8-oxoguanine in human DNA. Report on a workshop, DNA oxidation, held in Aberdeen. *Carcinogenesis.* **18**: 1833-1836
- Collins AR, Dušinská M, Gedik C and Štětina R (1996). Oxidative damage to DNA: do we have a reliable biomarker? *Environ Health Perspect.* **104**: 465-469
- Collins AR, Gedik C, Olmedilla B, Southon S and Bellizzi M (1998). Oxidative DNA damage measured in human lymphocytes: large differences between sexes and between countries, and correlations with heart disease mortality rates. *FASEB.* **12**: 1397-1400
- Cooke MS, Evans MD, Burd RM, Patel K, Barnard A, Lunec J and Hutchinson PE (2001). Induction and excretion of ultraviolet-induced 8-oxo-2'-deoxyguanosine and thymine dimers in vivo: implications for PUVA. *J Invest Dermatol.* **116**: 281-285
- Cooke MS, Evans MD, Podmore ID, Herbert KE, Mistry N, Mistry P, Hickenbotham PT, Hussieni A, Griffiths HR and Lunec J (1998). Novel repair action of vitamin C upon *in vivo* oxidative DNA damage. *FEBS letters.* **363**: 363-367
- Coven TR, Burack LH, Gilleaudeau R, Keogh M, Ozawa M and Krueger JG (1997). Narrowband UV-B produces superior clinical and histopathological resolution of moderate-to-severe psoriasis in patients compared with broadband UV-B. *Arch Dermatol.* **133**: 1514-1522
- Cunningham RP (1997). DNA Glycosylases. *Mutat Res.* **383**: 189-196
- Daya-Grosjean L, Robert C, Drougard C, Suarez HG and Sarasin A (1993). High mutation frequency in *ras* genes of skin tumors isolated from DNA repair deficient xeroderma pigmentosum patients. *Cancer Res.* **53**: 1625-1629
- de Boer J and Hoeijmakers JHJ (2000). Nucleotide excision repair and human syndromes. *Carcinogenesis.* **21**: 453-460
- de Boer J, van Steeg H, Berg RJW, Garssen J, de Wit J, van Oostrum CTM, Beems RB, van der Horst GTJ, van Kreijl CF, de Gruijl FR, Bootsma D, Hoeijmakers JHJ and Weeda G (1999). Mouse model for the DNA repair/basal transcription disorder trichothiodystrophy reveals cancer predisposition. *Cancer Res.* **59**: 3489-3494
- Degan P, Bonassi BS, De Caterina M, Korkina LG, Pinto L, Scopacasa F, Zatterale A, Calzone R and Pagano G (1995). *In vivo* accumulation of 8-hydroxy-2'-deoxyguanosine in DNA correlates with release of reactive oxygen species in Fanconi's anaemia families. *Carcinogenesis.* **16**: 735-742
- de la Asuncion JG, del Olmo ML, Sastre J, Millan A, Pellin A, Pallardo FV and Vina J (1998). AZT treatment induces molecular and ultrastructural oxidative damage to muscle mitochondria. Prevention by antioxidant vitamins. *J Clin Invest.* **102**: 4-9

- de Laat JMT and de Gruiji FR (1996). The role of UVA in the aetiology of non-melanoma skin cancer. *Cancer Surveys*. **26**: 173-191
- Demple B and Harrison L (1994). Repair of oxidative damage to DNA: enzymology and biology. *Annu. Rev Biochem.* **63**: 915-948
- Demple B, Herman T and Chen DS (1991). Cloning and expression of APE, the cDNA encoding the major human apurinic endonuclease: definition of a family of DNA repair enzymes. *Proc Natl Acad Sci USA*. **88**: 11450-11454
- de Murcia G, Menissier de Murcia J (1994). Poly (ADP-ribose) polymerase: a molecular nick-sensor. *Trends Biochem. Sci.* **19**: 172-176
- Department of Environment (1996). The potential effects of ozone depletion in the United Kingdom. Her Majesty's Stationery Office, London. pp2-9
- DePinho RA (2000). The age of cancer. *Nature*. **408**: 248-254
- Dhénaut A, Boiteux S and Radicella JP (2000). Characterisation of the *hOGG1* promoter and its expression during the cell cycle. *Mutat Res*. **461**: 109-118
- Dherin C, Radicella JP, Dizdaroglu M and Boiteux S (1999). Excision of oxidatively damaged DNA bases by the human  $\alpha$ -hOgg1 protein and the polymorphic  $\alpha$ -hOgg1 (Ser326Cys) protein which is frequently found in human populations. *Nucleic Acids Res*. **27**: 4001-4007
- Dianov G, Bischoff C, Piotrowski J and Bohr VA (1998). Repair pathways for processing of 8-oxoguanine in DNA by mammalian cell extracts. *J Biol Chem*. **273**: 33811-33816
- Diffey BL (1991). Solar ultraviolet radiation effects on biological systems. *Physics Medicine & Biol*. **36**: 299-328
- Digweed M, Reis A and Sperling K (1999). Nijmegen breakage syndrome: consequences of defective DNA double strand break repair. *Bioessays*. **21**: 649-656
- Divine KK, Gilliland FD, Crowell RE, Stidley CA, Bocklage TJ, Cook DL and Belinsky SA (2001). The XRCC1 glutamine allele is a risk factor for adenocarcinoma of the lung. *Mutat Res*. **461**: 273-278
- Dizdaroglu M, Jaruga P, Birincioglu M and Rodriguez H (2002). Free radical-induced damage to DNA: mechanisms and measurement. *Free Radical Res*. **32**: 1102-1115
- Dizdaroglu M, Karahalil B, Senturker S, Buckley TJ and Roldan-Arjona T (1999). Excision of products of oxidative DNA base damage by human NTH1 protein. *Biochemistry*. **38**: 243-246
- Dizdaroglu M, Zastawny TH, Carmical JR and Lloyd RS (1996). A novel DNA N-glycosylase activity of *Escherichia coli* T4 endonuclease-V that excises 4,6-diamino-5-formamidopyrimidine from DNA, a UV-radiation-induced and hydroxyl radical-induced product of adenine. *Mutat Res*. **362**: 1-8
- Doetsch PW, Zastawny TH, Martin AM and Dizdaroglu M (1995). Monomeric base damage products from adenine, guanine and thymine induced by exposure of DNA to ultraviolet radiation. *Biochemistry*. **34**: 737-747

- Douki T and Cadet J (2001). Individual determination of the yield of the main UV-induced dimeric pyrimidine photoproducts in DNA suggests a high mutagenicity of CC photolesions. *Biochemistry*. **40**: 2495-2501
- Douki T, Court M, Sauvaigo S, Odin F, Cadet J (2000). Formation of the main UV-induced thymine dimeric lesions within isolated and cellular DNA as measured by high performance liquid chromatography-tandem mass spectrometry. *J Biol Chem*. **275**: 11678-11685
- Driggers WJ, LeDoux SP, Wilson GL (1993). Repair of oxidative damage within the mitochondrial DNA of RINr 38 cells. *J Biol Chem*. **268**: 22042-22045
- Drummond JT, Li GM, Longley MJ and Modrich P (1995). Isolation of an hMSH-p160 heterodimer that restores DNA mismatch repair to tumour cells. *Science*. **268**: 1909-1912
- Duguid JR, Eble JN, Wilson TM and Kelley MR (1995). Differential cellular and subcellular expression of the human multifunctional apurinic/apyrimidinic endonuclease (APE/ref-1) DNA repair enzyme. *Cancer Res*. **55**: 6097-6102
- Dumaz N, Drougard C, Sarasin A and Daya-Grosjean L (1993). Specific UV-mutation spectrum in the P53 gene from DNA repair deficient xeroderma pigmentosum patients. *Proc Natl Acad Sci USA*. **90**: 10529-10533
- Dumaz N, Sary A, Soussi T, Daya-Grosjean L and Sarasin A (1994). Can we predict solar ultraviolet radiation as a casual event in human tumours by analysing the mutation spectra of the P53 gene? *Mutat Res*. **307**: 375-386
- Duval A and Hamelin R (2002). Genetic instability in human mismatch repair deficient cancers. *Ann Genet*. **45**: 71-75
- Eggset G, Volden G and Krokan H (1983). UV-induced DNA damage and its repair in human skin in vivo studied by sensitive immunohistochemical methods. *Carcinogenesis*. **4**: 745-750
- Eide L, Bjoras M, Pirovano M, Alseth I, Berdal KG and Seeberg E (1996). Base excision of oxidative purine and pyrimidine DNA damage in *Saccharomyces cerevisiae* by a DNA glycosylase with sequence similarity to endonuclease III from *Escherichia coli*. *Proc Natl Acad Sci USA*. **93**: 10735-10740
- Elder RH, Janseen JG, Weeks RJ, Willington MA, Deans B, Watson AJ, Mynett KJ, Bailey JA, Cooper DP, Rafferty JA, Heeran MC, Wijnhoven SW, van Zeeland AA and Margison GP (1998). Alkylpurine-DNA-N-glycosylase knockout mice show increased susceptibility to the induction of mutations by methyl methanesulfonate. *Mol Cell Biol*. **18**: 5828-5837
- Engelward BP, Weeda G, Wyatt MD, Broekhof JL, de Wit J, Donker I, Allan JM, Gold B, Hoeijmakers JH and Samson (1997). Base excision repair deficient mice lacking the Aag alkyladenine DNA glycosylase. *Proc Natl Acad Sci*. **94**: 13087-13092
- ESCODD. Comparison of different methods of measuring 8-oxoguanine as a marker of oxidative DNA damage. *Free Radical Res*. **32**: 333-341
- Evans AR, Limp-Foster M and Kelley MR (2000). Going APE over ref-1. *Mutat Res*. **461**: 83-108

- Evans MK, Robbins JH, Ganges MB, Tarone RE, Nairn RS and Bohr VA (1993). Gene-specific DNA repair in xeroderma pigmentosum complementation groups A, C, D, and F. Relation to cellular survival and clinical features. *J Biol Chem.* **268**: 4839-4847
- Eveno E, Quilliet X, Chevallier-Lagente O, Daya-Grosjean L, Stary A, Zeng L, Benoit A, Savini E, Ciarrocchi G and Kannouche P (1995). Stable SV40-transformation and characterisation of some DNA repair properties of fibroblasts from a trichothiodystrophy patient. *Biochimie.* **77**: 906-912
- Finkel T and Holbrook NJ (2000). Oxidants, oxidative stress and the biology of ageing. *Nature.* **408**: 239-247
- Fishel R and Kolodner RD (1995). Identification of mismatch repair genes and their role in the development of cancer. *Curr Opin Genet Dev.* **5**: 382-395
- Fishel R and Wilson T (1997). MutS homologs in mammalian cells. *Curr Opin Genet Dev.* **7**: 105-113
- Flindt-Hansen H, McFadden N, Eeg-Larsen T and Thune P (1991). Effect of a new narrow-band UVB lamp on photocarcinogenesis in mice. *Acta Derm. Venereol.* **71**: 245-248
- Floyd RA, Watson JJ, Wong PK, Altmiller DH and Rickard RC (1986). Hydroxyl free radical adduct of deoxyguanosine: sensitive detection and mechanism of formation. *Free Radical Res Commun.* **1**: 77-79
- Ford JM and Hanawalt PC (1996). Role of DNA excision repair gene defects in the etiology of cancer. In: Kastan MB ed. *Genetic instability and tumourigenesis*. Springer, New York. pp 47-70
- Försti A, Takala M, Laatikainen R and Hemminki K (1988). Excretion kinetics of the DNA adducts of cis-diamminedichloroplatinum(II) formed in vitro in rat urine. *Carcinogenesis.* **9**: 1745-1748
- Fraga CG, Motchnik PA, Shigenaga MK, Helbock HJ, Jacob RA and Ames BN (1991). Ascorbic acid protects against endogenous oxidative DNA damage in human sperm. *Proc Natl Acad Sci USA.* **88**: 11003-11006
- Frederick JE, Snell HE and Haywood EK (1989). Solar ultraviolet radiation at the earth's surface. *Photochem Photobiol.* **50**: 443-450
- Frelon S, Douki T, Ravanat J-L, Pouget J-P, Tornabene C and Cadet J (2000). High-performance liquid chromatography-tandem mass spectrometry measurement of radiation-induced base damaged to isolated and cellular DNA. *Chem Res Toxicol.* **13**: 1002-1010
- Friedberg EC (1996). Relationships between DNA repair and transcription. *Annu Rev Biochem.* **65**: 15-42
- Friedberg EC and Meira LB (2000). Databases of mouse strains carrying targeted mutations in genes affecting cellular responses to DNA damage: version 4. *Mutat Res.* **459**: 243-274
- Frosina G, Fortini P, Rossi O, Carrozzino F, Raspaglio G, Cox LS, Lane DP, Abbondandolo A and Dogliotti E (1996). 2 pathways for base excision-repair in mammalian cells. *J Biol Chem.* **271**: 9573-9578

- Fuchs E and Cleveland DW (1998). A structural scaffolding of intermediate filaments in health and disease. *Science*. **279**: 514-519
- Fung H, Kow YW, Van Houten B, Taatjes DJ, Hatahet Z, Janssen YMW, Vacek P, Faux SP, and Mossman BT (1998). Asbestos increases mammalian AP-endonuclease gene expression, protein and enzyme activity in mesothelial cells. *Cancer Res*. **58**: 189-194
- Futaki M and Liu JM (2001). Chromosomal breakage syndromes and the BRCA1 genome surveillance complex. *Trends Mol Med*. **7**: 560-565
- Gasparro FP and Brown DB (2000). Photobiology 102: UV sources and dosimetry - the proper use and measurement of "photons as a reagent". *J Invest Dermatol*. **114**: 613-615
- Gerard M, Fischer L, Moncollin V, Chipoulet JM, Chambon P and Egly JM (1991). Purification and interaction properties of the human RNA polymerase B(II) general transcription factor BTF2. *J Biol Chem*. **266**: 20940-20945
- Gillardon F, Bottiger B and Hossmann KA (1997). Expression of nuclear redox factor ref-1 in the rat hippocampus following global ischemia induced by cardiac arrest. *Brain Res Mol Brain Res*. **52**: 194-200
- Girard PM, Guibourt N and Boiteux S (1997). The Ogg1 protein of *Saccharomyces cerevisiae*: a 7,8-dihydro-8-oxoguanine DNA glycosylase/ AP lyase whose lysine 241 is a critical residue for catalytic activity. *Nucleic Acids Res*. **25**: 3204-3211
- Girard PM, D'Ham C, Cadet J and Boiteux S (1998). Opposite base-dependent excision of 7,8-dihydro-8-oxoadenine by the Ogg1 protein of *Saccharomyces cerevisiae*. *Carcinogenesis*. **19**: 1299-1305
- Gonda K, Nomizu T, Fukayama N, Sugano K and Takenosita S (2002). A novel germline mutation of hMLH1 in a patient with hereditary non-polyposis colorectal cancer. *Jpn J Clin Oncol*. **32**: 215-218
- Gown AM and Vogel AM (1984). Monoclonal antibodies to human intermediate filament proteins. II. Distribution of filament proteins in normal human tissues. *Am J Pathol*. **114**: 309-321
- Griffiths HR, Mistry P, Herbert KE and Lunec J (1998). Molecular and cellular effects of ultraviolet light-induced genotoxicity. *Crit Rev Clin Lab Sci*. **35**: 189-237
- Grishko VI, Driggers WJ, LeDoux SP and Wilson GL (1997). Repair of oxidative damage in nuclear DNA sequences with different transcriptional activities. *Mutat Res*. **384**: 73-80
- Grollman AP and Moriya M (1993). Mutagenesis by 8-oxoguanine: an enemy within. *Trends Biochem Sci*. **9**: 246-249
- Grombacher T and Kaina B (1995). Constitutive expression and inducibility of O<sup>6</sup>-methylguanine-DNA methyltransferase and N-methylpurine-DNA glycosylase in rat liver cells exhibiting different status of differentiation. *Biochem Biophys Acta*. **1270**: 63-72
- Grompe M and D'Andrea A (2001). Fanconi anemia and DNA repair. *Hum Mol Genet*. **10**: 2253-2259

- Grösch S, Fritz G and Kaina B (1998). Apurinic endonuclease (Ref-1) is induced in mammalian cells by oxidative stress and involved in clastogenic adaptation. *Cancer Res.* **58**: 4410-4416
- Grösch S and Kaina B (1999). Transcriptional activation of apurinic/aprimidinic endonuclease (Ape, Ref-1) by oxidative stress requires CREB. *Biochem Biophys Res Commun.* **261**: 859-863
- Gu H, Marth JD, Orban PC, Mossmann H and Rajewsky K (1994). Deletion of a DNA polymerase  $\beta$  gene segment in T-cells using cell type-specific gene targeting. *Science.* **265**: 103-106
- Gurley KE and Kemp CJ (2001). Synthetic lethality between mutation in Atm and DNA-PK(cs) during murine embryogenesis. *Curr Biol.* **11**: 191-194
- Ha HC, Woster PM, Yager JD and Casero RA (1997). The role of polyamine catabolism in polyamine analogue-induced programmed cell death. *Proc Natl Acad. Sci USA.* **94**: 11557-11562
- Haber JE (1999). DNA recombination: the replication connection. *Trends Biochem.Sci.* **24**: 271-275
- Halliwell B (2002). Effect of diet on cancer development: is oxidative DNA damage a biomarker. *Free Radical Biol Med.* **32**: 968-974
- Halliwell B and Dizdaroglu M (1992). The measurement of oxidative damage by HPLC and GC/MS techniques. *Free Radical Res Comms.* **16**: 75-87
- Halliwell B and Gutteridge JMC (1999). *Free radicals in biology and medicine.* 3<sup>rd</sup> Ed., Oxford University Press Oxford, UK.
- Hanawalt PC (1994). Transcription-coupled repair and human disease. *Science* **266**: 1457-1458
- Hanawalt PC (1995). DNA repair comes of age. *Mutat Res.* **336**: 101-113
- Hannuksela-Svahn A, Pukkala E, Laara E, Poikolainen K and Karvonen J (2000). Psoriasis, its treatment, and cancer in a cohort of Finnish patients. *J Invest Dermatol.* **114**: 587-590
- Harrison L, Ascione AG, Wilson DM 3<sup>rd</sup> and Demple B (1995). Characterization of the promoter region of the human apurinic endonuclease gene (APE). *J Biol Chem.* **270**: 5556-5564
- Harrison L, Ascione AG, Takiguchi Y, Wilson DM 3<sup>rd</sup>, Chen DJ and Demple B (1997). Comparison of the promoters of the mouse (APEX) and human (APE) apurinic endonuclease genes. *Mutat Res.* **385**: 159-72
- Hartwig A, Dally H and Schlegel R (1996). Sensitive analysis of oxidative DNA damage in mammalian cells: use of the bacterial Fpg protein in combination with alkaline unwinding. *Toxicol Lett.* **88**: 85-90

- Hattori Y, Nishigori C, Tanaka T, Uchida K, Nikaido O, Osawa T, Hiai H, Imamura S and Toyokuni S (1996). 8-Hydroxy-2'-deoxyguanosine is increased in epidermal cells of hairless mice after chronic ultraviolet B exposure. *J Invest Dermatol.* **107**: 733-737
- Haug T, Skropen F, Aas PA, Malm V, Skjelbred C and Krokan HE (1998). Regulation of expression of nuclear and mitochondrial forms of human uracil-DNA glycosylase. *Nucleic Acids Res.* **26**: 1449-1457
- Haushalter KA, Stikenberg T, Kirschner MW and Verdine GL (1999). Identification of a new uracil-DNA glycosylase family by expression cloning using synthetic inhibitors. *Curr Biol.* **9**: 174-185
- Hayes JD and Pulford DJ (1995). The glutathione S-transferase supergene family. Regulation of GST and contribution of the isoenzymes to cancer chemoprotection and drug resistance. *Crit Rev Biochem Mol Biol.* **30**: 445-460
- Hazra TK, Izumi T, Boldogh I, Imhoff B, Kow YW, Jaruga P, Dizdaroglu M and Mitra S (2002)<sup>1</sup>. Identification and characterization of a human DNA glycosylase for repair of modified bases in oxidatively damaged DNA. *Proc Natl Acad Sci USA.* **99**: 3523-3528
- Hazra TK, Izumi T, Maitl L, Floyd RA and Mitra S (1998). The presence of two distinct 8-oxoguanine repair enzymes in human cells: their potential complementary roles in preventing mutation. *Nucleic Acids Res.* **26**: 5116-5122
- Hazra TK, Kow YW, Hatahet Z, Imhoff B, Boldogh I, Mokkaapati SK, Mitra S and Izumi T (2002)<sup>2</sup>. Identification and characterization of a novel human DNA glycosylase for repair of cytosine derived lesions. *J Biol Chem.* **277**: 30417-30420
- He Z, Henricksen LA, Wold MS, and Ingles CJ (1995). Preferential binding of the xeroderma pigmentosum group A complementing protein to damaged DNA. *Nature.* **374**: 566-569
- Heinen CD, Wilson T, Mazurek A, Berardini M, Butz C and Fishel R (2002). HNPCC mutations in hMSH2 result in reduced hMSH2-hMSH6 molecular switch functions. *Cancer Cell.* **1**: 469-478
- Helbock HJ, Beckman KB, Shigenaga MK, Walter PB, Woodall AA, Yeo HC and Ames BN (1998). DNA oxidation matters: the HPLC-electrochemical detection assay of 8-oxo-deoxyguanosine and 8-oxo-guanine. *Proc Natl Acad Sci USA.* **95**: 288-293
- Hendrich B, Hardeland U, Ng HH, Jiricny and Bird A (1999). The thymine glycosylase MBD4 can bind to the product of deamination at methylated CpG sites. *Nature.* **401**: 301-304
- Henning KA, Li L, Iyer N, McDaniel LD, Reagan MS, Legerski R, Schultz RA, Stefanini M, Lehmann AR, Mayne LV and Friedberg EC (1995). The Cockayne syndrome group A gene encodes a WD repeat protein that interacts with CSB protein and a subunit of RNA polymerase II TFIIF. *Cell.* **82**: 555-564
- Henriksen EK, Moan J, Kaalhus O and Brunborg G (1996). Induction and repair of DNA damage in UV irradiated human lymphocytes. Spectral differences and repair kinetics. *J Photochem Photobiol B.* **32**: 39-48

- Herbert KE, Evans MD, Finnegan MTV, Farooq, Mistry N, Podmore ID, Farmer P and Lunec J (1994)<sup>1</sup>. A novel HPLC procedure for the analysis of 8-oxoguanine in DNA. *Free Radical Biol & Med.* **20**: 467-473
- Herbert K, Mistry N, Griffiths HR and Lunec J (1994)<sup>2</sup>. Immunochemical detection of sequence-specific modifications to DNA induced by UV light. *Carcinogenesis.* **15**: 2517-2521
- Herman JG, Umar A, Polyak K, Graff JR, Ahuja N, Issa JP, Markowitz S, Willson JK, Hamilton SR, Kinzler KW, Kane MF, Kolodner RD, Vogelstein B, Kunkel TA and Baylin SB (1998). Incidence and functional consequences of hMLH1 promoter hypermethylation in colorectal carcinoma. *Proc Natl Acad Sci USA.* **95**: 6870-6875
- Hickson ID, Davies SL, Li JL, Levitt NC, Mohaghegh P, North PS and Wu L (2001). Role of the Bloom's syndrome helicase in maintenance of genome stability. *Biochem Soc Trans.* **29**: 201-204
- Hilbert TP, Boorstein RJ, Kung HC, Bolton PH, Xing D, Cunningham RP and Teebor GW (1996). Purification of a mammalian homologue of *Escherichia coli* endonuclease III: Identification of a bovine pyrimidine hydrate-thymine glycol DNA-glycosylase/AP lyase by irreversible cross linking to a thymine glycol-containing oligonucleotide. *Biochemistry.* **35**: 2505-2511
- Hill JW, Hazra TK, Izumi T and Mitra S (2001). Stimulation of human 8-oxoguanine-DNA glycosylase by AP-endonuclease: potential coordination of the initial steps in base excision repair. *Nucleic Acids Res.* **29**: 430-438
- Hirano T, Yamaguchi Y and Kasai H (1997). Inhibition of 8-hydroxyguanine repair in testes after administration of cadmium chloride to GSH-depleted rats. *Toxicol & Applied Pharmacol.* **147**: 9-14
- Hiroyuki A, Hippo Y, Ishida T, Takashima R, Matsuba C, Kodama T, Takao M, Yasui A, Yamamoto K, Asano M, Fuasawa K, Yoshinari T, Inoue H, Ohtsuka E and Nishimura S (1997). Cloning and characterisation of mammalian 8-hydroxyguanine-specific DNA glycosylase/apurinic, apyrimidinic lysae, a functional mutM homologue. *Cancer Res.* **57**: 2151-2156
- Hoeijmakers JHJ (2001). Genome maintenance mechanisms for preventing cancer. *Nature.* **411**: 366-374
- Hollenbach S, Dhénaut A, Eckert I, Radicella JP and Epe B (1999). Overexpression of Ogg1 in mammalian cells: effects on induced and spontaneous oxidative DNA damage and mutagenesis. *Carcinogenesis.* **20**: 1863-1868
- Hsu DS, Zhao X, Zhao S, Kazantsev A, Wang RP, Todo T, Wei YF and Sancar A (1996). Putative human blue-light photoreceptors hCRY1 and hCRY2 are flavoproteins. *Biochemistry.* **35**: 13871-13877
- Huang JC, Hsu DS, Kazantsev A and Sancar A (1994). Substrate spectrum of human excinuclease-repair of abasic sites, methylated bases, mismatches and bulky adducts. *Proc Natl Acad Sci USA.* **91**: 12213-12217
- Ikenaga M, Patrick MH and Jagger J (1970). Action of photoreactivating light on pyrimidine heteroadduct in bacteria. *Photochem Photobiol.* **11**: 487-494

- Imlay JA and Linn S (1988). DNA damage and oxygen radical toxicity. *Science*. **240**: 1302-1309
- Itin PH and Pittelkow MR (1990). Trichothiodystrophy: review of sulfur-deficient brittle hair syndromes and association with the ectodermal dysplasias. *J Am Acad Dermatol*. **22**: 705-717
- Izumi T, Henner WD and Mitra S (1996). Negative regulation of the major human AP-endonuclease, a multifunctional protein. *Biochemistry*. **35**: 14679-14683
- Jaiswal M, Lipinski LJ, Bohr VA and Mazur SJ (1998). Efficient *in vitro* repair of 7-hydro-8-oxodeoxyguanosine by human cell extracts: involvement of multiple pathways. *Nucleic Acids Res*. **26**: 2184-2191
- Janseen K, Schlink K, Götte W, Hippler B, Kaina B and Oesch F (2001). DNA repair activity of 8-oxoguanine DNA glycosylase 1 (OGG1) in human lymphocytes is not dependent on genetic polymorphism Ser<sup>326</sup>/Cys<sup>326</sup>. *Mutat Res*. **486**: 207-216
- Jayaraman L, Murthy KGk, Zhu C, Curran T, Xanthoudakis S and Prives C (1997). Identification of redox/repair protein Ref-1 as a potent activator of p53. *Genes Dev*. **11**: 558-570
- Jeffreys AJ, Neil DL and Neumann R (1998). Repeat instability at human minisatellites arising from meiotic recombination. *EMBO J*. **17**: 4147-4157
- Jiricny J (1994). Colon cancer and DNA repair: have mismatches met their match? *Trends Genet*. **10**: 164-168
- Jiricny J (1998). Replication errors: cha(lle)nging the genome. *EMBO J*. **17**: 6427-6436
- Jones CJ and Wood RD (1993). Preferential binding of the xeroderma pigmentosum group A complementing protein to damaged DNA. *Biochemistry*. **32**: 12096-12104
- Jónsson ZO and Hübscher U (1997). Proliferating cell nuclear antigen: more than a clamp for DNA polymerases. *BioEssays*. **19**: 967-975
- Journe F, Leonard F and Kalis B (1994). Treatment for the prevention of benign summer light eruption (BSLE) caused by UVB of narrow spectrum (peak 312nm). *Nouv. Dermatol*. **13**: 348-353
- Kakolyris S, Kaklamanis L, Engles H, Turley H, Hickson ID, Gatter KC and Harris AL (1997). Human apurinic endonuclease 1 expression in a colorectal adenoma-carcinoma sequence. *Cancer Res*. **57**: 1794-1797
- Kamiya H and Kasai H (1995). Formation of 2-hydroxyadenosine triphosphate, an oxidatively damaged nucleotide, and its incorporation by polymerases: steady state kinetics of the incorporation. *J Biol Chem*. **270**: 19446-19450
- Kaneko T, Tahara S and Matsuo M (1997). Retarding effect of dietary restriction on the accumulation of 8-hydroxy-2'-deoxyguanosine in organs of Fischer 344 rats during aging. *Free Radical Biol Med*. **23**: 76-81

- Kantor GJ, Barsalou LS and Hanawalt PC (1990). Selective repair of specific chromatin domains in UV-irradiated cells from xeroderma pigmentosum complementation group C. *Mutat Res.* **235**: 171-180
- Karahall B, Girard P-M, Boiteux S and Dizdaroglu M (1998). Substrate specificity of the Ogg1 protein of *Saccharomyces cerevisiae*: excision of guanine lesions produced in DNA by ionising radiation- or hydrogen peroxide/ metal ion-generated free radicals. *Nucleic Acids Res.* **26**: 1228-1232
- Kasai H (1997). Analysis of a form oxidative DNA damage, 8-hydroxy-2'-deoxyguanosine, as a marker of cellular oxidative stress during carcinogenesis. *Mutat Res.* **387**: 147-163
- Kasai H. and Nishimura S (1984). Hydroxylation of deoxyguanosine at the C-8 position and other reducing agents. *Nucleic Acids Res.* **12**: 2137-2145
- Katiyar SK, Matsui MS and Mukhtar H (2000). Kinetics of UV light-induced cyclobutane pyrimidine dimers in human skin in vivo: an immunohistochemical analysis of both epidermis and dermis. *Photochem Photobiol.* **72**: 788-793
- Kato T Jr, Todo T, Ayaki H, Ishizaki K, Morita T, Mitra S and Ikenaga M (1994). Cloning of a marsupial DNA photolyase gene and the lack of related nucleotide sequences in placental mammals. *Nucleic Acids Res.* **22**: 4119-4124
- Kelley MR, Moore DH, Cheng L, Foster R, Michael H, Xu Y, Parsons S, Tritt R and Koch M (2000). Altered expression of the multifunctional DNA base excision repair and redox enzyme APE/Ref-1 in ovarian and prostate cancers. *Proceedings of the AACR Special Conference on DNA Repair Defects, San Diego, CA.*
- Kelley MR, Tritt R, Xu Y, New S, Freie B, Clapp DW and Deutsch WA (2001). The *Drosophila* S3 multifunctional DNA repair/ribosomal protein protects Fanconi anemia cells against oxidative DNA damaging agents. *Mutat Res.* **485**: 107-119
- Kendall TL, Byerley DJ and Dean R (1991). Isolation of DNA from blood. *Anal Biochem.* **195**: 74-76
- Khanna KK and Jackson SP (2001). DNA double-strand breaks: signalling, repair and cancer. *Nature Genet.* **27**: 247-254
- Kim J, Patel D and Choi B (1995). Contrasting structural impacts induced by *cis-syn* cyclobutane dimer and (6-4) adduct in DNA duplex decamers: Implications in mutagenesis and repair activity. *Photochem Photobiol.* **62**: 44-50
- Kim ST, Malhotra K, Smith CA, Taylor JS and Sancar A (1994). Characterization of (6-4)-photoproduct DNA photolyase. *J Biol Chem.* **269**: 8535-8540
- Kitao S, Lindor NM, Shiratori M, Furuichi Y and Shimamoto A (1999)<sup>1</sup>. Rothmund-thomson syndrome responsible gene, RECQL4: genomic structure and products. *Genomics.* **61**: 268-276
- Kitao S, Shimamoto A, Goto M, Miller RW, Smithson WA, Lindor NM and Furuichi Y (1999)<sup>2</sup>. Mutations in RECQL4 cause a subset of cases of Rothmund-Thomson syndrome. *Nature Genet.* **22**: 82-84

- Klatt P, Schmidt K, Brunner F, and Mayer B (1994). Inhibitors of brain nitric oxide synthase. Binding kinetics, metabolism, and enzyme inactivation. *J Biol Chem.* **269**: 1674-1680
- Klungland A, Rosewell I, Hollenbach S, Larsen E, Daly G, Epe B, Seeberg E, Lindahl T and Barnes DE (1999). Accumulation of premutagenic DNA lesions in mice defective in removal of oxidative base damage. *Proc Natl Acad Sci USA.* **96**: 13300-13305
- Kohn KW (1999). Molecular interaction map of the mammalian cell cycle control and DNA repair systems. *Mol Biol Cell.* **10**: 2703-2734
- Kohno T, Shinmura K, Tosaka M, Tani M, Kim S-R, Sugimura H, Nohmi T, Kasai H and Yokota J (1998). Genetic polymorphisms and alternative splicing of the *hOGG1* gene, that is involved in the repair of 8-hydroxyguanine in damaged DNA. *Oncogene.* **16**: 3219-3225
- Kolodner RD (1995). Mismatch repair: mechanisms and relationship to cancer susceptibility. *Trends Biochem Sci.* **20**: 397-401
- Kondo S, Toyokuni S, Tanaka T, Hiai H, Onodera H, Kasai H and Imamura M (2000). Overexpression of the *hOGG1* gene and high 8-hydroxy-2'-deoxyguanosine (8-OHdG) lyase activity in human colorectal carcinoma: regulation mechanism of 8-OHdG levels in DNA. *Clin Cancer Res.* **6**: 1394-1400
- Kotzin BL (1996). Systemic lupus erythematosus. *Cell.* **85**: 303-306
- Kraemer KH, Levy DD, Parris CN, Gozukara EM, Moriwaki S, Adelberg S and Seidman MM (1994). Xeroderma pigmentosum and related disorders: examining the linkage between defective DNA repair and cancer. *J Invest Dermatol.* **103**: 96S-101S
- Krokan HE, Nilsen H, Skorpen F, Otterlei M and Slupphaug G (2000). Base excision repair of DNA in mammalian cells. *FEBS Letters.* **476**: 73-77
- Krokan HE, Standal R and Slupphaug G (1997). DNA glycosylases in the base excision repair of DNA. *Biochem J.* **325**: 1-16
- Kuluncsics Z, Perdiz D, Brulay E, Muel B and Sage E (1999). Wavelength dependence of ultraviolet-induced DNA damage distribution: involvement of direct or indirect mechanisms and possible artefacts. *J Photochem Photobiol B.* **49**: 71-80
- Kupper JH, Van Gool L and Burkle A (1995). Molecular genetic systems to study the role of poly(ADP-ribosylation) in cellular response to DNA damage. *Biochimie.* **77**: 450-455
- Lackinger D, Ruppitsch W, Ramirez MH, Hirsch-Kauffmann M and Schweiger M (1998). Involvement of the Fanconi anemia protein FA-C in repair processes of oxidative DNA damages. *FEBS letters.* **440**: 103-106
- Lavin MF, Concannon P, and Gatti RA (1999). Eighth international workshop on Ataxia-telangiectasia (ATW8). *Cancer Res.* **59**: 3845-3849
- Leach FS, Nicolaides NC, Papadopoulos N, Liu B, Jen J, Parsons R, Peltomaki P, Sistonen P, Aaltonen LA, Nyström-Lahti M, Guan X-Y, Zhang J, Meltzer PS, Yu J-W, Kao F-T, Chen DJ, Cerosaletti KM, Fournier REK, Todd S, Lewis T, Leach RJ, Naylor SL, Weissenbach J, Mecklin J-P, Järvinen H, Petersen GM, Hamilton SR, Green J, Jass J, Watson

- P, Lynch HT, Trent JM, de la Chapelle A, Kinzler KW and Vogelstein B (1993). Mutations of a *mutS* homolog in hereditary nonpolyposis colorectal cancer. *Cell*. **75**: 1215-1225
- Le Curieux F and Hemminki K (2001). Cyclobutane thymidine dimers are present in human urine following sun exposure: quantitation using <sup>32</sup>P-postlabeling and high-performance liquid chromatography. *J Invest Dermatol*. **117**: 263-268
  - LeDoux SP, Wilson GL, Beecham EJ, Stevensner T, Wassermann K and Bohr VA (1992) Repair of mitochondrial DNA after various types of DNA damage in Chinese hamster ovary cells. *Carcinogenesis* **13**: 1967-1973
  - Lee Y-S, Choi J-Y, Park M-K, Choi E-M, Kasai H and Chung M-H (1996). Induction of <sup>8</sup>OHdG glycosylase in rat kidneys by potassium bromate (KBrO<sub>3</sub>), a renal carcinogen. *Mutat Res*. **364**: 227-233
  - Lee BM, Lee SK, and Kim HS (1998). Inhibition of oxidative DNA damage, 8-OHdG, and carbonyl contents in smokers treated with antioxidants (vitamin E, vitamin C, β-carotene and red ginseng). *Cancer Letters*. **132**: 219-227
  - Leech RW, Brumback RA, Miller RH, Otsuka F, Tarone RE and Robbins JH (1985). Cockayne syndrome: clinicopathologic and tissue culture studies of affected siblings. *Neuropathol Exp Neurol*. **44**: 507-519
  - Lehmann AR (1975). Postreplication repair of DNA in UV-irradiated mammalian cells. *Basic Life Sci*. **5B**: 617-623
  - Lehmann AR (1982). Three complementation groups in Cockayne's syndrome. *Mutat Res*. **106**: 347-356
  - Le Page F, Guy A, Cadet J, Sarasin A and Gentil A (1998). Repair and mutagenic potency of 8-oxoG:A and 8-oxoG:C base pairs in mammalian cells. *Nucleic Acids Res*. **26**: 1276-1281
  - Le Page F, Klungland A, Barnes DE, Sarasin A and Boiteux S (2000). Transcription coupled repair of 8-oxoguanine in murine cells: the Ogg1 protein is required for repair in nontranscribed sequences but not in transcribed sequences. *Proc Natl Acad Sci USA*. **97**: 8397-8402
  - Lestienne P and Bataille N (1994). Mitochondrial DNA alterations and genetic diseases: a review. *Biomed. Pharmacotherapeutics*. **48**: 199-214
  - Ley RD (1993). Photoreactivation in humans. *Proc Natl Acad Sci USA*. **90**: 4337
  - Li GM and Modrich P (1995). Restoration of mismatch repair to nuclear extracts of H6 colorectal tumour cells by a heterodimer of human MutL homologs. *Proc Natl Acad Sci USA*. **92**: 1950-1954
  - Lin L-H, Cao S, Yu L, Cui J, Hamilton WJ and Liu PK (2000). Up-regulation of base excision repair activity for 8-hydroxy-2'-deoxyguanosine in the mouse brain after forebrain ischemia-reperfusion. *J Neurochem*. **74**: 1098-1105
  - Lindahl T (1993). Instability and decay of the primary structure of DNA. *Nature*. **362**: 709-715

- Lindahl T, Karran P and Wood RD (1997). DNA excision repair pathways. *Curr Opin Genet Dev.* **7**: 158-169
- Lindahl T, Sedgwick B, Sekiguchi M and Nakabeppu Y (1988). Regulation and expression of the adaptive response to alkylating agents. *Annu. Rev. Biochem.* **57**: 133-157
- Lindahl T and Wood RD (1999). Quality control by DNA repair. *Science.* **286**: 1897-1905
- Loeb LA (1991). Mutator phenotype may be required for multistage carcinogenesis. *Cancer Res.* **51**: 3075-3079
- Loeb LA (2001). A mutator phenotype in cancer. *Cancer Res.* **61**: 3230-3239
- Loft S and Poulsen HE (2000). Antioxidant intervention studies related to DNA damage, DNA repair and gene expression. *Free Radical Res.* **33**: S67-83
- Lunec J (1998). ESCODD: European Standards Committee on Oxidative DNA Damage. *Free Radical Res.* **29**: 601-608
- Lunec J and Blake DR (1985). The determination of dehydroascorbic acid and ascorbic acid in the serum and synovial fluid of patients with rheumatoid arthritis (RA). *Free Radical Res Commun.* **1**: 31-39
- Lutsenko EA, Carcamo JM and Golde DW (2002). Vitamin C prevents DNA mutation induced by oxidative stress. *J Biol Chem.* **277**: 16895-16899
- Madhani HD, Bohr VA and Hanawalt PC (1986). Differential DNA repair in transcriptionally active and inactive proto-oncogenes: *c-abl* and *c-mos*. *Cell.* **45**: 417-423
- Maki H and Sekiguchi M (1992). MutT protein specifically hydrolyses a potent mutagenic substrate for DNA synthesis. *Nature.* **355**: 273-275
- Malins DC, Holmes EH, Polissar NL and Gunselman SJ (1993). The etiology of breast cancer. Characteristic alteration in hydroxyl radical-induced DNA base lesions during oncogenesis with potential for evaluating incidence risk. *Cancer.* **71**: 3036-3043
- Masutani C, Kusumoto R, Yamada A, Dohmae N, Yokoi M, Yuasa M, Araki M, Iwai S, Takio K and Hanaoka F (1999). The XPV (xeroderma pigmentosum variant) gene encodes human DNA polymerase  $\eta$ . *Nature.* **399**: 700-704
- Matsumoto Y, Kim K, Hurwitz J, Gary R, Levin DS, Tomkinson AE and Park MS (1999). Reconstitution of proliferating cell nuclear antigen-dependent repair of apurinic/apyrimidinic sites with purified human proteins. *J Biol Chem.* **274**: 33703-33708
- Matsunaga T, Mu D, Park CH, Reardon JT and Sancar A (1995). Human DNA repair excision nuclease analysis of the roles of the subunits involved in dual incisions by using anti-XPG and anti-ERCC1 antibodies. *J Biol Chem.* **270**: 20862-20869
- McLean WH and Lane EB (1995). Intermediate filaments in disease. *Curr Opin Cell Biol.* **7**: 118-125
- Mecocci P, MacGarvey U and Beal MF (1994). Oxidative damage to mitochondrial DNA is increased in Alzheimer's disease. *Ann Neurol.* **36**: 747-751

- Meister A (1981). Metabolism and functions of glutathione. *Trends Biochem. Sci.* 231-234
- Meyer M, Schreck R and Baeuerle PA (1993). H<sub>2</sub>O<sub>2</sub> and antioxidants have opposite effects on activation of NF-kappa B and AP-1 in intact cells: AP-1 as secondary antioxidant-responsive factor. *EMBO J.* 12: 2005-2015
- Michaels ML, Cruz C, Grollman AP and Miller JH (1992). Evidence that MutY and MutM combine to prevent mutations by a oxidatively damaged form of guanine in DNA. *Proc Natl Acad Sci USA.* 89: 7022-7025
- Miettinen M, Lehto V-P and Virtanen I (1985). Antibodies to intermediate filament proteins. The differential diagnosis of cutaneous tumors. *Arch Dermatol.* 121: 736-741
- Mitchell DL, Pfeiffer GP, Taylor JS *et al* (1993). Biological role of (6-4) photoproducts and cyclobutane dimers. In: Shima A, Ichihashi M, Fujiwara Y, Takebe H, eds. *Frontiers of Photobiology*, Elsevier Science, Amsterdam. pp 337-344
- Mitra S (1999). Repair of oxidative DNA damage and aging; central role of AP-endonuclease. In: Dizdaroglu and Karakaya, eds. *Advances in DNA Damage and Repair*, Kluwer Academic, Plenum Publishers, New York. pp 295-311
- Mizuno T, Matsunaga T, Ihara M and Nikaido O (1991). Establishment of a monoclonal antibody recognizing cyclobutane-type thymine dimers in DNA: a comparative study with 64M-1 antibody specific for (6-4)photoproducts. *Mutat Res.* 254: 175-184
- Mol CD, Kuo CF, Thayer MM, Cunningham R and Tainer JA (1995). Structure and function of the multifunctional DNA repair enzyme exonuclease III. *Nature.* 374: 381-386
- Moll R, Franke WW, Schiller DL, Geiger B and Krepler R (1982). The catalog of human cytokeratins: patterns of expression in normal epithelia, tumors and cultured cells. *Cell.* 31: 11-24
- Moore DH, Michael H, Tritt R, Parsons SH and Kelley MR (2000). Alterations in the expression of the DNA repair/ redox enzyme APE/Ref-1 in epithelial ovarian cancers. *Clin Cancer Res.* 6: 602-609
- Mori T, Matsunaga T, Hirose T, and Nikaido O (1988). Establishment of a monoclonal antibody recognizing ultraviolet light-induced (6-4) photoproducts. *Mutat Res.* 194: 263-270
- Moynahan ME, Cui TY and Jasin M (2001). Homology-directed DNA repair, mitomycin-c resistance, and chromosome stability is restored with correction of a Brca1 mutation. *Cancer Res.* 61: 4842-4850
- Mu D, Hsu D and Sancar A (1996). Reaction mechanism of human DNA repair excision nuclease. *J Biol Chem.* 271: 8285-8294
- Muller JM, Rupec RA and Baeuerle PA (1997). Study of gene regulation by NF-κB and AP-1 in response to reactive oxygen intermediates. *Methods in Enzymol.* 11: 301-312
- Murata-Kamiya N, Kamiya H, Iwamoto N and Kasai H (1995). Formation of a mutagen, glyoxal, from DNA treated with oxygen free radicals. *Carcinogenesis* 16: 2251-2253

- Murata-Kamiya N, Kamiya H, Kaji H and Kasai H (1997). Glyoxal, a major product of DNA oxidation, induces mutations at G:C sites on a shuttle vector plasmid replicated in mammalian cells. *Nucleic Acids Res.* **25**: 1897-1902
- Nagashima M, Sasaki A, Morishita K, Takenoshita S, Nagamachi Y, Kasai K and Yokota J (1997). Presence of human cellular protein(s) that specifically binds and cleaves 8-hydroxyguanine containing DNA. *Mutat Res.* **383**: 49-59
- Nakae D, Denda A, Kobayashi Y, Akai H, Kishida H, Tsujiuchi T, Konishi Y, Suzuki T and Muramatsu M (1998). Inhibition of early-phase exogenous and endogenous liver carcinogenesis in transgenic rats harbouring a rat glutathione-S-transferase placental form gene. *Jpn J Cancer Res.* **89**: 1118-1125
- Nakajima-Iijima S, Hamada H, Reddy P and Kakunaga T (1985). Molecular structure of the human  $\beta$ -actin gene: Interspecies homology of sequences in the introns. *Proc Natl Acad Sci USA.* **82**: 6133-6137
- Nance MA and Berry SA (1992). Cockayne syndrome: review of 140 cases. *Am J Med Genet.* **42**: 68-84
- Nash HM, Bruner SD, Scharer OD, Kawate T, Addona TA, Spooner E, Lane WS and Verdine G (1996). Cloning of a yeast 8-oxoguanine DNA glycosylase reveals the existence of a base-excision DNA repair protein superfamily. *Current Biol.* **6**: 968-980
- Neddermann P and Jiricny J (1994). Efficient removal of uracil from G.U mispairs by the mismatch-specific thymine DNA glycosylase from HeLa cells. *Proc Natl Acad Sci USA.* **91**: 1642-1646
- Nigg EA (1996). Cyclin-dependent kinase 7: at the cross-roads of transcription, DNA repair and cell cycle control? *Curr Opin Cell Biol.* **8**: 312-317
- Nilakantan V, Spear BT and Glauert HP (1998). Effect of the peroxisome proliferator ciprofibrate on lipid peroxidation and 8-hydroxydeoxyguanosine formation in transgenic mice with elevated hepatic catalase activity. *Free Radical Biol Med.* **24**: 1430-1436
- Nilsen H and Krokan HE (2001). Base excision repair in a network of defence and tolerance. *Carcinogenesis.* **22**: 987-998
- Nilsen H, Otterlei M, Haug T, Solum K, Nagelhus TA, Skorpen F, and Krokan HE (1997). Nuclear and mitochondrial uracil-DNA glycosylases are generated by alternative splicing and transcription from different positions in the *UNG* gene. *Nucleic Acids Res.* **25**: 750-755
- Nishikawa T, Edelstein D, Du XL, Yamagishi S, Matsumura T, Kaneda Y, Yorek MA, Beebe D, Oates PJ, Hammes H, Giardino I and Brownlee M (2000). Normalizing mitochondrial superoxide production blocks three pathways of hyperglycaemic damage. *Nature.* **404**: 787-790
- Nishioka K, Ohtsubo T, Oda H, Fujiwara T, Kang D, Sugimachi K and Nakabeppu Y (1999). Expression and differential intracellular localisation of two major forms of humana 8-oxoguanine DNA glycosylase encoded by alternatively spliced OGG1 mRNAs. *Mol Cell Biol.* **10**: 1637-1652

- Njoo MD, Bos JD and Westerhof W (2000). Treatment of generalized vitiligo in children with narrow-band (TL-01) UVB radiation therapy. *J. Am. Acad. Dermatol.* **42**: 245-253
- Nunomura A, Perry G, Pappolla MA, Wade R, Hirai K, Chiba S and Smith MA (1999). RNA oxidation is a prominent feature of vulnerable neurons in Alzheimer's disease. *J Neurosci.* **19**: 1959-1964
- Okamoto K, Toyokuni S, Uchida K, Ogawa O, Takenawa J, Kakehi Y, Kinoshita H, Hattori-Nakakuki Y, Hiai H and Yoshida O (1994). Formation of 8-hydroxy-2'-deoxyguanosine and 4-hydroxy-2-nonenal-modified proteins in human renal-cell carcinoma. *Int J Cancer.* **58**: 825-829
- Okazaki T, Chung U, Nishishita T, Ebisu S, Usuda S, Mishiro S, Xanthoudakis S, Igarashi T and Ogata E (1994). A redox factor protein, ref1, is involved in negative gene regulation by extracellular calcium. *J Biol Chem.* **269**: 27855-27862
- Olinski R, Zastawny T, Budzbon J, Skokowski J, Zegarski W and Dizdaroglu M (1992). DNA base modifications in chromatin of human cancerous tissues. *FEBS Lett.* **309**: 193-198
- Oliva MR, Ripoll F, Muñiz P, Iradi A, Ramón T, Valls V, Drehmer E and Sáez GT (1997). Genetic alterations and oxidative metabolism in sporadic colorectal tumors from a Spanish community. *Mol Carcinogenesis.* **18**: 232-243
- Olken NM, Osawa Y and Marletta MA (1994). Characterization of the inactivation of nitric oxide synthase by NG-methyl-L-arginine: evidence for heme loss. *Biochem.* **33**: 14784-14791
- Olkowski ZL (1998). Mutant AP endonuclease in patients with amyotrophic lateral sclerosis. *Neuro Report.* **9**: 239-242
- Otterlei M, Warbrick E, Slupphaug G, Nagelhus T, Haug T, Akbari M, Aas PA, Steinsbekk K, Bakke O and Krokan HE (1999). Post-replicative base excision repair in replication foci. *EMBO J.* **18**: 3834-3844
- Palombo F, Iaccarino I, Nakajima E, Ikejima M, Shimada T, and Jiricny J (1996). hMutS $\beta$ , a heterodimer of hMSH2 and hMSH3, binds to insertion/deletion loops in DNA. *Curr Biol.* **6**: 1181-1184
- Park CH, Bessho T, Matsunaga T and Sancar A (1995)<sup>2</sup>. Purification and characterization of the XPF-ERCC1 complex of human DNA-repair excision nuclease. *J Biol Chem.* **270**: 22657-22660
- Park CH, Mu D, Reardon JT and Sancar A (1995)<sup>1</sup>. The general transcription-repair factor TFIIH is recruited to the excision repair complex by the XPA protein independent of the TFIIIE transcription factor. *J Biol Chem.* **270**: 4896-4902
- Park JB and Levine M (1996). Purification, cloning and expression of dehydroascorbic acid reduction activity from human neutrophils: Identification as glutaredoxin. *Biochem J.* **315**: 931-938
- Parsons R, Li G-M, Longley MJ, Fang W-h, Papadopoulos N, Jen J, de la Chapelle A, Kinzler KW, Vogelstein B and Modrich P (1993). Hypermutability and mismatch repair deficiency in RER<sup>+</sup> tumour cells. *Cell.* **75**: 1227-1236

- Pascucci B, Stucki M, Jonsson ZO, Dogliotti E and Hübscher U (1999). Long patch base excision repair with purified human proteins: DNA ligase I as patch size mediator for DNA polymerases delta and epsilon. *J Biol Chem.* **274**: 33696-33702
- Patrick MH (1970). Near-U.V. photolysis of pyrimidine heteroadducts in E. coli DNA. *Photochem Photobiol.* **11**: 477-485
- Peak MJ and Peak JG (1989). Solar-ultraviolet-induced damage to DNA. *Photodermatol.* **6**: 1-15
- Peak JG and Peak MJ (1991). Comparison of initial yields of DNA to protein crosslinks and single strand breaks induced in cultured cells by far and near UV light, blue light and X-rays. *Mutat. Res.* **246**: 187-196
- Pfeiffer P, Goedecke W and Obe G (2000). Mechanisms of DNA double-strand break repair and their potential to induce chromosomal aberrations. *Mutagenesis.* **15**: 289-302
- Pflaum M, Will O and Epe B (1997). Determination of steady-state levels of oxidative DNA base modifications in mammalian cells by means of repair endonuclease. *Carcinogenesis.* **18**: 2225-2231
- Piersen CE, McCullough AK and Lloyd RS (2000). AP lyases and dRPases: commonality of mechanism. *Mutat Res.* **459**: 43-53
- Pinkus R, Bergelson S and Danial V (1996). Role of oxidants and antioxidants in the induction of AP-1, NF-kappaB and glutathione-S-transferase gene expression. *J Biol Chem.* **271**: 13422-13429
- Podmore ID, Cooke MS, Herbert KE and Lunec J (1996). Quantitative determination of cyclobutane thymine dimers in DNA by stable isotope-dilution mass spectrometry. *Photochem Photobiol.* **64**: 310-315
- Podmore ID, Farmer PB, Herbert KE, Jones GDD and Martin EA (1997). <sup>32</sup>P-post labelling approaches for the detection of 8-oxo-2'-deoxyguanosine-3'-monophosphate in DNA. *Mutat Res.* **178**: 139-149
- Podmore ID, Griffiths HR, Herbert KE, Mistry N, Mistry P and Lunec J (1998). Vitamin C exhibits pro-oxidant properties. *Nature.* **392**: 559
- Poulsen HE, Jensen BR, Weimann A, Jensen SA, Sørensen M and Loft S (2000). Antioxidants, DNA damage and gene expression. *Free Radical Res.* **33**: S33-39
- Prasad R, Singhal RK, Srivastava DK, Molina Jt, Tomkinson AE and Wilson SH (1996). Specific interaction of DNA polymerase beta and DNA ligase I in a multiprotein base excision repair complex from bovine testis. *J Biol Chem.* **271**: 16000-16007
- Prolla TA, Pang Q, Alani E, Kolodner RD and Liskay RM (1994). MLH1, PMS1 and MSH2 interactions during the initiation of DNA mismatch repair in yeast. *Science.* **265**: 1091-1093
- Prowse AH, Webster AR, Richards FM, Richard S, Olschwang S, Resche F, Affara NA and Maher ER (1997). Somatic inactivation of the VHL gene in Von Hippel-Lindau disease tumors. *Am J Hum Genet.* **60**: 765-771

- Purkis PE, Steel JB, Mackenzie IC, Nathrath WB, Leigh IM and Lane EB (1990). Antibody markers of basal cells in complex epithelia. *J Cell Sci.* **97**: 39-50
- Purmal AA, Rabow LE, Lampman GW, Cunningham RP and Kow YW (1996). A common mechanism of action for the N-glycosylase/ AP lyase from *E.coli* and T4. *Mutat Res.* **364**: 193-207
- Purohit S and Arenaz P (1999). Molecular cloning, sequence and structure analysis of hamster apurinic/apyrimidinic endonuclease (*chAPE1*) gene. *Mutat Res.* **435**: 215-224
- Qin X, Zhang S, Nakatsuru Y, Oda H, Yamazaki Y, Suzuki T, Nikaido O and Ishikawa T (1994). Detection of active UV-photoproduct repair in monkey skin in vivo by quantitative immunohistochemistry. *Cancer Lett.* **83**: 291-298
- Radak Z, Kaneko T, Tahara S, Nakamoto H, Ohno H, Sasvari M, Nyakas C and Goto S (1999). The effect of exercise training on oxidative damage of lipids, proteins and DNA in rat skeletal muscle: evidence for beneficial outcomes. *Free Radical Biol Med.* **27**: 69-74
- Radicella JP, Dherin C, Desmaze C, Fox MS and Bioteux S (1997). Cloning and characterization of *hOGG1*, a human homolog of the *OGG1* gene of *Saccharomyces cerevisiae*. *Proc Natl Acad Sci USA.* **94**: 8010-8015
- Rady P, Scinicaiello F, Wagner RF Jr and Trying SK (1992). p53 mutations in basal cell carcinomas. *Cancer Res.* **53**: 2961-2964
- Ramana CV, Boldogh I, Izumi T and Mitra S (1998). Activation of apurinic/apyrimidinic endonuclease in human cells by reactive oxygen species and its correlation with their adaptive response to genotoxicity of free radicals. *Proc Natl Acad Sci USA.* **95**: 5061-5066
- Ravanat JL, Turesky RL, Gremaud E, Trudel LJ and Stadler RH (1995). Determination of 8-oxoguanine in DNA by Gas-Chromatography-Mass Spectrometry and HPLC-Electrochemical detection: overestimation of the background level of the oxidized base by the Gas Chromatography-Mass Spectrometry method. *Chem Res Toxicol.* **8**: 1039-1045
- Ravanat JL, Douki T, Duez P, Gremaud E, Herbert K, Hofer T, Lasserre L, Saint-Pierre C, Favier A and Cadet J (2002). Cellular background level of 8-oxo-7,8-dihydro-2'-deoxyguanosine: an isotope based method to evaluate artefactual oxidation of DNA during its extraction and subsequent work-up. *Carcinogenesis.* **23**: 1911-1918
- Reardon JT, Bessho T, Kung HC, Bolton PH and Sancar A (1997). *In vitro* repair of oxidative DNA damage by human nucleotide excision repair system: possible explanation for neurodegeneration in Xeroderma pigmentosum patients. *Proc Natl Acad Sci USA.* **94**: 9463-9468
- Reardon JT, Mu D, Sancar A (1996). Overproduction, purification and characterization of the XPC subunit of the human DNA-repair excision nuclease. *J Biol Chem.* **271**: 19451-19456
- Redaelli A, Magrassi R, Bonassi S, Abbondandolo A and Frosina G (1998). AP endonuclease activity in humans: development of a simple assay and analysis of ten normal individuals. *Teratog Carcinog Mutagen.* **18**: 17-26

- Rehman A, Collis CS, Yang M, Kelly M, Diplock AT Halliwell and Rice-Evans C (1998). The effects of iron and vitamin C co-supplementation on biomarkers on oxidative damage to DNA in healthy volunteers. *Biochem Biophys Res Comm.* **246**: 293-298
- Reusch MK, Meager K, Leadon SA and Hanawalt PC (1988). Comparative removal of pyrimidine dimers from human epidermal keratinocytes in vivo and in vitro. *J Invest Dermatol.* **91**: 349-352
- Riballo E, Critchlow SE, Teo SH, Doherty AJ, Priestley A, Broughton B, Kysela B, Beamish H, Plowman N, Arlett CF, Lehmann AR, Jackson SP and Jeggo PA (1999). Identification of a defect in DNA ligase IV in a radiosensitive leukaemia patient. *Curr Biol.* **9**: 699-702
- Rich T, Allen RL, and Wyllie AH (2000). Defying death after DNA damage. *Nature.* **407**: 777-783
- River J (1996). Melanoma. *Lancet.* **347**: 803-807
- Rivier C and Shen GH (1994). In the rat, endogenous nitric oxide modulates the response of the hypothalamic-pituitary-adrenal axis to interleukin-1 beta, vasopressin, and oxytocin. *J Neurosci.* **14**: 1985-1993
- Robbins JH (1988). Xeroderma pigmentosum. Defective DNA repair causes skin cancer and neurodegeneration. *J Amer Med Assoc.* **260**: 384-388
- Robbins JH, Kraemer KH, Lutzner MA, Festoff BW and Coon HG (1974). Xeroderma pigmentosum. An inherited disease with sun sensitivity, multiple cutaneous neoplasms, and abnormal DNA repair. *Ann Intern Med.* **80**: 221-248
- Robertson KA, Hill DP, Xu Y, Liu L, Van Epps S, Hockenbery DM, Park J, Wilson TM and Kelley MR (1997). Down-regulation of apurinic/apyrimidinic endonuclease expression is associated with the induction of apoptosis differentiating myeloid leukemia cells. *Cell Growth & Different.* **8**: 443-449
- Robson CN and Hickson ID (1991). Isolation of cDNA clones encoding a human apurinic/apyrimidinic endonuclease that corrects DNA repair and mutagenesis defects in *E.coli xth* (exonuclease III) mutants. *Nucleic Acids Res.* **19**: 5519-5523
- Robson CN, Hochhauser D, Craig R, Rack K, Buckle VJ and Hickson ID (1992). Structure of the human DNA repair gene HAP1 and its localisation to chromosome 14q 11.2-12. *Nucleic Acid Res.* **20**: 4417-4421
- Röhrdanz E and Kahl R (1998). Alterations of antioxidant enzyme expression in response to hydrogen peroxide. *Free Radical Biol & Med.* **24**: 27-38
- Roldán-Arjona T, Wei YF, Carter KC, Klungland A, Anselmino C, Wang RP, Augustus M and Lindahl T (1997). Molecular cloning and functional expression of a human cDNA encoding the antimutator enzyme 8-hydroxyguanine-DNA glycosylase. *Proc Natl Acad Sci USA.* **94**: 8016-8020
- Rosenquist TA, Zharkov DO and Grollman AP (1997). Cloning and characterization of a mammalian 8-oxoguanine DNA glycosylase. *Proc Natl Acad Sci USA.* **94**: 7429-7434

- Rosenstein BS, Rosenstein RB, Zamansky GB (1992). Repair of DNA damage induced in systemic lupus erythematosus skin fibroblasts by simulated sunlight. *J Invest Dermatol.* **98**: 469-474
- Roth DB and Craig NL (1998). VDJ recombination: a transposase goes to work. *Cell.* **94**: 411-414
- Rotman G and Shiloh Y (1998). ATM: from gene to function. *Hum Mol Genet.* **7**: 1555-1563
- Rothwell DG and Hickson ID (1996). Asparagine 212 is essential for abasic site recognition by the human DNA repair endonuclease HAP1. *Nucleic Acids Res.* **24**: 4217-4221
- Rumsey SC, Daruwala R, Al-Hasani H, Zarnowski MJ, Simpson IA and Levine M (2000). Dehydroascorbic acid transport by GLUT4 in *Xenopus* oocytes and isolated rat adipocytes. *J Biol Chem.* **275**: 28246-28253
- Runger TM, Epe B and Moller K (1995). Repair of ultraviolet B and singlet oxygen-induced DNA damage in xeroderma pigmentosum cells. *J Invest Dermatol.* **104**: 68-73
- Ruven HJ, Berg RJ, Seelen CM, Dekkers JA, Lohman PH and Mullenders LH (1993). UV induced cyclobutane pyrimidine dimers are selectively removed from transcriptionally active genes in the epidermis of hairless mice. *Cancer Res.* **53**: 1642-1645
- Saitoh T, Shinmura K, Yamaguchi S, Tani M, Seki S, Murakami H, Nojima Y and Yokota J (2001). Enhancement of OGG1 protein AP lyase activity by increase of APEX protein. *Mutat Res.* **486**: 31-40
- Sancar A (1994). Structure and function of DNA photolyase. *Biochemistry.* **43**: 2-9
- Sancar A (1995)<sup>1</sup>. DNA repair in humans. *Annu Rev Gen.* **29**: 60-105
- Sancar A (1995)<sup>2</sup>. Excision repair in mammalian cells. *J. Biol. Chem.* **270**: 15915-15918
- Sancar A (1996). DNA excision repair. *Annu Rev Biochem.* **65**: 43-81
- Sarasin A (1999). The molecular pathways of ultraviolet-induced carcinogenesis. *Mutat Res.* **428**: 5-10
- Satoh MS, Jones CJ, Wood RD and Lindahl T (1993). DNA excision-repair defect of xeroderma pigmentosum prevents removal of a class of oxygen free radical-induced base induced base lesions. *Proc Natl Acad Sci USA.* **90**: 6335-6339
- Savva R, McAuley-Hecht K, Brown T and Pearl L (1995). The structural basis of specific base excision repair by uracil-DNA glycosylase. *Nature.* **373**: 487-493
- Schaeffer L, Moncollin V, Roy R, Staub A, Mezzina M, Sarasin A, Weeda G, Hoeijmakers JH and Egly JM (1994). The ERCC2/DNA repair protein is associated with the class II BTF2/TFIIH transcription factor. *EMBO J.* **13**: 2388-2392
- Schaeffer L, Roy R, Humbert S, Moncollin V, Vermeulen W, Hoeijmakers JH, Chambon P and Egly JM (1993). DNA repair helicase: a component of BTF2 (TFIIH) basic transcription factor. *Science.* **260**: 58-63

- Schapira AHV (1995). Nuclear and mitochondrial genetics in Parkinson's disease. *J Med Genet.* **32**: 411-414
- Schär P (2001). Spontaneous DNA damage, genome instability and cancer-when DNA replication escapes control. *Cell.* **104**: 329-332
- Schmickel RD, Chu EHY, Trosko JE (1977). Cockayne's syndrome: a cellular sensitivity to ultraviolet light. *Pediatrics.* **60**: 135-139
- Scully R and Livingston DM (2000). In search of the tumour-suppressor functions of BRCA1 and BRCA2. *Nature.* **408**: 429-432
- Seeberg E, Eide L and Bjoras M (1995). The pathway of base excision repair. *Trends Biochem Sci.* **20**: 391-397
- Seki S, Hatsushika M, Watanabe S, Akiyama K, Nagao K and Tsutuni K (1992). cDNA cloning, sequencing, expression and possible domain structure of human APEX nuclease homologous to *Escherichia coli* exonuclease III. *Biochem Biophys Acta.* **1131**: 287-299
- Sekiguchi M, Nakabeppu Y, Sakumi K and Tuzuki T (1996). DNA-repair methyltransferase as molecular device for preventing mutation and cancer. *J Cancer Res Clin Oncol.* **122**: 199-206
- Selby CP and Sancar A (1993). Molecular mechanisms of transcription-repair coupling. *Science.* **260**: 53-58
- Sen CK and Packer L (1996). Antioxidant and redox regulation of gene transcription. *FASEB J.* **10**: 709-720
- Setlow P (1992). I will survive: Protecting and repairing spore DNA. *J Bacteriol.* **174**: 2737-2741
- Shen JC and Loeb LA (2000). The Werner syndrome gene: the molecular basis of RecQ helicase-deficiency diseases. *Trends Genet.* **16**: 213-220
- Shin CS, Moon BS, Park KS, Kim SY, Park SJ, Chung MH and Lee HK (2001). Serum 8-hydroxy-guanine levels are increased in diabetic patients. *Diabetes Care.* **24**: 733-737
- Shinmura K, Kasai H, Sasaki A, Sugimura H and Yokota J (1997). 8-hydroxyguanine (7,8-dihydro-8-oxoguanine) DNA glycosylase and AP lyase activities of hOGG1 protein and their substrate specificity. *Mutat Res.* **385**: 75-82
- Shivji KK, Kenny MK and Wood RD (1992). Proliferating cell nuclear antigen is required for DNA excision repair. *Cell.* **69**: 367-374
- Singhal RK, Prasad R and Wilson SH (1995). DNA polymerase conducts the gap filling uracil-initiated base excision repair in a bovine testis nuclear extract. *J Biol Chem.* **270**: 949-957
- Slupphaug G, Eftedal I, Kavli B, Bharati S, Helle NM, Haug T, Levine DW and Krokan HE (1995). Properties of recombinant human uracil-DNA glycoylase from the UNG gene and evidence that UNG encodes the major uracil-DNA glycoylase. *Biochemistry.* **34**: 128-138

- Smith G, Stanely LA, Sim E, Strange RC and Wolf CR (1996). Metabolic polymorphisms and cancer susceptibility. *Cancer Surv.* **25**: 27-65
- Soultanakis RP, Melamede RJ, Bepalov IA, Wallace SS, Beckman KB, Ames BN, Taatjes DJ and Janssen-Heininger YM (2000). Fluorescence detection of 8-oxoguanine in nuclear and mitochondrial DNA of cultured cells using a recombinant Fab and confocal scanning laser microscopy. *Free Radical Biol Med.* **28**: 987-998
- Staal FJT, Roederer M, Herzenberg LA and Herzenberg LA (1990). Intracellular thiols regulate activation of nuclear factor  $\kappa$ B and transcription of human immunodeficiency virus. *Proc Nat. Acad Sci USA.* **87**: 9943-9947
- Strydom A and Sarasin A (1996). The genetic basis of xeroderma pigmentosum and trichothiodystrophy syndromes. *Cancer Surv.* **26**: 155-171
- Strydom A and Sarasin A (2000). Ultraviolet A- and singlet oxygen-induced mutation spectra. *Methods Enzymol.* **319**: 153-165
- Stedeford T, Cardozo-Pelaez F, Nemeth N, Song S, Harbison RD and Sanchez-Ramos J (2001). Comparison of base-excision repair capacity in proliferating and differentiated PC 12 cells following acute challenge with dieldrin. *Free Radical Biol Med.* **31**: 1272-1278
- Stefanini M, Lagomarsini P, Arlett CF, Marinoni S, Borrone C, Crovato F, Trevisan G, Cordone G and Nuzzo F (1986). Xeroderma pigmentosum (complementation group D) mutation is present in patients affected by trichothiodystrophy with photosensitivity. *Hum Genet.* **74**: 107-112
- Stern RS, Nichols KT and Vakeva LH (1997) Malignant melanoma in patients treated for psoriasis with methoxsalen (psoralen) and ultraviolet A radiation (PUVA). The PUVA Follow-Up Study. *N Engl J Med.* **336**: 1041-5
- Struthers L, Patel R, Clark J and Thomas S (1998). Direct detection of 8-oxodeoxyguanosine and 8-oxoguanine by avidin and its analogues. *Anal. Biochem.* **255**: 20-31
- Sturgis EM, Castillo EJ, Li L, Zheng R, Eicher SA, Clayman GL, Strom SS, Spitz MR and Wei Q (1999). Polymorphisms of DNA repair gene XRCC1 in squamous cell carcinoma of the head and neck. *Carcinogenesis.* **20**: 2125-2129
- Sugawara K, Ng JM, Masutani C, Iwai S, van der Spek PJ, Eker APM, Hanaoka F, Bootsma D and Hoeijmakers JHJ (1998). Xeroderma pigmentosum group C protein complex is the initiator of global genome nucleotide excision repair. *Mol Cell.* **2**: 223-232
- Sun H, Treco D, Schultes NP and Szostak JW (1989). Double-strand breaks at the initiation site for meiotic gene conversion. *Nature.* **338**: 87-90
- Sutherland BM, Harber LC and Kochevar IE (1980). Pyrimidine dimer formation and repair in human skin. *Cancer Res.* **40**: 3181-5
- Szatrowski TP and Nathan CF (1991). Production of large amounts of hydrogen peroxide by human tumour cells. *Cancer Res.* **51**: 794-798
- Tagesson C, Kallberg M, Klintonberg C and Starkhammer H (1995). Determination of urinary 8-hydroxydeoxyguanosine by automated coupled-column high performance liquid

chromatography: a powerful technique for assaying *in vivo* oxidative DNA damage in cancer patients. *Euro J Cancer*. **31A**: 934-940

- Takao M, Aburatani H, Kobayashi K, and Yasui A (1998). Mitochondrial targeting of human DNA glycosylases for repair of oxidative DNA damage. *Nucleic Acids Res*. **26**: 2917-2922
- Takeuchi T and Morimoto K (1993). Increased formation of 8-hydroxydeoxyguanosine, an oxidative DNA damage, in lymphoblasts from Fanconi's anemia patients due to possible catalase deficiency. *Carcinogenesis*. **14**: 1115-1120
- Taniguchi N (1992). Clinical significances of superoxide dismutases: Changes in aging, diabetes, ischemia and cancer. *Adv Clin Chem*. **29**: 1-59
- Taylor E, Broughton BC, Botta E, Stefanini M, Sarasin A, Jaspers N, Fawcett H, Harcourt SA, Arlett CF and Lehmann AR (1997). Xeroderma pigmentosum and trichothiodystrophy are associated with different mutations in the XPD (ERCC2) repair/transcription gene. *Proc Natl Acad Sci USA*. **94**: 8658-8663
- Tebbs RS, Flannery ML, Meneses JJ, Hartmann A, Tucker JD, Thompson LH, Cleaver JE and Pedersen RA (1999). Requirement for *Xrcc1* DNA base excision repair gene during early mouse development. *Dev Biol*. **208**: 513-529
- Tell G, Crivellato E, Pines A, Paron I, Pucillo C, Manzin G, Bandiera A, Kelley MR, Loreto CD and Damante G (2001). Mitochondrial localisation of APE/Ref-1 in thyroid cells. *Mutat Res*. **485**: 143-152
- Thomas D, Scot AD, Barbey R, Padula M and Boiteux S (1996). Inactivation of OGG1 increases the incidence of G.C→T.A transversions in *Saccharomyces cerevisiae*: evidence for endogenous oxidative damage to DNA in eukaryotic cells. *Mol Gen Genet*. **254**: 171-178
- Thomson B, Tritt R, Davis M and Kelley MR (2001). Histology-specific expression of a DNA repair protein in pediatric rhabdomyosarcomas. *J Pediatr Hematol Oncol*. **23**: 234-239
- Timme TL and Moses RE (1988). Diseases with DNA damage-processing defects. *Am. J Med Sci*. **295**: 40-48
- Todo T, Takemori H, Ryo H, Ihara M, Matsunaga T, Nikaido O, Sato K and Nomura T (1993). A new photoreactivating enzyme that specifically repairs ultraviolet light-induced (6-4) photoproducts. *Nature*. **361**: 371-374
- Tomkinson AE, Bonk RT and Linn S (1988). Mitochondrial endonuclease activities specific for apurinic/apyrimidinic sites in DNA from mouse cells. *J Biol Chem*. **263**: 12532-12537
- Tornaletti S and Pfeifer GP (1994). Slow repair of pyrimidine dimers at *p53* mutation hotspots in skin cancer. *Science*. **263**: 1436-1440
- Tornaletti S and Pfeifer GP (1996). UV damage and repair mechanisms in mammalian cells. *BioEssays*. **18**: 221-228
- Toyokuni S, Iwasa Y, Kondo S, Tanaka T, Ochi H and Hiai H (1999). Intranuclear distribution of 8-hydroxy-2'-deoxyguanosine. An immunocytochemical study. *J Histochem Cytochem*. **47**: 833-836

- Toyokuni S, Tanaka T, Hattori Y, Nishiyama Y, Yoshida A, Uchida K, Hiai H, Ochi H and Osawa T (1997). Quantitative immunohistochemical determination of 8-hydroxy-2'-deoxyguanosine by a monoclonal antibody N45.1: Its application to ferric nitriloacetate-induced carcinogenesis model. *Lab Invest.* **76**: 365-374
- Tsukaguchi H, Tokui T, Mackenzie B, Berger UV, Chen XZ, Wang Y, Brubaker RF and Hediger MA (1999). A family of mammalian Na<sup>+</sup>-dependent L-ascorbic acid transporters. *Nature.* **399**: 70-75
- Tsurudome Y, Hirano T, Yamato H, Tanaka I, Sagai M, Hirano H, Nagata N, Itoh H and Kasai H (1999). Changes in the levels of 8-hydroxyguanine in DNA, its repair and *OGG1* mRNA in rat lungs after intratracheal administration of diesel exhaust particles. *Carcinogenesis.* **20**: 1573-1576
- Umlas ME, Franklin WA and Chan GL (1985). Ultraviolet light irradiation of defined-sequences DNA under conditions of chemical photosensitisation. *Photochem Photobiol.* **42**: 265-273
- van der Kemp PA, Thomas D, Barbey R, Oliveira RD and Boiteux S (1996). Cloning and expression in *Escherichia coli* of the OOG1 gene of *Saccharomyces cerevisiae*, which codes for a DNA glycosylase that excises 7,8-dihydro-8-oxoguanine and 2,6-diamino-4-hydroxy-5-N-methylformidopyrimidine. *Proc Natl Acad Sci USA.* **93**: 5197-5202
- van der Spek PJ, Kobayashi K, Bootsma D, Takao M, Eker AP and Yasui A (1996). Cloning, tissue expression, and mapping of a human photolyase homolog with similarity to plant blue-light receptors. *Genomics.* **37**: 177-182
- van Gool AJ, Citterio E, Rademakers S, van Os R, Vermuelen W, Bootsma D and Hoeijmakers JHJ (1997). The Cockayne syndrome B protein, involved in transcription-coupled DNA repair, resides in an RNA polymerase II-containing complex. *EMBO J.* **16**: 5955-5965
- van Steeg H and Kraemer KH (1999). Xeroderma pigmentosum and the role of UV-induced DNA damage in skin cancer. *Mol Med Today.* **5**: 86-94
- Venema J, van Hoffen A, Karcagi V, Natarajan AT, van Zeeland AA and Mullenders LH (1991). Xeroderma pigmentosum complementation group C cells remove pyrimidine dimers selectively from the transcribed strand of active genes. *Mol. Cell. Biol.* **11**: 4128-4134
- Venema J, van Hoffen A, Natarajan AT, van Zeeland AA and Mullenders LH (1990). The residual repair capacity of xeroderma pigmentosum complementation group C fibroblasts is highly specific for transcriptionally active DNA. *Nucleic Acids Res.* **18**: 443-448
- Vera JC, Rivas CI, Fischbarg J and Golde DW (1993). Mammalian facilitative hexose transporters mediate the transport of dehydroascorbic acid. *Nature.* **364**: 79-82
- Vera JC, Rivas CI, Velasquez FV, Zhang RH, Concha II and Golde DW (1995). Resolution of the facilitated transport of dehydroascorbic acid from its intracellular accumulation as ascorbic acid. *J Biol Chem.* **270**: 23706-23712
- Verjat T, Dhénaut A, Radicella JP and Araneda S (2000). Detection of 8-oxoG DNA glycosylase activity and *OGG1* transcripts in the rat CNS. *Mutat Res.* **460**: 127-138

- Vermeulen W, Scott RJ, Rodgers S, Muller HJ, Cole J, Arlett CF, Kleijer WJ, Bootsma D, Hoeijmakers JH and Weeda G (1994). Clinical heterogeneity within xeroderma pigmentosum associated with mutations in the DNA repair and transcription gene ERCC3. *Am J Hum Genet.* **54**: 191-200
- Vidal AE, Hickson ID, Boiteux S and Radicella JP (2001). Mechanism of stimulation of the DNA glycosylase activity of hOGG1 by the major human AP endonuclease: bypass of the AP lyase activity. *Nucleic Acids Res.* **29**: 1285-1292
- Wagner JR., Hu CC and Ames BN (1992). Endogenous oxidative damage of deoxycytosine in DNA. *Proc Natl Acad USA.* **89**: 3380-3384
- Walter SD, King WD and Marret LD (1999). Association of cutaneous malignant melanoma with intermittent exposure to ultraviolet radiation: results of a case-control study in Ontario, Canada. *Int J Epidemiol.* **28**: 418-427
- Wang JC (1996). DNA topoisomerases. *Annu Rev Biochem.* **65**: 635-692
- Wang L, Hirayasu K, Ishizawa M and Kobayashi Y (1994). Purification of genomic DNA from human whole blood by isopropanol-fractionation with concentrated NaI and SDS. *Nucleic Acids Res.* **22**: 1774-1775
- Wang YC, Maher VM, Mitchell DL and McCormick JJ (1993). Evidence from mutation spectra that the UV hypermutability of xeroderma pigmentosum variant cells reflects abnormal, error-prone replication on a template containing photoproducts. *Mol Cell Biol.* **13**: 4276-4283
- Wani AA, D'Ambrosio SM and Alvi NK (1987). Quantitation of pyrimidine dimers by immunoslot blot following sublethal UV-irradiation of human cells. *Photochem. Photobiol.* **46**: 477-482
- Wei Q, Matanoski GM, Farmer ER, Hedayati MA, Grossman L (1994). DNA repair and susceptibility to basal cell carcinoma: a case-control study. *Am. J. Epidemiol.* **140**: 598-607
- Weimann A, Belling HE and Poulsen HE (2001). Measurement of 8-oxo-2'-deoxyguanosine and 8-oxo-2'-deoxyadenosine in DNA and human urine by high performance liquid chromatography-electrospray tandem mass spectrometry. *Free Radical Biol Med.* **30**: 757-764
- Welch RW, Wang Y, Crossman A Jr, Park JB, Kirk KL and Levine M (1995). Accumulation of vitamin C (ascorbate) and its oxidized metabolite dehydroascorbic acid occurs by separate mechanisms. *J Biol Chem.* **270**: 12584-12592
- Wells WW and Xu DP (1994). Dehydroascorbic acid reduction. *J Bioenerg Biomembr.* **26**: 369-377
- Westerdahl J Ingvar C, Masback A, Jonsson N and Olsson H (2000). Risk of cutaneous malignant melanoma in relation to use of sunbeds: further evidence of UV-A carcinogenicity. *Br J Cancer.* **82**: 1593-1599
- Whitehouse CJ, Taylor RM, Thistlethwaite A, Zhang H, Karimi-Busheri F, Lasko DD, Weinfeld M and Caldecott KW (2001). XRCC1 stimulates human polynucleotide kinase activity at damaged DNA termini and accelerates DNA single-strand break repair. *Cell.* **104**: 107-117

- Wikman H, Risch A, Klimek F, Schmezer P, Spiegelhalder B, Dienemann H, Kayser K, Drings P and Bartsch H (2000). *hOGG1* polymorphism and loss of heterozygosity (LOH): significance for lung cancer susceptibility in a Caucasian population. *Int J Cancer*. **88**: 932-937
- Will O, Schlindler D, Boiteux S and Epe B (1998). Fanconi's anaemia cells have normal steady-state levels and repair of oxidative DNA base modifications sensitive to Fpg protein. *Mutat Res*. **409**: 65-72
- Williams MD, Van Remmen H, Conrad CC, Huang TT, Epstein CJ and Richardson A. (1998). Increased oxidative damage is correlated to altered mitochondrial function in heterozygous manganese superoxide dismutase knockout mice. *J Biol Chem*. **273**: 28510-28515
- Wilson TM, Rivkees SA, Deutsch WA and Kelley MR (1996). Differential expression of the apurinic/apyrimidinic endonuclease (APE/ref-1) multifunctional DNA base excision repair gene during fetal development and in adult rat brain and testis. *Mutat Res*. **362**: 237-248
- Wilson DM and Thompson LH (1997). Life without DNA repair. *Proc Natl Acad Sci USA*. **94**: 12754-12757
- Winkler GS and Hoeijmakers JHJ (1998). From DNA helicase to brittle hair. *Nature Genet*. **20**: 106-107
- Winkler BS, Orselli SM and Rex TS (1994). The redox couple between glutathione and ascorbic acid: a chemical and physiological perspective. *Free Radical Biol Med*. **17**: 333-349
- Wood RD (1999). Variants on a theme. *Nature*. **399**: 639-640
- Wood R and Shivji M (1997). When DNA polymerases are used for DNA repair in eukaryotes? *Carcinogenesis*. **8**: 605-610
- Woollons A, Clingen PH, Kipp C, Arlett CF, Green MHL and Young AR (1998)<sup>1</sup>. Tanning lamp pyrimidine dimer induction in normal human epidermal keratinocytes reduced by the use of UVB filters. *Br J Dermatol*. **138**: 730
- Woollons A, Clingen PH, Price ML, Kipp C, Arlett CF, Green MHL and Young AR (1998)<sup>2</sup>. A study of the effect of UVB filters on the spectrum of DNA damage induced in normal human epidermal keratinocytes by tanning lamps. *Br J Dermatol*. **139**: 26-27
- Woollons A, Kipp C, Young AR, Petit-Frere C, Arlett CF, Green MH and Clingen PH (1999). The 0.8% ultraviolet B content of an ultraviolet A sunlamp induces 75% of cyclobutane pyrimidine dimers in human keratinocytes in vitro. *Br J Dermatol*. **140**: 1023-1030
- Wu L, Karow JK and Hickson ID (1999). Genetic recombination: Helicases and topoisomerases link up. *Curr. Biol*. **9**: R518-R520
- Xanthoudakis S and Curran T (1992). Identification and characterisation of Ref-1, a nuclear protein that facilitates AP-1 DNA-binding activity. *EMBO J*. **11**: 653-665

- Xanthoudakis S, Miao G, Wang F, Pan Y-CE and Curran T (1992). Redox activation of Fos-Jun DNA binding activity is mediated by a DNA repair enzyme. *EMBO J.* **11(9)**: 3323-3335
- Xanthoudakis S, Smeyne RJ, Wallace JD and Curran T (1996). The redox/DNA repair protein, Ref-1, is essential for early embryonic development in mice. *Proc Natl Acad Sci USA.* **93**: 8919-8923
- Xie Z, Kometiani P, Liu J, Li J, Shapiro JI and Askari A (1999). Intracellular reactive oxygen species mediate the linkage of Na/K-ATPase to hypertrophy and its marker genes in cardiac myocytes. *J Biol Chem.* **274**: 19323-19328
- Xu G, Marcusson JA and Hemminki K (2001). DNA photodamage induced by UV phototherapy lamps and sunlamps in human skin in situ and its potential importance for skin cancer. *J Invest Dermatol.* **116**: 194-195
- Xu Y, Moore DH, Broshears J, Liu L, Wilson TM and Kelley MR (1997) The apurinic/aprimidinic endonuclease (APE/ref-1) DNA repair enzyme is elevated in premalignant and malignant cervical cancer. *Anticancer Res.* **17**: 3713-19
- Xu Y-J, Kim EY and Demple B (1998). Excision of C-4' -oxidized lesions from double-stranded DNA by human apurinic/aprimidinic endonuclease (Ape1 protein) and DNA polymerase  $\beta$ . *J Biol Chem.* **273**: 28837-28844
- Yacoub A, Kelley MR and Deutsch WA (1997). The DNA repair activity of human redox/repair protein APE/Ref-1 is inactivated by phosphorylation. *Cancer Res.* **57**: 5457-5459
- Yamaguchi R, Hirano T, Asami S, Chung MH, Sugite A and Kasai H (1996). Increased 8-hydroxyguanine levels in DNA and its repair activity in rat kidney after administration of a renal carcinogen, ferric nitrilotriacetate. *Carcinogenesis.* **17**: 2419-2422
- Yamamoto F, Kasai H, Bessho T, Chung MH, Inoue H, Ohtsuka E, Hori T and Nishimura S (1992). Ubiquitous presence in mammalian cells of enzymatic activity specifically cleaving 8-hydroxyguanine-containing DNA. *Jpn. J Cancer Res.* **83**: 351-357
- Yao KS, Xanthoudakis S, Curran T and O'Dwyer PJ (1994). Activation of AP-1 and of a nuclear redox factor, Ref-1, in the response of HT29 colon cancer cells to hypoxia. *Mol Cell Biol.* **14**: 5997-6003
- Yengi L, Inskip A, Gilford J, Alldersea J, Bailey L, Amith A, Lear JT, Heagerty AH, Bowers B, Hand P, Hayes JD, Jones PW, Strange RC and Fryer AA (1996). Polymorphism at the glutathione-S-transferase locus *GSTM3*: Interactions with cytochrome P450 and glutathione-S-transferase genotypes as risk factors for multiple cutaneous basal cell carcinoma. *Cancer Res.* **56**: 1974-1977
- Young AR, Chadwick CA, Harrison GI, Hawk JL, Nikaido O and Potten CS (1996). The *in situ* repair kinetics of thymine dimers and 6-4 photoproducts in human skin types I and II. *J Invest Dermatol.* **106**: 1307-1313
- Young AR, Chadwick CA, Harrison GI, Nikaido O, Ramsden J and Potten CS (1998). The similarity of action spectra for thymine dimers in human epidermis and erythema suggests that DNA is the chromophore for erythema. *J Invest Dermatol.* **111**: 982-988

- Zhao B, Grandy DK, Hagerup JM, Magenis RE, Smith L, Chauhan BC and Henner WD (1992). The human gene for apurinic/apyrimidinic endonuclease (HAP1): sequence and localization to chromosome 14 band q12. *Nucleic Acids Res.* **20**: 4097-4098
- Zheng Y, Pao A, Adair GM and Tang M (2001). Cyclobutane pyrimidine dimers and bulky chemical DNA adducts are efficiently repaired in both strands of either a transcriptionally active or promoter-deleted APRT gene. *J Biol Chem.* **276**: 16786-16796
- Zhou BB and Elledge SJ (2000). The DNA damage response: putting checkpoints into perspective. *Nature.* **408**: 433-439